THE EFFECTS OF AQUIFER HETEROGENEITY ON THE NATURAL ATTENUATION RATES OF CHLORINATED SOLVENTS

A THESIS SUBMITTED TO
THE GRADUATE SCHOOL OF NATURAL AND APPLIED SCIENCES
OF
MIDDLE EAST TECHNICAL UNIVERSITY

BY

BAŞAK ÖNKAL

IN PARTIAL FULFILLMENT OF THE REQUIREMENTS
FOR
THE DEGREE OF MASTER OF SCIENCE
IN
ENVIRONMENTAL ENGINEERING

DECEMBER 2005

Approval of the Graduate School of Natural and Applied Sciences

_____

Prof. Dr. Canan ÖZGEN
Director

I certify that this thesis satisfies all the requirements as a thesis for the degree of Master of Science.

_____

Prof. Dr. Filiz B. DİLEK
Head of Department

This is to certify that we have read this thesis and that in our opinion it is fully adequate, in scope and quality, as a thesis for the degree of Master of Science.

_____

Prof. Dr. Kahraman ÜNLÜ
Supervisor

Examining Committee Members

Assoc. Prof. Dr. F. Dilek SANİN (METU,ENVE) _____

Prof. Dr. Kahraman ÜNLÜ (METU,ENVE) _____

Prof. Dr. Gürdal TUNCEL (METU,ENVE) _____

Asst. Prof. Dr. Ayşegül AKSOY (METU,ENVE) _____

Prof. Dr. Nurkan KARAHANOĞLU (METU,GEOE) _____

I hereby declare that all information in this document has been obtained and presented in accordance with academic rules and ethical conduct. I also declare that, as required by these rules and conduct, I have fully cited and referenced all material and results that are not original to this work.

Name, Last name: Başak ÖNKAL
Signature :

ABSTRACT

THE EFFECTS OF AQUIFER HETEROGENEITY ON
THE NATURAL ATTENUATION RATES OF
CHLORINATED SOLVENTS

Önkal, Başak
M.Sc., Department of Environmental Engineering
Supervisor: Prof. Dr. Kahraman Ünlü

December 2005, 186 pages

Monitored natural attenuation has been particularly used at sites where petroleum hydrocarbons and chlorinated solvents have contaminated soil and groundwater. One of the important aspects of the methodology that has been recognized recently is that the mass removal rates, the most important parameter to determine effectiveness of the methodology, is controlled by the groundwater flow regime and the aquifer heterogeneity. Considering this recognition, the primary objective of this study is to quantitatively describe the relationship between the natural attenuation rates and aquifer heterogeneity using numerical simulation techniques. To represent different levels of aquifer heterogeneity, the hydraulic conductivity distribution (ln K) is statistically simulated with the numerical algorithm, Turning Bands Random Field Generator, by changing the statistical parameters, Coefficient of

Variation (CV) and correlation length (h) and Visual MODFLOW and RT3D software programs are used for the simulation of groundwater flow and chlorinated solvent transport. Simulation results showed that degradation rates and the shape of the contaminant plumes show variations for different heterogeneity levels. Increasing CV resulted in the decrease in the transport of the plume and shrinkage in the areal extend. On the other hand, “h” determined the shape and the size of the plume through its affect on mechanical dispersion. For a given “h”, degradation rates increased with increasing CV, but change in “h” did not show a regular trend. Such findings are expected to be beneficial when assessing the effectiveness of natural attenuation process for a selected site during the feasibility studies without need for detailed site characterization.

Keywords: Natural Attenuation, Chlorinated Solvents, Aquifer Heterogeneity, Numerical Simulations

ÖZ

AKİFER HETEROJENLİĞİNİN KLORLU HİDROKARBON BİLEŞİKLERİNİN DOĞAL GİDERİM ORANLARI ÜZERİNDEKİ ETKİSİ

Önkal, Başak
Yüksek Lisans, Çevre Mühendisliği Bölümü
Tez Yöneticisi : Prof. Dr. Kahraman Ünlü

Aralık 2005, 186 sayfa

İzlemeli Doğal Giderim, İDG, özellikle petrol hidrokarbonları ve klorlu solventlerle kirlenmiş akiferlerin temizlenmesinde ciddi bir alternatif yöntem olarak görülmektedir. Giderek yaygınlaşan İDG uygulamalarında karşılaşılan en önemli konulardan bir tanesi, yöntemin etkinliğini belirlemede en önemli parametre olan kirletici giderim oranlarının belirlenmesinin büyük ölçüde yeraltı suyu (YAS) akış rejimine bağlı olması ve YAS akış rejiminin de akifer heterojenliği tarafında kontrol ediliyor olmasıdır. Bu çerçevede bu tez çalışmasının temel amacı klorlu hidrokarbon bileşiklerinin akifer ortamındaki doğal giderim oranları ile akifer heterojenliği arasındaki ilişkinin nümerik simülasyon yöntemi kullanılarak irdelenmesi ve niceliksel olarak tanımlanmasıdır. Akiferin heterojenlik düzeyi, hidrolik iletkenlik (ln K) dağılımının homojen bir dağılımdan başlayarak değişkenlik katsayısı, CV, ve korelasyon uzunluğu ile değişim gösterecek şekilde ‘Turning Bands Random

Field Generator' algoritması kullanılarak istatiksel yöntemle simüle edilmiştirv e Visual MODFLOW ve RT3D programları kullanılarak klorlu hidrokarbon bileşiklerinin akifer ortamındaki taşınımı modellenmiştir. Sonuçlar akifer heterojenliğinin değişimi ile kirlilik bulutu şeklinin ve kirletici giderim oranlarının ciddi bir şekilde değiştiğini göstermektedir. Değişkenlik katsayısı, CV, arttıkça kirlilik bulutunun taşınımı ve kapladığı alan azalmıştır. Diğer yandan, değişen korrelasyon uzunluğu mekanik dağılım katsayısı üzerindeki etkisinden dolayı daha çok kirlilik bulutunun şeklini ve büyüklüğünü belirlenmiştir. Giderim oranlarında, sabit "h" değeri için, artan CV ile artış gözlenmesine rağmen artan "h" ile belirgin bir trend gözlenememiştir. Elde edilecek bulgular İGD uygulaması ile ilgili fizibilite çalışmaları aşamasında, yöntemin kullanılması düşünülen saha için ne ölçüde etkili olacağının çok detaylı saha karakterizasyonuna gerek duyulmaksızın öngörülmesini sağlayacaktır.

Anahtar Kelimeler: İzlemeli Doğal giderim, Klorlu Hidrokarbon Bileşikleri, Akifer heterojenliği, Nümerik Simülasyonlar

To My Dear Family….

ACKNOWLEDGEMENTS

I owe a dept o graditude to my thesis sopervisor, Prof. Dr. Kahraman Ünlü, for his invaluable guidance, insight, advice, criticism and assistance he has provided constantly through out this thesis.

My deepest appreciation goes to my family for their kind support, encouragement, love and patiance through out this study.

I also owe a deep of gratitude to Tuğba Uçankuş, Environmental Engineer, for her support and fellowship during this study. She gave the most moral support and shared the her knowledge through out this study.

I should particularly like to emphasize that, I owe a dept of graditude more than I can readily express to Ceyda Düzyol for her kind help, encouragement and moral and material support.

TABLE OF CONTENTS

LIST OF TABLES

TABLES

LIST OF FIGURES

FIGURES

CHAPTER 1

INTRODUCTION

1.1. General

The contamination and degradation of groundwater resources throughout the world brought the necessity of taking precautions and using these resources more carefully. During the last few decades the contamination of groundwater has been intensified through industrial and agricultural activities. As a result, attempts for development of groundwater remediation technologies have gained much attention. Various remediation technologies have been developed within last ten years and applied at field scale. The common feature of all of these active cleanup based technologies is the fact that they require high investment and operational costs. Therefore, being a more economical and a less resource demanding technology, Monitored Natural Attenuation lately become an attractive alternative for most clean up activities.

The term ‘‘monitored natural attenuation’’ refers to the reliance on natural processes to achieve site-specific cleanup objectives within a reasonable time frame (U.S . EPA, 1997). The attenuation processes that are at work in such a remediation approach include a variety of in situ physical, chemical, and biological processes that, under favorable conditions, act without human intervention to reduce mass, toxicity, mobility, volume, or concentration of

contaminants in soil and groundwater. The in situ processes may include biodegradation, dispersion, dilution, adsorption, volatilization, and chemical or biological stabilization, transformation or destruction of contaminants (U.S. EPA, 1997)

Natural attenuation processes (biodegradation, dispersion, sorption, and volatilization) affect the fate and transport of chlorinated solvents in all hydrologic systems. When these processes are shown to be capable of attaining site-specific remediation objectives in a time period that is reasonable compared to other alternatives, they may be selected alone or in combination with other more active remedies as the preferred remedial alternative. Monitored Natural Attenuation (MNA) is a term that refers specifically to the use of natural attenuation processes as part of overall site remediation (U.S. EPA, 1998).

1.1.1. Natural Attenuation of Chlorinated Solvents

Natural attenuation in ground-water systems results from the integration of several subsurface attenuation mechanisms that are classified as either destructive or nondestructive. The processes that are known to cause a reduction in the concentration and/or mass of a contaminant dissolved in groundwater and that result only in the reduction of a contaminant's concentration but not of the total contaminant mass in the system are termed as "nondestructive." Nondestructive processes include advection, hydrodynamic dispersion (mechanical dispersion and diffusion), sorption, dilution, and volatilization. The processes that result in the degradation of contaminants are termed as "destructive." The processes relevant to natural attenuation of Carbonaceous Volatile Organic Compounds (CVOCs) in ground water include destructive processes such as abiotic and biotic degradation and the most important process for the natural biodegradation of the more highly chlorinated solvents is reductive dechlorination. Figure 1.1.

shows the reductive dechlorination pathway of the chlorinated solvents. During this process, the chlorinated hydrocarbon species are used as an electron acceptor, not as a source of carbon, and a chlorine atom is removed and replaced with a hydrogen atom.

In general, reductive dechlorination occurs by sequential dechlorination from tetrachloroethene (PCE) to trichloroethene (TCE) to dichloroethene (DCE) to vinyl chloride (VC) to ethane (ETH) and dissolved chloride. During reductive dechlorination, all three isomers of DCE (cis1,2-DCE, trans-1,2-DCE and 1,1-DCE) can theoretically be produced. However, it is believed that under the influence of biodegradation, cis1,2-DCE is a more common intermediate than trans-1,2-DCE, and that 1,1-DCE is the least prevalent of the three DCE isomers when they are present as daughter products (Bouwer, 1994). Reductive dechlorination of chlorinated solvent compounds is associated with the accumulation of daughter products and an increase in the concentration of chloride ions.

Reductive dechlorination affects each of the chlorinated ethenes differently. Of these compounds, PCE is the most susceptible to reductive dechlorination because it is the most oxidized compound. Conversely, VC is the least susceptible to reductive dechlorination because it is the least oxidized of these compounds. As a result, the rate of reductive dechlorination decreases as the degree of chlorination decreases (Vogel and McCarty, 1985; Bouwer, 1994). This rate decrease may explain the accumulation of VC in PCE and TCE plumes that are undergoing reductive dechlorination (Murray and Richardson (1993). Reductive dechlorination has been demonstrated to occur under nitrate- and iron reducing conditions, but the most rapid biodegradation rates, affecting the widest range of chlorinated aliphatic hydrocarbons, occur under sulfate-reducing and methanogenic conditions (Weidemeier and Chappelle, 1998).

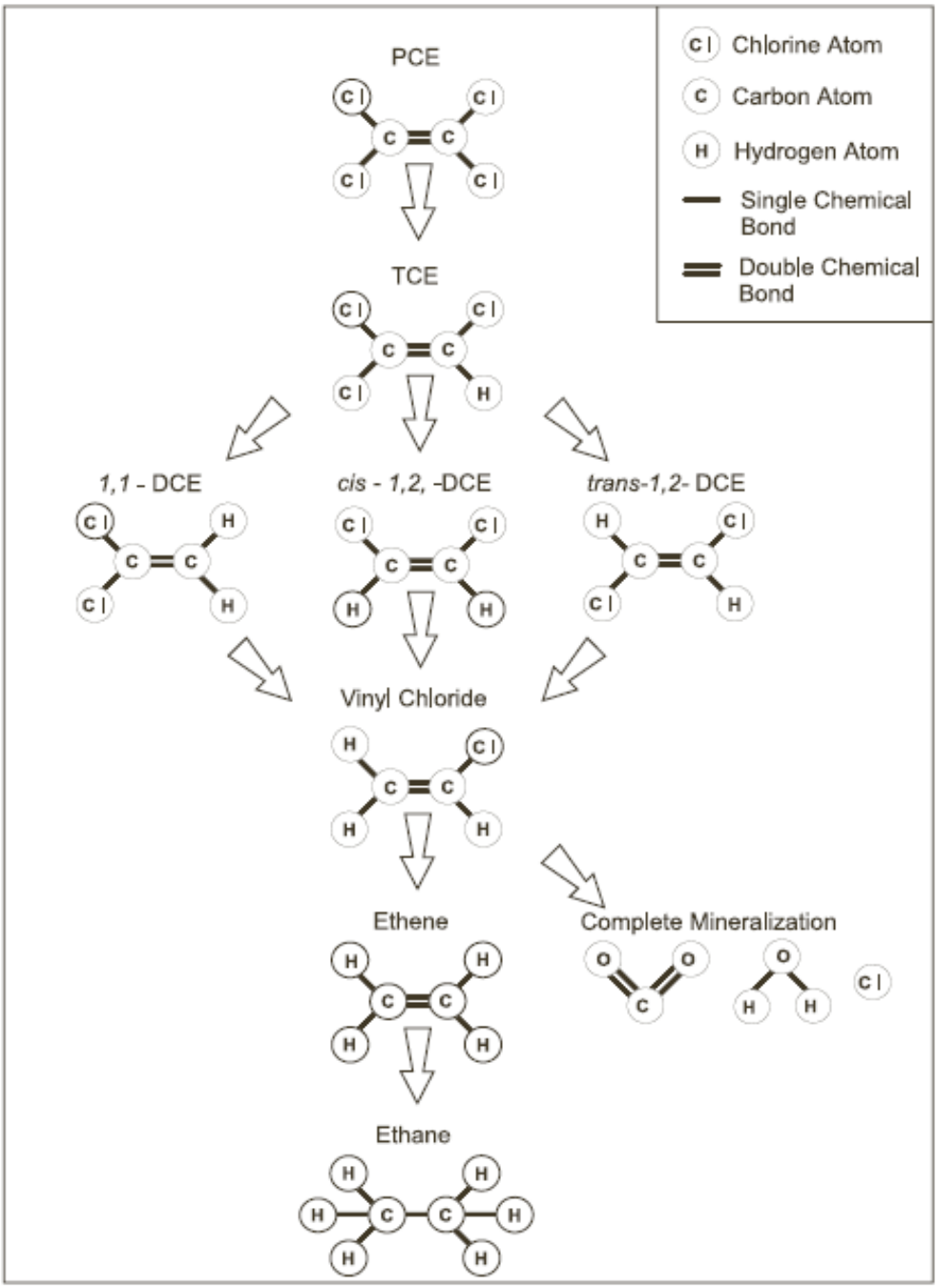

Figure 1.1. Reductive Dechlorination of Chlorinated Ethenes
(U.S. EPA, 1998)

Biodegradation of fuel hydrocarbons, especially benzene, toluene, ethylbenzene, and xylenes (BTEX), are mainly limited by electron acceptor

availability, and generally will proceed until all of the contaminants biochemically accessible to the microbes are destroyed (Wiedemeier, 1996b). On the other hand, the more highly chlorinated solvents such as perchloroethene (PCE) and trichloroethene (TCE) typically are biodegraded under natural conditions via reductive dechlorination, a process that requires both electron acceptors (the chlorinated aliphatic hydrocarbons) and an adequate supply of electron donors (Weidemeier and Chappelle, 1998). Electron donors include fuel hydrocarbons or other types of anthropogenic carbon (e.g., landfill leachate) or natural organic carbon. In case of depletion of electron donors in the subsurface environment before the removal of chlorinated aliphatic hydrocarbons, biological reductive dechlorination will cease. This is the most significant difference between the processes of fuel hydrocarbon and chlorinated aliphatic hydrocarbon biodegradation. Therefore, predicting the long-term behavior of chlorinated aliphatic hydrocarbon plumes is more difficult than fuel hydrocarbon plumes. Thus, it is important to have a good understanding of the important natural attenuation mechanisms. Data collection should include all parameters to evaluate the efficacy of natural attenuation. It is necessary to better quantify biodegradation besides a better understanding of the processes of advection, dispersion, dilution from recharge, and sorption (U.S. EPA, 1998). Detailed site characterization is required to adequately document and understand these processes. The long-term monitoring strategy should consider the possibility that the behavior of a plume may change over time and monitor for the continued availability of a carbon source to support reductive dechlorination.

Nondestructive natural attenuation processes include those that reduce contaminant concentration but do not reduce the total contaminant mass in a system. The most important nondestructive attenuation processes for tetrachloroethene (PCE) to trichloroethene (TCE) and trichloroethene (TCE)

to dichloroethene (DCE) in ground water are volatilization, dispersion, dilution and sorption.

1.1.2. Behavior of Chlorinated Solvent Plumes

Chlorinated solvent plumes can exhibit three types of behavior depending on the amount of solvent, the amount of biologically available organic carbon in the aquifer, the distribution and concentration of natural electron acceptors, and the types of electron acceptors being used. Three major types of chlorinated solvent plumes are identified. Type 1 behavior occurs where the primary substrate is anthropogenic carbon (e.g., BTEX or landfill leachate), and microbial degradation of this anthropogenic carbon drives reductive dechlorination. Type 2 behavior dominates in areas that are characterized by relatively high concentrations of biologically available native organic carbon. Microbial utilization of this natural carbon source drives reductive dechlorination (i.e., it is the primary substrate for microorganism growth. Finally, Type 3 behavior dominates in areas that are characterized by inadequate concentrations of native and/or anthropogenic carbon, and concentrations of dissolved oxygen that are greater than 1.0 mg/L or that do not contain microbes capable of biodegradation of chlorinated solvents. Under these aerobic conditions, reductive dechlorination will not occur (Weidemeier and Chappelle, 1998).

Individual plumes may exhibit all three types of behavior in different portions of the plume and this can be beneficial for the biodegradation of chlorinated aliphatic hydrocarbon plumes. For example, Figure 1.2. shows a plume that exhibits Type 1 behavior in the source area and Type 3 behavior downgradient from the source (Wiedemeier et al.,1996a). In this kind of plumes PCE, TCE, and DCE are reductively dechlorinated with accumulation of VC near the source area (Type 1 or Type 2 behavior), then VC is oxidized (Type 3 behavior), either aerobically or via iron reduction further

downgradient. Vinyl chloride is oxidized to carbon dioxide in this type of plume and does not accumulate. Another scenario of plume behavior is that all chlorinated aliphatic hydrocarbons are reductively dechlorinated via Type 1 or Type 2 behavior and in this type of plumes VC is reduced to ethene, which may be further reduced to ethane or methane (Freedman and Gossett, 1989). In this type of plume, VC degrades more slowly than TCE, and thus tends to accumulate.

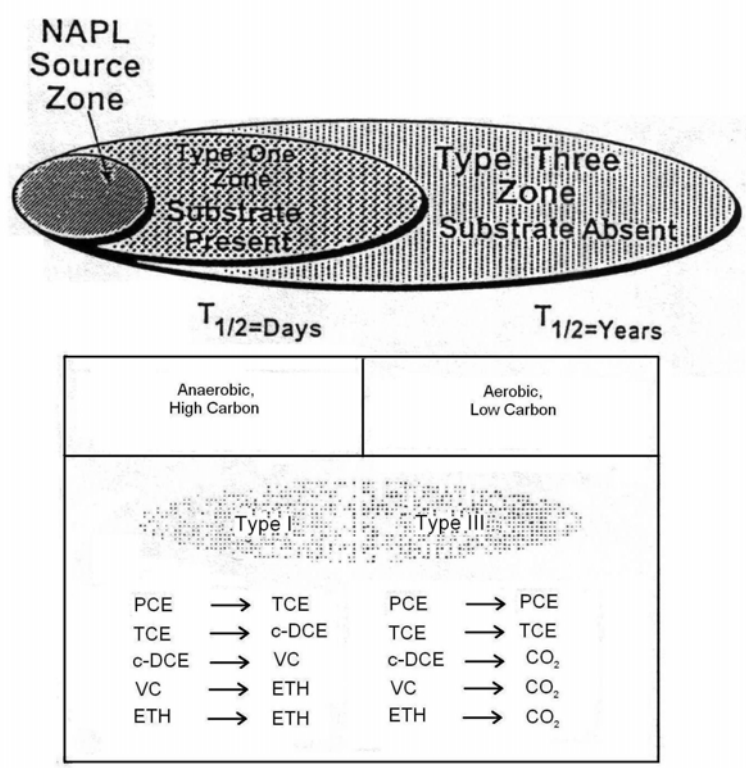

Figure 1.2. A NAPL plume exhibiting the Type 1 and Type 3 plume behavior (Wiedemeier et al.,1996a)

1.2. Literature Survey

The research findings of the past years have shown that the groundwater flow systems that are contaminated by petroleum hydrocarbons can be remediated by naturally occurring systems. However, the fact that the chlorinated solvents can also be naturally remediated is a relatively new

issue (Wiedemeie, et al., 1999; National Research Council, 2000). Since the natural attenuation capacity of a site depends mainly on the site and contaminant specific properties, studies have been performed to investigate the degradation pathways of the chlorinated solvents and the effect of aquifer specific properties on the transport and attenuation rates. Being the most effective property on the distribution of the water head and the groundwater velocity field, hydraulic conductivity has gained the much attention in this study.

Chapell and Bradley (1998) identified the remediation goals for the source areas of a chlorinated ethane-contaminated groundwater plume by assessing the natural attenuation capacity of an aquifer system. The study have shown that in an aquifer system while near the source of contamination sulfate reducing conditions occurring, at the down gradient of the source area the Fe(III) reducing conditions take place. The sulfate reducing conditions yield in the transformation of PCE to TCE and subsequently to DCE and finally to VC which is followed by transformation of DCE and VC to carbon dioxide and chloride in the Fe (III) reducing conditions (Chapell and Bradley, 1998). This sequence of transformation of chlorinated solvents show that the aquifers has the capacity of biological removal of chlorinated hydrocarbons and this natural degradation mechanism of the aquifer, meaning that the decrease in the contaminant concentrations along the groundwater flow regime, depends on the biodegradation rates, aquifer dispersive characteristics and groundwater flow velocity (Chapell and Bradley, 1998).

Natural attenuation of TCE was evaluated for a groundwater plume at IDAHO National Engineering and Environmental Laboratory (Sorenson, et al., 2000). Significant evidence demonstrated that reductive dechlorination is occurring and three first-order rate estimation methods were used to understand the transport processes affecting TCE. Two of the methods gave attenuation results as 8 years; however, these methods did not adequately distinguish

between degradation and dispersion. In the third method tracers were used to distinguish between dispersion and degradation. The aerobic degradation rate was between 13 and 21 years. The study has demonstrated that, in general, the rate of contaminant concentration decrease is not constant with time after the source is removed. It is important to distinguish the affect of aquifer dispersive characteristics on the biodegradation rates for a better understanding of the long term effects of the natural attenuation in the contaminated sites (Sorenson, et al., 2000).

The redox chemistry of the sites showing that the contaminant concentrations decreases along the groundwater flow direction can be accepted as a direct evidence of the natural attenuation is effectively taking place in the subsurface environment. Also USEPA has developed three lines of evidence approach to estimate natural attenuation (USEPA, 1998). These are the documented loss of contaminants at the field scale:, the presence and distribution of geochemical and biochemical indicators of natural attenuation and direct microbiological evidence. This approach has been used to demonstrate that the most important and effective way of natural attenuation of chlorinated solvents takes place in anaerobic conditions (Wiedemeie, et al., 1999).

Researches to understand the process of natural attenuation of the chlorinated solvents and the processes and parameters that affect natural attenuation capacity of a site have took place in the literature as mentioned below. The “lines of evidence” approach was used to examine the potential for monitored natural attenuation of PCE and TCE in the groundwater and aquifer sediments of a test site, Area-6 site in Dover Air Force Base (Dover, DE). The studies about the conditions in which the chlorinated solvents can undergo natural attenuation was examined and a site-specific conceptual model was developed where both anaerobic and aerobic biological processes are responsible for destruction of PCE, TCE, and daughter

products using the chlorinated hydrocarbon and biogeochemical data (Wit, et all, 2002). Clement (1997) and Clement et al. (2000) have developed a multi-dimensional and multi-species reactive transport code, RT3D, for simulating the bioremediation scenarios in subsurface environments. The developed model was applied to analyze field-scale transport and biodegradation of PCE, TCE, DCE and VC plumes at Area-6 site in Dover Air Force Base (Dover, DE). The model was calibrated to field data and the general groundwater flow patterns and the distribution of contaminant plumes were recreated. The sensitivity analysis was carried out considering the results that showed the anaerobic degradation rate, source loading rate and groundwater transport rate are the important model parameters. The results of the sensitivity analysis indicated that the shape and extend of the predicted TCE plume is most sensitive to transmissivity values which is an aquifer parameter directly related with hydraulic conductivity and aquifer thickness (Clement, et al., 2000).

To understand the behavior of contaminant plumes in groundwater, MacQuarrie and Sudicky (1990)performed 2-dimensional toluene and dissolved oxygen transport simulations. The simulations were carried out in fields having uniform and random hydraulic conductivity distributions. Turning Bands Random Field Generator (Tompson, 1987) was used for the generation of random hydraulic conductivity fields. The heterogeneity level, average groundwater velocity, retardation factor of the contaminant is the physical and chemical parameters that affect the degradation rate of the organic contaminant. The results of the simulations that were carried out in the uniform flow field showed that increase in the groundwater velocity resulted in an increase in the mass loss of the contaminant due to increase in the mechanical mixing of the organic plume with the oxygenated groundwater. The dissolved organic and oxygen distributions were demonstrated to be very irregular in the random hydraulic conductivity fields because of small-scale groundwater velocity variations (MacQuarrie and

Sudicky-2, 1990). It is stated by MacQuarrie and Sudicky (1990) that the local scale dispersivities and the groundwater velocities control the transport behavior, shape and size of the dissolved organics.

Buscheck & Alcantar, 1995, applied regression techniques and analytical solutions to illustrate the effects of naturally occurring processes in the subsurface such as advection, dispersion, sorption and biodegradation on the overall attenuation of petroleum hydrocarbons. The analyses were based on the assumption that the transport was 1-dimensional and the contaminant had reached a steady state. The regression results of concentration versus distance was coupled with the analytical solution of 1-dimensional transport equation with first order decay under steady-state conditions that is presented by Bear, (1979). Buscheck & Alcantar, (1995) stated that as the contaminant velocity increases, the decay becomes less effective in reducing the contaminant concentrations as a function of distance. Hence retardation enhances biodegradation as retarded transport velocities favor biodecay over transport (Domenico & Schwartz, 1990), whereas dispersion results in further spreading of contaminant, reducing concentrations.

1.3. Scope and Objectives

The level of heterogeneity of a site has an effect on various mechanisms and processes in an aquifer system such as the groundwater flow regime and the fate and transport of the contaminants. Eventually, the natural attenuation capacity of a site changes at different heterogeneity levels. The objectives of this study are to investigate the effects of aquifer heterogeneity on the transport of Chlorinated Hydrocarbons, more specifically PCE, TCE and their degradation by products, and their mass attenuation rates and to develop quantitative relationships between degradation rates and the parameters of aquifer heterogeneity, CV and h. The study is performed in three stages. At first place, the statistical distributions of spatially correlated random hydraulic

conductivity fields representing different levels of aquifer heterogeneity levels were generated, and then these fields were subsequently used to simulate flow and fate and transport of contaminant species. The hydraulic conductivity (ln K) field will be statistically simulated starting with a homogeneous uniform distribution and then changing the heterogeneity level which is determined by the Coefficient of Variation (CV), a ratio of standard deviation to mean, and the spatial correlation length (h), the maximum separation distance for which the sample pairs seem correlated. The fields with CV ratios of 50%, 100%, 150% and correlation length of 5 m, 10 m and 20 m have been generated. Turning Bands Random Field Generator is used for the generation of hydraulic conductivity fields having different heterogeneity levels. In the second part of the study, through using groundwater flow and contaminant transport models, Visual MODFLOW and RT3D, the groundwater flow regime and the chlorinated solvent transport and degradation has been simulated for fields having different hydraulic conductivity distributions. Then the biodegradation rates of the contaminants have been evaluated for each heterogeneous field. As the final step, multiple regression analyses were conducted to develop quantitative functional relationships between the biodegradation rate constants of PCE and ir degradation species and the aquifer heterogeneity parameters, coefficient of variation and spatial correlation length.

Development of an adequate database during the iterative site characterization process is an important step in the documentation of natural attenuation. Detailed and extensive monitoring strategy should be performed for better site characterization to understand the groundwater flow regime and level of heterogeneity. The findings of this study (functional relationship between k and CV and h) of this study will produce a range of degradation rate constants as a function of CV and correlation length. Thus, with a minimal site characterization effort to determine the ranges of CV and h values may give a working estimation of degradation rate constant that can

be used while assessing the effectiveness of natural attenuation to achieve the clean up goals at a given contaminated site.

CHAPTER 2

MATERIALS AND METHODS

The theoretical background of the fate and transport of the contamination and software programs used in the random field generation and contaminant fate and transport simulations are explained in this section.

2.1. Random Field Generation

Random fields are the 1-, 2-, 3-dimensional analogues of stochastic processes; they are used to model spatial data as observed in environmental, atmospheric, and geological sciences. (Schlather, 2001). Numerical techniques are used for the generation of spatially correlated random fields.

In this study, Turning Bands Random Field Generator (Tompson, 1987) was used to generate random hydraulic conductivity fields. The turning bands method implemented numerically using a FORTRAN code developed by Zimmermann and Wilson (1990). The main reason to generate random fields of physical quantities such as hydraulic conductivity is that although detailed site characterization is carried out, it is very difficult to predict and measure the in situ distribution of these variables over large spatial and temporal distances. Besides, the mathematical representation as correlated random

fields of these kinds of spatial and temporal variables allow larger scale characterization or prediction of these parameters for the site of interest (e.g. Mejia and Rodriguez-Iturbe 197; Smith and Freeze, 1979; Smith and Schwartz, 1980; Gelhar, 1984; Gelhar and Axness, 1983). Since the detailed and complete prediction and measurement of these parameters and their distributions are very difficult, these artificial random distributions of parameters can be used instead of the reality while checking the theoretical results.

2.1.1. Random Field Theory

The turning bands method has been widely used to create artificial fields of physical quantities. The Turning Bands Method (TBM), as originally suggested by Matheron [1973], involves the simulation of isotropic and anisotropic random fields in two- or higher-dimensional space by using a sequence of one-dimensional processes along lines crossing the space. This method can be used to generate a second order, stationary random field whose marginal density functions are all normal of mean zero and variance one (Tompson, et al., 1987). $z(x)$ is defined as the desired, three-dimensional field realization, normally distributed $N(0,\sigma^2)$

Transformation of such a normal field into another normal field $z^*(x)$ with mean m and variance σ^2 can be accomplished as

$$z^*(x) = \sigma_f \, z(x) + m \qquad (2.1)$$

or transformation a lognormal field, e.g., a hydraulic conductivity K(x) distribution and can be defined as:

$$K(x) = \exp(z^*(x)) = e^m e^{\sigma_f z(x)} = K_G e^{\sigma_f z(x)} \qquad (2.2)$$

where K_G is the geometric mean of K(x). Equation 2.1 takes the form as

$$\sigma_f \; z(x) = z^*(x) - m \qquad (2.3)$$

where $z^*(x)$ is the log normal hydraulic conductivity distribution and can be defined as $ln\,(K(x))$. The mean of any normally distributed population $z(x)$ can be defined as the expected value of $z(x)$ or the mathematical expectation of $z(x)$ denoted by $E(z(x))$. Then the exponential term $\sigma_f \, z(x)$ in equation 2.2 can be rewritten as

$$\sigma_f \; z(x) = f(x) = ln\,(K(x)) - E[ln(K(x))]. \qquad (2.4)$$

Besides mean and variance, spatial correlation length is also another parameter that determines the degree of heterogeneity within the generated random field. The effect of mean and variance in field heterogeneity is stated by the coefficient of variation, CV, which is the ratio of standard deviation to mean.

$$\mathrm{CV} = \frac{\sigma}{m} \qquad (2.5)$$

In order to determine the effect of heterogeneity on the fate and transport of the contaminant, spatially correlated random hydraulic conductivity fields having different CV and correlation length (h) values are generated using Turning Bands Random Field Generator. The correlation length (h) is defined as the maximum separation distance for which the sample pairs of hydraulic conductivity seem correlated (Warrick, et al., 1986).

Since the generator gives the lognormal field, the mean and variance has to be input to the program accordingly, in order to have a field with a specified mean and variance. For log normally distributed variables, such as hydraulic

conductivity, the following conversion formulas are used to determine the log mean $m_{\ln}$ and log variance $\sigma^2_{\ln}$ as

$$m_{\ln} = \ln(m) - \frac{\sigma^2_{\ln}}{2} \tag{2.6}$$

$$\sigma^2_{\ln} = \ln\left(\frac{\sigma^2}{m^2} + 1\right) \tag{2.7}$$

where *m* and σ^2 are the mean and variance of the original random variable, respectively. Log normally distributed random variables, e.g. hydraulic conductivity, are generated form the transformed normal distribution $N(m_{\ln}, \sigma^2_{\ln})$ by using the $m_{\ln}$ and $\sigma^2_{\ln}$ values (Ünlü, 1994).

The turning bands generator uses Monte Carlo Simulation technique for the generation of random fields. Monte Carlo simulation is a stochastic technique that uses the random selection process repeatedly many times to create multiple realizations of the random process.

2.1.2. Generation of Hydraulic Conductivity Fields

For the construction of model domain, which has a random heterogeneity, turning bands random field generator is used and 2- dimensional hydraulic conductivity distributions are generated. In the generation of these randomly distributed isotropic hydraulic conductivity fields and exponential covariance structure of the following form is used.

$$C(l) = \sigma^2 e^{-l/h} \tag{2.8}$$

where σ^2 is the variance, l is the spatial lag distance and h is the spatial correlation length. For a hydraulic conductivity field with anisotropic covariance structure equation 2.8 takes the form

$$C(l) = \sigma^2 \exp\left[\left(-\left(\frac{l}{h_x}\right)^2 + \left(\frac{l}{h_y}\right)^2\right)^{1/2}\right] \qquad (2.9)$$

where h_x and h_y are the correlation lengths in x- and y- directions, respectively.

The generator requires some physical and parametric data to be specified (Tompson, et al., 1987). The physical data determines the dimensions of the model domain through defining the number of grid points and the grid spacing in the x- and y- directions. The size of the domain for which random K fields were generated was 150 m in x- and 100m in y-direction. The grid spacing was taken as 0.5 m in both directions. In addition, the statistical properties, spatial correlation length (h), mean (K_G) and variance (σ_f) of the log-normally distributed hydraulic conductivity field was also assigned as physical input data group that will be read in subroutine input of the generator.

The parametric data is required for the numerical definition of the line processing technique used in the generation of the fields as number of lines, and number of points simulated on any line together with the magnitude of the physical spacing on the lines, the number of Monte Carlo Simulations that the generator will perform.

As it is mentioned before in Monte Carlo Simulation technique the random selection process is repeated many times to create multiple scenarios. In the

generation of nine random fields 10 replicate Monte Carlo Simulations (MCS) are performed and spatial estimates of the mean, variance and covariance for the ten replicate of each random field generated were presented and discussed in Chapter 3 Results and Conclusion.

The generated random K fields have CV values of 50%, 100% and 150% with correlation lengths of 5 m, 10 m and 20 m. The mean value of the log-normally distributed hydraulic conductivity fields was 1.8 x 10^{-4} m/sec. The field was discretized into square grids taking into account that at least 5 nodal K values should fall within the specified correlation length in order to maintain the numerical robustness during generation of random K fields.

The log mean, $m_{\ln}$ and log variance, $\sigma^2_{\ln}$ which are inputs for the Turning Bands Random Field Generator, were calculated for each of the fields that using the equations 2.4 and 2.5. Calculations of the mean and variance of the log normally distributed hydraulic conductivity fields are carried out as

$$K_G = e^{m_{\ln}} \tag{2.10}$$

$$\sigma_f = \sigma_{\ln} \tag{2.11}$$

Since the parametric data is related to the simulation technique of the generated randomly distributed data, same parametric data file is used for all simulations of the random field generation. The complete physical data and the parametric data used for the simulation of the random fields are given in Appendix A.

In order to see the effect of anisotropy on the hydraulic conductivity distribution and in turn on the groundwater flow and contaminant transport, two K fields with anisotropic spatial correlation structure were also generated for the corresponding fields having the least and most mass loss at the end of the contaminant transport simulation times. In the random field generator the anisotropy is determined in the physical input data by the correlation

length in the x and y directions. For the two dimensional anisotropic random filed generation, the anisotropy ratio is selected such that,

$$\frac{h_x}{h_y} = 5 \qquad (2.12)$$

The physical input data of the generated anisotropic fields are also given in Appendix A.

2.2. Modeling Chlorinated Compound Transport in Aquifers

The simulations of the chlorinated solvent fate and transport were carried out by Visual MODFLOW, which is a software package for the simulation of groundwater flow (MODFLOW), and a module for the contaminant transport (RT3D). The flow and transport of the contaminants were simulated for a uniform and for each random field generated.

2.2.1. Overview of Visual MODFLOW

Visual MODFLOW is the most complete and easy-to-use modeling environment for practical applications in three-dimensional groundwater flow and contaminant transport simulations graphics (Visual MODFLOW, 2002).

2.2.1.1. MODFLOW Package

Modeling studies has gained much attention in past few years because they are useful tools in representing the real field situations. They are used for the conceptual representation of the physical, chemical and biological processes taking place in the field of interest. The important and the first step is to develop a conceptual model for the site regarding the processes that take place within the system and the site specific properties. The software programs are then used for the implementation of the numerical model which is used to solve the mathematical model, equations

The following partial differential equation represents the 3-dimensional groundwater flow through subsurface:

$$\frac{\partial}{\partial x}(K_{xx}\frac{\partial H}{\partial x})+\frac{\partial}{\partial y}(K_{yy}\frac{\partial H}{\partial y})+\frac{\partial}{\partial z}(K_{zz}\frac{\partial H}{\partial z})-W=S_S\frac{\partial H}{\partial t}) \qquad (2.13)$$

where K_{xx}, K_{yy} and K_{zz} are the hydraulic conductivity values along x, y and z directions which are assumed to be parallel to the major axis of hydraulic conductivity, (LT^{-1}); H is the potentiometric head, (L); W is the volumetric flux per unit volume of aquifer and represents source/sinks, (T^{-1}); S_s is the specific storage of the aquifer, (L^{-1}); and t is time, (T).

MODFLOW simulates steady and nonsteady flow in an irregularly shaped flow system in which aquifer layers can be confined, unconfined, or a combination of confined and unconfined. Flow from external stresses, such as flow to wells, area recharge, evapotranspiration, flow to drains, and flow through river beds, can be simulated. Hydraulic conductivities or transmissivities for any layer may differ spatially and be anisotropic (restricted to having the principal directions aligned with the grid axes), and the storage coefficient may be heterogeneous. Specified head and specified flux boundaries can be simulated as can a head dependent flux across the model's outer boundary.

Equation 2.13 is solved using the finite-difference approximation and the defined model domain boundary and the initial head conditions. The flow region is subdivided into blocks in which the medium properties are assumed to be uniform. In plan view the blocks are made from a grid of mutually perpendicular lines that may variably spaced. Model layers can have varying thickness. A flow equation is written for each block, called a cell and the

equation yields for solution for nodal heads and the flow rate within the individual cells. Several solvers are provided for solving the resulting matrix problem; the user can choose the best solver for the particular problem. Flow-rate and cumulative-volume balances from each type of inflow and outflow are computed for each time step.

2.2.1.2. RT3D Package

RT3D is a program for simulating reactive multi-species mass transport in three-dimensional groundwater aquifers and it is included in the Visual MODFLOW as transport package. RT3Dv1.0 was first developed and subsequently released into the public domain and quickly became an accepted standard for reactive transport modeling (Clement, 1997)

RT3DV1 (Reactive Transport in 3-Dimensions) is a computer code that solves the coupled partial differential equations that describe reactive-flow and transport of multiple mobile and/or immobile species in three-dimensional saturated groundwater systems. RT3D is a generalized multi-species version of the U.S. Environmental Protection Agency (EPA) transport code, MT3D (Zheng, 1990). As with MT3D, RT3D also requires the groundwater flow code MODFLOW (McDonald and Harbaugh, 1988) for computing spatial and temporal variations in groundwater head distribution. The RT3D code was originally developed to support the contaminant transport modeling efforts at natural attenuation demonstration sites (Clement and Johnson 1998; Lu et al., 1998). As a research tool, RT3D has also been used to model several laboratory and pilot-scale active bioremediation experiments (Johnson et al. 1998). The performance of RT3D has been validated by comparing the code results against various numerical and analytical solutions (Clement et al., 1998; Sun and Clement, 1998; Sun et al. 1998). The code is currently being used to model field-scale natural attenuation at multiple sites. The RT3D includes an implicit reaction solver

that makes the code sufficiently flexible for simulating various types of chemical and microbial reaction kinetics. RT3D v1.0 supports seven pre-programmed reaction modules that can be used to simulate different types of reactive contaminants including bezene-toluene-xylene mixtures (BTEX), and chlorinated solvents such as tetrachloroethene (PCE) and trichloroethene (TCE). In addition, RT3D has a user-defined reaction option that can be used to simulate any other types of user-specified reactive transport systems.

The RT3D code always requires a reaction module to define the problem-specific reactions (i.e., how the contaminants react with each other and with the subsurface). It includes seven pre-programmed reaction modules.

Among these modules, the Aerobic/anaerobic Model for PCE/TCE Degradation reaction module was used in this study. This module simulates the degradation of PCE/TCE and their degradation products via both aerobic and anaerobic pathways.

The conceptual model for all chlorinated solvent degradation reactions, mediated by aerobic and anaerobic dechlorination processes, is described in Figure 2.1.

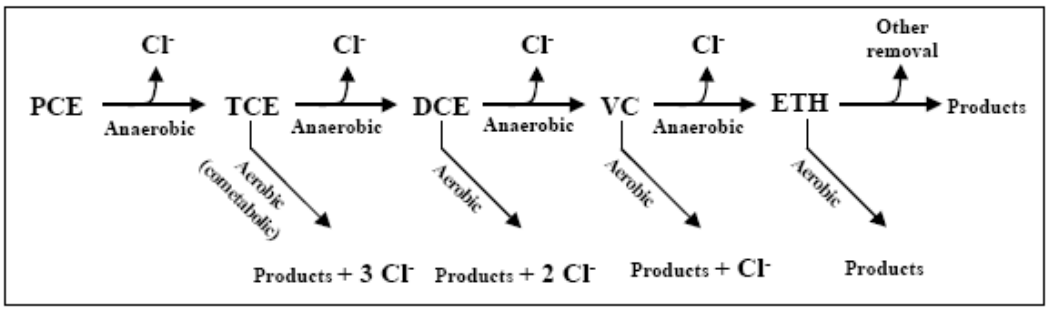

Figure 2.1. Conceptual Model for Chlorinated Solvent Biodegradation (Vogel and McCarty, 1985)

Assuming first-order biodegradation kinetics, the mass transport and transformation of PCE, TCE, DCE, VC, ETH, and Cl can be simulated by solving the following set of partial differential equations. For most natural attenuation modeling applications, the first-order assumption can be considered as a reasonable approximation (Weidemeier et al., 1996)

$$R_P \frac{\partial [PCE]}{\partial t} = \frac{\partial}{\partial x_i}\left(D_{ij} \frac{\partial [PCE]}{\partial x_i} \right) \frac{\partial (v_i [PCE])}{\partial x_i} + \frac{q_s}{\phi}[PCE] - K_P [PCE] \tag{2.14}$$

$$\begin{aligned} R_T \frac{\partial [TCE]}{\partial t} = {} & \frac{\partial}{\partial x_i}\left(D_{ij} \frac{\partial [TCE]}{\partial x_i} \right) \frac{\partial (v_i [TCE])}{\partial x_i} + \frac{q_s}{\phi}[TCE]_S + Y_{T/P} K_P [PCE] \\ & - K_{T1}[TCE] - K_{T2}[TCE] \end{aligned} \tag{2.15}$$

$$\begin{aligned} R_D \frac{\partial [DCE]}{\partial t} = {} & \frac{\partial}{\partial x_i}\left(D_{ij} \frac{\partial [DCE]}{\partial x_i} \right) \frac{\partial (v_i [DCE])}{\partial x_i} + \frac{q_s}{\phi}[DCE]_S + Y_{D/T} K_{T1} [TCE] \\ & - K_{D1}[DCE] - K_{D2}[DCE] \end{aligned} \tag{2.16}$$

$$\begin{aligned} R_V \frac{\partial [VC]}{\partial t} = {} & \frac{\partial}{\partial x_i}\left(D_{ij} \frac{\partial [VC]}{\partial x_i} \right) \frac{\partial (v_i [VC])}{\partial x_i} + \frac{q_s}{\phi}[VC]_S + Y_{V/D} K_{D1} [DCE] \\ & - K_{V1}[VC] - K_{V2}[VC] \end{aligned} \tag{2.17}$$

$$\begin{aligned} R_E \frac{\partial [ETH]}{\partial t} = {} & \frac{\partial}{\partial x_i}\left(D_{ij} \frac{\partial [ETH]}{\partial x_i} \right) \frac{\partial (v_i [ETH])}{\partial x_i} + \frac{q_s}{\phi}[ETH]_S + Y_{E/V} K_{V1} [VC] \\ & - K_{E1}[ETH] - K_{E2}[ETH] \end{aligned} \tag{2.18}$$

$$\begin{aligned} R_C \frac{\partial [Cl]}{\partial t} = {} & \frac{\partial}{\partial x_i}\left(D_{ij} \frac{\partial [Cl]}{\partial x_i} \right) \frac{\partial (v_i [Cl])}{\partial x_i} + \frac{q_s}{\phi}[Cl]_S + Y1_{C/P} K_{P1} [PCE] \\ & + Y1_{C/T} K_{T1} [TCE] + Y1_{C/D} K_{D1} [DCE] + Y1_{C/V} K_{V1} [VC] \\ & + Y2_{C/T} K_{T2} [TCE] + Y2_{C/D} K_{D2} [DCE] + Y2_{C/V} K_{V2} [VC] \end{aligned} \tag{2.19}$$

where [PCE], [TCE], [DCE], [VC], [ETH], and [Cl] represent contaminant concentrations of various species, M/L^3; K_P, K_{T1}, K_{D1}, K_{V1}, and K_{E1} are first-

order anaerobic degradation rates, day^{-1}; K_{T2}, K_{D2}, K_{V2}, and K_{E2} are first-order aerobic degradation rates, T^{-1}, R_P, R_T, R_D, R_V, R_E, and R_C are retardation factors; $Y_{T/P}$, $Y_{D/T}$, $Y_{V/D}$, and $Y_{E/V}$ are chlorinated compound yields under anaerobic reductive dechlorination conditions, $Y1_{C/P}$, $Y1_{C/T}$, $Y1_{C/D}$, and $Y1_{C/V}$ are yield values for chloride under anaerobic conditions, and $Y2_{C/T}$, $Y2_{C/D}$, and $Y2_{C/V}$ are yield values for chloride under aerobic conditions. The yield values are estimated from the reaction stoichiometry and molecular weights; for example, anaerobic degradation of one mole of PCE would yield one mole of TCE, therefore $Y_{T/P}$ = molecular weight of TCE/molecular weight of PCE (131.4/165.8 = 0.79). v_i is the linear pore water velocity, LT^{-1}, q_s is the volumetric flow rate per unit volume of the aquifer representing source/sinks, T^{-1}, D_{ij} is the hydrodynamic dispersion coefficient, L^2T^{-1}

The reaction models presented above assume that the biological degradation reactions occur only in the aqueous phase, which is a conservative assumption. Using the reaction operator-split strategy, the biological reaction kinetics included in the transport equations 2.14-2.19 are separated and assembled as a set of ordinary differential equations:

$$\frac{d[PCE]}{dt} = \frac{K_P[TCE]}{R_P} \tag{2.20}$$

$$\frac{d[TCE]}{dt} = \frac{Y_{T/P}K_P[PCE] - K_{T1}[TCE] - K_{T2}[TCE]}{R_T} \tag{2.21}$$

$$\frac{d[DCE]}{dt} = \frac{Y_{D/T}K_{T!}[TCE] - K_{D1}[DCE] - K_{D2}[DCE]}{R_D} \tag{2.22}$$

$$\frac{d[VC]}{dt} = \frac{Y_{V/D}K_{D1}[DCE] - K_{V1}[VC] - K_{V2}[VC]}{R_V} \tag{2.23}$$

$$\frac{d[ETH]}{dt} = \frac{Y_{E/V}K_{V1}[VC] - K_{E1}[ETH] - K_{E2}[ETH]}{R_E} \tag{2.24}$$

$$\frac{d[Cl]}{dt} = \frac{\begin{array}{c} Y1_{C/P}K_{P1}[PCE] + Y1_{C/T}K_{T1}[TCE] + Y1_{C/D}K_{D1}[DCE] + Y1_{C/V}K_{V1}[VC] \\ + Y2_{C/T}K_{T2}[TCE] + Y2_{C/D}K_{D2}[DCE] + Y2_{C/V}K_{V2}[VC] \end{array}}{R_C} \quad (2.25)$$

These equations 2.20-2.25 are coded into the Aerobic/Anaerobic Model for PCE/TCE Degradation reaction module available in RT3D package.

2.2.2. Description of Simulated Aquifer System

The contaminant transport simulations are carried out with Visual MODFLOW by describing the model domain and assigning the aquifer properties, initial and boundary conditions of the aquifer and contaminant degradation pathways. The steps that are carried out within the program are described below.

2.2.2.1. Size of the Domain and Discretization

Firstly, the size of the problem domain is determined according to the scale of the question. The graphical representation of the simulated aquifer system as it is created in Visual MODFLOW is presented in Figure 2.2. The length in x-direction is 150 m, and in y-direction is 100 m. In order to assign randomly distributed K values of the generated fields to the corresponding nodes in model domain generated in the Visual MODFLOW and to preserve the spatial random structure, the gird spacing is adjusted to $\Delta x = \Delta y =$ 0.5 m.

m in both directions. 2-D groundwater flow and contaminant transport simulations were carried out.

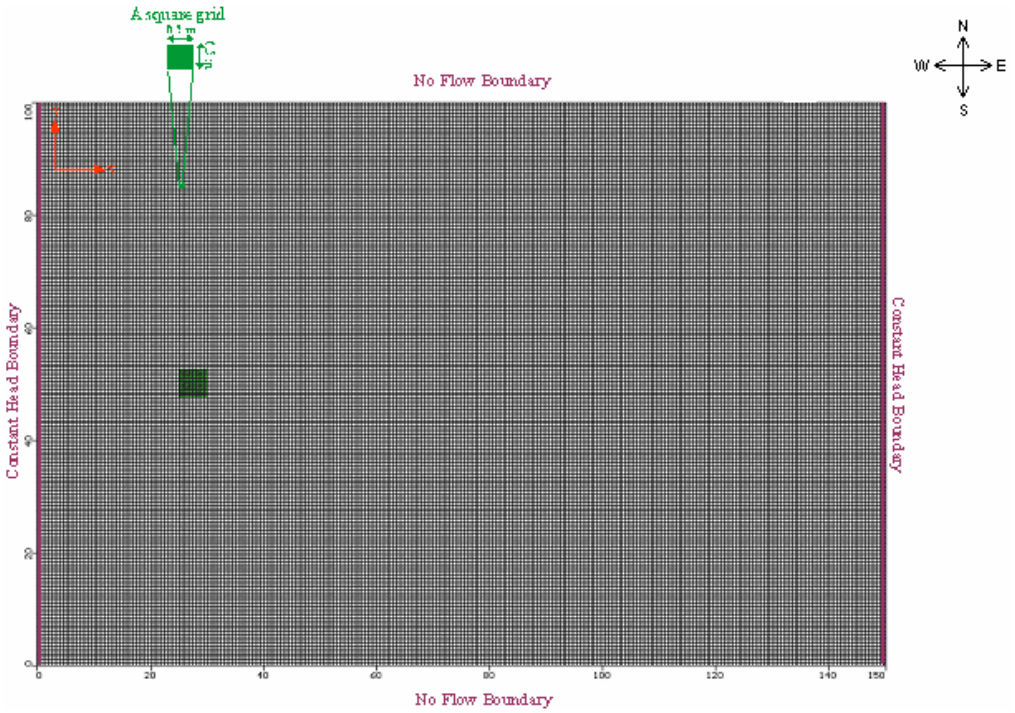

Figure 2.2. Model domain created in Visual MODFLOW

2.2.2.2. Input Data File Preparation

Following the creation of the model domain, the site specific properties for the groundwater flow simulations and contaminant specific properties for the contaminant transport simulations has to be determined. The site specific and contaminant specific parameters are obtained from the site of Cape Carnaveal Air Station, Florida (BIOCHLOR, 2000).

The groundwater flow in a subsurface system is determined by the velocity field and head distribution within the site. Flow boundary conditions are defined for the created model domain to generate a head distribution and subsequently a velocity field. The head gradient across the site was specified as 1.2×10^{-3} m/m. Then, the specified head boundaries are adjusted accordingly as indicated in Table 2.1.

Table 2.1. Flow boundary conditions of the model domain.

West	Constant Head Boundary; $H\big\vert_{0,y)} = H_0 = 5\,\mathrm{m}$ and $0 \le y \le 100\,m$
East	Constant Head Boundary; $H\big\vert_{(y,150)} = H_0 = 4.82\,\mathrm{m}$ and $0 \le y \le 100\,m$
North	no-flow boundary
South	no-flow boundary

Also, the aquifer specific properties have an effect on the groundwater flow regime in an aquifer system. The material properties of the aquifer system are shown in Table 2.2. Besides the aquifer properties and the boundary conditions, recharge has also an effect on the rate of the groundwater flow. The annual recharge rate is specified as 45 mm/year for the whole model domain.

Table 2.2. Flow boundary conditions of the model domain.

Aquifer Property	**Value**
Specific Storage (S_s)	1 x 10^{-7}
Total Porosity (ϕ)	0.3
Specific Yield (S_y)	0.2
Bulk Density (ρ_b)	1.6 g/cm^3
Longitudinal Dispersivity (σ_L)	12 m
Transverse Dispersivity (σ_T)	1.2 m

Besides the aquifer properties, the contaminant transport simulation requires some contaminant specific properties, possible degradation mechanism and source characterization. The input data for the contaminant transport simulation is entered to the RT3D transport package of Visual MODFLOW.

Within the transport submenu, for sorption of contaminant, linear isotherm (equilibrium-controlled) sorption was selected. Additionally, the model determining the degradation mechanism of the chlorinated solvents was selected as 'Aerobic/anaerobic model for PCE/TCE degradation'. The values and the units of contaminant specific properties and kinetic parameters used as input in RT3D package are shown in Table 2.3. Initial background concentrations of each chlorinated hydrocarbon species (PCE, TCE, DCE, VC and ETH) were taken as "0" within the model domain. The initial background concentration of the chloride was taken as '0.01 mg/l'. Since reductive dechlorination is the degradation of these chlorinated hydrocarbons in the anaerobic conditions, the aerobic degradation (λ_2), rates were set to "0". The program simulates the degradation of the contaminants in the aqueous phase, thus, the soil water partition coefficients (K_d) of the contaminants are also input to the program.

Table 2.3. Values of initial concentrations and degradation kinetic parameters.

Contaminant	**Initial Concentration (mg/L)**	**K_d (L/mg)**	**λ_1 (d^{-1})***	**λ_2 (d^{-1})***
PCE	0	0.784×10^{-6}	1.739×10^{-3}	-
TCE	0	0.239×10^{-6}	1.301×10^{-3}	0
DCE	0	0.23×10^{-6}	4.767×10^{-3}	0
VC	0	0.0545×10^{-6}	3.726×10^{-3}	0
ETH	0	0.556×10^{-6}	1.8×10^{-2}	0

* λ_1 is the first-order anaerobic degradation rate, T^{-1}, and λ_2 is the first-order aerobic degradation rates

Jut as the determination of flow boundary conditions for the groundwater flow simulations, the transport boundary conditions are also determined for the contaminant transport simulations. The transport boundary conditions of the model domain are shown in Table 2.4. In order to eliminate the effects of boundary concentrations on the contaminant transport, they are determined and assigned according to the initial background concentrations of the hydrocarbon species and chloride. Therefore, the concentrations of the chlorinated hydrocarbon species (PCE, TCE, DCE, VC and ETH) at the west boundary of the model domain were set to "0". Since the initial background concentration of chloride is 0.01 mg/l the boundary condition for chlorine is adjusted to that value for the simulation time. Visual MODFLOW uses default no flux boundary for the boundaries of the model domain if no concentration is assigned for the contaminants. Therefore, East, North and South boundaries of the model domain assigned as default no flux boundaries.

Table 2.4. Transport boundary conditions of the model domain.

West	Constant Concentration Boundary; $C\big\|_{(0,y)} = C_0$ and $C_0 = 0$ for PCE, TCE, DCE, VC , ETH and 0.01 mg/l for Cl^- $0 \le y \le 100\, m$
East	no flux
North	no flux
South	no flux

Assuming first-order biodegradation kinetics, transport and transformation of PCE, TCE, DCE, VC, ETH, and Cl can be simulated by solving the following set of partial differential equations given in equations 2.14 through 2.19. For most natural attenuation modeling applications, the first-order assumption can be considered as a reasonable approximation (Weidemeier et al., 1996)

RT3D uses the first order biodegradation kinetics for transport and transformation of chlorinated hydrocarbon species (PCE, TCE, DCE, VC and ETH). RT3D uses default yield coefficients in the solution of equations 2.14-2.19. YT/P, YD/T, YV/D, and YE/V are chlorinated compound yields under anaerobic reductive dechlorination conditions (their values are: 0.79, 0.74, 0.64 and 0.45, respectively); Y1C/P, Y1C/T, Y1C/D, and Y1C/V are yield values for chloride under anaerobic conditions (their values are: 0.21, 0.27, 0.37, and 0.57, respectively); and Y2C/T, Y2C/D, and Y2C/V are yield values for chloride under aerobic conditions (their values are: 0.81, 0.74, and 0.57, respectively).

The contaminant source also needs to be specified as contaminant boundary condition. The properties of the source such as dimensions, the duration and the concentration of the contaminants are presented in Table 2.5 and Figure 2.3. As it is indicated in the table below, the source is a two-step pulse source. In the second step, between days 200 and 220, the source concentrations of all of the hydrocarbon species are set to the one tenth of the source concentrations of the first step lasting 200 days.

After assigning all of the input parameters required for the groundwater flow and contaminant transport simulations, the outputs of the Turning Bands Random Field Generator are used to assign the hydraulic conductivity distribution for each of the generated fields. A total of nine random and a uniform hydraulic conductivity fields were used in Visual MODFLOW and RT3D. The total simulation time is set to 2000 days.

Table 2.5. Contaminant source characteristics

Size of the source	**Width** = 10 m
	Length = 10 m
Duration of contamination	0 – 200 days
Species concentration	**PCE** = 0.056 mg/L
	TCE = 15.8 mg/L
	DCE = 98.5 mg/L
	VC = 3.080 mg/L
Duration of contamination	200 – 220 days
Species concentration	**PCE** = 0.0056 mg/L
	TCE = 1.58 mg/L
	DCE = 9.85 mg/L
	VC = 0.3080 mg/L

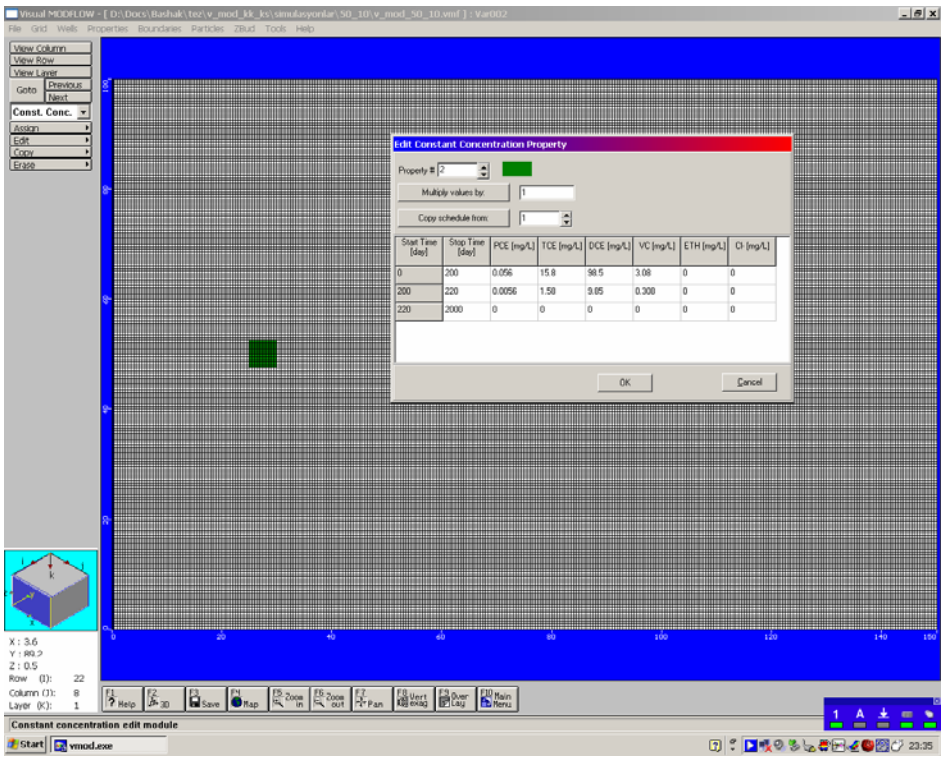

Figure 2.3. Location, duration and concentration of the contaminant source in the model domain.

2.2.2.3. Wells Submenu

At the end of the simulations, in order to monitor the contaminant concentrations, observation wells are located along the flow paths of each field within the flow domain taking into account the velocity field and the shape of contaminant plume.

2.2.2.4. Model Output

For modeling of groundwater flow and contaminant transport, the model was run at transient state for a period of 2000 days. The obtained model output includes the head, velocity and contaminant concentration distributions as a function of both time and space for one uniform and nine spatially correlated random hydraulic conductivity fields.

2.3. Calculation of Biodegradation

Using the output of the Visual MODFLOW simulations, the biodegradation rates of the contaminants are calculated. These biodegradation rate constants are required to accurately simulate the fate and transport of contaminants dissolved in ground water. Biodegradation of contaminants can usually be approximated using first-order kinetics; however, the apparent degradation rate must be normalized (corrected) for the effects of dilution, sorption, and volatilization. Two methods are applied for the determination of first-order rate constants. The first method involves the use of a normalized data set to compute the biodegradation rates (Wiedemeier *et al.,* 1996b). The second method was derived by Buscheck and Alcantar (1995) and applicable for steady-state plumes. These methods require contaminant concentrations measured at different locations within the contaminant plume along the flow path.

2.3.1. Conservative Tracer Method

In order to calculate biodegradation rates accurately, measured contaminant concentrations must be normalized for the effects of dispersion, dilution, and sorption. A convenient way to do this is to use compounds or elements associated with the contaminant plume that are relatively unaffected or predictably affected by biological processes occurring within the aquifer. These are called tracers. An ideal tracer would have air/water partitioning coefficient Henry's constant, K_H, and soil/water distribution coefficient, K_d [L^3/M] or organic carbon/water partition coefficient, K_{oc}, [L^3/M], identical to the contaminant of interest. For many chlorinated solvent plumes, the sum of ionic chloride and organic chloride associated with the solvents can be considered as a conservative tracer. Tracer experiments in ground water showed that chloride moved through most of the soils tested more conservatively (i.e., with less retardation and loss) than any of the other tracers tested (Kaufman and Orlob, 1956). Total chlorine can be calculated by multiplying the measured concentration of a chlorinated organic compound by the mass fraction of chloride in the molecule, then summing that quantity for all the chlorinated organic compounds represented in the plume (Wiedemeier *et al.,* 1998). The stoichiometry for chlorinated ethenes is presented in Table 2.6.

Table 2.6. Stoichiometry for chlorinated ethenes and produced chloride.

Contaminant	Stoichiometry	Chloride Produced (moles)	Mass ratio of Chloride (%)
PCE	$C_2Cl_4 \rightarrow C_2H_4 + 4Cl$	4	86
TCE	$C_2Cl_3H \rightarrow C_2H_4 + 3Cl$	3	81
DCE	$C_2Cl_2H_2 \rightarrow C_2H_4 + 2Cl$	2	73
VC	$C_2ClH_3 \rightarrow C_2H_4 + Cl$	1	57

The tracer is affected by adsorption, dilution and dispersion to the same degree as the contaminant of interest and is not affected by biological processes. The equation 2.31 uses these assumptions to solve for the expected down gradient contaminant concentration if biodegradation had been the only attenuation process operating between two points along the flow path. Then normalized (corrected) concentration of PCE, TCE, DCE and VC can be calculated as

$$C_{OWB,corr} = C_{OWB}\left(\frac{T_{OWA}}{T_{OWB}}\right) \quad (2.31)$$

where $C_{OWB,corr}$ is the corrected contaminant concentration at sampling location, observation well B, OWB down gradient; C_{OWA} is the measured contaminant concentration at sampling location, observation well A, OWA; T_{OWA} is the tracer concentration at sampling location OWA up gradient; and T_{OWB} is the tracer concentration at sampling location OWB.

The corrected concentration of a compound is the concentration that would be expected at one point (B) located down gradient from another point (A) if the process of dispersion and dilution had not been occurring between the points A and B. First-order degradation rate can be estimated between any two points (A and B) of a corrected data set (where point A is up gradient of point B) as:

$$C_{OWB,corr} = C_{OWA}e^{-\lambda t} \quad (2.32)$$

where $C_{OWB,corr}$ is the corrected contaminant concentration at sampling location OWB down gradient (M/L^3); C_{OWA} is the measured TCE concentration at up gradient sampling location OWA, (M/L^3); λ is the first

order biological decay rate (T^{-1}) ; and *t* is the time of contaminant travel between sampling locations (T);

Taking the natural logarithm of equation 2.32 yields,

$$\ln\left(C_{OWB,corr}\right) = -\lambda(t) + \ln C_{OWA} \qquad (2.33)$$

The travel time between the two sampling locations is related with the average linear velocity of the dissolved contaminant; however, it is affected by the sorption process in which dissolved contaminant partition from the ground water and adheres to the particles comprising the aquifer matrix. This process results in the slowing down of the contaminant relative to the average linear groundwater velocity and it is defined as:

$$v_c = \frac{v_x}{R} \qquad (2.34)$$

where v_c is the contaminant velocity, v_x is the groundwater flow velocity within the field and R is the contaminant specific retardation factor. Given the distance, x, between sampling points, the travel time, t, can be calculated as,

$$t = \frac{x}{v_C} \qquad (2.35)$$

The retardation factors of the chlorinated hydrocarbon species are given in Table 2.7 (BIOCHLOR,2000).

Table 2.7. The Retardation Factors of the contaminants.

	Contaminant				
	PCE	**TCE**	**DCE**	**VC**	**ETH**
Retardation Factor	7.1	2.9	2.8	1.4	5.03

Since there are more than two sampling locations, all the locations are considered in calculations. From a linear regression analysis involving the plot of $\ln(C_{corr})$ versus time, the first order reaction rate can be obtained.

The measured contaminant concentration at the first sampling location is used directly in the biodegradation rate computations since no affect of adsorption, dilution and dispersion relatively to the down gradient sampling locations.

2.3.2. Buscheck – Alcantar Method

Buscheck and Alcantar (1995) derive a relationship that allows calculation of first order decay rate constants for steady-state plumes and it is based on the one-dimensional steady-state analytical solution to the advection, dispersion, sorption and decay equation presented by Bear (1979). It is appropriate for plumes where contaminant concentrations are in dynamic equilibrium, meaning that the contaminant plume has reached a steady-state condition.

A plume is said to be at steady state when the plume is no longer migrating downgradient and that contaminant concentrations are not changing significantly through time. The first order equation for the concentration as a function of distance (Kemblowski et al., 1987) is given as

$$C(x) = C_0 \exp\left[-k \frac{x}{v_x} \right] \qquad (2.36)$$

where k is the first-order mass attenuation rate constant [T^{-1}].

Buscheck and Alcantar method involves coupling the regression of contaminant concentration (plotted on a logarithmic scale) versus downgradient distance (plotted on a linear scale) to an analytical solution for one dimensional, steady-state, contaminant transport that includes advection, dispersion, sorption, and biodegradation. The general one-dimensional

transport equation, with first order decay of the contaminant can be expressed as:

$$\frac{\partial C}{\partial t} = \frac{1}{R}\left[\mathrm{D_x} \frac{\partial^2 C}{\partial x^2} - v_x \frac{\partial C}{\partial x} \right] - \lambda \mathrm{C} \qquad (2.37)$$

where D_x, (L^2/T) is the dispersion coefficient, v_x (L/T) is the linear groundwater velocity, R (-) is the retardation coefficient, and $\lambda(T^{-1})$ is the biodegradation rate coefficient. Equation 2.37 assumes that D_x is constant and independent of distance, x. The mass transport by dispersion and advection are described by the terms in brackets, respectively and the retardation coefficient represents the contribution of sorption in the transport of contaminants.

Both advection and dispersion are related with the longitudinal dispersivity, α_x (L), a parameter that is the characteristic of the porous medium through the contaminant migrates and it represents the spreading of the contaminant over a given length of flow, is described by the empirical equation (Fetter, 1993) as:

$$\mathrm{D_x} = \alpha_x v_x \qquad (2.38)$$

The steady state solution of the equation 2.37 for concentration is given (Bear, 1979) as:

$$C(x) = C_0 \exp\left[\frac{x}{2\alpha_x} \left[1 - \left(1 + \frac{4\lambda\alpha_x}{v_c} \right)^{\frac{1}{2}} \right] \right] \qquad (2.39)$$

As the Buscheck and Alcantar Method indicate the exponential regression of the concentration versus distance gives the reciprocal of the attenuation

distance, λ/v_x, in equation 2.36 and the solution of one-dimensional steady-state transport equation gives the slope m $= \frac{k}{v_x}$ of the log linear data as:

$$m = \frac{k}{v_x} = \left(\frac{1}{2\alpha_x}\right)\left[1-\left(1+\frac{4\lambda\alpha_x}{v_x}\right)^{\frac{1}{2}}\right] \quad (2.40)$$

Both equations 2.36 and 2.40 describe the slope of the log linear data and they can be equated to solve for the decay rate. Then for a steady-state plume, the first-order decay rate is given (Buscheck and Alcantar, 1995) as:

$$\lambda = \frac{v_C}{4\alpha_x}\left(\left[1+2\alpha_x m\right]^2 - 1\right) \quad (2.41)$$

$$\lambda = \frac{v_C}{4\alpha_x}\left(\left[1+2\alpha_x\left(\frac{k}{v_x}\right)\right]^2 - 1\right) \quad (2.42)$$

where λ is the first-order biodegradation rate constant (T^{-1}), v_c is the retarded contaminant velocity in the x-direction ($L.T^{-1}$), v_x is the groundwater velocity, α_x dispersivity (L), and k/v_x is the slope of line formed by making a log-linear plot of contaminant concentration versus downgradient distance along flow path.

CHAPTER 3

RESULTS AND DISCUSSION

A numerical modeling study was conducted for the determination of fate and transport of the chlorinated solvent plumes for different fields having different heterogeneity levels. In the first part of the study, the fields having different spatially correlated hydraulic conductivity distributions are generated. In the second part, the groundwater flow system and contaminant transport modeling simulations are carried out to investigate the variations in the chemical plume migration and degradation rates of the contaminants. The differences in the plume development, and the fate and transport of the chlorinated solvent plumes with the changing hydraulic conductivity distributions are discussed in the following sections.

3.1. Random Hydraulic Conductivity Field

Using the Turning Bands Random Field Generator, two-dimensional fields having spatially correlated random hydraulic conductivity distributions are generated. Under field conditions, K field has rarely uniform distribution, mostly it shows a spatial random variation. Therefore, hydraulic conductivity distributions showing a large spatial variation will be a realistic approximation to the real field situations.

Randomly distributed nine different hydraulic conductivity fields were generated having the same mean conductivity but different coefficient of

variations and correlation length (h) values, representing different realizations of K field.

3.1.1. Validation of generated random fields

The turning bands random field generator uses Monte Carlo Simulation technique to calculate the random distributions called “base distributions” and this process is carried out many times to create multiple “base distribution”. These normally distributed “base distributions” are then transformed by using the equations 2.1. and 2.2. to log normal distributions of hydraulic conductivity. To make sure that these generated hydraulic conductivity fields preserve the statistical properties that are prescribed at the beginning of the generation process, the generated fields must be validated prior to using them in the groundwater flow and transport simulations. The mean and variance and the spatial correlation length of the generated fields should be close to the specified theoretical values.

The generator gives mean and variance of the base distributions for multiple realizations of Monte Carlo Simulation technique. Therefore, it is expected that the mean and variance of these distributions should be close the 0 and 1, respectively. The generator also estimates the covariance function of the generated hydraulic conductivity distribution. As another way of validation, this estimated covariance function is compared with the theoretical covariance function calculated by equation 2.8. It is required that both functions should be close to each other. An example for the graphical representation of this validation of spatial estimates of mean, variance and covariance for the isotropic field having CV = % 50 and h = 5 m is illustrated in Figure 3.1. Similar plots for the other isotropic K fields are presented in Appendix B. It is seen from these figures that as the correlation length increase from 5 to 20 m, the mean and variance values slightly differ from zero and one, respectively. Although the deviations from the expected values

of mean and variance increase with the increase in correlation length, the fields illustrate the statistical properties of pre-specified fields. Also the figures of calculated and estimated covariance functions of all fields are fit closely, meaning that the correlation structure of the generated fields mimics the theoretically specified spatial correlation structure.

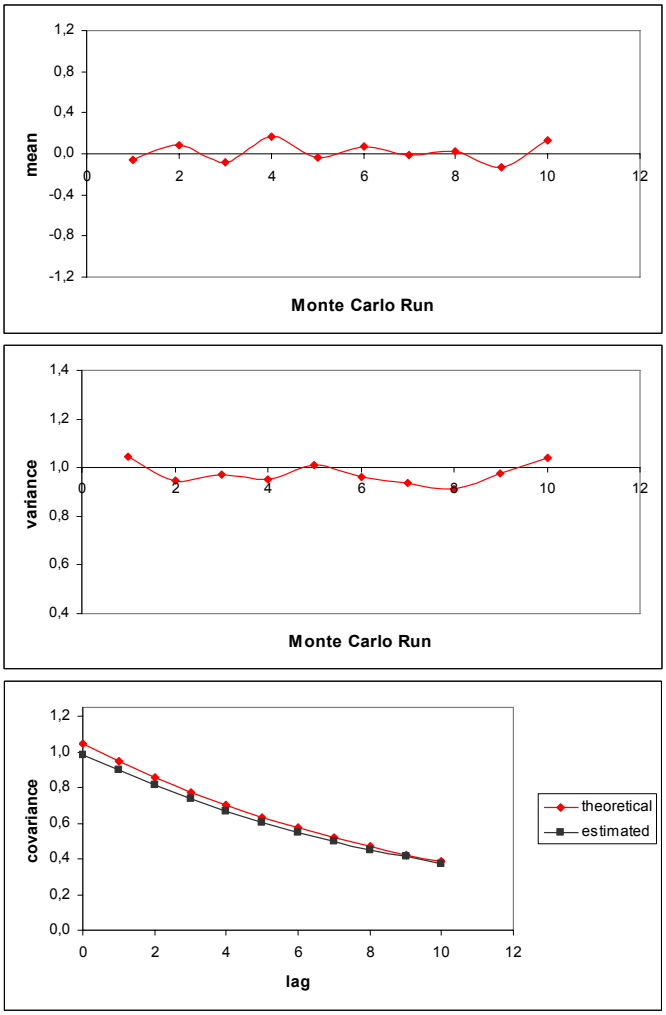

Figure 3.1. Mean and variance and covariance estimate for the 10 realizations of the isotropic K field having CV=%50 and h=5 m.

The same validation is carried out for the anisotropic hydraulic conductivity fields. The graphical representation of this validation of spatial estimates of mean, variance and covariance for the anisotropic field having CV = % 50, h_x = 10 m and h_y = 2 m and for the field CV = % 150, h_x = 20 m and h_y = 4 m is

illustrated in Figure 3.2 and 3.3, respectively. Close proximity of the calculated statistics to theoretical values show that the statistical properties and the spatial correlation structure of simulated anisotropic K field mimicked the theoretical fields reasonably well.

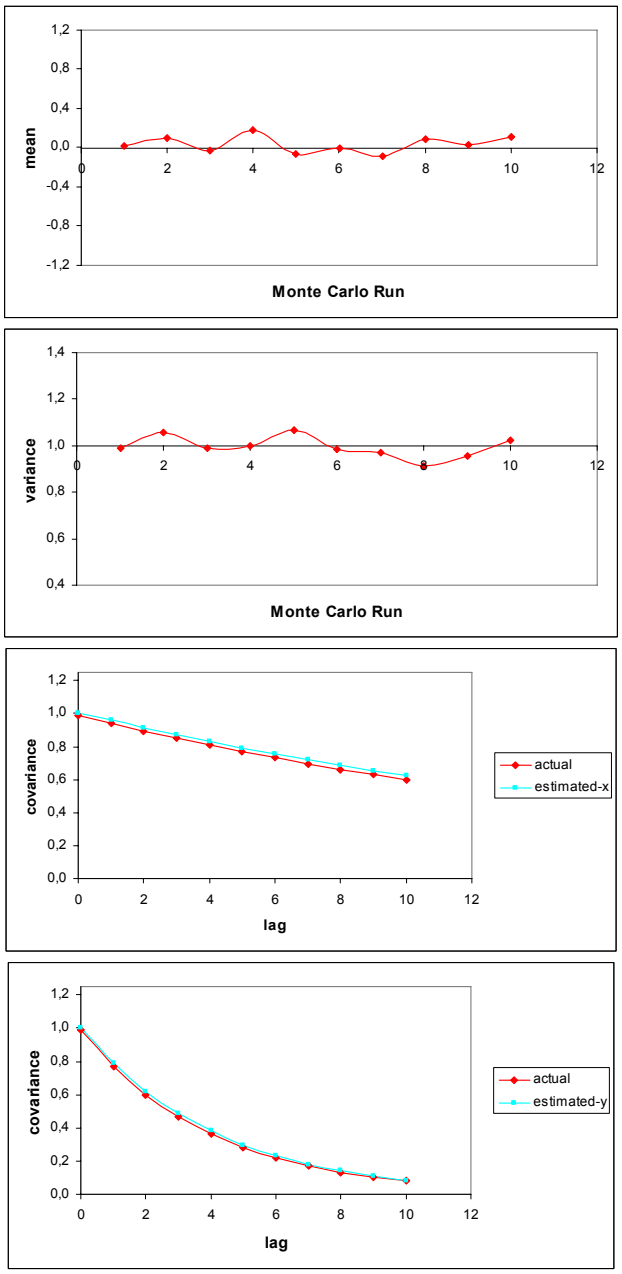

Figure 3.2. Mean and variance and covariance estimate for the 10 realizations of the anisotropic K field having CV=%50, hx= 10 m and hy= 2 m

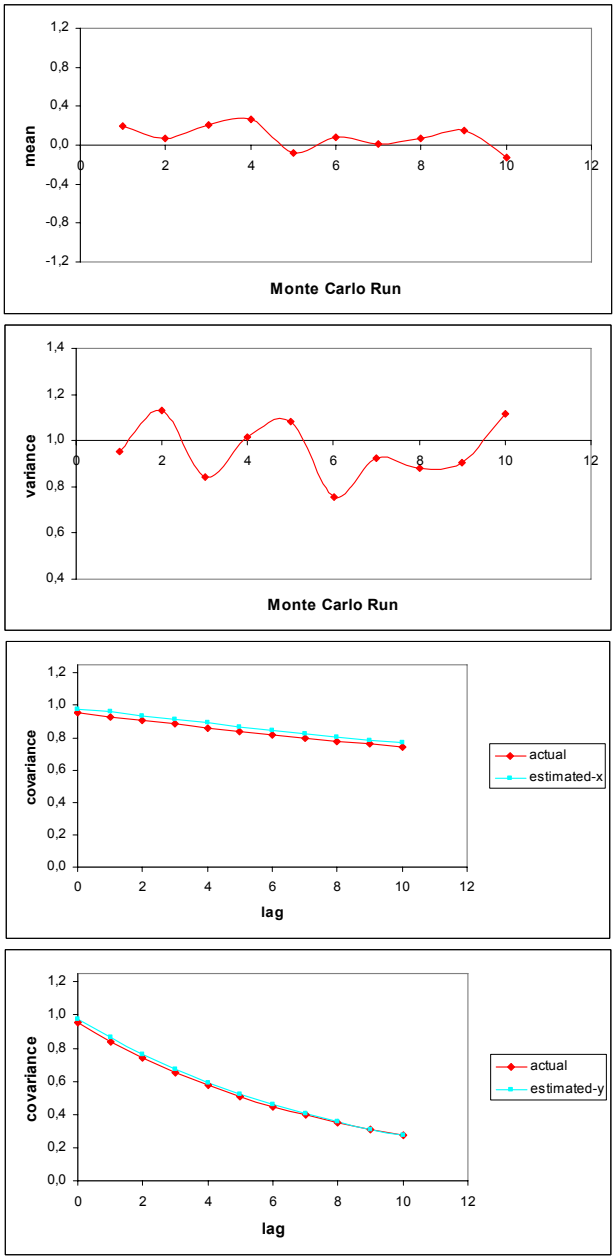

Figure 3.3. Mean and variance and covariance estimate for the 10 realizations of the anisotropic K field having CV=% 150, hx=20m and hy=4m

3.1.2. Isotropic hydraulic conductivity fields

The generated isotropic hydraulic conductivity fields and the histograms of the hydraulic conductivity data are illustrated in figures 3.4, 3.5 and 3.6.

From the figures it is seen that for a given CV value, the contrast in high and low conductivity zones occurs in longer distances as the h increases. The areas of the high and low conductivity zones are smaller and spread all over the entire flow field when the correlation length is 5 m. However, as h increases these areas of low and high conductivity fields get longer. For the field having CV = % 50 and h = 5 m, from the figure and the hydraulic conductivity data the highest conductivity is determined to be 0.0011 m/sec and the histogram tells that the number of the cells that has this conductivity value is around 2300 out of total cell number of 45000. The cells having the highest hydraulic conductivity can be observed across the entire flow field in smaller areas. The same can be said for the low conductivity zones. For the field having CV = % 50 and h = 20 m, the highest conductivity is 0.0009 m/sec and the number of cells having this value is around 1500. However, these conductivity values are more densely occurring at the southwest of the flow field. Same is also true for the low conductivity values that are also more closely occurring in larger areas of the flow field. The same effect is also observed for the other CV when correlation length is changing.

For a given correlation length value, the location of the areal distributions of the high and low conductivity zones are the same. However, the conductivity contrast becomes much more evident as CV increases. The highest conductivity value within each field increases as CV increases. Also increasing CV results decrease in the lowest hydraulic conductivity value. The histograms of the hydraulic conductivity data also support the forgoing result, that the number of the cells having these high and low conductivity zones increases as the CV of the generated field increases. The number of cells that have the hydraulic conductivity value of 0.0001 m/sec is around 1000 for CV = % 50, 3800 for CV = % 100 and 9000 for CV = % 150 when h = 20 m.

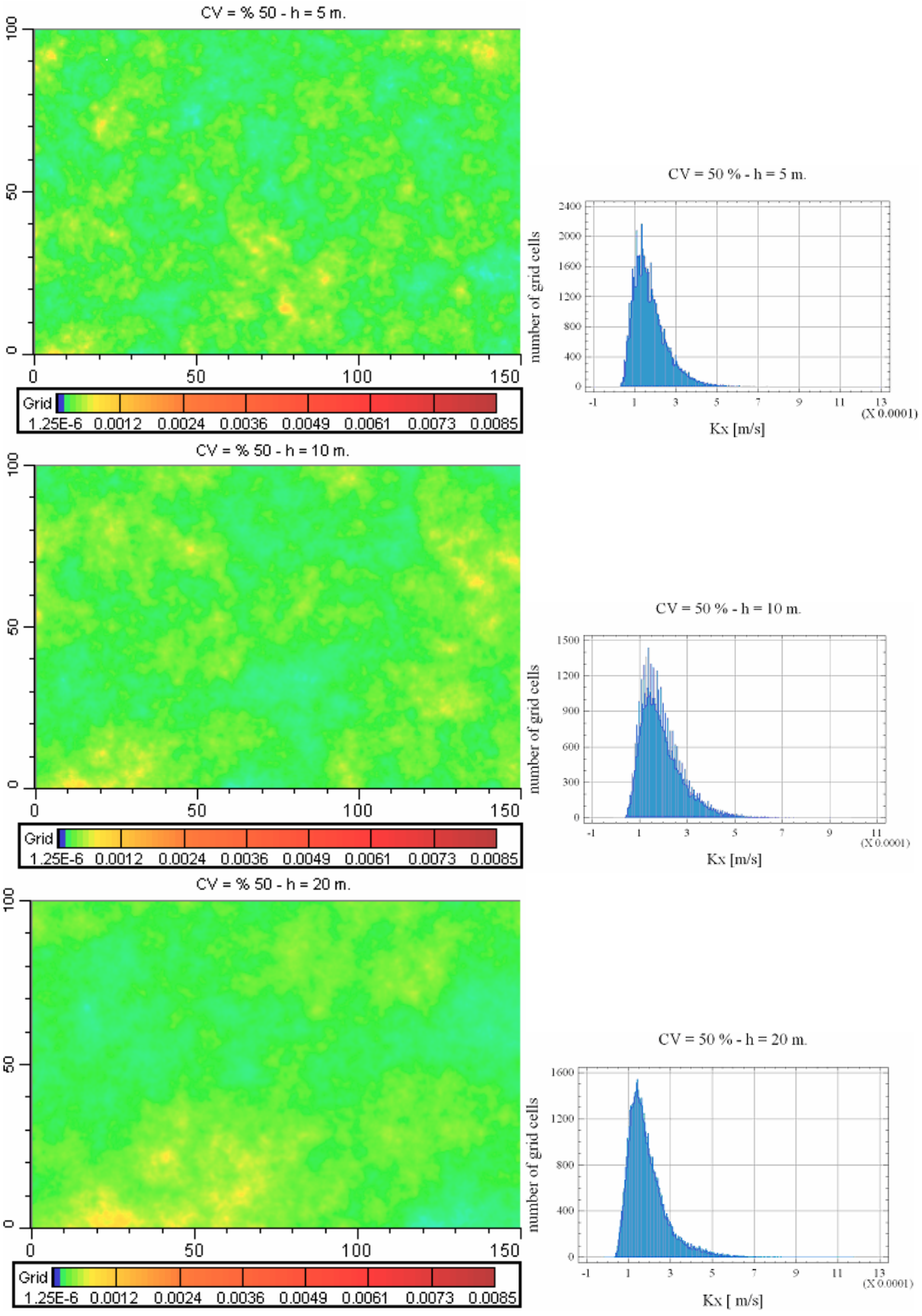

Figure 3.4. The Hydraulic Conductivity distribution for the isotropic field with CV = 50% and h = 5, 10 and 20 m.

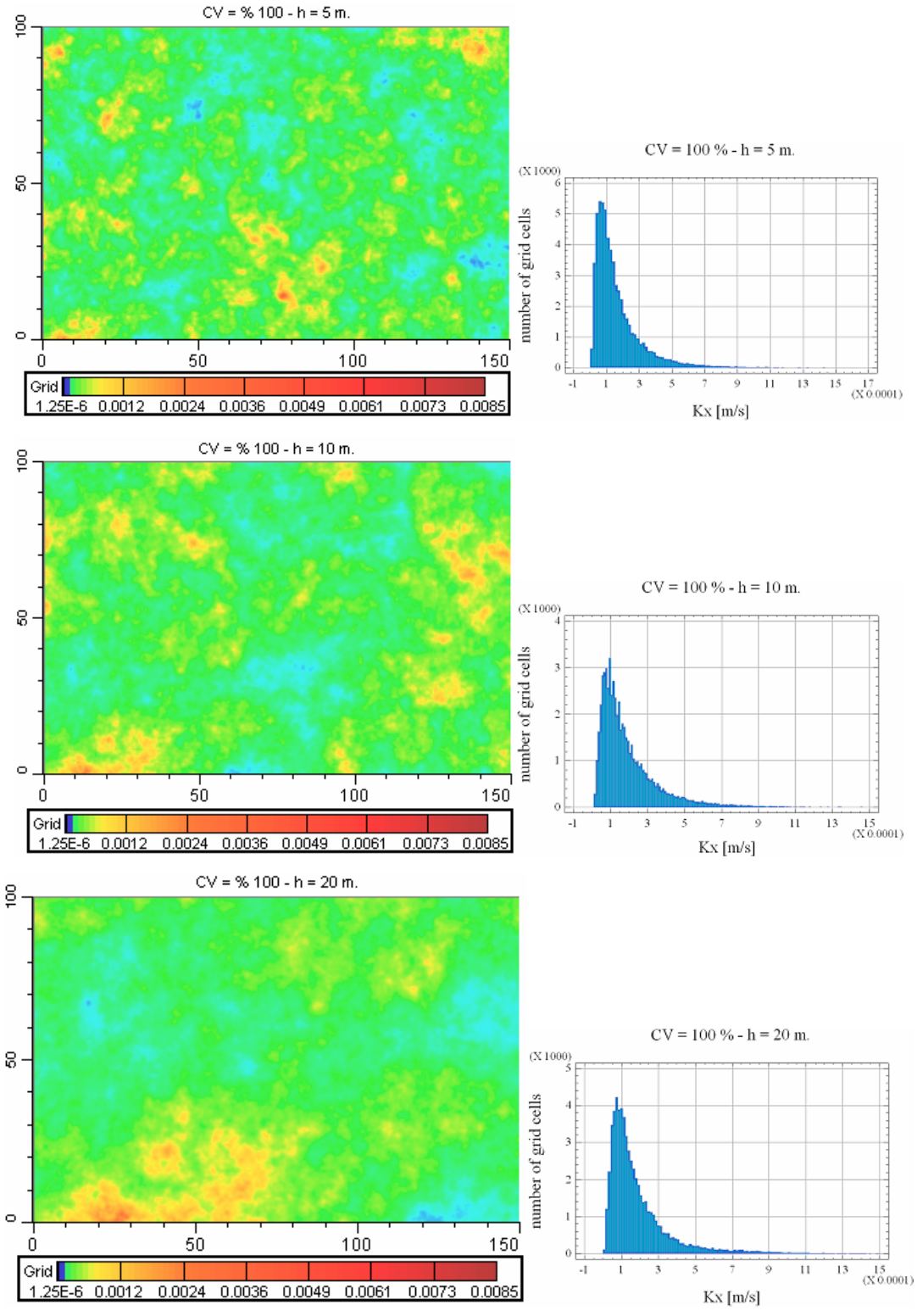

Figure 3.5. The Hydraulic Conductivity distribution for the isotropic field with CV = % 100 and h = 5, 10 and 20 m.

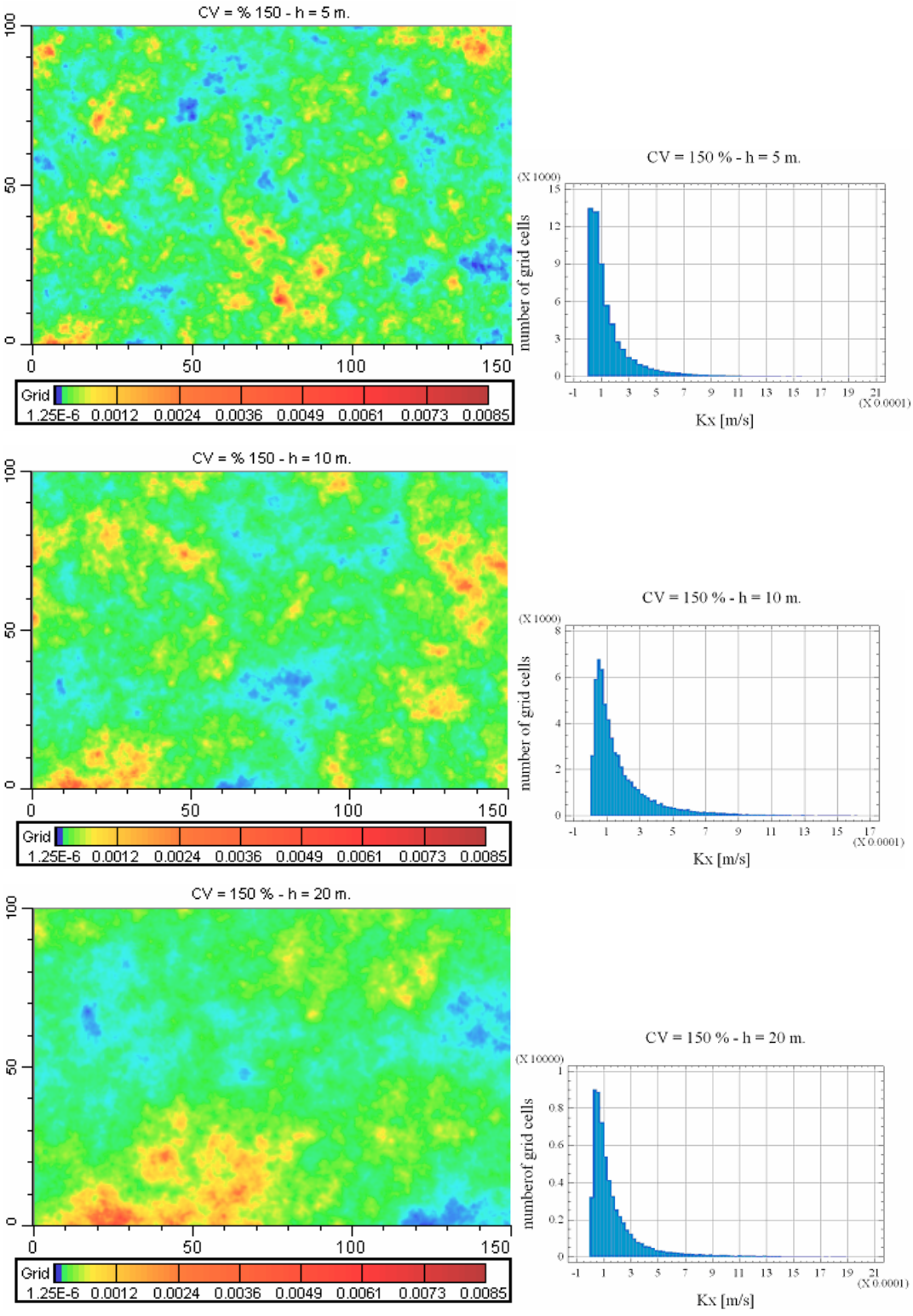

Figure 3.6. The Hydraulic Conductivity distribution for the isotropic field with CV = % 150 and h = 5, 10 and 20 m.

3.1.3. Anisotropic hydraulic conductivity fields

The anisotropic random fields generated having CV = % 50 and CV = % 150 are shown in figure 3.7. It is seen from the figures that the areas of high and low conductivity zones are more elongated in the x-(flow) direction in the anisotropic fields and are narrower in the transverse y- direction. Also, the distribution of the low and high conductivity zones is more random at various locations across the field, covering smaller areas compared to the corresponding isotropic fields.

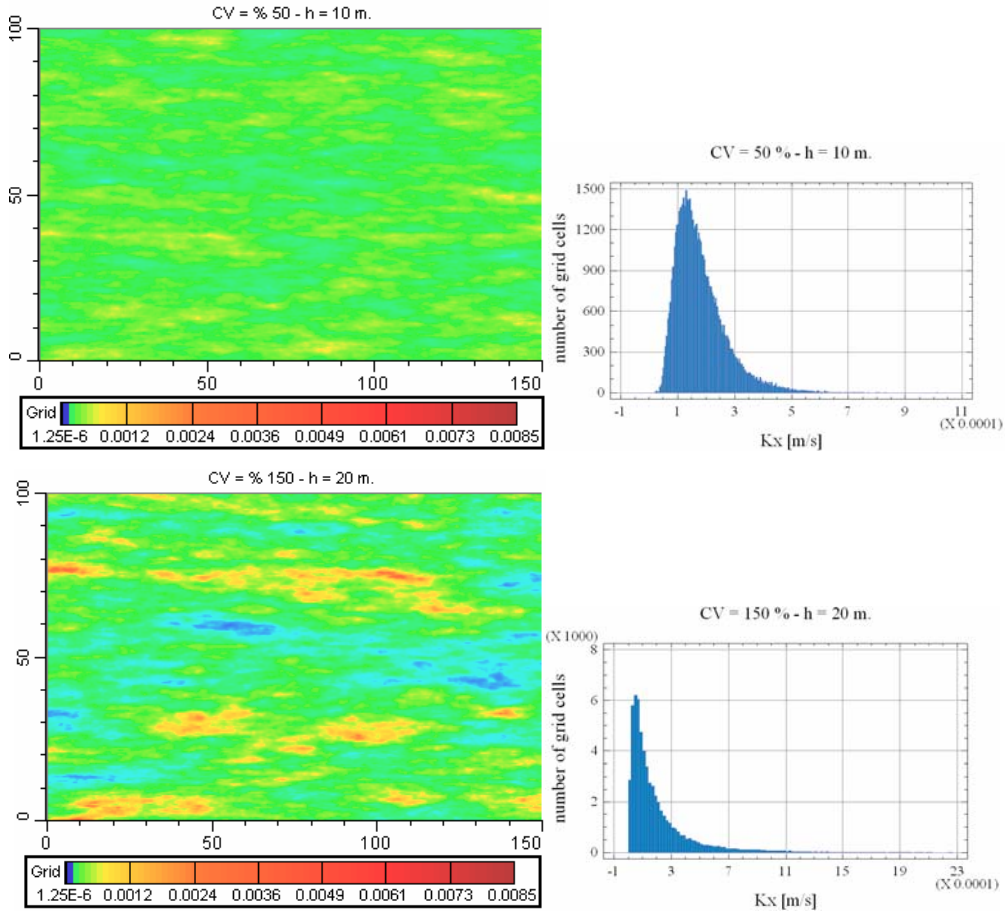

Figure 3.7. Hydraulic Conductivity distribution for the anisotropic fields with CV = % 50 and hx = 10 m, hy = 2 m and CV = % 150 and hx = 20 m, hy = 4 m.

3.2. Simulation of Flow Fields and Chlorinated Compound Plumes

Visual MODFLOW and RT3D are used for two-dimensional groundwater flow and contaminant transport simulations. Simulations are carried out for the generated uniform flow field and the isotropic and anisotropic random fields. Uniform flow field simulations for various contaminated species are considered to form a base case for the purpose comparison with heterogeneous fields and in turn to demonstrate the affect of different levels of heterogeneity on the plume behavior. MODFLOW simulates and gives the head distribution and groundwater velocity distributions within the model domain. Figure 3.8 shows the steady state head distribution for the uniform flow field.

As stated earlier due to imposed BCs, a 1-D flow field is generated from west to east boundary of the model domain. The groundwater head at the west and east boundary are 5 m and 4.82 m, respectively. Uniform field has a uniform distribution of hydraulic conductivity meaning that the same value is assigned to each cell across the model domain as 1.8×10^{-3} m/sec, which is the man value for random K fields. Hydraulic conductivity distribution affects the groundwater flow regime in an aquifer system; therefore, the head distributions are controlled by the hydraulic conductivity distributions. From Figure 3.8 it is seen that the head distribution is also uniform across the model domain, just as the uniform hydraulic conductivity distribution. There is a constant head decline with distance along the x-direction. The velocity field across the model domain is also uniform and constant at each cell as 1.08×10^{-6} m/sec.

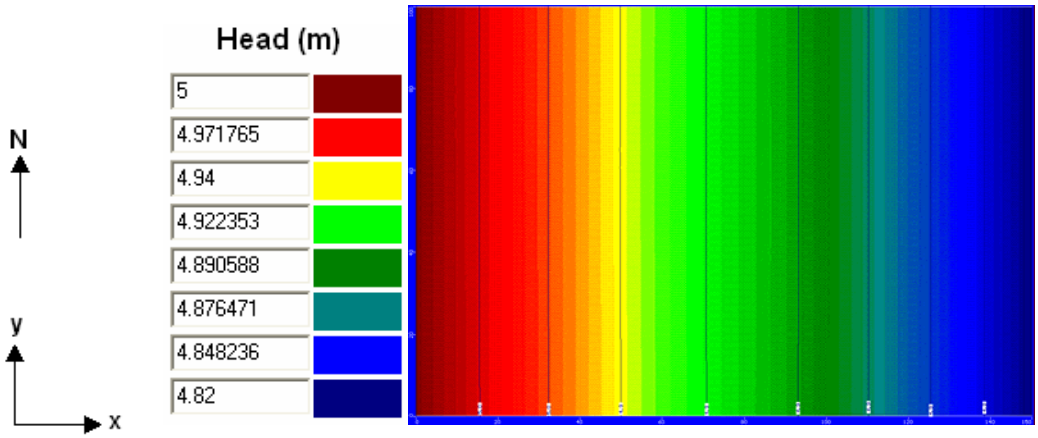

Figure 3.8. Steady state head distribution for the uniform field

The steady state head distributions of the generated isotropic and anisotropic random hydraulic conductivity fields are given in Appendix C. These figures also support that the change in the hydraulic conductivity distribution also changes the head distribution. High hydraulic conductivity values create high groundwater velocities; therefore, at the zones where the higher hydraulic conductivities are dense, the water flows faster and slows down when it comes to a zone of low hydraulic conductivity. This causes the accumulation of the water behind the low conductivity zone and generating larger areas having higher and the same head distribution. In the figures this phenomenon can be observed as larger areas having the same colors. The spacing between the contour lines is high within the zones of high hydraulic conductivity and less within the areas of low hydraulic conductivity for a unit decline in the head contours. Since water will prefer to flow through the high conductivity zones, the different zones of high and low hydraulic conductivity causes water to flow in different directions and velocities. Eventually, this behavior causes the bending of the head contours along west to east direction. This bending of the head contours and thus the change in the direction of the velocity vectors become obvious with the increase in the CV and h. The field having the highest and the lowest hydraulic conductivity value is the one having CV = % 150 and h =20 m, it is obvious form the head

distribution in this fields that the most irregular shape of the head contours are observed within this field. The highest and the lowest velocities are also observed within this field.

The simulations of chlorinated solvent transport for the uniform, isotropic and anisotropic fields are performed by the sub program RT3D of Visual MODFLOW to investigate the lateral and transverse extend of contaminant plume. The simulations are performed for nine generated random fields and the uniform field. The model domain, input parameters of flow and transport are all the same except the hydraulic conductivity distributions. As stated earlier, all the fields had the same mean hydraulic conductivity but different CV and correlation lengths. Figure 3.9 shows the VC plume of 100th and 1250th days for the uniform field.

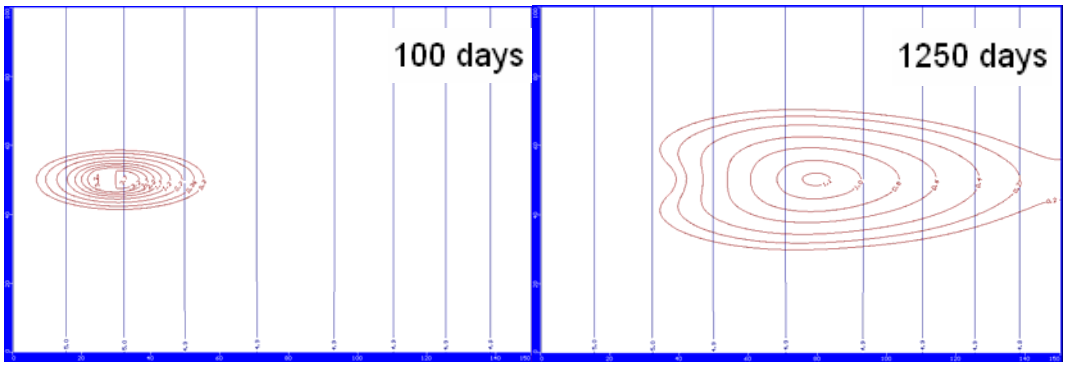

Figure 3.9. VC plumes at 100th and 1250th days for the uniform field

The maximum VC concentration is 3.7 mg/l at the center of mass of the plume at the 100th day and 1.1. mg/l at the 1250th day of the simulation. The minimum VC concentrations are shown as the outer concentration contour as 0.2 mg/l for both of the plumes. The figures indicate that the plume has a regular shape. Since the head distribution and the velocity fields are also uniform depending, the center of mass of the plume and the plume front is not distorted form the direction of groundwater flow. As seen from the figures,

the locations of the center of mass of the plumes are controlled by the advective flow velocity, *v,* while the spreading of the contaminant mass, σ, along the longitudinal and transverse directions are controlled by the respective directional dispersivities, σ_L and σ_T. Equation 2.38 also shows that the mechanical dispersion is directly proportional to the groundwater velocity and it is the mechanical dispersion that results in the mixing and spreading of the plume both in the groundwater flow direction (longitudinal) and in the transverse direction. The plume is said to have an ellipsoidal shape.

3.2.1. Isotropic hydraulic conductivity fields

The steady state head distribution and the shape of the VC plume at the 100^{th} and 1250^{th} days for fields having CV = % 50, 100 and 150 and correlation lengths 5, 10 and 20 m are illustrated in Figures 3.10 - 3.12. Minimum VC concentration contour at the plume front is 0.2 mg/l in all of the figures. Figure 3.10 shows that the shapes of the plumes are irregular and distorted when compared with the shape of the plume in the uniform hydraulic conductivity field due to the fact that the velocity fields spatially variable depending on the non uniform hydraulic conductivity distributions. The size of the plume in the transverse direction is large in the field when the correlation length is 5 m. On the other hand, the size in the x-direction is less with a center of mass that is almost at the same location as it is in the uniform field showing that the directional velocity change caused more spreading in the y-direction while it is less in the x-direction. In the field having the correlation length as 10 m, the plume is narrower; however, it is much more elongated in the x-direction showing that the groundwater velocity in the x direction is high.

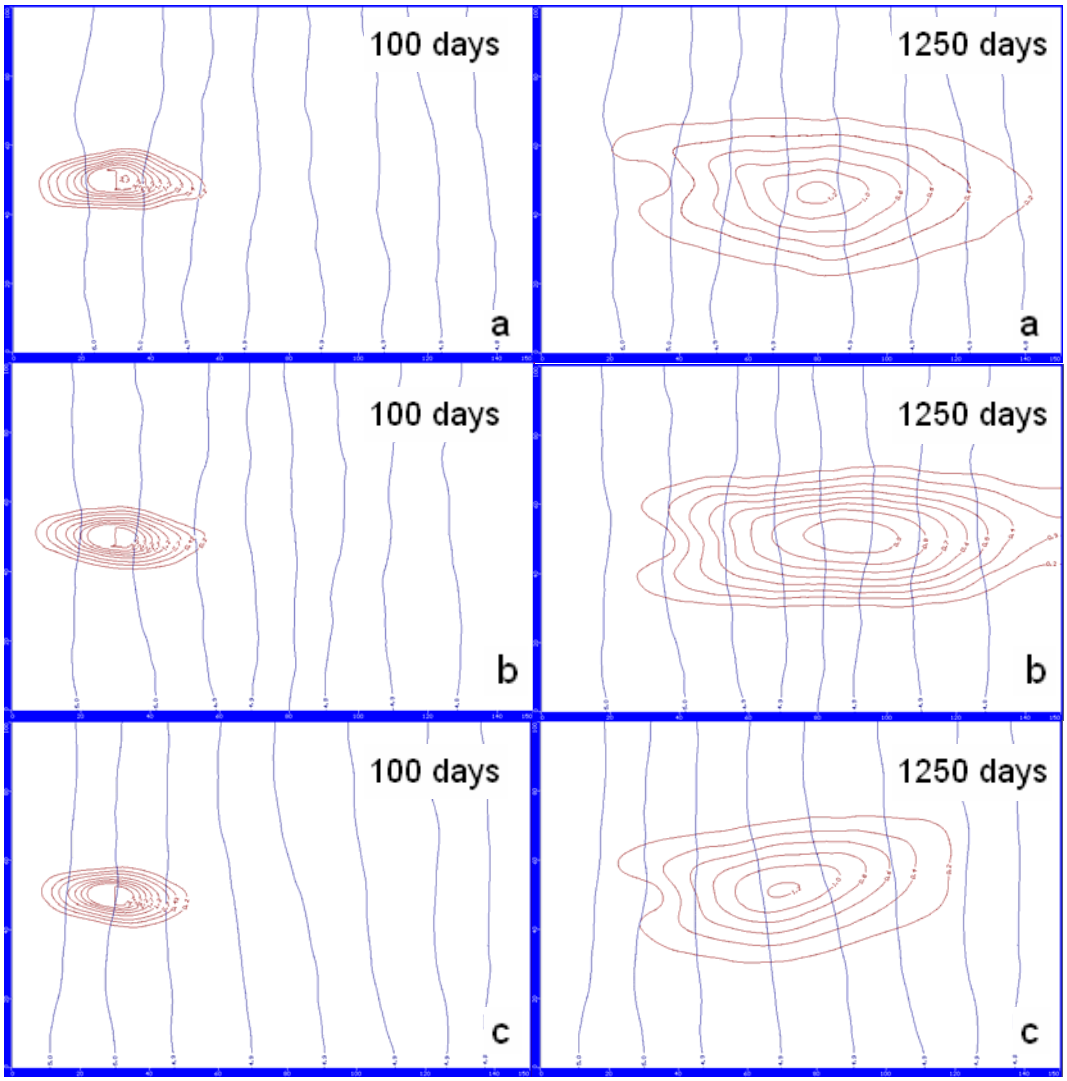

Figure 3.10. VC plumes at 100th and 1250th days for (a) h= 5 m, (b) h= 10 m, (c) h= 20 m when CV = 50 %

The plume formed in the field with correlation length of 20 m is smaller especially in the x-direction. Also the direction of the plume front shows that the change in the direction of groundwater flow is high. The maximum concentrations at the center of mass of the plumes also support that the mass loss or the transport of the contaminant by dispersive and advective processes is less in the field having correlation length 5 m and is high in the field having correlation length 10 m., however, it is less for the field having correlation length 20 m.

The shapes of the plumes become more irregular and distorted and the concentration contours become much more irregular when CV is increased to % 100. Figure 3.11 shows that the size of the plume with correlation length of 5 m is almost the same when compared with the plume of uniform field. When the correlation length is 10 m, the size of the plume in the x-direction is bigger, although it is small in the y-direction. When CV = % 100, the smallest plume is formed in the field with correlation length of 20 m. But the change in the direction of the plume pathway is much more obvious than the plume formed in the field having CV = % 50 m and correlation length 20 m. The locations of the center of mass of the three plumes show that the average groundwater velocity is less than the uniform field and the field having CV = % 50. The maximum VC concentrations at the center of mass of the plumes are more or less the same with the field with CV = % 50. However, it is obvious that the most mass loss or spreading of the plume is again occurred for the field having correlation length 10 m.

Figure 3.12 depicts that like the fields having CV % 50 and 100, in the field with CV= % 150 the biggest plume formed in the field with correlation length of 10 mi but its size is narrower in y-dire and shorter in the x- direction. The smallest plume is also formed in the field with correlation length 20 m and also there is a directional change in the plume pathway. However, an enlargement in the size of the plume in the y-direction is observed. This may be due to the fact that the directional velocity changes and the occurrence of larger low conductivity zones in the x-direction along the flow path of the plume with increase in h. Unlike the plumes in the fields having different CV's, the plume in the field having correlation length 10 m has an obvious change in the direction of the plume path way; this shows that there is a high conductivity zone and since the groundwater prefers to flow through that zone the plume is spread and transported.

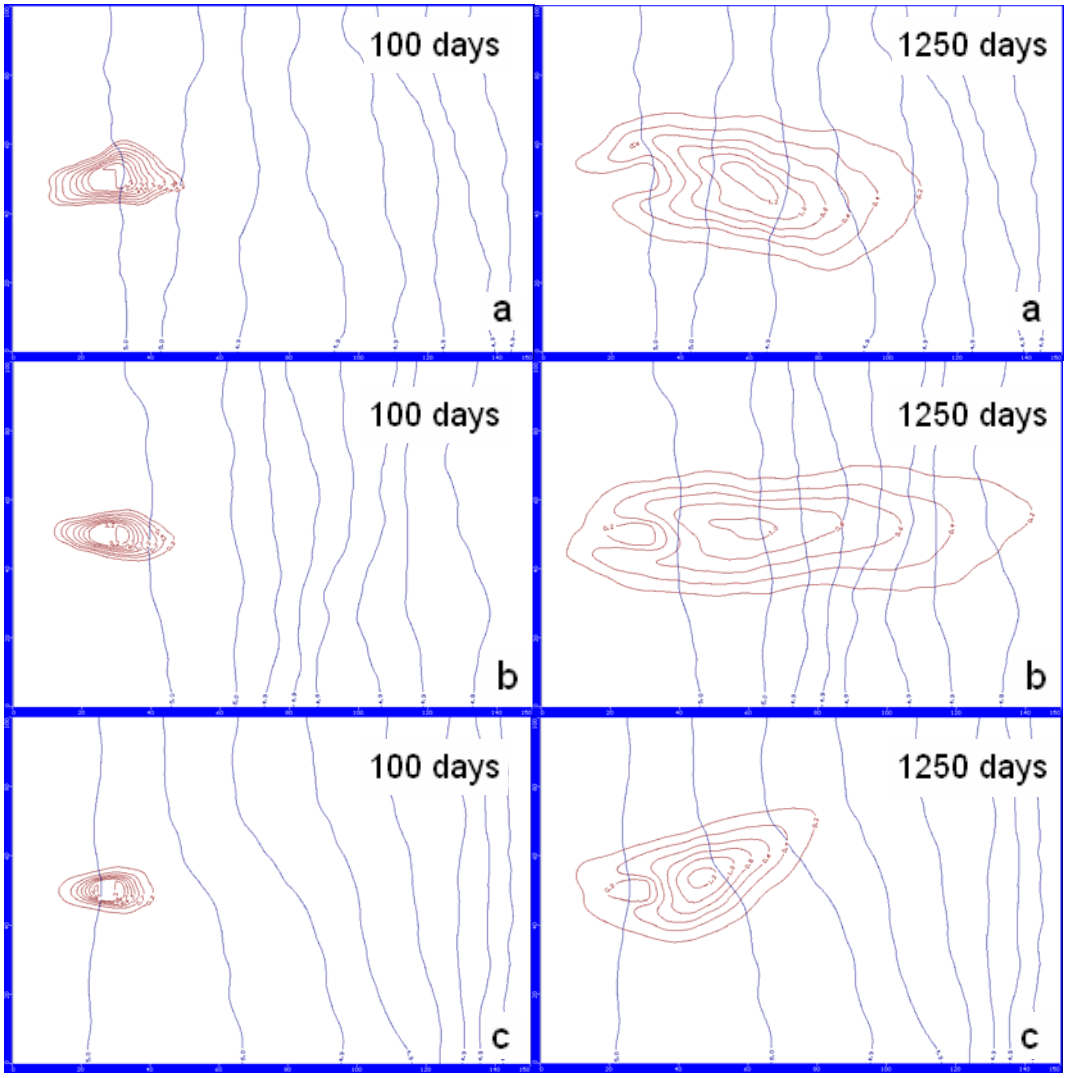

Figure 3.11. VC plumes at 100th and 1250th days for (a) h= 5 m, (b) h= 10 m, (c) h= 20 m when CV = 100 %

Figure 3.12 shows that the size of the high and low conductivity zones become larger and conductivity contrast become steeper at various locations of the model as CV and h of the field increases. This results in the high variations in the direction and magnitude of the groundwater flow. The water tends to flow through a high conductivity zone and changes its direction through that way when it comes to a low conductivity zone. If the difference in the high and low conductivity zones becomes higher, than the change in the

direction of the plume pathway is much more obvious due to the high directional velocities. The center of mass of the three plumes for the field with CV % 150 shows that the average groundwater velocities are less than the fields having CV % 50 and 100. The steady state head distribution and the shape of the PCE, TCE, DCE and ETH plumes at the 100th and 1250th days for fields having CV = % 50, 100 and 150 and correlation lengths 5, 10 and 20 m are given in Appendix C in Figures C.1 – C.3.

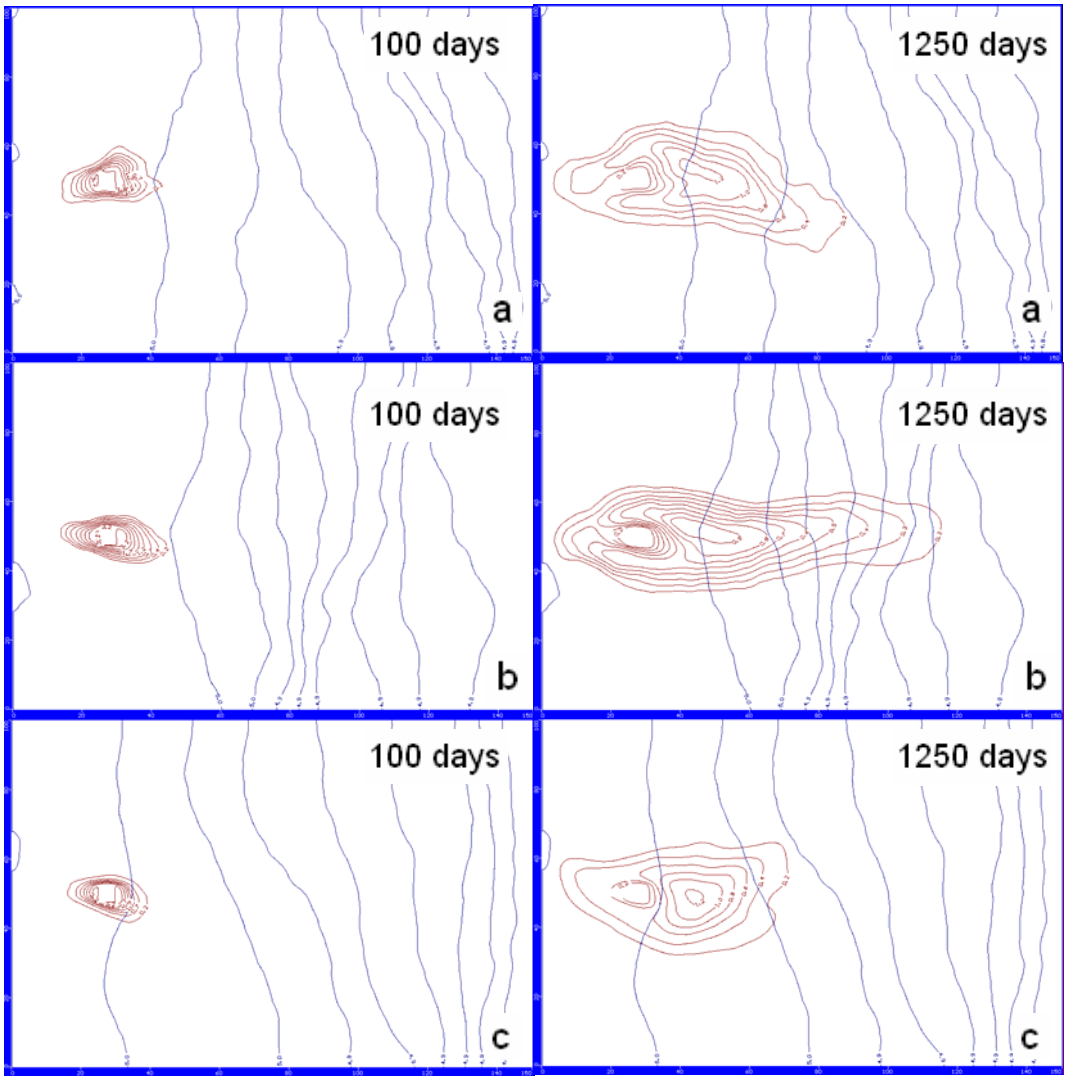

Figure 3.12. VC plumes at 100th and 1250th days for (a) h= 5 m, (b) h= 10 m, (c) h= 20 m when CV = 150 %

All three figures of VC and the other chlorinated solvent plumes at the generated fields having different CV's and correlation lengths show that the shapes of the plumes becomes more irregular and distorted as CV of the generated field increases. Regardless of the correlation length, the locations of the center of mass of the plumes show that the increase in CV results in the slowing down of the plume. The displacement of the center of mass of the plumes in the x-direction becomes less when CV increases indicating that the average groundwater velocities decrease with the increasing CV. This is due to the fact that the non uniform hydraulic conductivity fields generate non uniform velocity fields. Since the conductivity contrast between the zones of high and low conductivity increases as CV increases regardless of the correlation length, the groundwater velocity contrast also increases. Although the main direction of the groundwater flow is in the x-direction, the high and low conductivity zones results in the divergence in the direction of flow and results in the smaller displacement in the x-direction. The increasing irregularity and the distortion of the plumes with increasing CV also depend on the high and low velocity fields generated within the model domains. These high and low velocity fields generated by the high and low conductivity zones cause the plume to be trapped in the low conductivity zones and to flow through high conductivity zones. Another affect of the CV is in the sizes of the plumes; that is the sizes of the plumes become smaller in both longitudinal and transverse directions as CV increases which implies that there is shrinkage of the plume in the areal extent with increasing CV. As mentioned before, the mixing and spreading of the plume depends on the mechanical dispersion, which is also directly proportional to the directional dispersivity and the groundwater velocity. Thus, the shrinkage of the plume as CV increases can be explained with the decreasing mechanical dispersion with decreasing velocity.

As mentioned earlier, for a given CV value, correlation length affects the areal extent and the frequency of the distribution of high and low conductivity zones. As correlation length increases the high and low conductivity zones repeat themselves in longer distances. It is clear from the figures that the shapes of the plumes depend on these distributions. Since the areas of the high and low conductivity zones are smaller and spread all over the entire flow field when the correlation length is 5 m, the plume is also spread both in longitudinal and transverse directions in the same extend. However, as correlation length increases these areas of low and high conductivity fields gets larger. The plume developed the fields having correlation length 10 m, has spread more in the x-direction since there are relatively larger conductivity zones along the flow path of the plume. Hence, the plume is trapped less by low conductivity zones and spreading is less in the transverse direction. The plume shape is affected by the high conductivity zones formed within the fields having correlation length 20 m. The higher conductivity values that are collected at specific locations of the model area create change in the direction of groundwater flow hence the velocity field and the in the transport of the contaminant plume. The dispersion of the contaminant through the high conductivity zone located at the southwest of the fields is observed best for the field with CV = % 150 and correlation length 20 m and the VC plume front is directed towards another high conductivity zone northern east of the field since water tends to flow through high conductivity zone. The low conductivity zones located in the middle of the model domain along x-direction decreases the transport of the plume along the x-direction in Figure 3.12.

Figures 3.13., 3.14. and figures 3.15., 3.16 are showing the change in the location of peak concentration and plume front for the VC plume with time as a function of CV and h. Figure 3.13. also supports the idea that the average groundwater velocity in the x-direction decreases with the increasing CV, as the displacement of the center of mass of the plume in x-direction decreases

with increasing CV. However, Figure 3.16 reveals that the fields having correlation length 10 m. has the highest velocity in the x-direction, in other words the displacement of the center of mass of the plume is the highest among the three correlation lengths. This may be due to the fact that the relatively high conductivity zone present along the main groundwater flow, x-, direction. This affect is also obvious in figure 3.17. that the location of the plume front is more distant for the field having correlation length 10 m. The spreading of the plume along the x-direction decreases as CV increases.

The graphs of peak concentration distribution of VC plume with distance for different correlation length and CV values are shown in figures 3.17 and 3.18, respectively. The figures show that the change in the peak concentrations does not change gradually with CV or correlation length. Although the peak concentration show variations for different CV and correlation length values, they are very close to each other, almost same. However, it is observed once more with these graphs that the displacement of the center of mass of the plumes changes gradually with changing CV while changing slightly with changing correlation length.

The graphs of the change in the location of peak concentration and plume front of the PCE, TCE, DCE and ETH plumes with time and the graphs of peak concentration distribution of PCE, TCE, DCE and ETH plumes with distance are given in Appendix C in Figures C.22 – C.43.

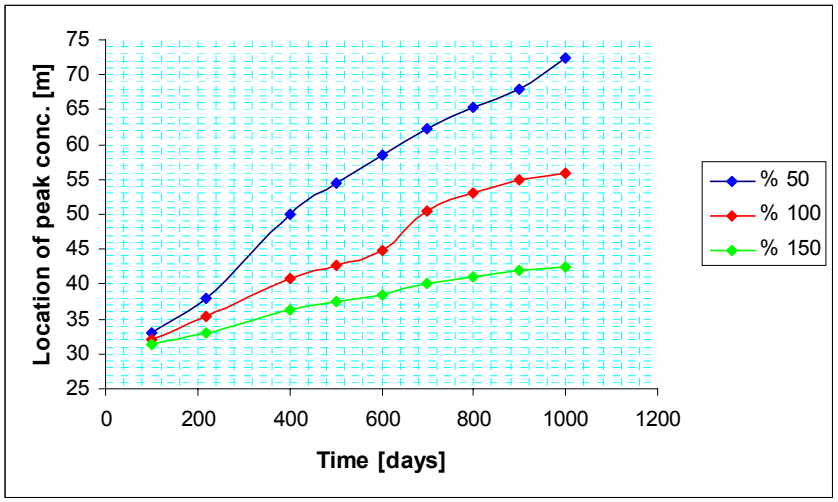

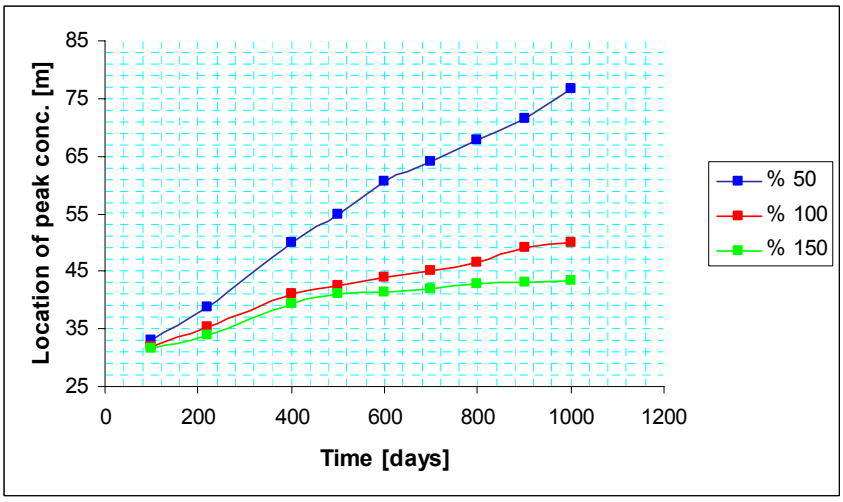

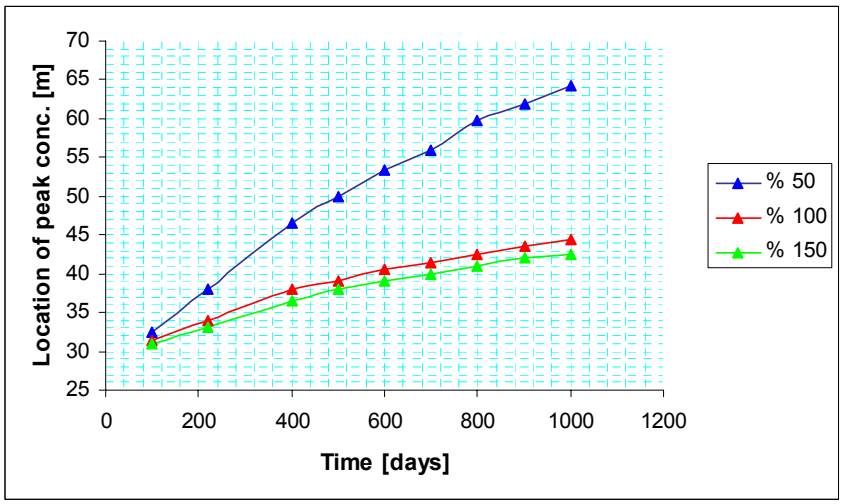

Figure 3.13. Location of peak concentration of VC plume with time for (a) h = 5 m, (b) h = 10 m, (c) h = 20 m.

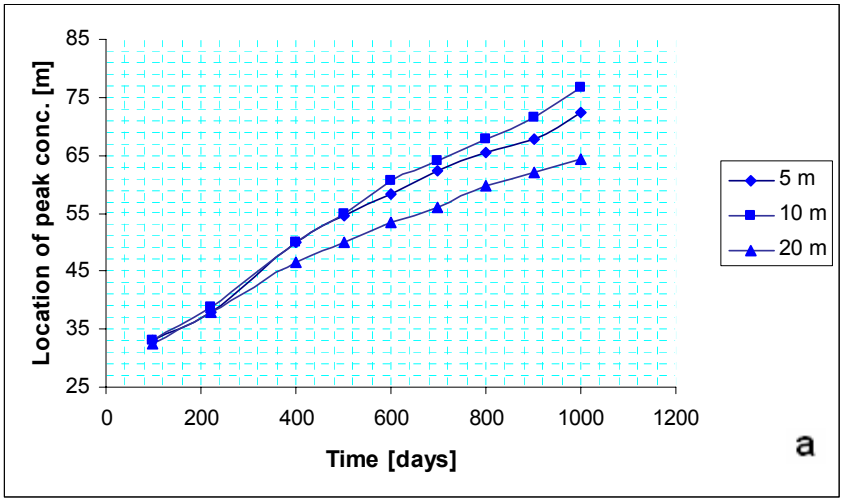

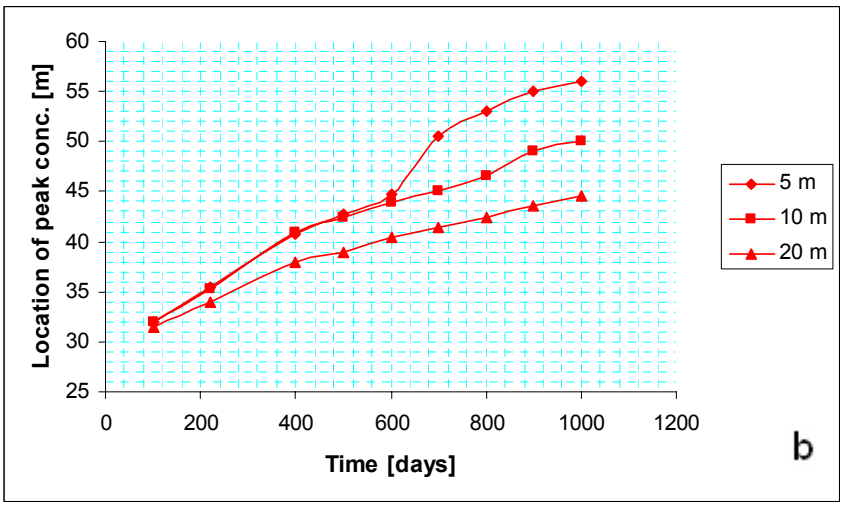

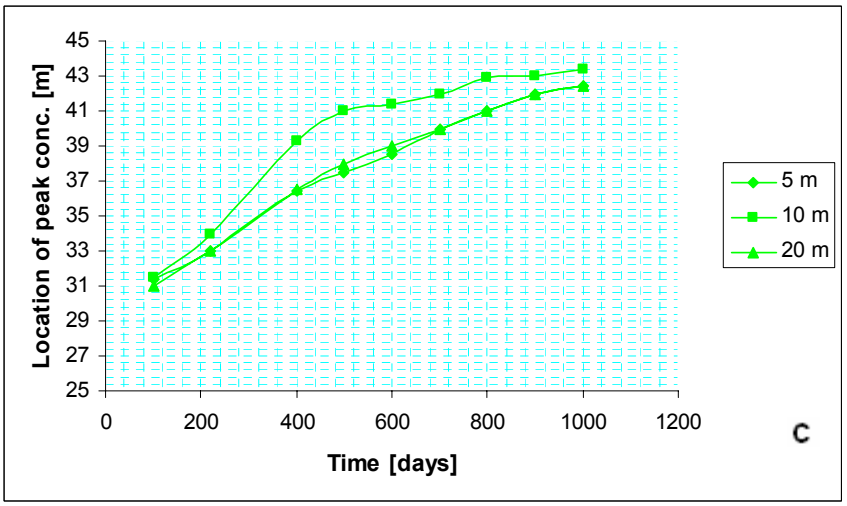

Figure 3.14. Location of peak concentration of VC plume with time for (a) CV = % 50, (b) CV = % 100, (c) CV = % 150

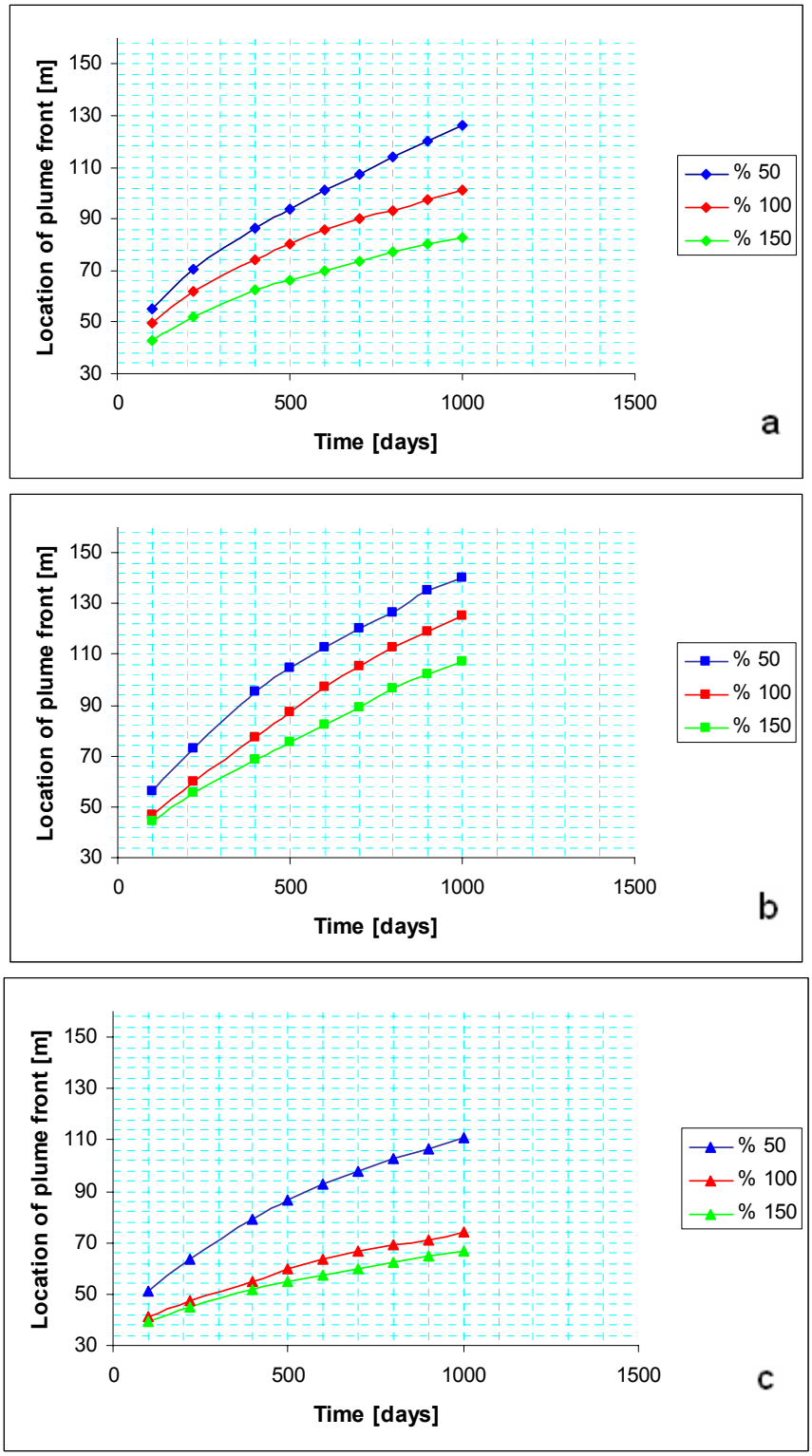

Figure 3.15. Location of VC plume front with time for (a) h = 5 m, (b) h = 10 m, (c) h = 20 m.

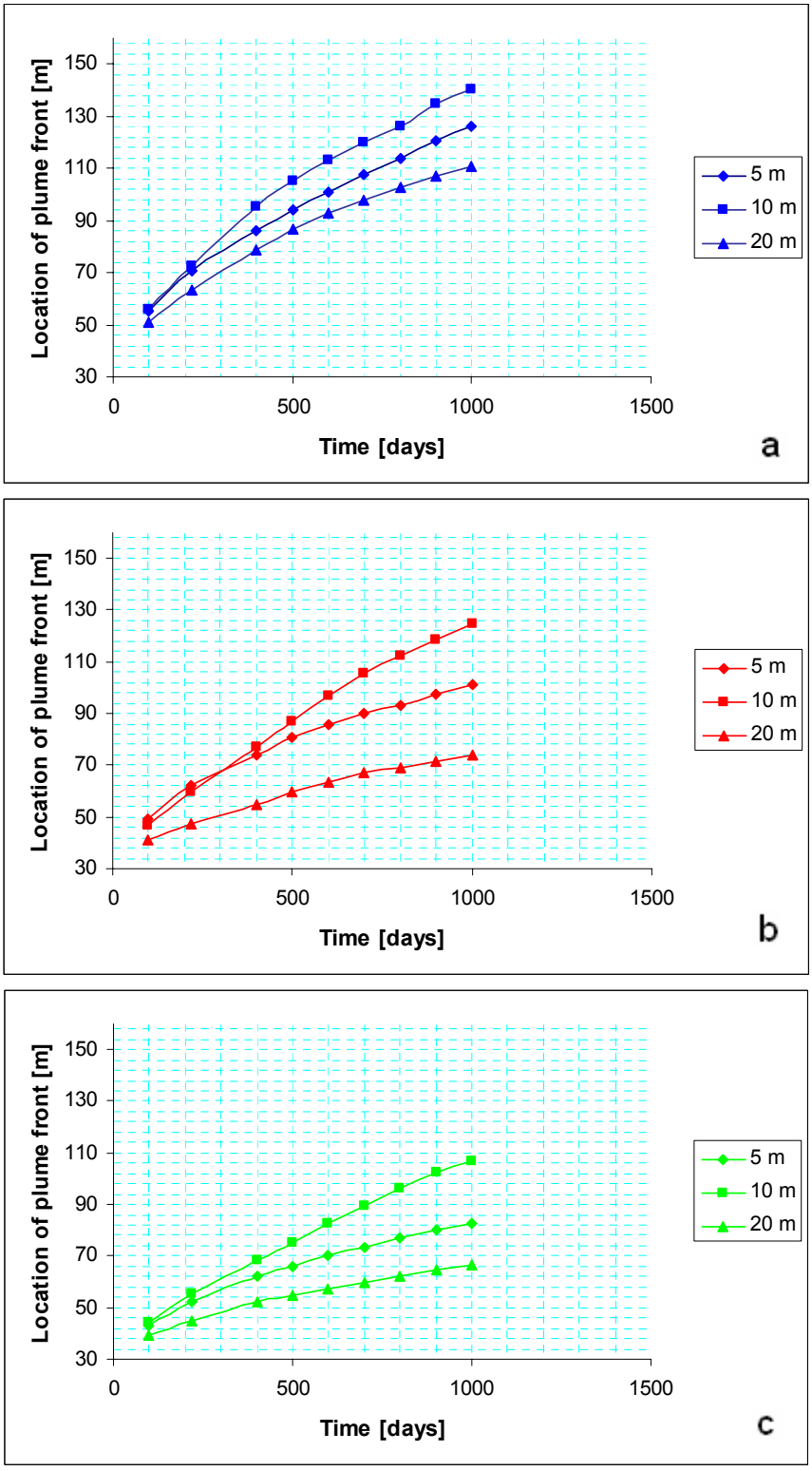

Figure 3.16. Location of VC plume front with time for (a) CV = % 50, (b) CV = % 100, (c) CV = % 150

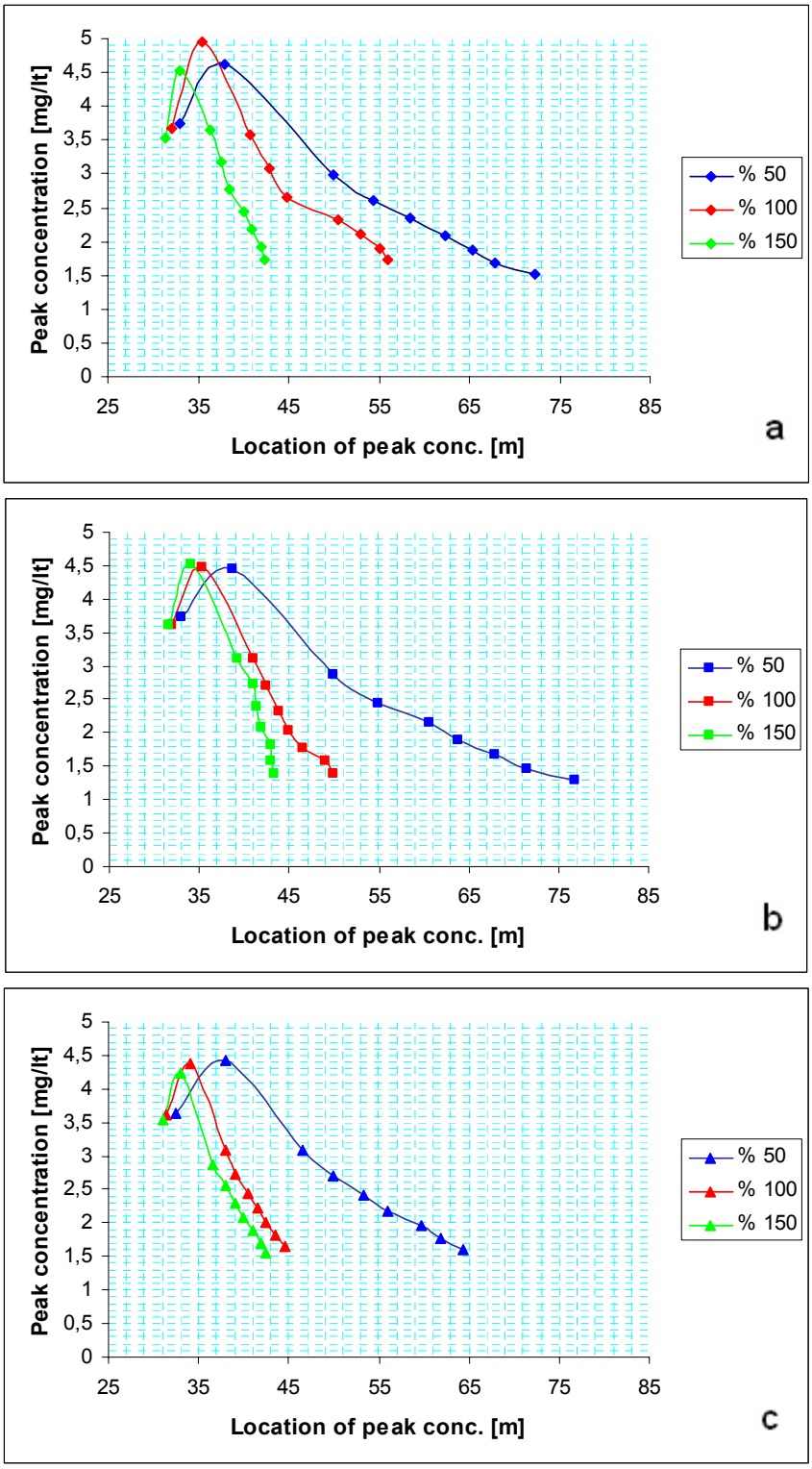

Figure 3.17. Peak concentration distribution of VC plume with distance for (a) h = 5 m, (b) h = 10 m, (c) h = 20 m

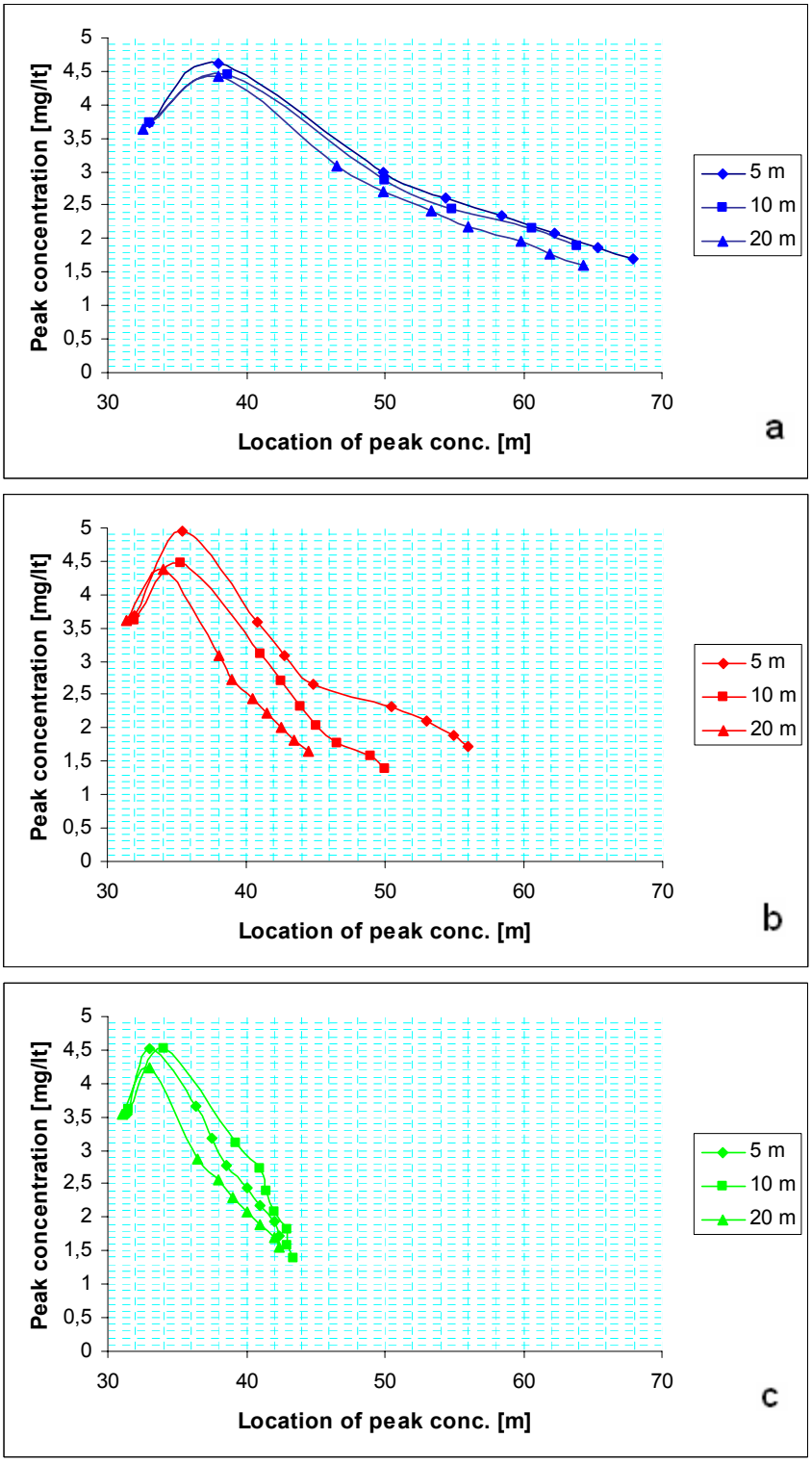

Figure 3.18. Peak concentration distribution of VC plume with distance for (a) CV = % 50, (b) CV = % 100, (c) CV = % 150

3.2.2. Anisotropic hydraulic conductivity fields

Figure 3.19. shows the steady state head distribution and the shape of the VC plume at the 100th and 1250th days for the isotropic field and anisotropic field when CV = % 50 . The irregular shape and the transport in the groundwater flow direction of the plume does not change too much, however, the spreading of the plume increased in the transverse direction. Since the randomness in the conductivity values in smaller distance in y-direction, the high and low conductivity zones are observed through out the model field and more in the y-direction when compared with the isotropic field. Therefore these high conductivity zones resulted in the mixing and spreading of the plume more in the transverse direction.

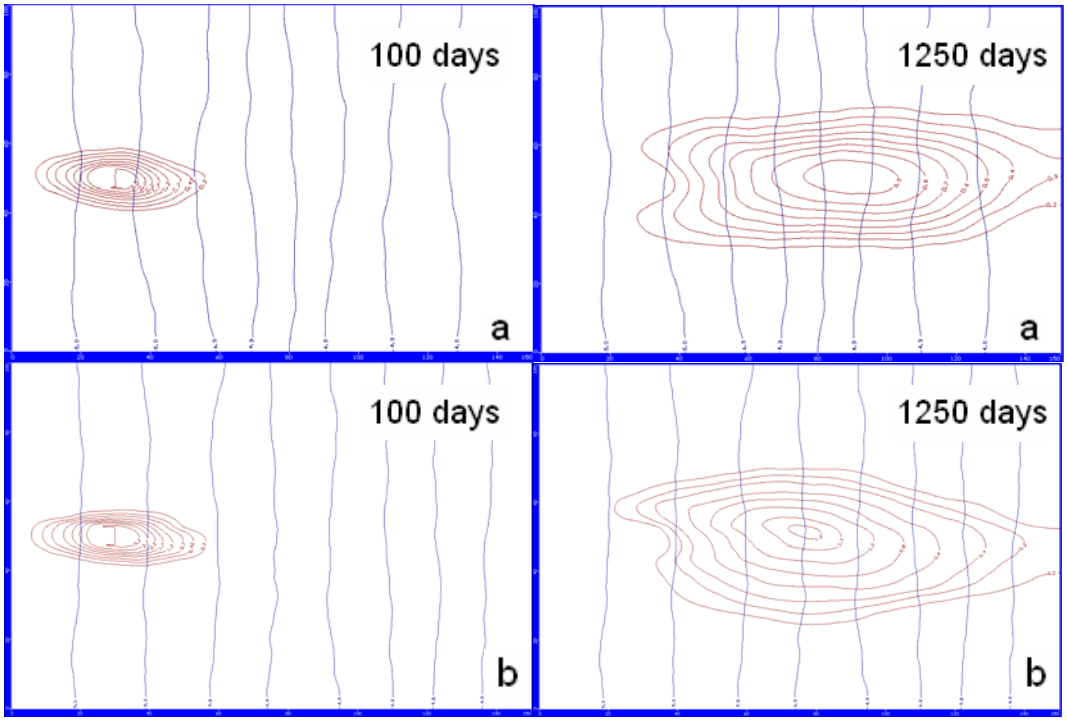

Figure 3.19. VC plumes at 100th and 1250th days for (a) isotropic, h = 10 m, (b) anisotropic, h_x = 10 m, h_y = 2 m when CV = 50 %

Figure 3.20. shows the steady state head distribution and the shape of the VC plume at the 100th and 1250th days for the isotropic field and anisotropic field when CV = % 150. Although the conductivity contrast is same as it is in the isotropic field, the zones of high and low conductivity are not located densely at specific areas within the model domain meaning that the hydraulic conductivity values that are close to each other do not observed to have bigger areas. The zones spread all over the model domain as being elongated in the x-direction since the randomness occurs in 5 times greater distances in the x-direction. Therefore, the plume is elongated in the x-direction in the anisotropic field through mixing and spreading in the flow direction. The displacement of the center of mass of the plume is also increased in the anisotropic field showing the average velocity in the x-direction has also increased.

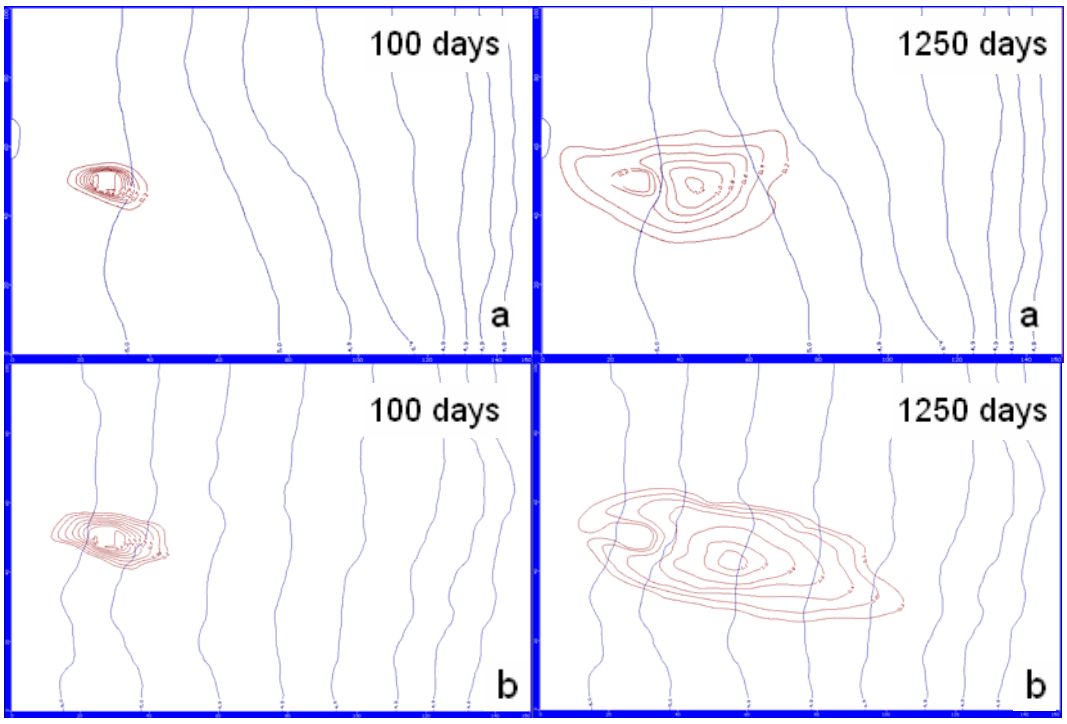

Figure 3.20. VC plumes at 100th and 1250th days for (a) isotropic, h = 20 m, (b) anisotropic, h_x = 20 m, h_y = 4 m when CV = 150 %

The steady state head distribution and the shape of the PCE, TCE, DCE and ETH plumes at the 100^{th} and 1250^{th} days for the anisotropic fields having CV = % 50 and 150 are given in Appendix C in Figures C.4 and C.5.

Figures 3.21. and 3.22. are the graphical representations of change in the location of peak concentration and plume front of the VC plume with time for the anisotropic fields. Figures 3.21 shows that the displacement of the center of mass of the plume is higher than the isotropic field when CV ratio % 50 and lower when CV ratio is % 150. Same behavior is observed for in Figure 3.22 for the plume front in isotropic and anisotropic fields. The graphs of peak concentration distribution of VC plume with distance for the anisotropic fields are shown in figure 3.23. Although there is a slight difference in the peak concentrations, the final peak concentrations are almost same. These results indicate that the dispersion in the transport due to dispersion and advection increased in the anisotropic field having CV % 50 in y-direction and in the anisotropic field having CV % 150 in x-direction.

The graphs of the change in the location of peak concentration and plume front of the PCE, TCE, DCE and ETH plumes with time and the graphs of peak concentration distribution of PCE, TCE, DCE and ETH plumes with distance at the same days of simulations for CV = % 50 and 150 are given in Appendix C in Figures C.46 – C.57.

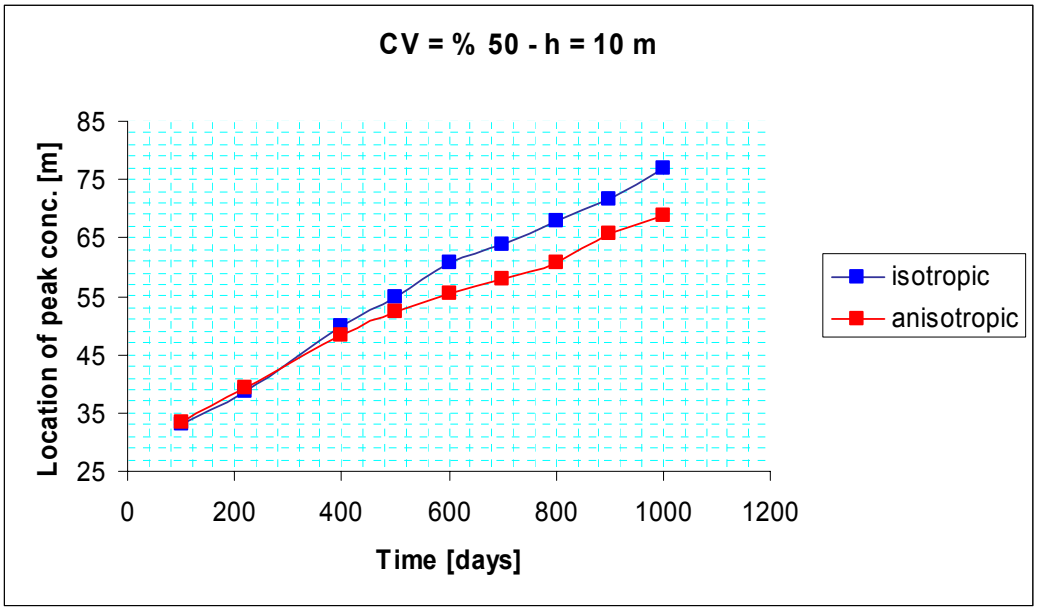

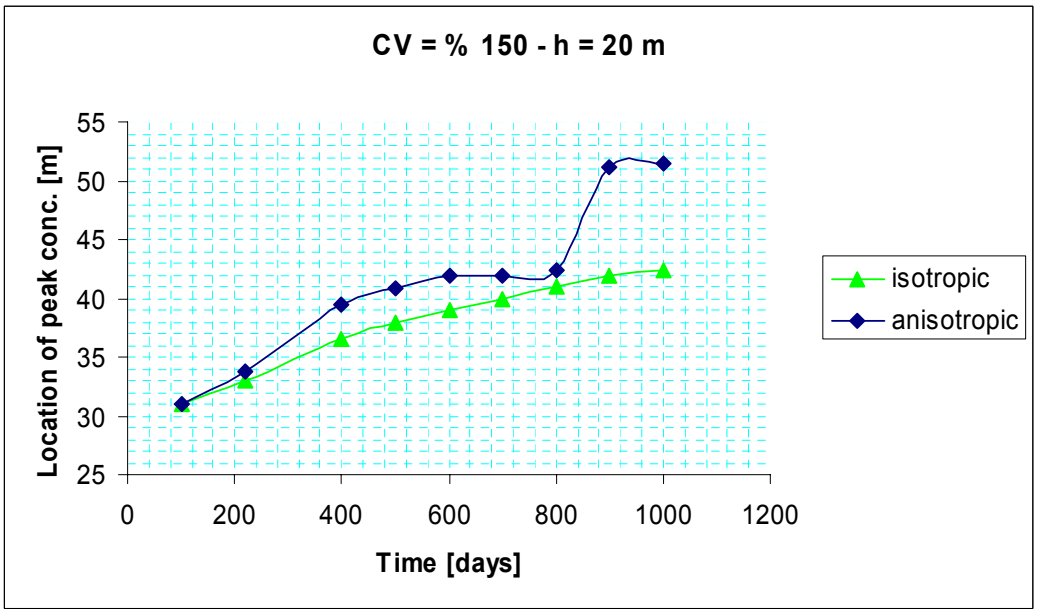

Figure 3.21. Location of peak concentration of VC plume with time for isotropic (h = 10 m when CV = % 50 and h = 20 m when CV = % 150) and anisotropic (h_x = 10 m, h_y = 2 m when CV = % 50 and h_x = 20 m, h_y = 4 m when CV = % 150) fields.

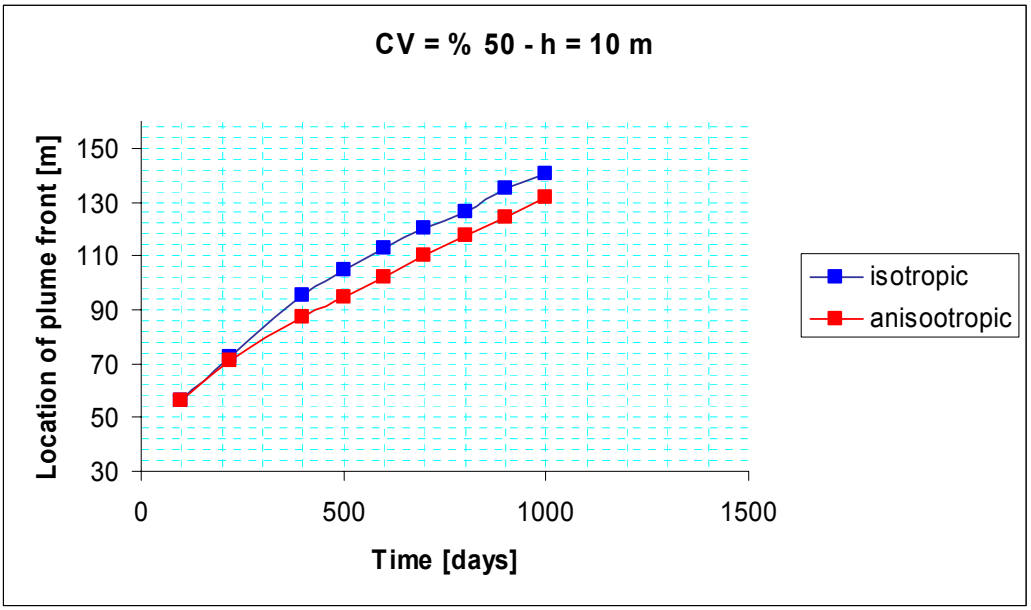

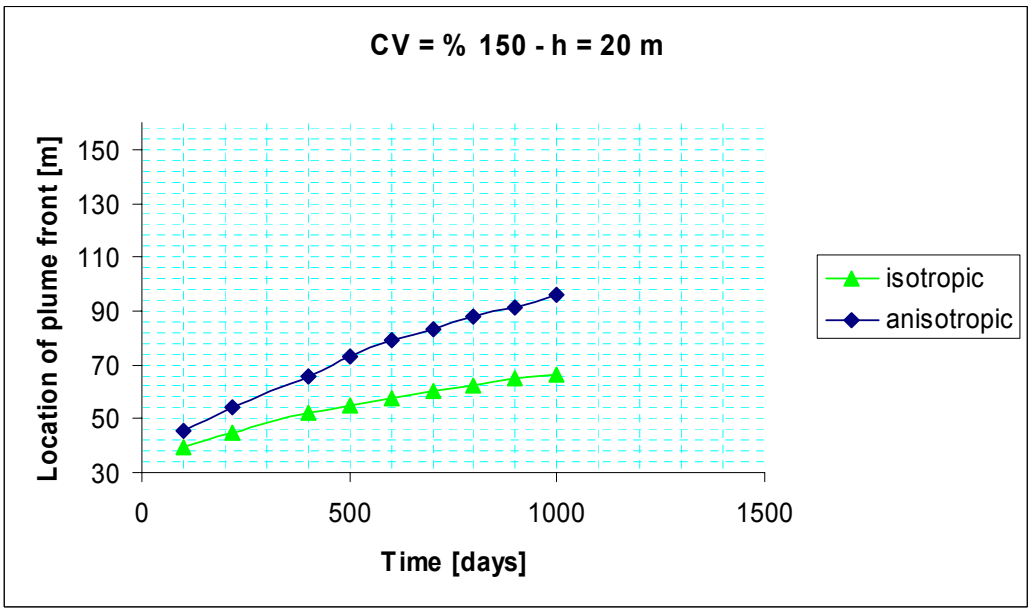

Figure 3.22. Location of VC plume front with time for isotropic (h = 10 m when CV = % 50 and h = 20 m when CV = % 150) and anisotropic (h_x = 10 m, h_y = 2 m when CV = % 50 and h_x = 20 m, h_y = 4 m when CV = % 150) fields.

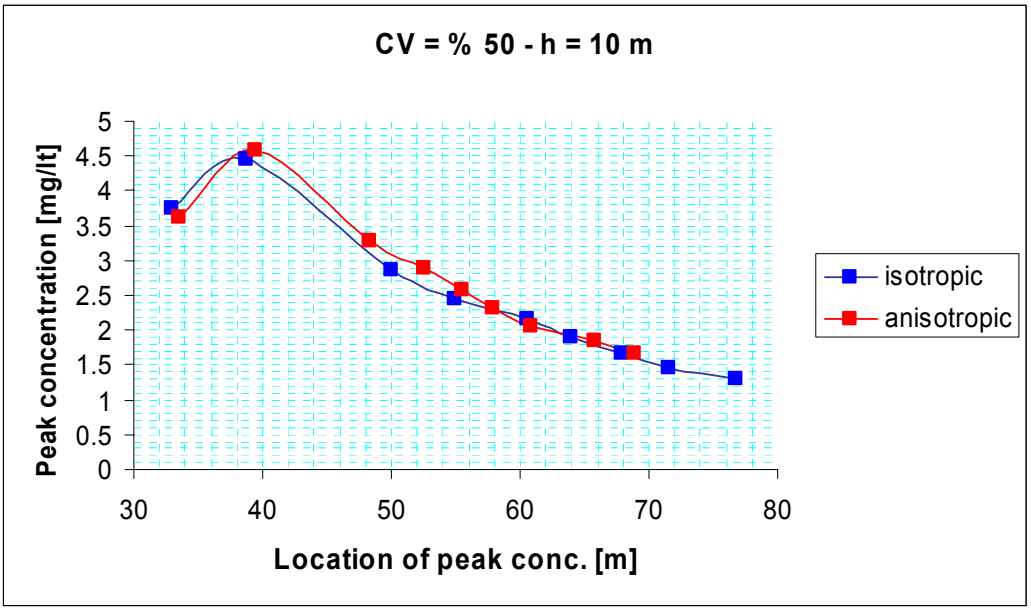

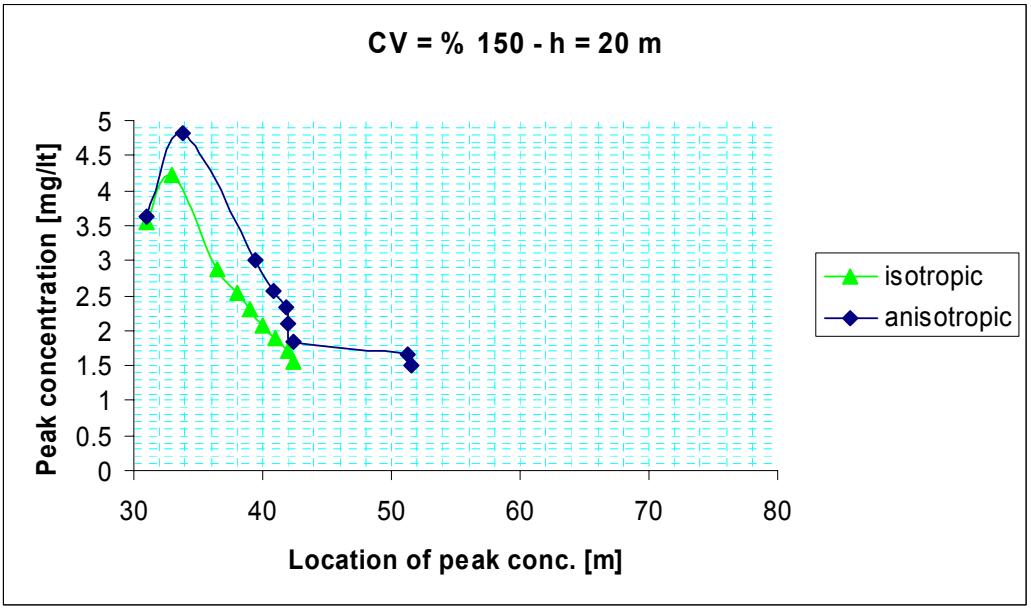

Figure 3.23. Peak concentration distribution of VC plume with distance for isotropic (h = 10 m when CV = % 50 and h = 20 m when CV = % 150) and anisotropic (h_x = 10 m, h_y = 2 m when CV = % 150 and h_x = 20 m, h_y = 4 m when CV = % 50) fields.

3.3. Assessment of Degradation Rates as a Function of Heterogeneity

Conservative Tracer and Buscheck and Alcantar Methods are used for the calculation of the biodegradation rates of the chlorinated solvents, PCE, TCE, DCE, VC and ETH, for all of the generated random hydraulic conductivity fields.

The plumes obtained from results of the contaminant transport simulations for the generated random fields and the uniform field are assumed to reach almost at steady state at the 1000^{th} day when the plume migration and downgradient concentrations are observed with time. At the 1000^{th} day of the simulation time, plumes are no longer migrating downgradient and contaminant concentrations are not changing significantly with time. Therefore, the degradation rate constant determination is carried out using the data of 1000^{th} day of the simulation. Both of the methods require contaminant concentrations measured along the groundwater flow direction. Chlorinated compound sampling transects are determined and observation wells are located for each of the generated random fields and the uniform field along the flow direction. Since the plume migration behavior and the shapes of the plumes are significantly different for each simulation, different transects are determined for each field. The observation wells on the selected transects that are used to obtain the measured contaminant concentrations along the flow path for each of the field are presented in Appendix D in Figures D.1 – D.6.

The center of the mass of the plume is considered as the beginning of the pathway and since the change in the location of the center of mass of the PCE plume is less, the first observation well is located at the center of mass of the PCE plume in all simulations. The center of mass of the plume for other chlorinated compounds also observed along the flow path of the PCE

plume, therefore, observation wells are located at the center of mass of other plumes. The other observation well locations are determined according to the shape and the downgradient length of the plume. The downgradient distance of the observation wells located at each field and the measured contaminant concentrations are given in Appendix E in Tables E.1 – E.12.

Contaminant velocities are required in the calculation of degradation rates. Visual MODFLOW calculates the groundwater velocity at each cell through the model domain and gives the magnitude of the directional velocity components in both, x- and y-, directions. The averages of the vector sum of these velocities are calculated for each field for the determination of the average groundwater velocity. Then, the contaminant velocities are calculated using equation 2.34 using the contaminant specific retardation factors presented in Table 2.6. The calculated average contaminant velocities are shown in Table 3.1.

3.3.1. Conservative Tracer Method

To calculate the biodegradation rates of chlorinated compounds, PCE, TCE, DCE, VC and ETH, accurately, measured contaminant concentrations must be corrected for the effects of dispersion, dilution, and sorption using the measured concentrations of a conservative tracer. In this study like for many chlorinated solvent plumes, the sum of ionic chloride and organic chloride associated with the chlorinated compounds are considered as a conservative tracer. The conservative tracer concentration is using equation 2.30. The slope of the line in the linear regression line given equation 2.33 yields the anaerobic biodegradation rates of the contaminant species. Therefore, ln $C_{corrected}$ (corrected concentrations) of PCE, TCE, DCE, VC and ETH versus time graphs are plotted.

Table 3.1. The average groundwater (GW) and contaminant velocities for random fields.

Field		Velocities [m/sec]					
CV (%)	h (m)	GW	PCE	TCE	DCE	VC	ETH
Uniform		1.08×10^{-6}	1.52×10^{-7}	3.72×10^{-7}	3.86×10^{-7}	7.71×10^{-7}	2.04×10^{-7}
50	5	9.43×10^{-7}	1.33×10^{-7}	3.25×10^{-7}	3.37×10^{-7}	6.74×10^{-7}	1.78×10^{-7}
	10	1.69×10^{-7}	2.38×10^{-8}	5.84×10^{-8}	6.04×10^{-8}	1.21×10^{-7}	3.19×10^{-8}
	20	1.67×10^{-7}	2.35×10^{-8}	5.75×10^{-8}	5.96×10^{-8}	1.19×10^{-7}	3.15×10^{-8}
100	5	1.86×10^{-7}	2.62×10^{-8}	6.42×10^{-8}	6.65×10^{-8}	1.33×10^{-7}	3.51×10^{-8}
	10	2.10×10^{-7}	2.96×10^{-8}	7.25×10^{-8}	7.51×10^{-8}	1.5×10^{-7}	3.97×10^{-8}
	20	2.16×10^{-7}	3.04×10^{-8}	7.45×10^{-8}	7.72×10^{-8}	1.54×10^{-7}	4.08×10^{-8}
150	5	1.90×10^{-7}	2.67×10^{-8}	6.55×10^{-8}	6.78×10^{-8}	1.36×10^{-7}	3.58×10^{-8}
	10	2.15×10^{-7}	3.03×10^{-8}	7.42×10^{-8}	7.69×10^{-8}	1.54×10^{-7}	4.06×10^{-8}
	20	2.18×10^{-7}	3.08×10^{-8}	7.53×10^{-8}	7.8×10^{-8}	1.56×10^{-7}	4.12×10^{-8}

3.3.1.1. Isotropic hydraulic conductivity fields

The plotted ln $C_{corrected}$ versus time graphs are given in Appendix F. The slopes of the regression lines give us the first order anaerobic biodegradation rate coefficients of the chlorinated solvent plumes and these degradation rates calculated for each compound at each field are given in Table 3.2. for the isotropic fields. Calculated uniform rate constants are within the same order of magnitude as input rate constants in Table 2.3 except ETH. Calculated biodegradation rates of the contaminants in the uniform field are different than the biodegradation rate coefficients that are input to the program in Table 2.3, which are taken from the Cape Carnaveal Air Station, Florida (BIOCHLOR, 2000). This may be due to the fact that the input

degradation rates are based on calibration field data using a simulation time of 32 years (field data collected in 1997). Also there are three contaminant source areas, however, the source having the highest contaminant concentrations is used in this study. Besides, the duration of the contamination is continuous in the simulations performed with BIOCHLOR and the real site situations while the duration of the contamination is stopped after 220 days in the simulations performed with Visual MODFLOW.

Table 3.2. Biodegradation rates for the contaminants for the uniform field and the generated random fields calculated by Conservative Tracer Method.

Fields		**Biodegradation rate, λ, [d-1]**				
CV (%)	**h (m)**	**PCE**	**TCE**	**DCE**	**VC**	**ETH**
Uniform		0.0015	0.0019	0.0019	0.0025	6.0x10-4
50	**5**	0.0011	0.0016	0.0021	0.0023	7.0x10-4
	10	0.001	0.0011	0.0011	0.0014	6.0x10-4
	20	0.0012	0.0014	0.0013	0.0025	9.0x10-4
100	**5**	0.0009	0.0012	0.001	0.0026	8.0x10-4
	10	0.001	0.0011	0.0011	0.0014	6.0x10-4
	20	0.0021	0.0019	0.0019	0.0033	9.0x10-4
150	**5**	0.001	0.001	0.001	0.0014	5.0x10-4
	10	0.001	0.001	0.001	0.0016	5.0x10-4
	20	0.0031	0.003	0.003	0.0037	1.4x10-4

The degradation rate values of the contaminants in the fields are less than the ones in the uniform field except in the fields having CV %100 and % 150 when the correlation length is 20 m. For a given CV value the highest degradation rates are in the field having correlation length 20 m. For h = 20

m the size of the plume is the smallest among the other two plumes of the fields having correlation lengths 5 and 10 m at each CV value. The lowest biodegradation rates are calculated in the fields having correlation length 10 m for each CV ratio and the size of the plumes are the biggest among the plumes formed at the fields with correlation length 5 and 20 m. As mentioned before the size of the plumes gets smaller as CV increases for a given correlation length and the calculated degradation rates also increase with the increasing CV. These results show that the degradation of the contaminants is directly related with the size of the plume that as the size of the plume decreases the degradation rate increases.

3.3.1.2. Anisotropic hydraulic conductivity fields

Same ln $C_{corrected}$ versus time graphs are plotted for the anisotropic fields and they are given in Appendix F. The first order anaerobic biodegradation rates of the chlorinated solvent plumes for the fields with isotopic and anisotropic hydraulic conductivity fields are given in Table 3.4.

Table 3.3. Biodegradation rates for the contaminants for the isotropic and fields anisotropic having calculated by Conservative Tracer Method.

	Biodegradation rate, λ, [d^{-1}]			
Contaminant	**CV = 50 %, h = 10 m**	**CV = 50 %, h_x = 10 m and h_y =2 m**	**CV = 150 %, h = 20 m**	**CV = 150 %, h_x = 20 m and h_y =4 m**
PCE	0.0009	0.0012	0.0031	0.0016
TCE	0.0009	0.0012	0.003	0.0014
DCE	0.0008	0.0011	0.003	0.0013
VC	0.002	0.002	0.0037	0.0024
ETH	5.00E-04	6.00E-04	1.40E-03	0.0007

The biodegradation rates in the anisotropic field when CV is % 50 are higher than the ones in the isotropic field; however, the biodegradation rates in the anisotropic field when CV is % 150 are less than the ones in the isotropic field. Anisotropy increases biodegradation rate constants at low CV, whereas it cause decrease in the rate constants at high CV. The result that as the size of the contaminant plume gets smaller due to the decrease in the mechanical dispersion and the velocity, the degradation rate increases, obtained for isotropic field, is also valid for anisotropic fields.

3.3.2. Buscheck and Alcantar Method

As mentioned in section 2.3.2 Buscheck and Alcantar (1995) derived a relationship for the calculation of first order decay rate constants for steady-state plumes as expressed in equation 2.41. Linear regression analysis is conducted for ln $C_{measured}$ (measured concentrations) of the chlorinated compounds and the downgradient distance of the located observation wells for each field. The regression plots of Buscheck-Alcantar Method are also given in Appendix F. The calculated slope of the regression lines are used in the calculations of the first order anaerobic degradation rate calculations of the chlorinated solvent plumes using equation 2.41.

3.3.2.1. Isotropic hydraulic conductivity fields

The calculated first-order anaerobic biodegradation rates of the chlorinated solvent plumes for the isotropic fields are given in Table 3.4 for the isotropic fieldds The calculated degradation rates of the contaminants in the uniform field are also different than the degradation rates that are input to the program taken from the Cape Carnaveal Air Station, Florida (BIOCHLOR, 2000). However, the same effects of CV and h are observed on the biodegradation rates.

The biodegradation rate values of the contaminants in the fields are less than the ones in the uniform field except in the fields having CV %100 and % 150 when the correlation length is 20 m. For a given CV value, the highest biodegradation rates are mostly in the field having correlation length 20 m and, for which the size of the plume is the smallest. For a given CV the lowest biodegradation rates are calculated in the fields having correlation length 10 m, and for which the size of the plumes are the largest. The biodegradation rates calculated by Buscheck-Alcantar Method also show that the biodegradation of the contaminants is directly related with the size of the plume; as the size of the plume decreases the degradation rate increases.

Table 3.4. Biodegradation rates for the contaminants for the uniform field and the generated random fields calculated by Buscheck-Alcantar Method.

Fields		**Biodegradation rate, λ, [d-1]**				
CV (%)	**h (m)**	**PCE**	**TCE**	**DCE**	**VC**	**ETH**
Uniform		0.00455	0.003194	0.00378	0.003655	0.001223
50	**5**	0.00279	0.00381	0.00473	0.00423	0.00142
	10	0.00180	0.00243	0.00209	0.00275	0.00106
	20	0.00292	0.00441	0.00435	0.00641	0.00227
100	**5**	0.00240	0.00319	0.00280	0.00610	0.00138
	10	0.00261	0.00202	0.00198	0.00265	0.00087
	20	0.00998	0.00704	0.00691	0.00919	0.00272
150	**5**	0.00367	0.00294	0.00291	0.00402	0.00143
	10	0.00280	0.00187	0.00184	0.00281	0.00089
	20	0.01918	0.01420	0.01410	0.01281	0.00472

3.3.2.2. Anisotropic hydraulic conductivity fields

The regression plots of Buscheck-Alcantar Method for the anisotropic fields are also given in Appendix F and the calculated first-order anaerobic biodegradation rates of the chlorinated solvent plumes for the fields with isotopic and anisotropic hydraulic conductivity distribution are given in Table 3.4. The effect of anisotropy on the biodegradation rates of the contaminants calculated by Buschek-Alcantar are same as the ones calculated by Conservative Tracer Method. The degradation rates in the anisotropic field when CV is % 50 are higher than those in the isotropic field; however, the biodegradation rates in the anisotropic field when CV is % 150 are less than the ones in the isotropic field. Biodegradation rate of the contaminants are higher for the smaller size plumes.

Table 3.8. Biodegradation rates for the contaminants for the isotropic and fields anisotropic having calculated by Buscheck-Alcantar Method.

	Biodegradation rate, λ, [d^{-1}]			
Contaminant	**CV = 50 %, h = 10 m**	**CV = 50 %, h_x = 10 m and h_y =2 m**	**CV = 150 %, h = 20 m**	**CV = 150 %, h_x = 20 m and h_y =4 m**
PCE	0.00180	0.0031	0.01918	0.00522
TCE	0.00243	0.00261	0.01420	0.00387
DCE	0.00209	0.00257	0.01410	0.00381
VC	0.00275	0.0035	0.01281	0.00466
ETH	0.00106	0.00113	0.00472	0.00121

3.4. Functional Relationship between Rate Constants and Heterogeneity

As a final step of the study, a non-linear regression analysis study was performed to fit the calculated biodegradation rates to a model that would depend on the aquifer heterogeneity parameters, CV and correlation length. The surface plots of the calculated biodegradation rates of the chlorinated solvent species were presented in Appendix G. The degradation rates and the surface plots showed that there was a nonlinear relationship between the degradation rates and the aquifer heterogeneity parameters in the following form,

$$\lambda = a + (b\,x\,(CV)^c) + (d\,x\,(h)^e) \qquad 3.1$$

where λ is the first order anaerobic degradation rate, T-1, CV is the coefficient of variation, h is the correlation length, L, and a, b, c, d and e were the constants.

Multiple nonlinear regression analyses were carried out for biodegradation rates of PCE, TCE, DCE, VC and ETH calculated by both Conservative Tracer and Buscheck-Alcantar Methods using the software, STATGRAPHICS Plus. The constants that are defined in equation 3.1 were estimated through the best fit of the defined model with the calculated biodegradation rate and corresponding aquifer heterogeneity parameters. In order to achieve the best fit of the estimated model and the data, the initial values of the parameters was adjusted to the estimated results of the regression analyses. The regression repeated until the best fit was obtained. The final forms of the nonlinear equations describing the relationship between the biodegradation rates and the CV and correlation length are presented for Conservative Tracer and Buscheck-Alcantar Methods in Tables 3.9 and 3.10, respectively. The R2, Coefficient of Determination, is an

indicator of how well the model fits the data. The R2 values of each regression analysis were also given in the tables. It is seen that the biodegradation rates calculated Buscheck-Alcantar Method produce a better than Conservative Tracer Method.

Table 3.9. Nonlinear equations of first-order anaerobic degradation rates calculated by Conservative Tracer Method

Equation	R^2
$\lambda_{PCE} = -0.02247 + (0.02429 \times (CV)^{0.012224}) + (6.05E\text{-}9 \times (h)^{4.06666})$	0.63
$\lambda_{TCE} = -0.00873 + (0.00926 \times (CV)^{0.013901}) + (9.68E\text{-}14 \times (h)^{7.68578})$	0.54
$\lambda_{DCE} = -0.00518 + (0.00641 \times (CV)^{-0.001974}) + (1.02E\text{-}15 \times (h)^{9.17555})$	0.41
$\lambda_{VC} = -0.02438 + (0.02563 \times (CV)^{0.004986}) + (1.96E\text{-}8 \times (h)^{3.7038})$	0.60
$\lambda_{ETH} = -0.02188 + (0.02216 \times (CV)^{0.003101}) + (1.53E\text{-}9 \times (h)^{4.21839})$	0.64

Table 3.10. Nonlinear equations of first-order anaerobic degradation rates calculated by Buscheck-Alcantar Method.

Equation	R^2
$\lambda_{PCE} = -0.03836 + (0.02241 \times (CV)^{0.013232}) + (6.14E\text{-}8 \times (h)^{3.94076})$	0.68
$\lambda_{TCE} = -0.03372 + (0.02703 \times (CV)^{0.065485}) + (3.05E\text{-}9 \times (h)^{4.83165})$	0.64
$\lambda_{DCE} = -0.03329 + (0.02742 \times (CV)^{0.059603}) + (8.51E\text{-}9 \times (h)^{4.48229})$	0.59
$\lambda_{VC} = -0.03265 + (0.02857 \times (CV)^{0.053196}) + (2.806E\text{-}9 \times (h)^{4.84961})$	0.75
$\lambda_{ETH} = -0.03072 + (0.02911 \times (CV)^{0.019931}) + (4.66E\text{-}9 \times (h)^{4.34329})$	0.74

CHAPTER 4

SUMMARY AND CONCLUSION

Groundwater contamination by various organic and inorganic compounds is a common environmental problem. Being a more economical and a less resource demanding technology, Monitored Natural Attenuation has lately become an attractive alternative for groundwater cleanup at chlorinated solvent contaminated sites. Natural attenuation processes (biodegradation, dispersion, sorption, and volatilization) affect the fate and transport of contaminants and in all hydrologic systems; however, the natural attenuation capacities are different in these hydrologic systems depending on the site specific aquifer characteristic. The level of heterogeneity of a site is one parameter that has an effect on these attenuation processes in an aquifer system. Although the research findings of the past years have shown that the ground water flow systems contaminated by petroleum hydrocarbons can be remediated by naturally occurring systems, the chlorinated hydrocarbon degradation under natural attenuation processes is relatively a new issue.

In order to demonstrate and quantify the affect of heterogeneity on the groundwater flow regime, and in turn on the degradation rates of the chlorinated hydrocarbons, more specifically PCE, TCE, DCE, VC and ETH, a 2-dimensional numerical flow and transport modeling study was conducted. Turning Bands Random Field Generator is used for the generation of the statistical distributions of spatially correlated random hydraulic conductivity fields representing different levels of aquifer heterogeneity levels, and then

these fields were used to simulate flow and fate and transport of contaminant species. First-order anaerobic biodegradation rates of the chlorinated hydrocarbon species were calculated using Conservative Tracer and Buscheck-Alcantar Methods. Finally, multiple non-linear regression analysis were carried out and to derive empirical functional relationship between the degradation rates and aquifer heterogeneity.

Major findings of this numerical modeling study can be summarized as follows.

The results of 2-dimensional contaminant transport simulations revealed that the chlorinated solvent plumes at the generated fields became more irregular and distorted as CV of the generated field increases. The increase in the CV ratio also resulted in the slowing down of the contaminant plume migration. This is due to the fact that the average groundwater velocities also decreased with increasing CV ratio. Shrinkage of the contaminant plume in the areal extend was also another affect of increasing CV ratio which may be explained with the decreasing mechanical dispersion with decreasing velocity and eventually with increasing CV ratio.

Although the plume shape and size depends on CV and h, the chlorinated solvent transport simulation results showed that the shape of the contaminant plumes depend mainly on the correlation length since it was the correlation length that determines the spreading of the high and low conductivity zones within the model domain. However, it is mainly the CV that has changed the size of the plume, while it is also changing the shape of the plume but not at a degree as the correlation length. Although the size of the plume was different significantly in the fields having different correlation lengths, the displacement of center of mass of the plumes, hence the transport of the contaminants were not affected that much. The effect of anisotropy was best observed for the plume having CV ratio 150 %. Since high and low

conductivity zones were spread within the model domain and elongated in x-direction. The displacement of the center of mass was high and the plume size in the x-direction. Anisotropy mainly affected the shape and the directional size of the plume since it affected the local groundwater velocity and eventually mechanical dispersion as well.

The degradation rates calculated by Conservative Tracer Method and Buscheck-Alcantar Method showed that rates are directly related with the size of the contaminant plume. Results showed that the degradation of the contaminants was directly related with the size of the plume that as the size of the plume decreased the degradation rates increased. Therefore, biodegradation rates increased as the CV ratio increased. However, the change in correlation length did not show a clear trend. The biggest plume was observed when correlation length was 10 m and hence the smallest degradation rate was calculated for these fields when CV ratio kept constant. This affect of plume size on the degradation rate may be due to the fact that the less mixing and spreading through mechanical dispersion and the less transport through advection of the contaminants made the contaminant much more available to the microorganisms to degrade. The same affect of size on the degradation rates was observed for the anisotropic fields.

Although, the results of the Conservative Tracer and Buscheck-Alcantar Methods were different, the trends in the change of the degradation rates according to CV and correlation length were same. The degradation rates calculated by Buscheck-Alcantar Method were greater than those calculated by Conservative Tracer Method. Buscheck-Alcantar Method depends on the assumption that the plume has reached steady state that is the plume no longer migrating downgradient and that contaminant concentrations are not changing significantly through time. The 1000^{th} day of the simulation time was the time the least migration of the plume and concentration change was

occurring. The difference may be due to the fact that the plume did not reached a complete steady state at the 1000th day of the simulation.

The results of this study showed that the for the fields having CV less than % 100 and having CV close to % 50, hydraulic conductivity distribution may be treated as uniform since the changes in the plume shapes, sizes and the degradation rates of the contaminants are more observable for the field with CV higher than % 100.

Finally, a multiple non-linear regression analysis of the degradation rates calculated for each chlorinated solvent specie at each random field generated were performed for the rates calculated by two methods. It is observed that the data din not fit well as it is expected. This behavior may be due to the fact that as MacQuarrie and Sudicky, 1990 stated and as the results of this study indicates, the local groundwater velocity variations within the model domain makes the behavior of the organic plumes and the degradation rates less predictable. However, the presented numerical relationship between the degradation rate and the aquifer heterogeneity will be beneficial in assessing the natural attenuation capacity of a contaminated site during the feasibility studies and will be a better approximation to the estimated field scale degradation rates of the chlorinated solvent species. The heterogeneity level of a contaminated site can be determined by using drill holes and the CV and the correlation length values of the site can be obtained from the drill log data. Then, using these equations that represents the degradation of the chlorinated solvents as a function of CV and h can be used to predict the natural attenuation capacity of the contaminated site. This will give the chance of getting quantitative results by using qualitative data.

REFERENCES

Bear, J. 1979. **Hydraulics of Groundwater**, McGraw-Hill, New York, NY.

Bouwer, EJ. **Bioremediation of chlorinated solvents using alternate electron acceptors,** In: RD Norris et al. (Eds.), Handbook of bioremediation, pp. 149-175, 1994.

BIOCHLOR, Natural Attenuation Decision Support System, User's Manual Version 1.0, EPA/600/R-00/008, USEPA, Office of Research and Development Washington DC, 2000.

Buscheck, T.E., Alcantar, C.M**., Regression Techniques and Analytical Solutions to Demonstrate Intrinsic Bioremediation**, In Proceedings of the 1995 Battelle International Conference on In-Situ and On Site Bioreclamation, April 1995.

Chapelle, F.H., and Bradley, P.M., **Selecting Remediation Goals by Assessing the Natural Attenuation Capacity of Groundwater Systems**, Bioremediation Journal, 2(3): 227-238, December 1998.

Clement, T.P., Johnson, C.D., Sun, Y., Klecka, G.M., Bartlett, C., **Natural attenuation of chlorinated ethane compounds: model development and field-scale application at the Dover site.** Journal of Contaminant Hydrology. 42, 113–140, 2000.

Clement, T.P., RT3D- **A modular computer code fr simulating reactive multi-species transport in groundwater aquifers**. Ground Water Monitoring Remediation, 18 (2), 79-92, 1997.

Freedman, D. L. and J. M. Gossett. 1989. "**Biological Reductive Dechlorination of Tetrachloroethylene and Trichloroethylene to Ethylene under Methanogenic Conditions.**" Appl. Environ. Microbiol. 55(9): 2144-2151.

Fetter, C. W., **Contaminant Hydrogeology**, Macmillan Publishing Company, New York, NY, 1993.

Johnson, C.D., R.S. Skeen, D.P. Leigh, T.P. Clement, and Y. Sun**, Modeling natural attenuation of chlorinated ethenes at a Navy site using the RT3D code**, Proceedings of WESTEC 98 conference, sponsored by Water Environmental Federation, Orlando, Florida, 1998.

MacQuarrie, K. T. B., Sudicky, E. A., **Simulation of Biodegradable Organic Contaminants in Groundwater 2. Plume Behavior in Uniform and Random Flow Fields, Water Resources Research**, 26(2): 223-239, 1990.

Matheron, G., **The intrinsic random functions and their application**, Adv. Appl. Probab., 5 439-468, 1973.

McDonald, M.D., and Harbaugh, A.W., A modular three-dimensional finite-difference flow model, Techniques in Water Resources Investigations of the U.S. Geological Survey, Book 6., 586 pp., 1988.

Murray, W.D. and Richardson, M., **Progress toward the biological treatment of C1 and C2 halogenated hydrocarbons**, Crit. Rev. Environ. Sci. Technol., 23(3):195-217, 1993.

Natural Attenuation of Chlorinated Solvents in Groundwater: Principles and Practices (prepared by Interstate Technology and Regulatory

Cooperation Work Group, In Situ Bioremediation Work Team and Industrial Members of the Remediation Technologies Development Forum (RTDF))

Schlather, M. **Simulation and Analysis of Random Fields**, R News, 1 (2), p. 18-20, 2001.

Sorenson, K.S., Peterson, L.N., Hinchee, R.E., and Ely, R.L., **An Evaluation of Aerobic Trichloroethene Attenuation Using First-Order Rate Estimation**, Bioremediation Journal, 4(4): 337-357, 2000.

Sun, Y., J.N. Petersen, T.P. Clement, B.S. Hooker, **Effects of reaction kinetics on predicted concentration profies during subsurface bioremediation,** Journal of Contamianant Hydrology, vol. 31, 359-372, 1998.

Sun, Y. and T.P. Clement, 1998, **A decomposition method for solving coupled multispecies reactive transport problems**, Transport in Porous Media Journal, 1404, p. 1-20, 1998.

USEPA, **Use of monitored natural attenuation at superfund, RCRA Corrective Action, and Underground Storage Tank Sites**, OSWER Directive 9200.4-17, 1997.

USEPA, **Technical Protocol for Evaluating Natural Attenuation of Chlorinated Solvents in Ground Water,** EPA/600/R-98/128, Office of Research and Development Washington DC, 1998.

Tompson A.F.B., Ababou R., and Gelhar L.W., **"Application And Use of The Three-Dimensional Turning Bands Random Field Generator: Single Realization Problems"**, March 1987.

Tompson A.F.B., Ababou R., and Gelhar L.W., **"Implementation of the Three-Dimensional Turning Bands Random Field Generator"**, Water Resources Research, Vol. 25 No 10, pp 2227-2243, October 1989.

Ünlü K., **"Assessing Risk of Groundwater Pollution From Land-Disposed Wastes"**, Journal of Environmental Engineering, Vol 120 No 6, November/December 1994.

Visual MODFLOW v.3.0 User's Manual, Waterloo Hydrogeologic Inc.,2002

Vogel, T. M. and P. L. McCarty, **Abiotic and Biotic Transformations of 1,1,1-Trichloroethane Under Methanogenic Conditions**, Environ. Sci. Technol., 21, pp. 1208-1213, 1987.

Vogel, T. M. and P. L. McCarty, **Biotransformation of Tetrachloroethylene to Trichloroethylene, Dichloroethylene, Vinyl Chloride and Carbon Dioxide Under Methanogenic Conditions**, Appl. Environ. Microbiol., 49, pp. 1080-1083, 1985.

Warrick, A.W., Myers, D.E., Nielsen. D.R., **Geostatistical Methods Applied to Soil Science**, Methods of Soil Analysis, Part 1. Physical and Mineralogical Methods-2nd Edition, Madison, WI, USA.

Wiedemeier, T.H., Swanson, M.A., Wilson, J.T., Kampbell, D.H., Miller, R.N., and Hansen, J.E., 1996b, "**Approximation of biodegradation rate constants for monoaromatic hydrocarbons (BTEX) in ground water"** Ground Water Monit. Remed., 16(3):186-194.

Wiedemeier, T.H., Swanson, M. A., Moutoux, D. E., Gordon, E. K., Wilson, J. T., Wilson, B. H., Haas, P. E., Kampbel, D. H., Hansen, J. E., Haas and Chapelle, F. H., **Technical Protocol for Evaluating Natural Attenuation of**

Chlorinated Solvents in Ground Water, EPA/600/R-98/128, USEPA, Office of Research and Development Washington DC, 1998.

Witt, M.E., Klecka, G.M., Lutz, E.J., Ei, T.A., Grosso, N.R., Chapelle, F.H., **Natural Attenuation of chlorinated solvents at Area 6, Dover Air Force Base: groundwater biogeochemistry**, Journal of Contaminant Hydrology. 57, 61–80, 2002.

Zheng, C., MT3D, **A modular three-dimensional transport model for simulation of advection, dispersion and chemical reactions of contaminants in groundwater systems**, U.S.E.P.A Report, 1990.

APPENDICES A – INPUT DATA OF RANDOM FIELD GENERATOR

Table A.1. Physical input data of the random field generator for the field having CV = % 50

	CV = 50 % h = 5 m	**CV = 50 % h = 5 m**	**CV = 50 % h = 5 m**
Line 1: IDATE, IRUN			
Line 2: NX, NY, NZ	301, 201, 0	301, 201, 0	301, 201, 0
Line 3: DX, DY, DZ	0.5, 0.5, 0	0.5, 0.5, 0	0.5, 0.5, 0
Line 4: XL1, XL2, XL3	5,5,0	10,10,0	20,20,0
Line 5: CONDG, SIG	1.61×10^{-4} 0.47	1.61×10^{-4} 0.47	1.61×10^{-4} 0.47

Table A.2. Physical input data of the random field generator for the field having CV = % 100

	CV = 100 % h = 5 m	**CV = 100 % h = 10 m**	**CV = 100 % h = 20 m**
Line 1: IDATE, IRUN			
Line 2: NX, NY, NZ	301, 201, 0	301, 201, 0	301, 201, 0
Line 3: DX, DY, DZ	0.5, 0.5, 0	0.5, 0.5, 0	0.5, 0.5, 0
Line 4: XL1, XL2, XL3	5,5,0	10,10,0	20,20,0
Line 5: CONDG, SIG	1.27×10^{-4}, 0.83	1.27×10^{-4}, 0.83	1.27×10^{-4}, 0.83

Table A.3. Physical input data of the random field generator for the field having CV = % 150

	CV = 150 % h = 5 m	**CV = 150 % h = 10 m**	**CV = 150 % h = 20 m**
Line 1: IDATE, IRUN			
Line 2: NX, NY, NZ	301, 201, 0	301, 201, 0	301, 201, 0
Line 3: DX, DY, DZ	0.5, 0.5, 0	0.5, 0.5, 0	0.5, 0.5, 0
Line 4: XL1, XL2, XL3	5,5,0	10,10,0	20,20,0
Line 5: CONDG, SIG	9.99x 0^{-5}, 1.09	9.99x10^{-5}, 1.09	9.99x10^{-5}, 1.09

Table A.4. Parametric input data of the random field generator

	CV = % 50, % 100, % 150 and h = 5 m, 10 m, 20m
Line 1: NLINE,DELZET,NZTEST	100, 0.1, 2000
Line 2: BIGK, DK	100, 0.25
Line 3: NMONT, IU, NL	10, 210467, 11
Line 4: CMIN, CMAX, NDELT	-3, 3, 20
Line 5: KS(J), J=1, 3	1, 1, 0
Line 6: ILOG	1
Line 7: NFILE, TFILE	NSCALEF.OUT TSCALEF.OUT

Table A.5. Physical input data of the random field generator for the anisotropic fields

	CV = 50 % h_x **= 10 m and** h_y **= 2 m**	**CV = 150 %** h_x **= 20 m and** h_y **= 4 m**
Line 1: IDATE, IRUN		
Line 2: NX, NY, NZ	301, 201, 0	301, 201, 0
Line 3: DX, DY, DZ	0.5, 0.5, 0	0.5, 0.5, 0
Line 4: XL1, XL2, XL3	10,2,0	20,4,0
Line 5: CONDG, SIG	1.61×10^{-4} 0.47	9.99×0^{-5}, 1.09

APPENDICES B – VALIDATION GRAPHS OF RANDOM FIELD GENERATOR

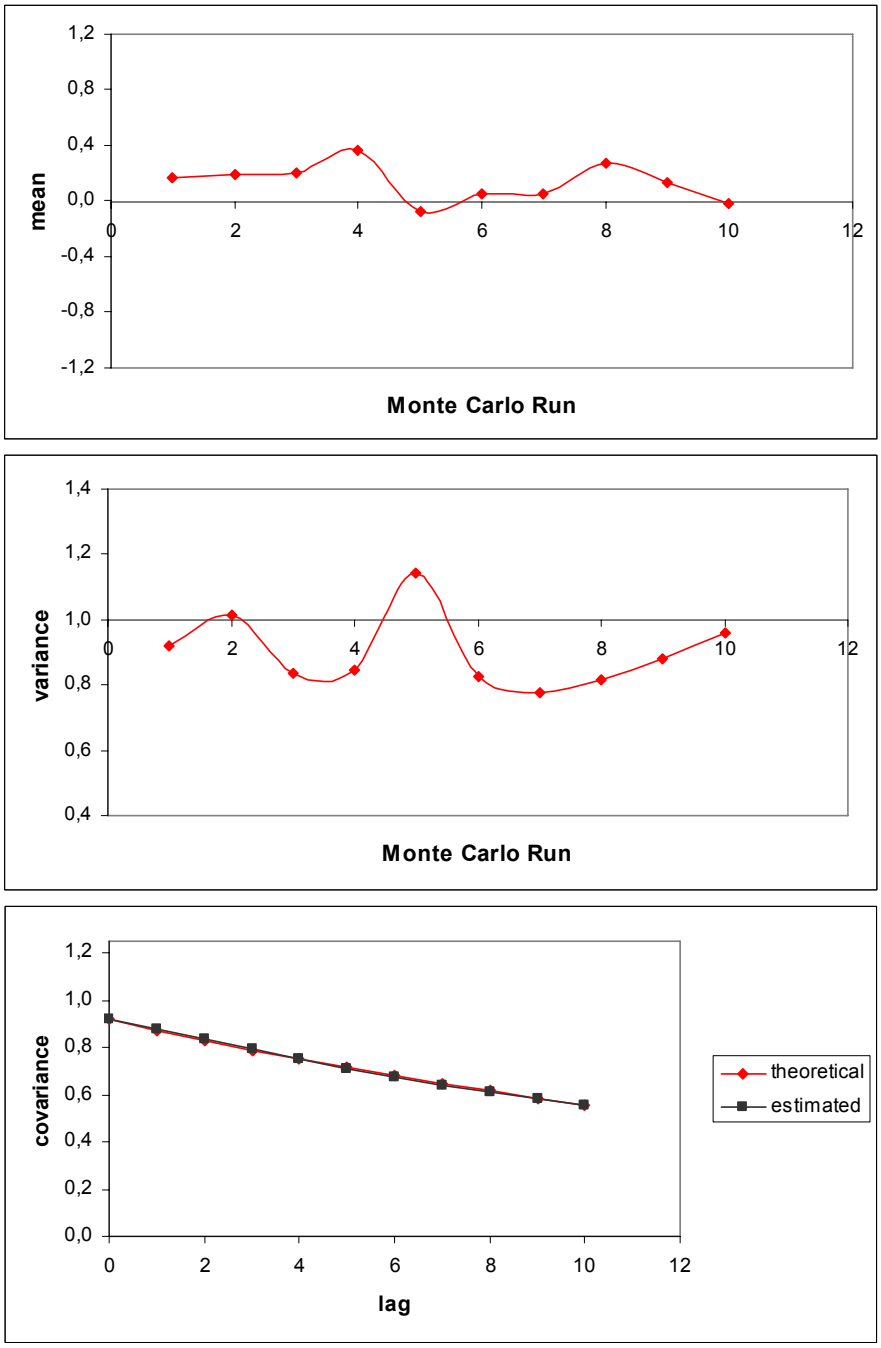

Figure B.1. Mean and variance and covariance estimate for the 10-replicate runs for the field having CV=%50 and h=10 m.

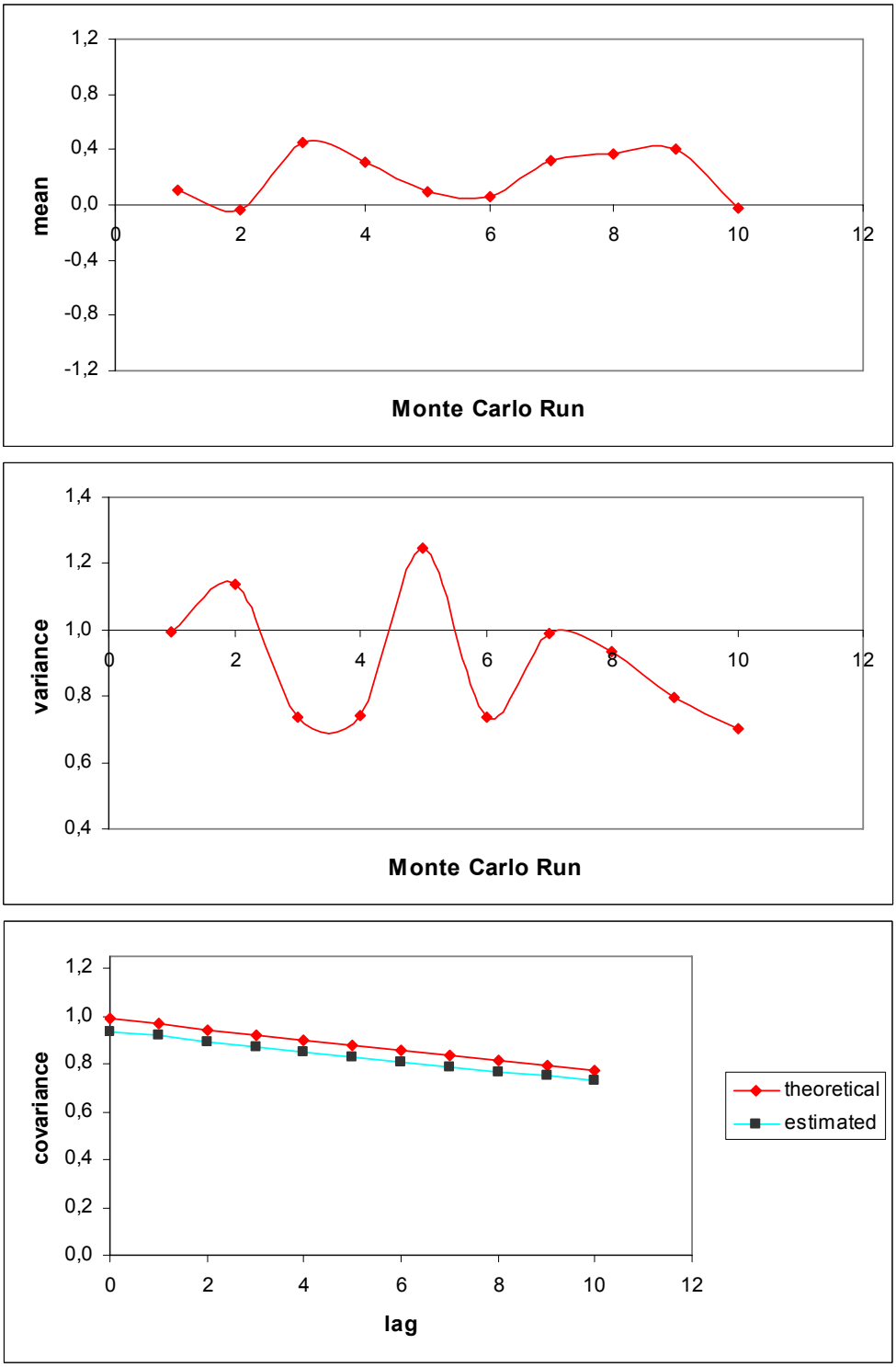

Figure B.2. Mean and variance and covariance estimate for the 10-replicate runs for the field having CV=%50 and h=20 m.

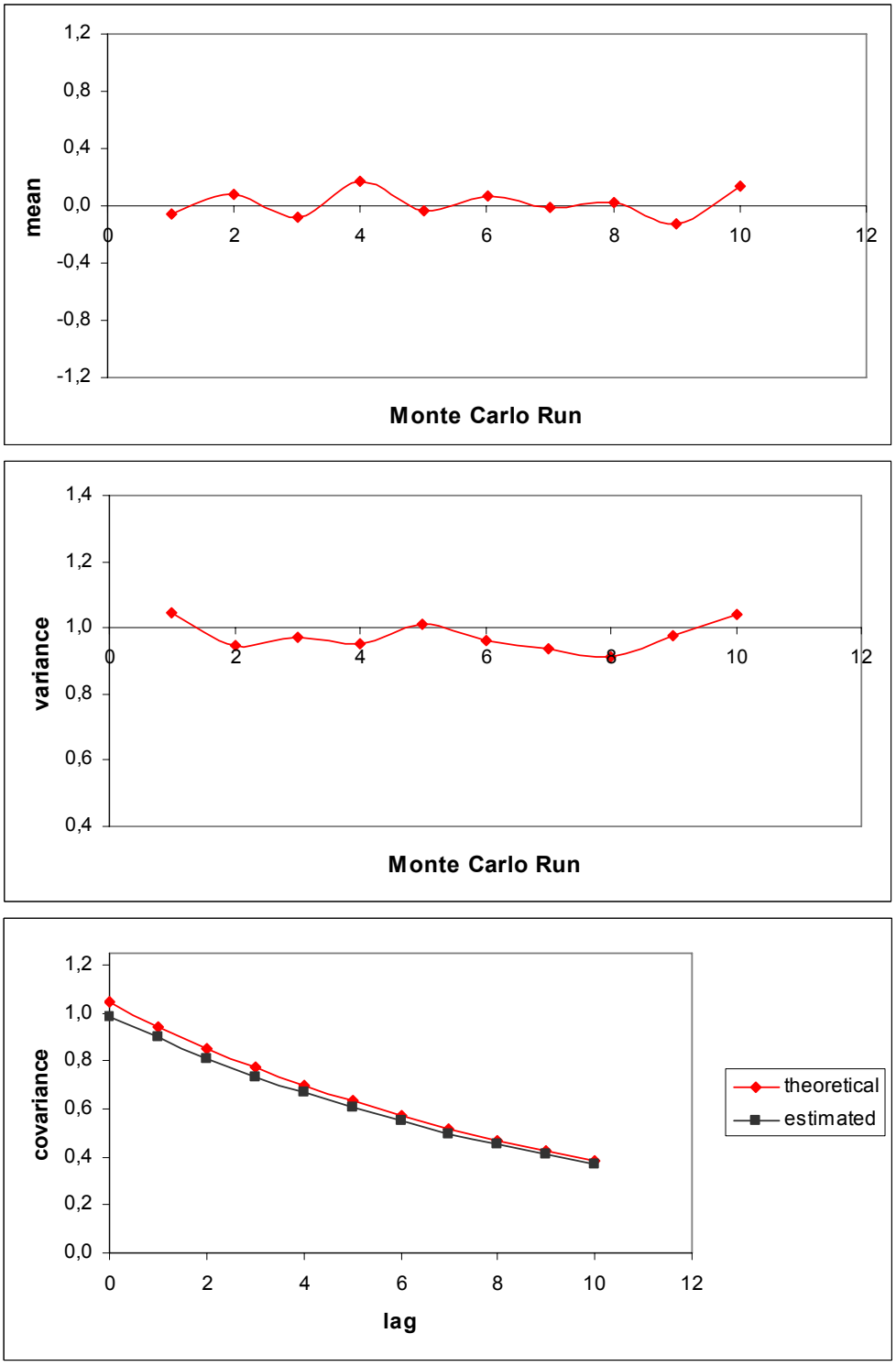

Figure B.3. Mean and variance and covariance estimate for the 10-replicate runs for the field having CV=%100 and h=5 m.

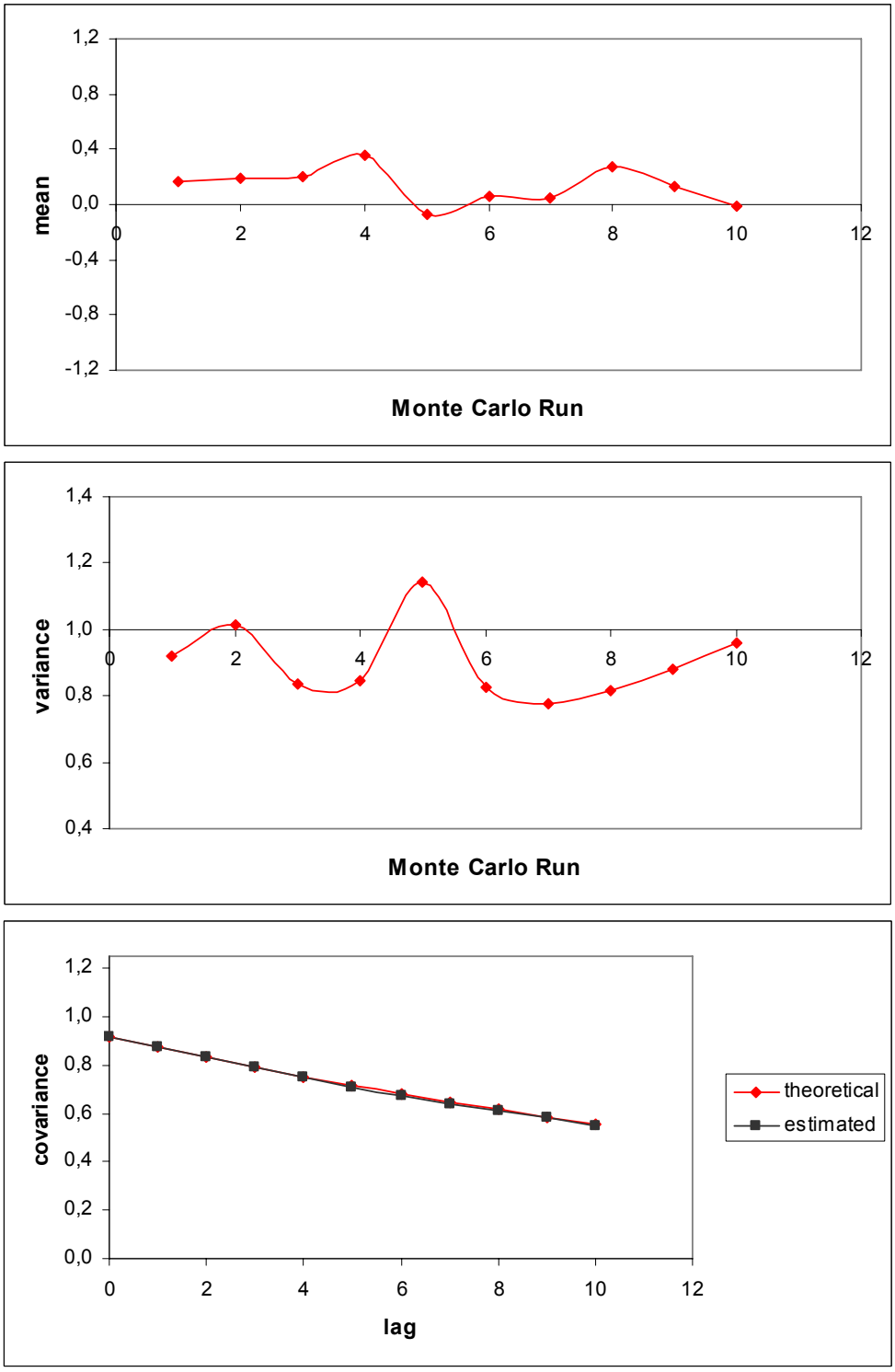

Figure B.4. Mean and variance and covariance estimate for the 10-replicate runs for the field having CV=%100 and h=10 m.

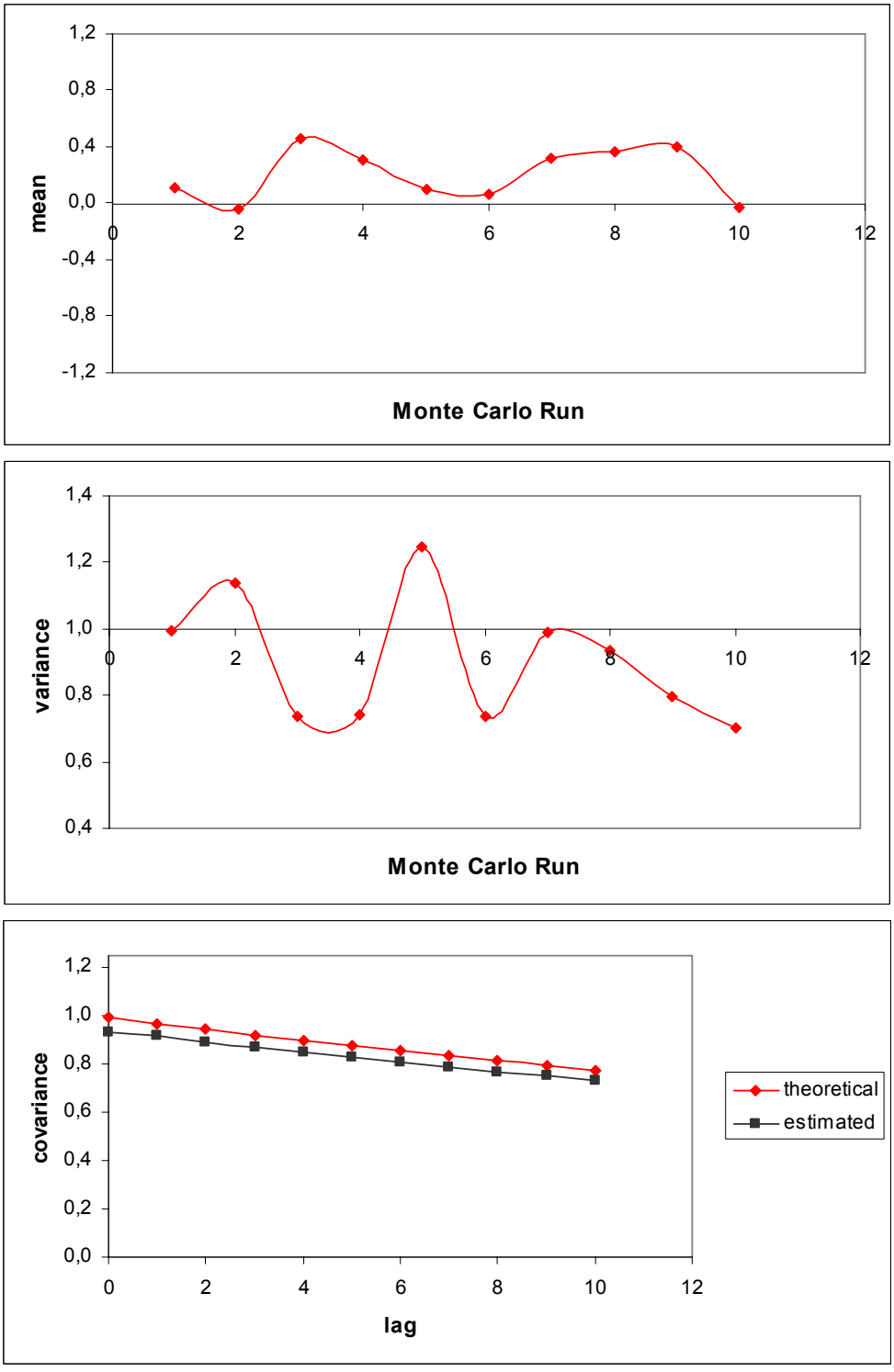

Figure B.5. Mean and variance and covariance estimate for the 10-replicate runs for the field having CV=%100 and h=20 m.

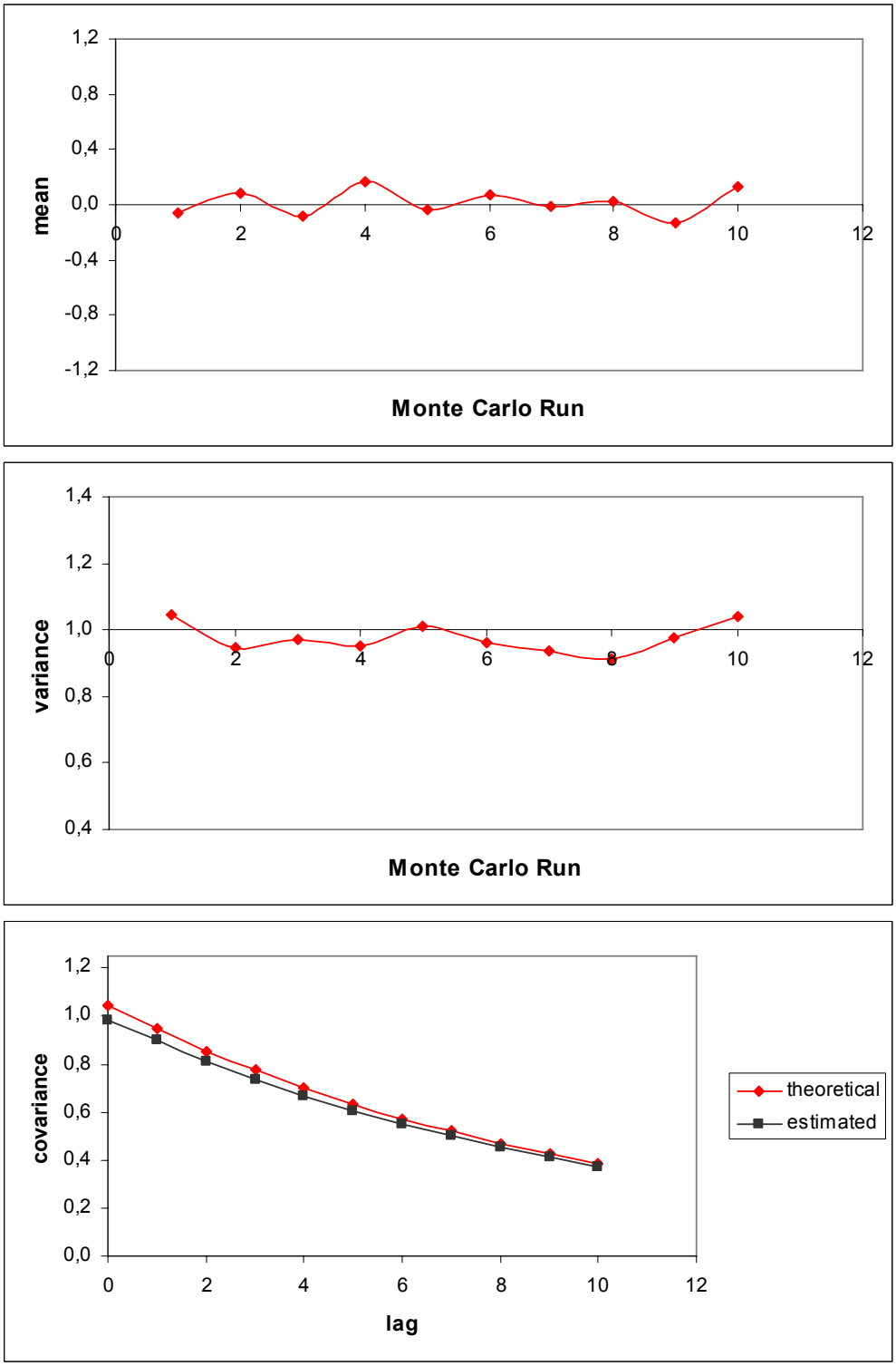

Figure B.6. Mean and variance and covariance estimate for the 10-replicate runs for the field having CV=%150 and h=5 m.

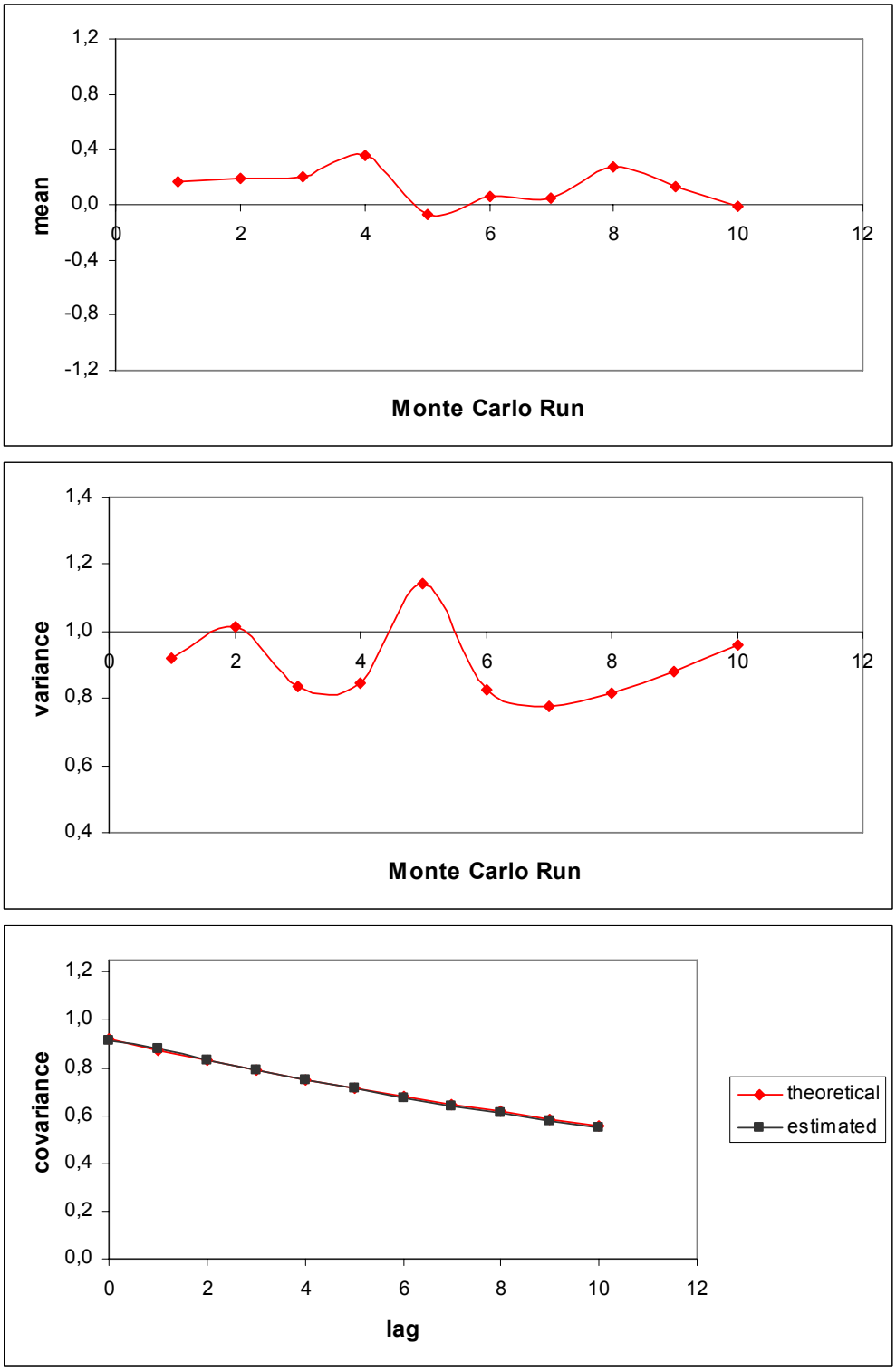

Figure B.7. Mean and variance and covariance estimate for the 10-replicate runs for the field having CV=%150 and h=10 m.

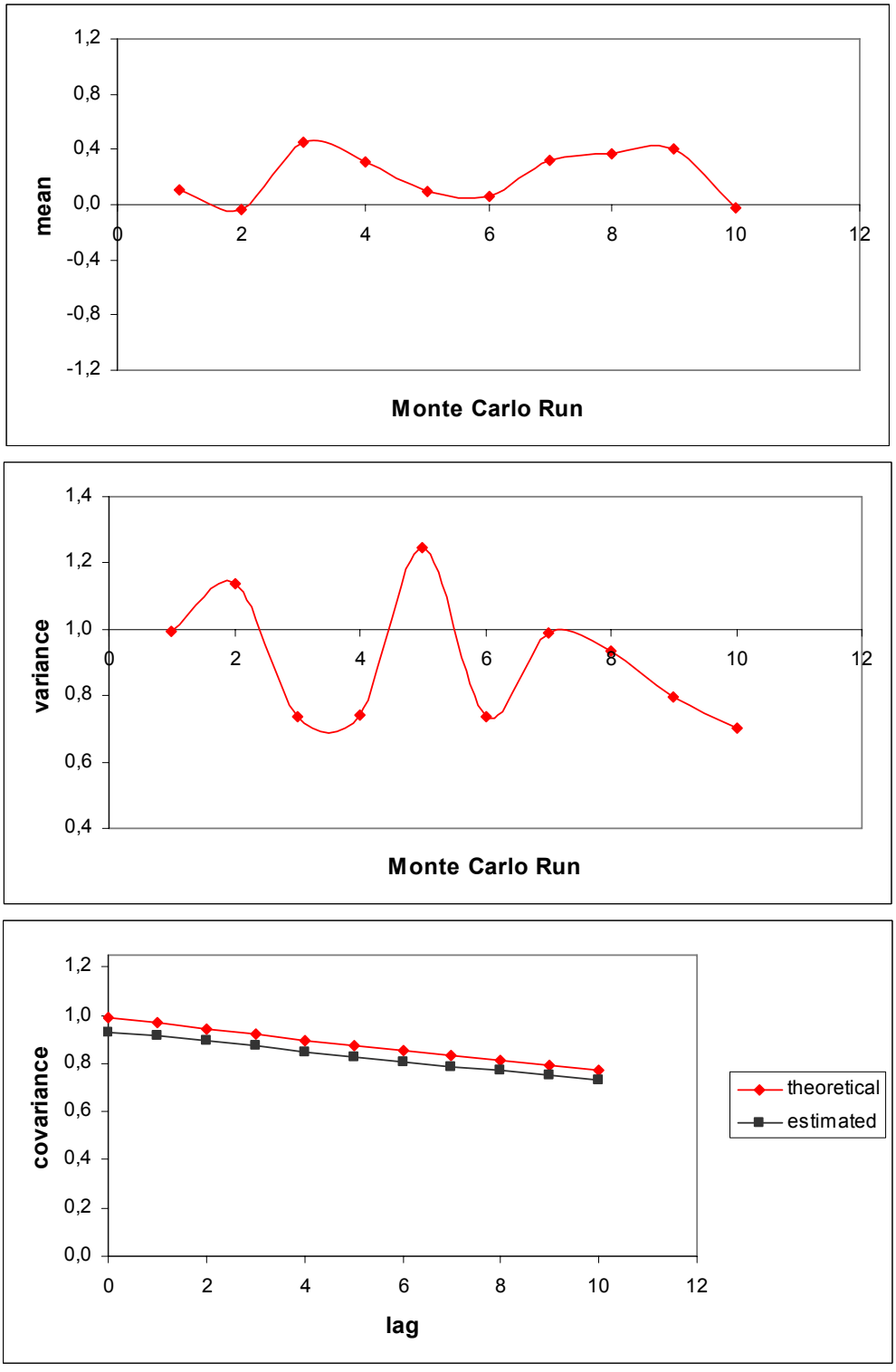

Figure B.8. Mean and variance and covariance estimate for the 10-replicate runs for the field having CV=%150 and h=20 m.

APPENDICES C – FATE and TRANSPORT of CHLORINATED SOLVENT PLUMES

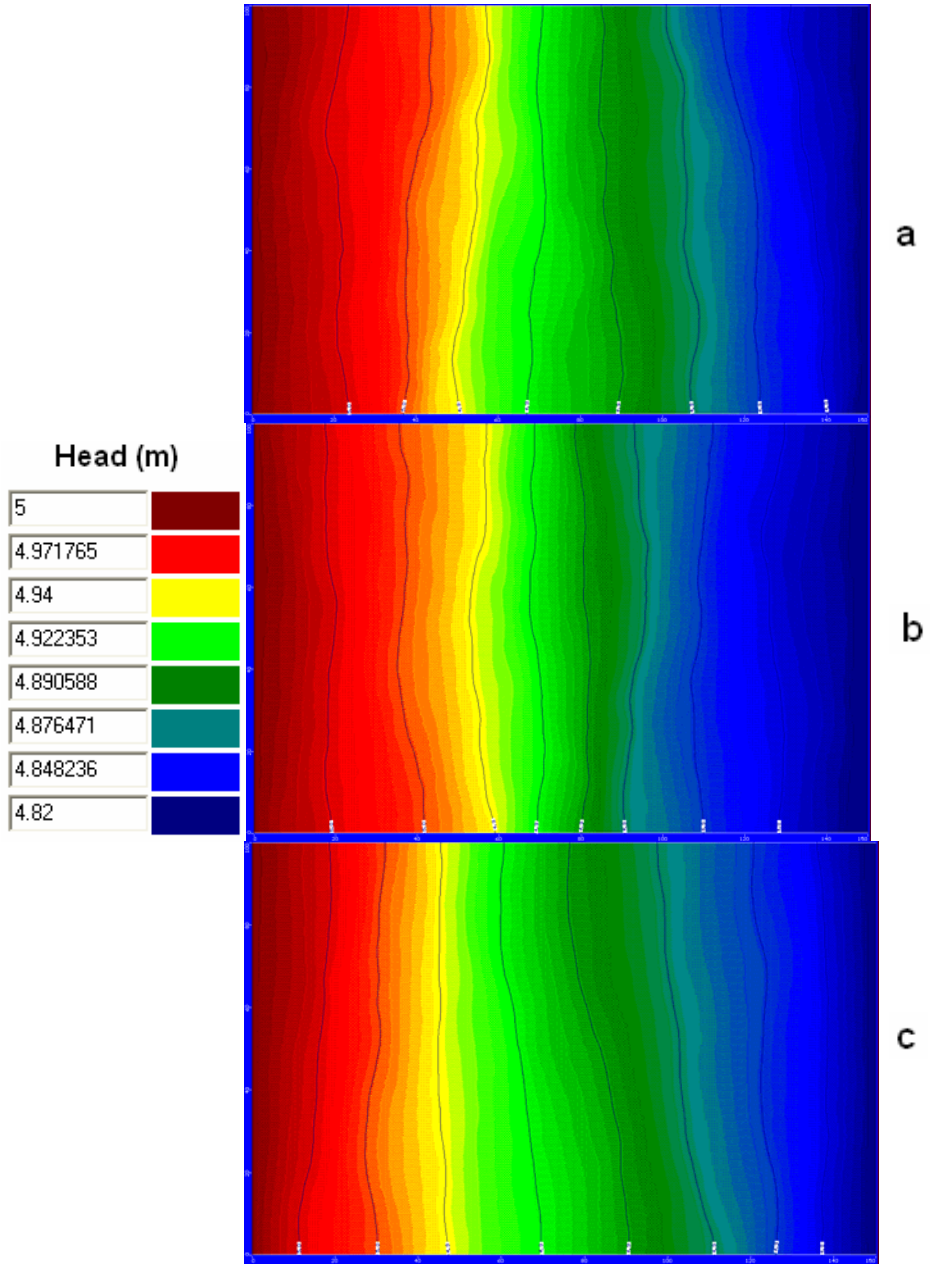

Figure C.1. Steady state head distribution for the isotropic field with CV = 50% and h = 5, 10 and 20 m.

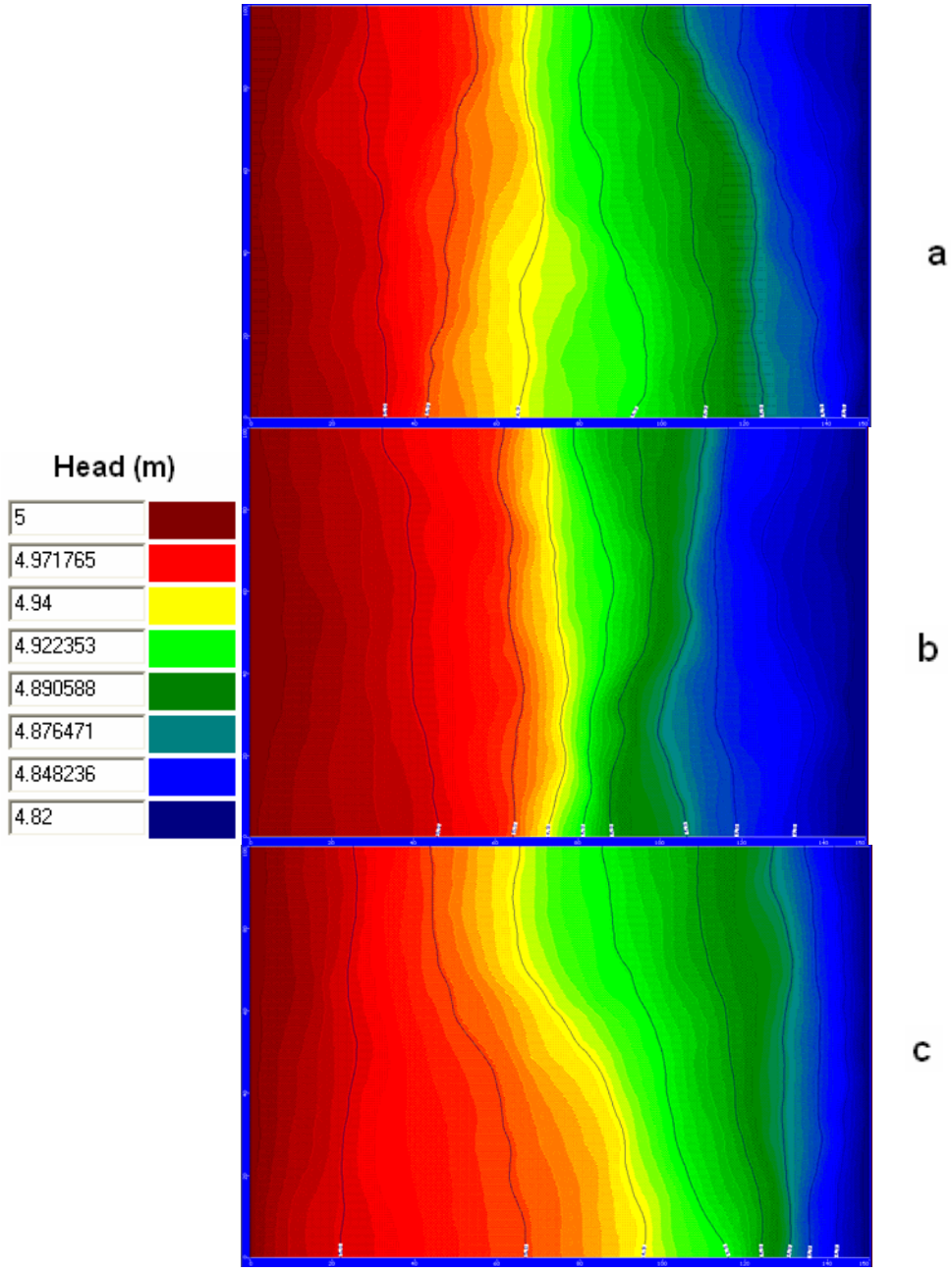

Figure C.2. Steady state head distribution for the isotropic field with CV = 100 % and h = 5, 10 and 20 m.

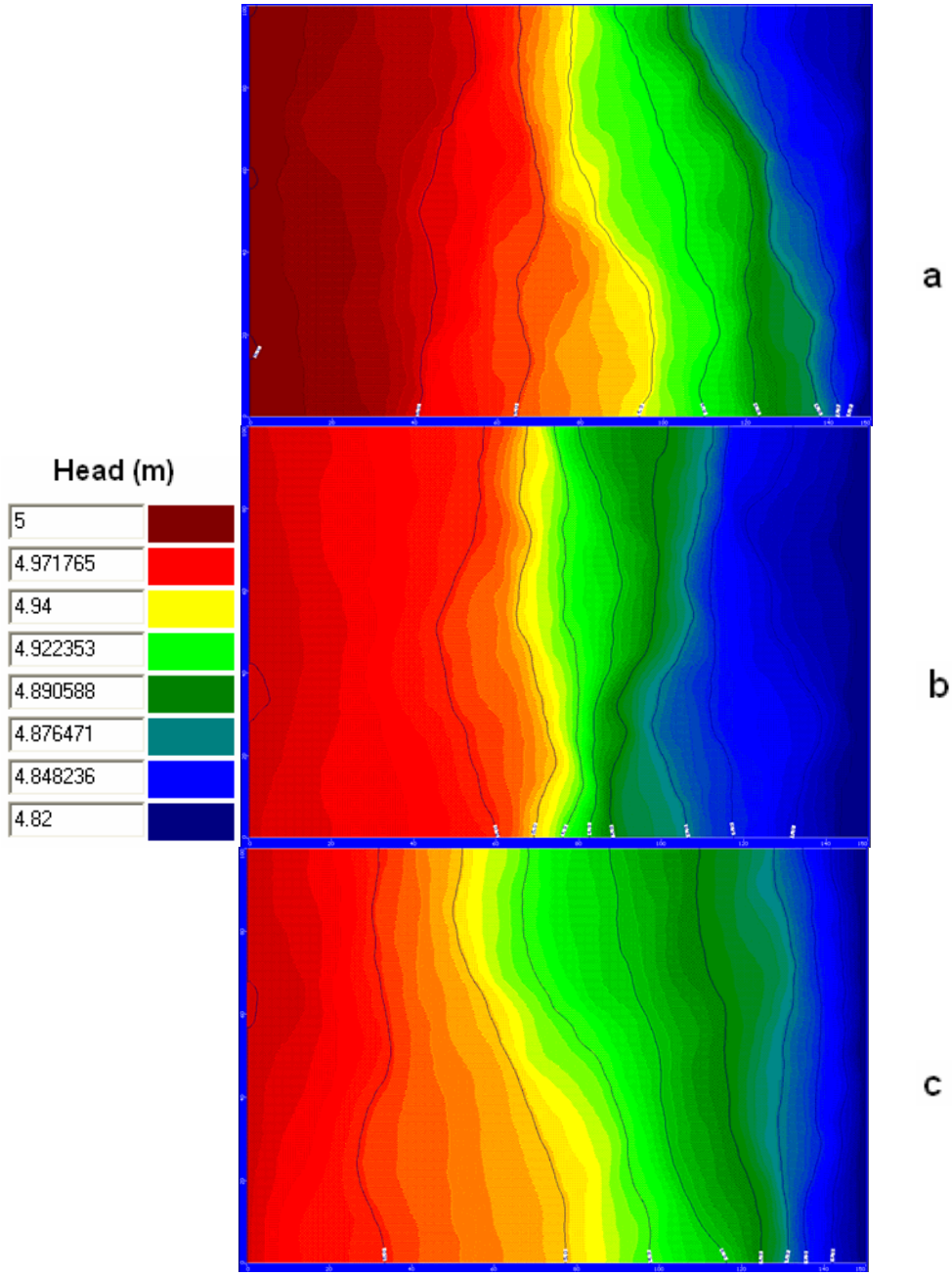

Figure C.3. Steady state head distribution for the isotropic field with CV = 150 % and h = 5, 10 and 20 m.

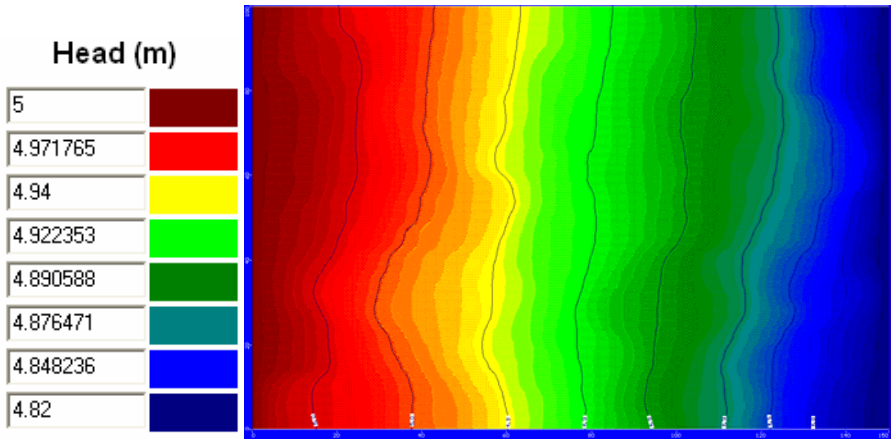

Figure C.4. Steady state head distribution for the anisotropic field with CV = % 50 and h_x = 10 m, h_y = 2 m

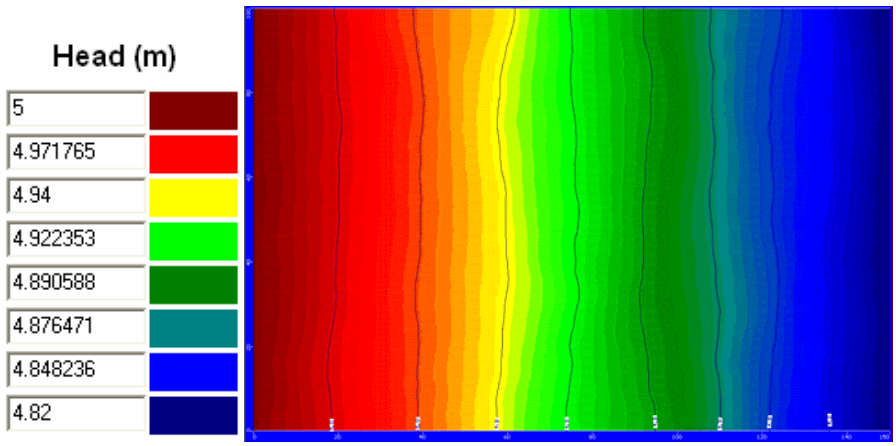

Figure C.5. Steady state head distribution for the anisotropic field with CV = % 150 and h_x = 20 m, h_y = 4 m

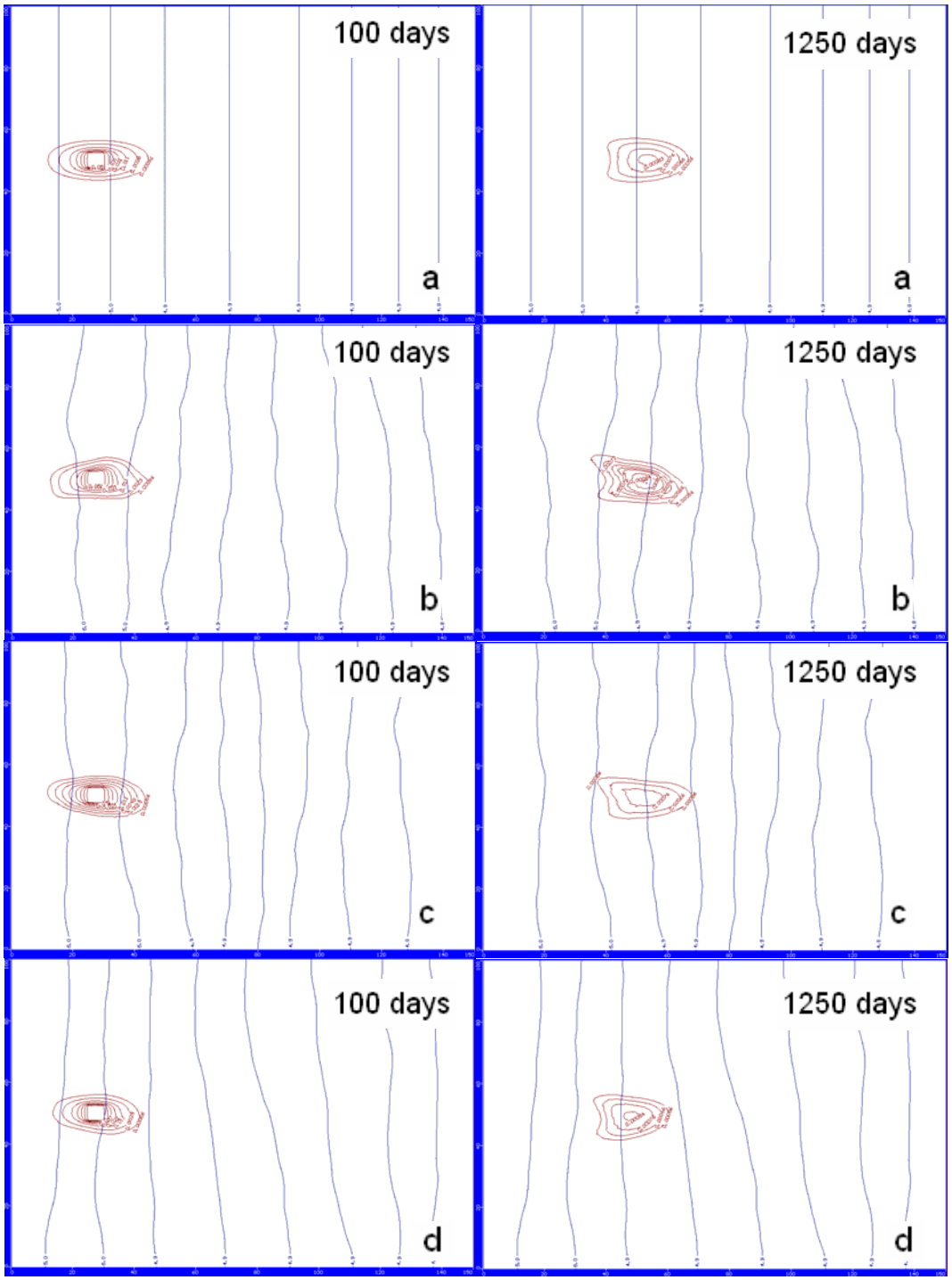

Figure C.6. PCE plumes at 100th and 1250th days for the uniform field and for (a) uniform field, (b) h= 5 m, (c) h= 10 m, (d) h= 20 m when CV = 50 %

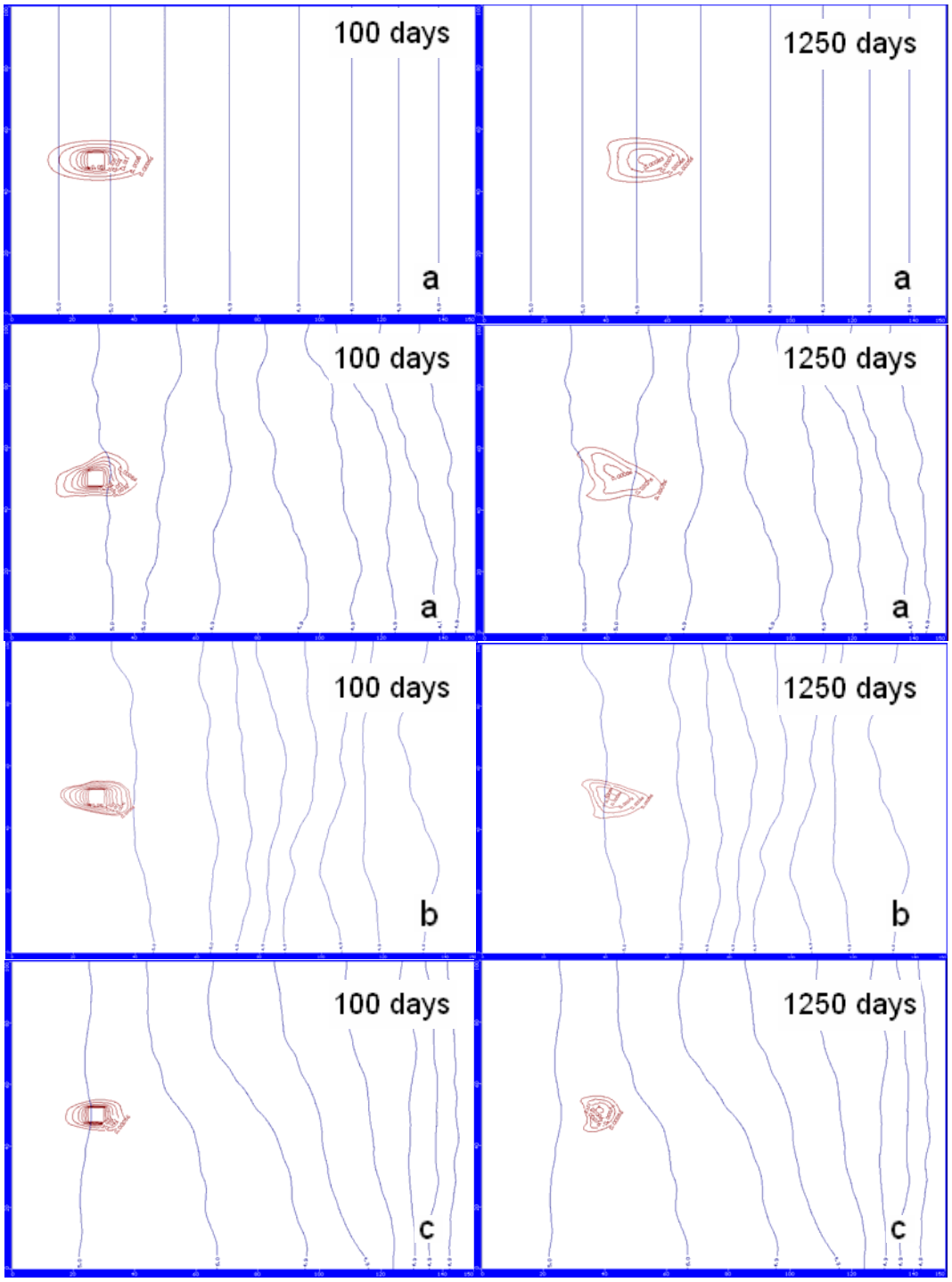

Figure C.7. PCE plumes at 100th and 1250th days for the uniform field and for (a) uniform field, (b) h= 5 m, (c) h= 10 m, (d) h= 20 m when CV = 100 %

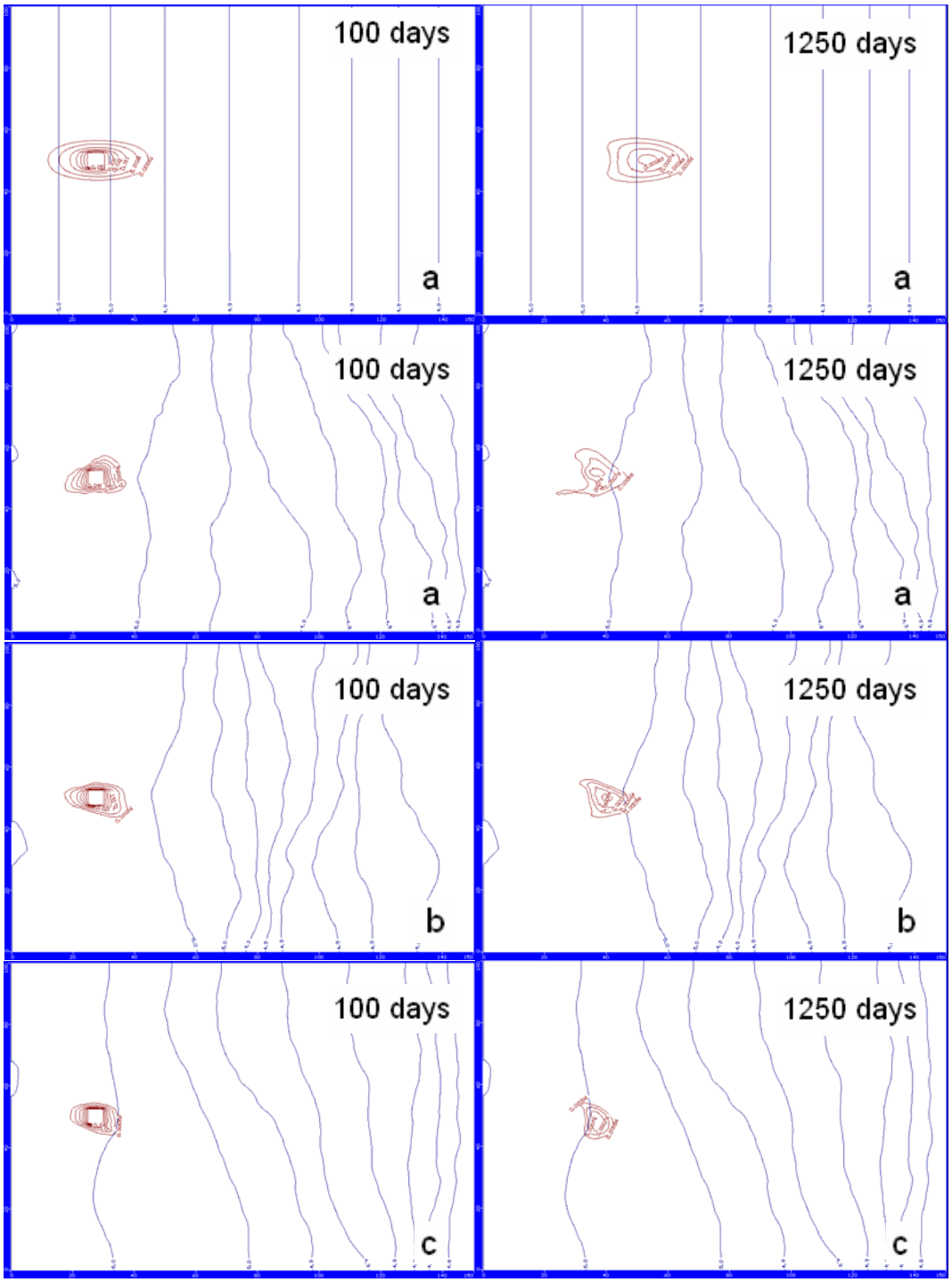

Figure C.8. PCE plumes at 100th and 1250th days for the uniform field and for (a) uniform field, (b) h= 5 m, (c) h= 10 m, (d) h= 20 m when CV = 150 %

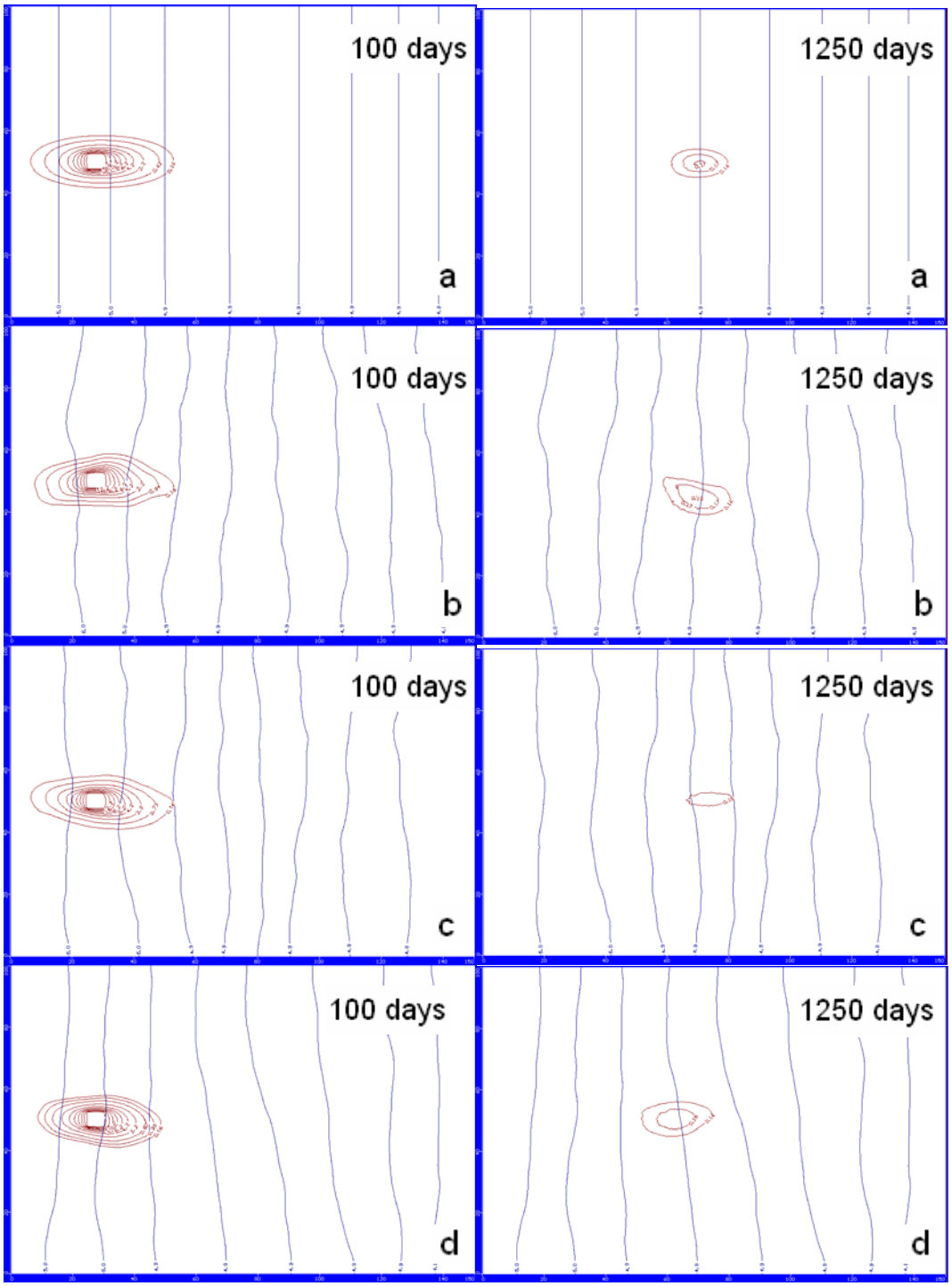

Figure C.9. TCE plumes at 100th and 1250th days for the uniform field and for (a) uniform field, (b) h= 5 m, (c) h= 10 m, (d) h= 20 m when CV = 50 %

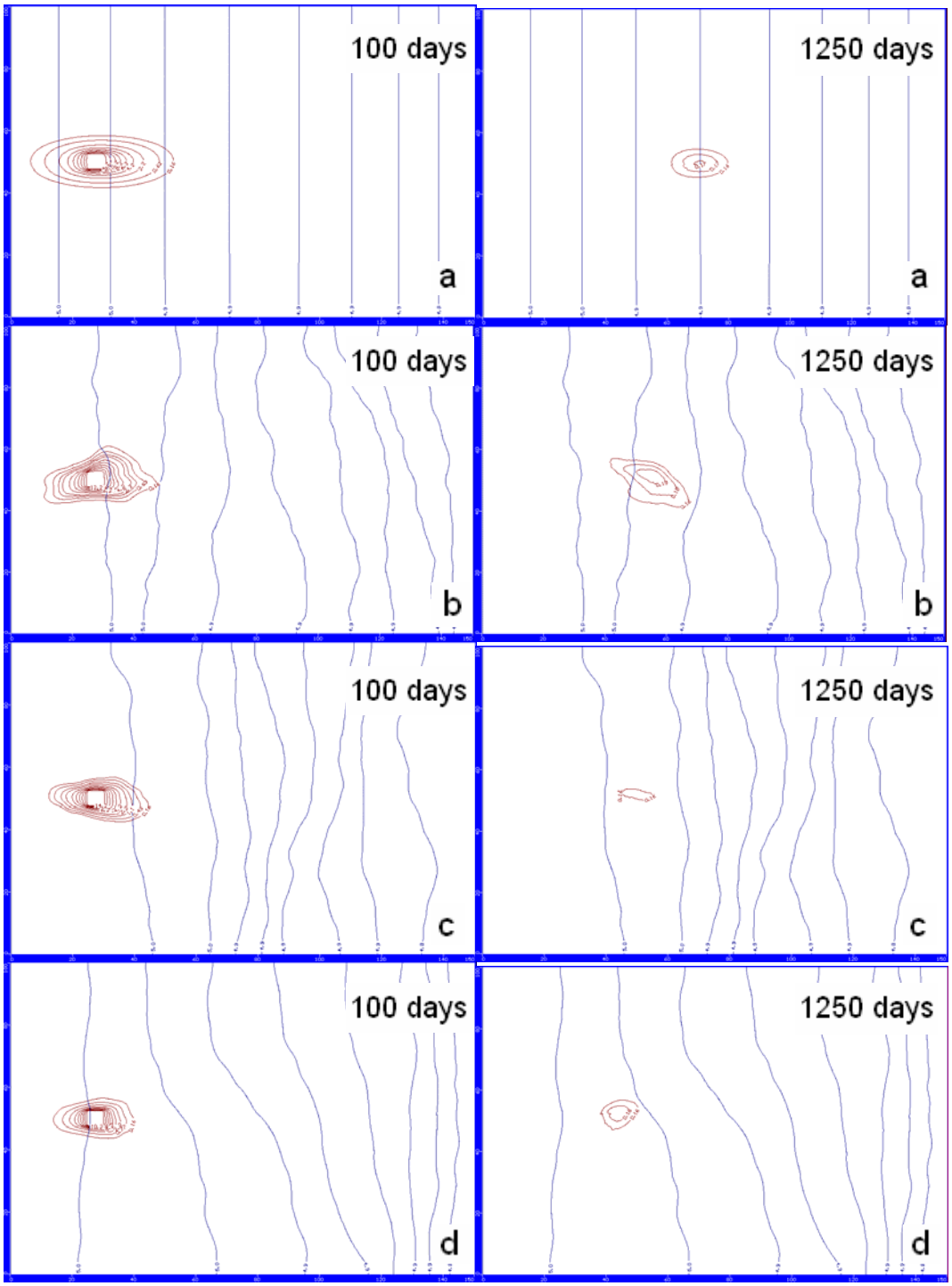

Figure C.10. TCE plumes at 100th and 1250th days for the uniform field and for (a) uniform field, (b) h= 5 m, (c) h= 10 m, (d) h= 20 m when CV = 100 %

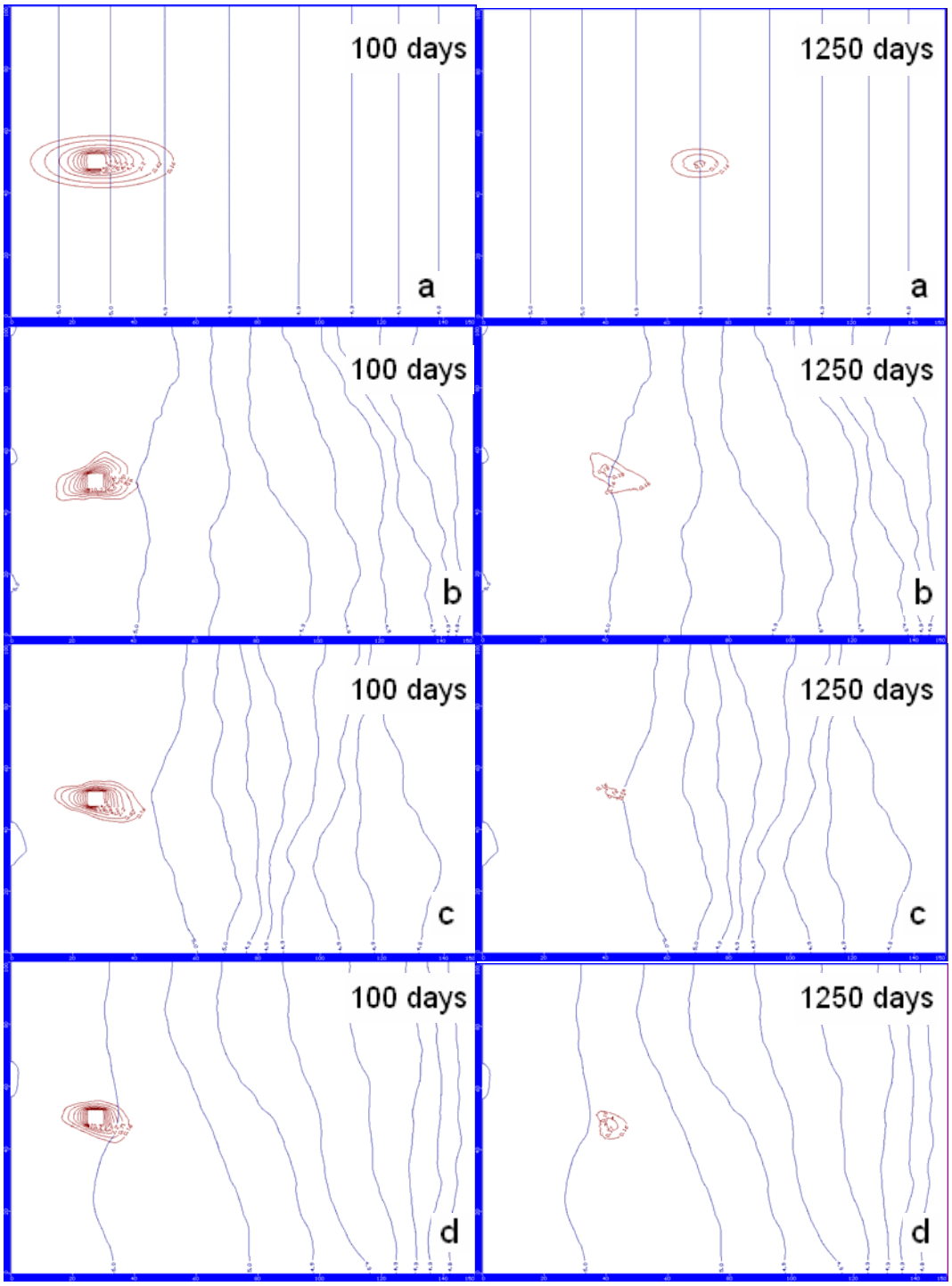

Figure C.11. TCE plumes at 100th and 1250th days for the uniform field and for (a) uniform field, (b) h= 5 m, (c) h= 10 m, (d) h= 20 m when CV = 150 %.

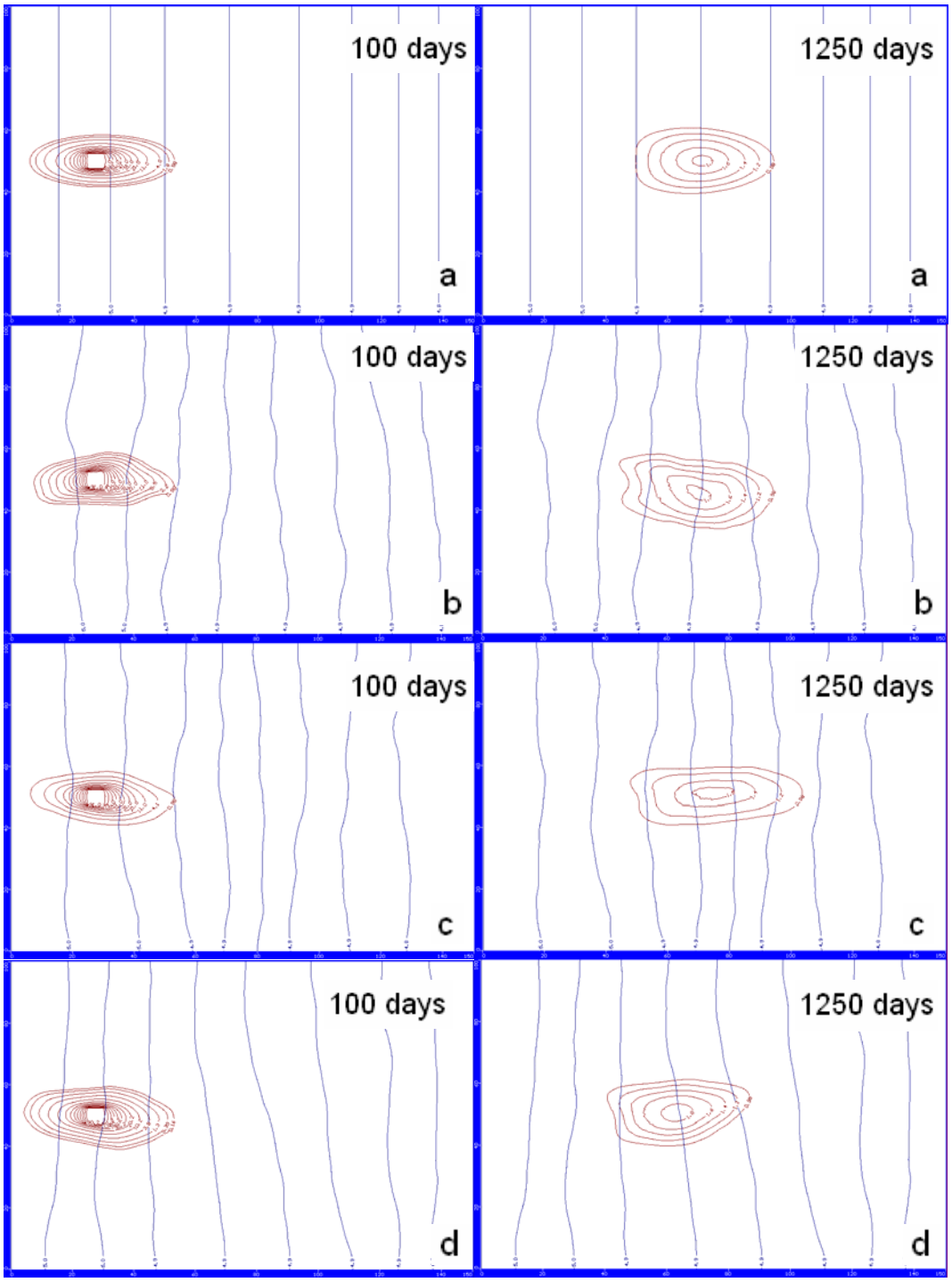

Figure C.12. DCE plumes at 100th and 1250th days for the uniform field and for (a) uniform field, (b) h= 5 m, (c) h= 10 m, (d) h= 20 m when CV = 50 %

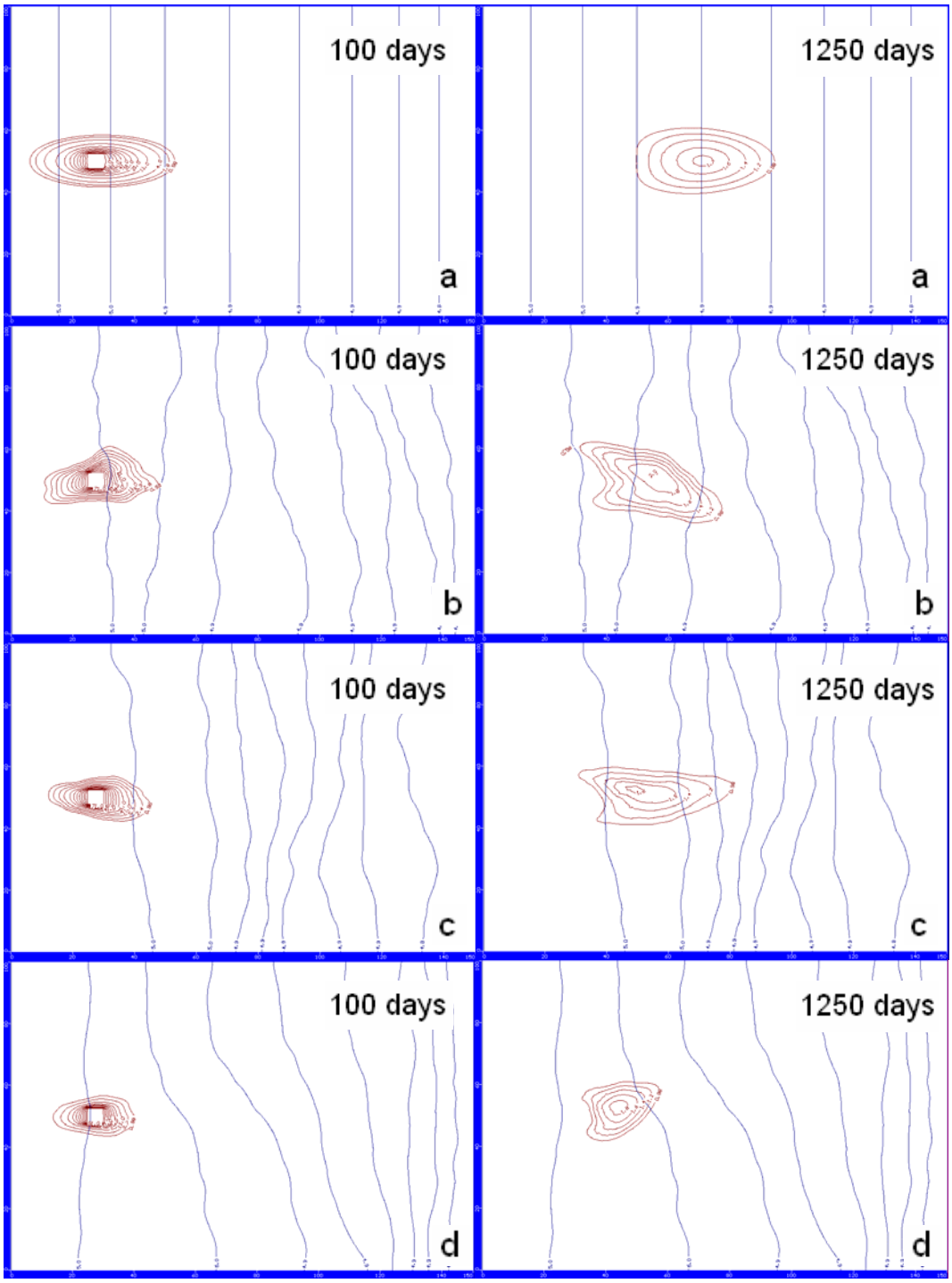

Figure C.13. DCE plumes at 100th and 1250th days for the uniform field and for (a) uniform field, (b) h= 5 m, (c) h= 10 m, (d) h= 20 m when CV = 100 %

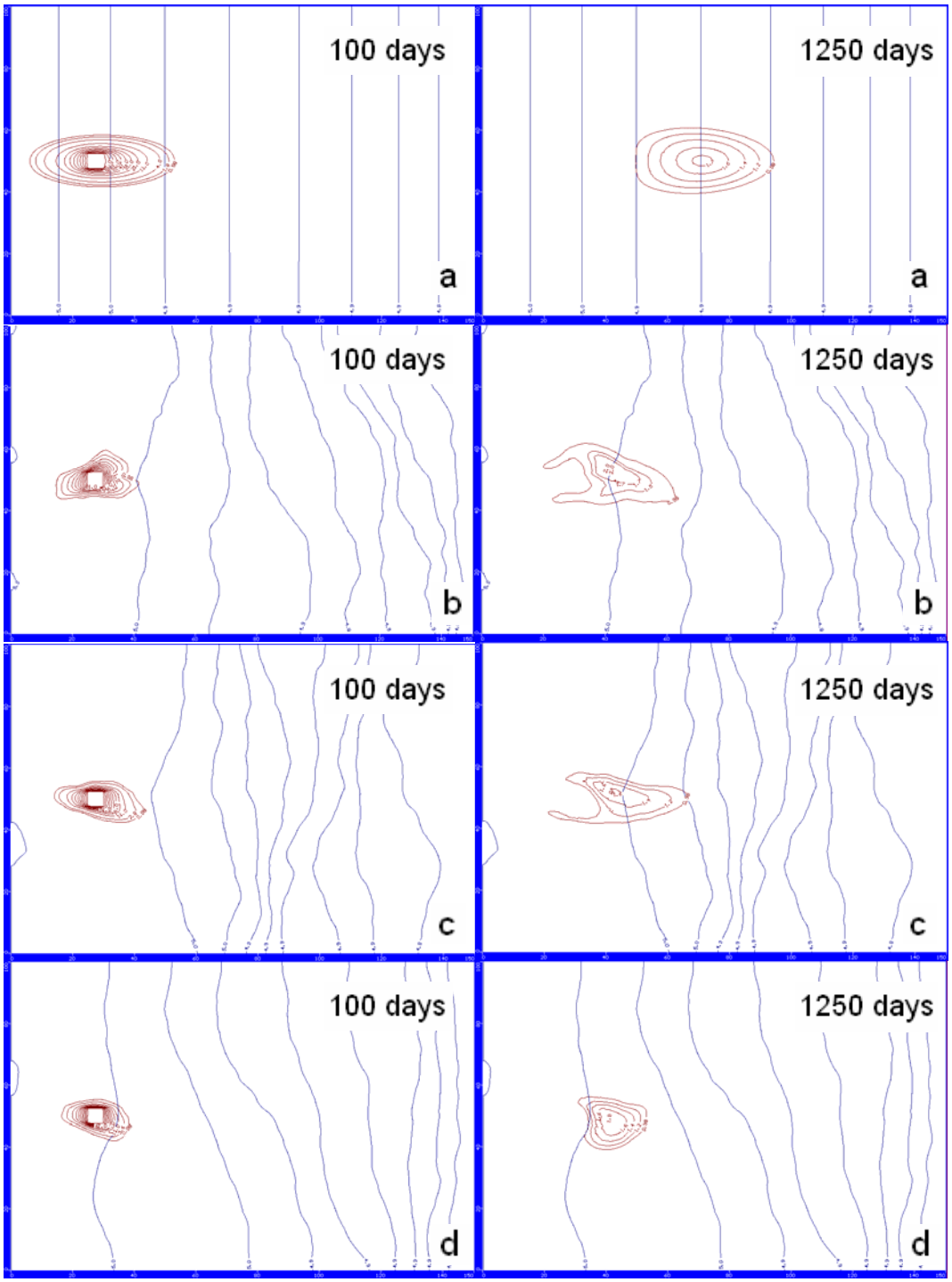

Figure C.14. DCE plumes at 100th and 1250th days for the uniform field and for (a) uniform field, (b) h= 5 m, (c) h= 10 m, (d) h= 20 m when CV = 150 %

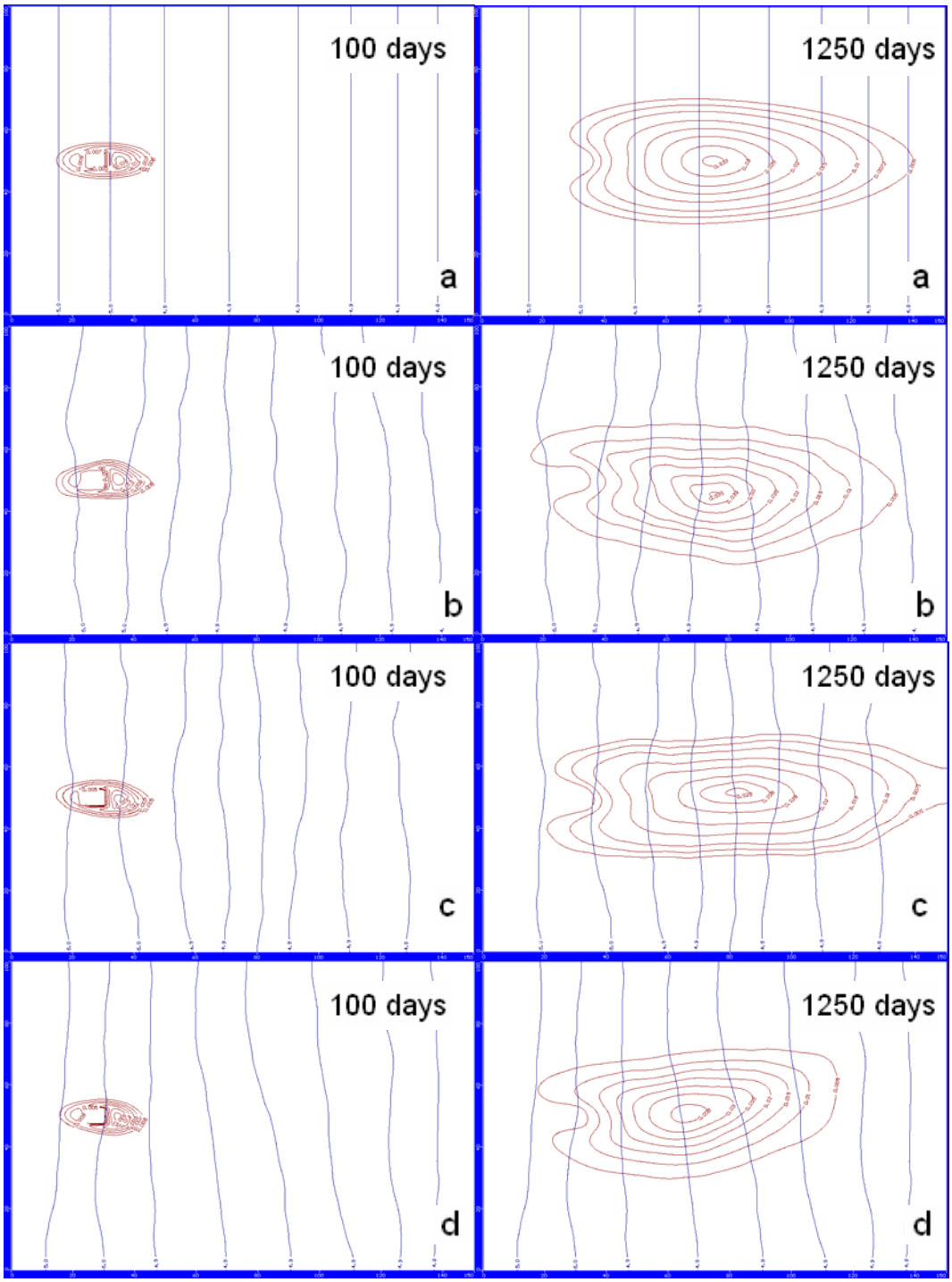

Figure C.15. ETH plumes at 100th and 1250th days for the uniform field and for (a) uniform field, (b) h= 5 m, (c) h= 10 m, (d) h= 20 m when CV = 50 %

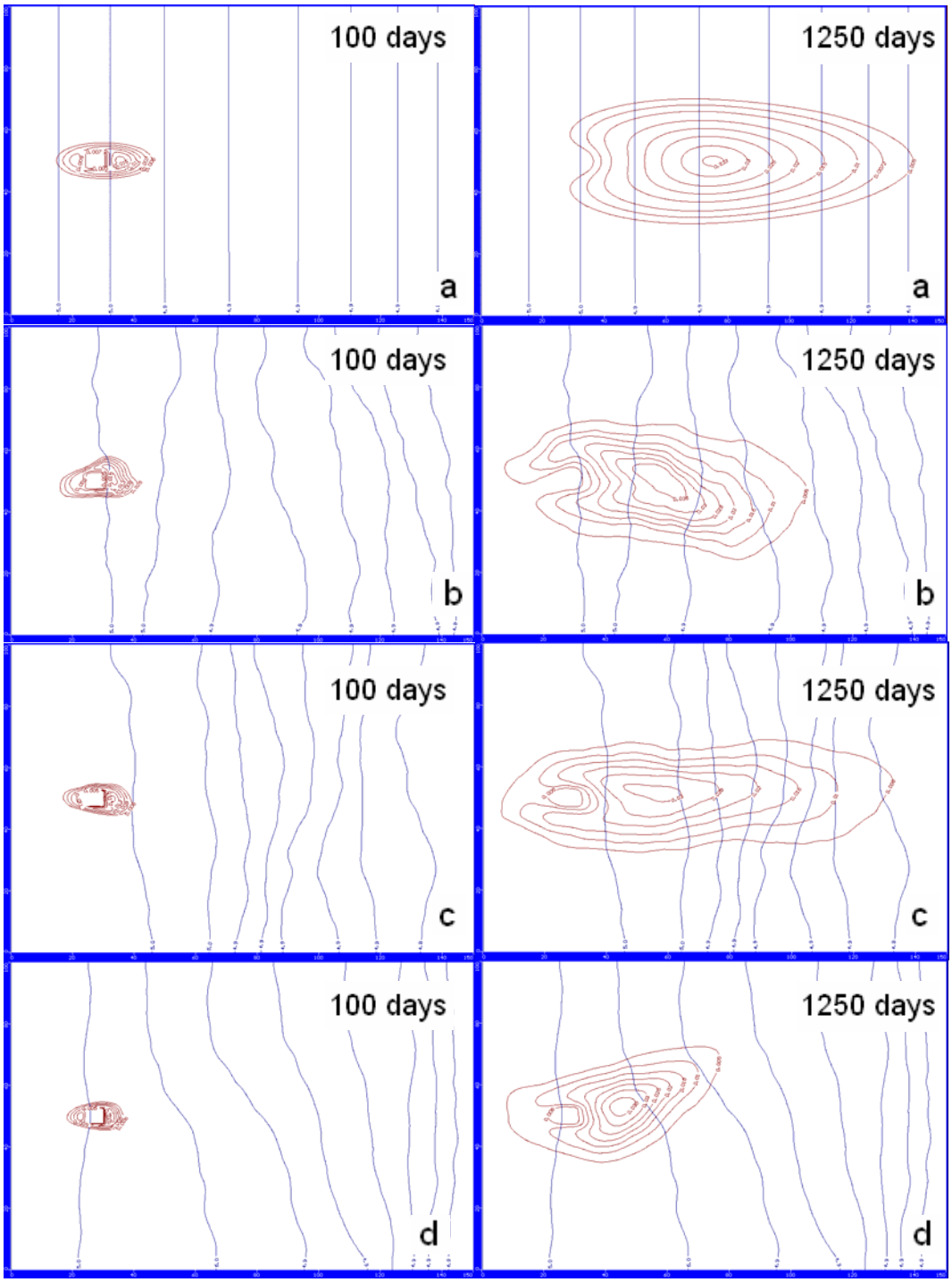

Figure C.16. ETH plumes at 100th and 1250th days for the uniform field and for (a) uniform field, (b) h= 5 m, (c) h= 10 m, (d) h= 20 m when CV = 100 %

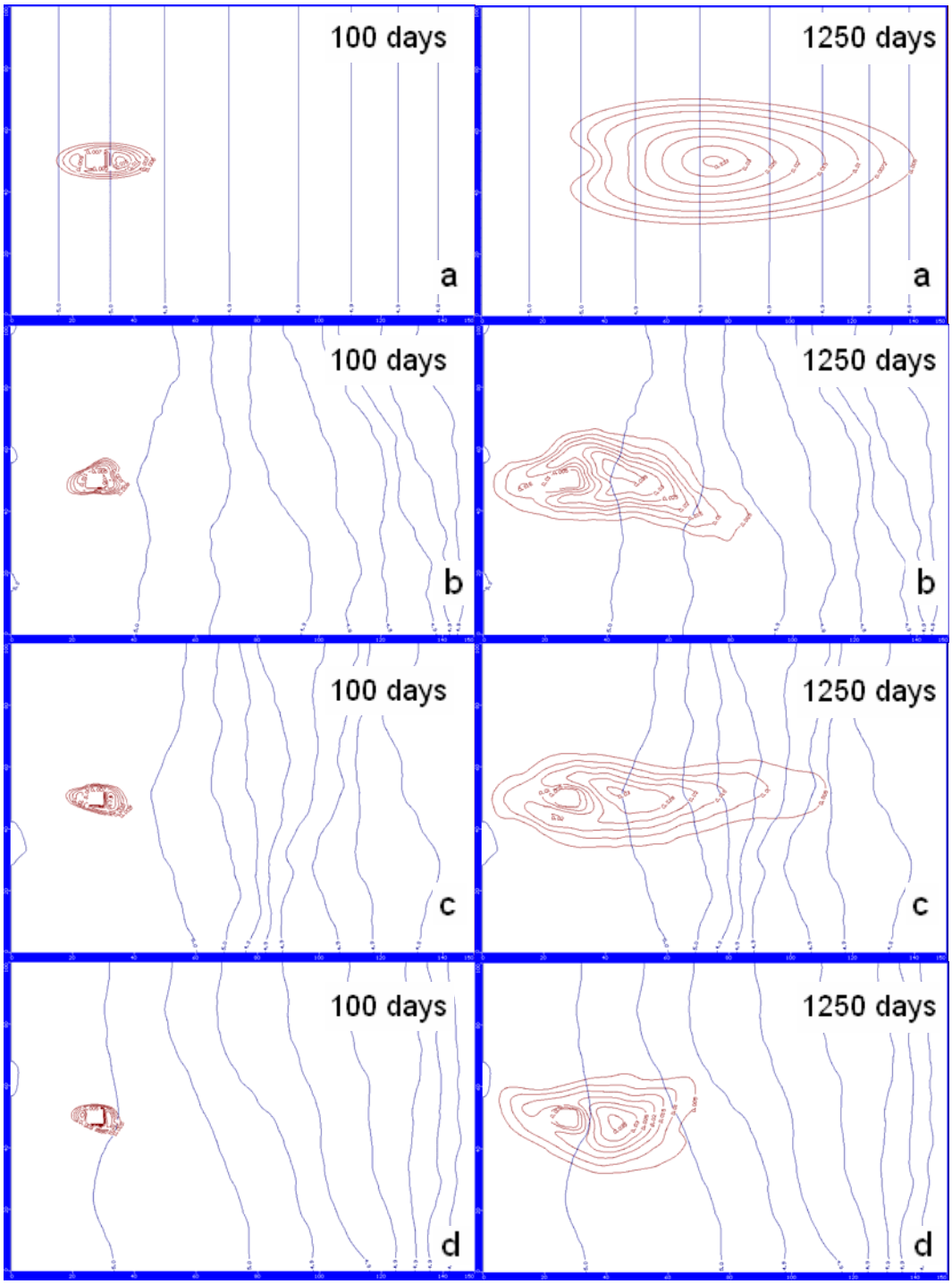

Figure C.17. ETH plumes at 100th and 1250th days for the uniform field and for (a) uniform field, (b) h= 5 m, (c) h= 10 m, (d) h= 20 m when CV = 150 %

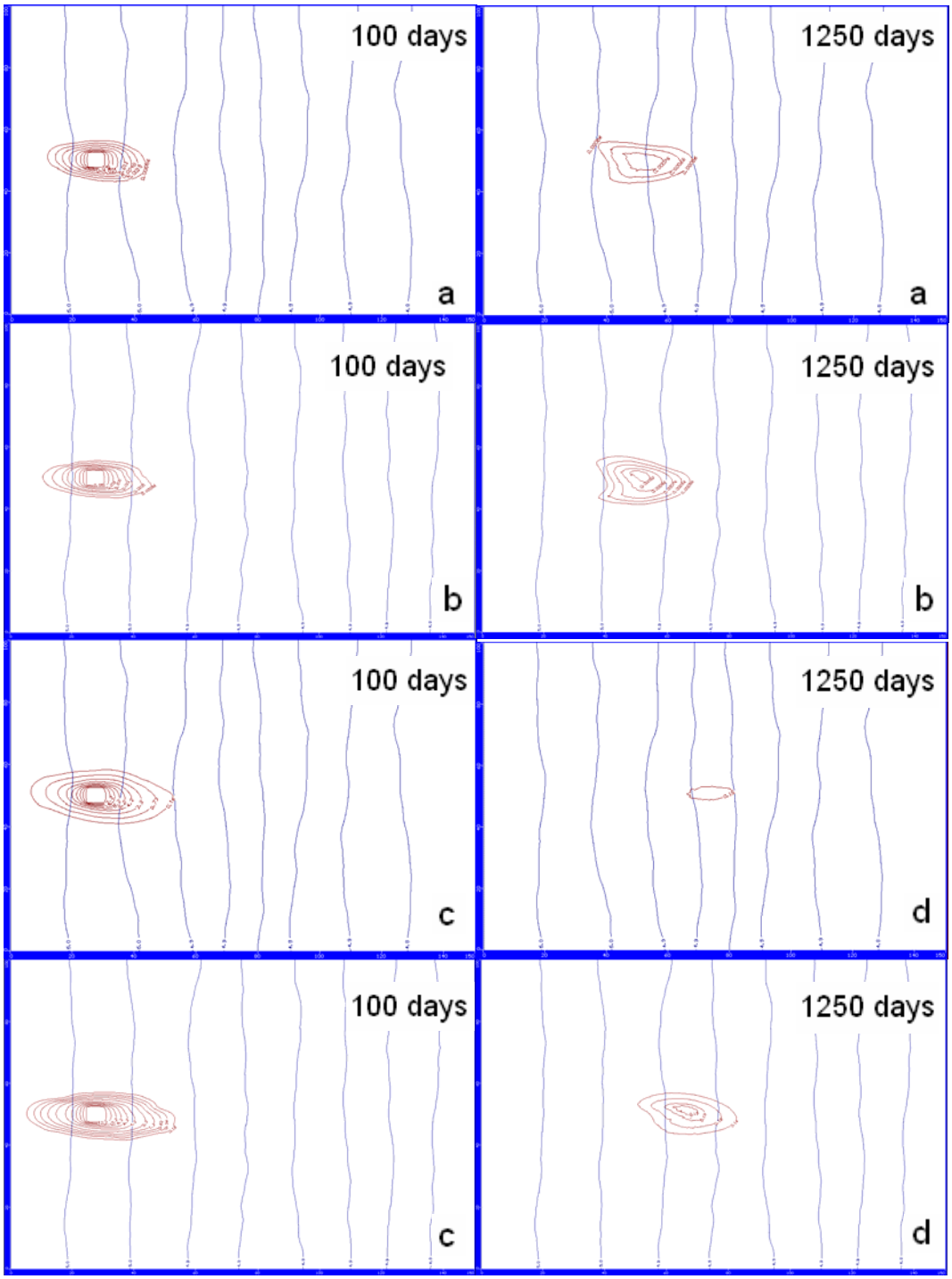

Figure C.18. PCE plumes at 100th and 1250th days for (a) h = 10 m, (b) h_x = 10 m, h_y = 2 m when CV = 50 % and TCE plumes at 100th and 1250th days for (c) h = 10 m, (d) h_x = 10 m, h_y = 2 m when CV = 50 %

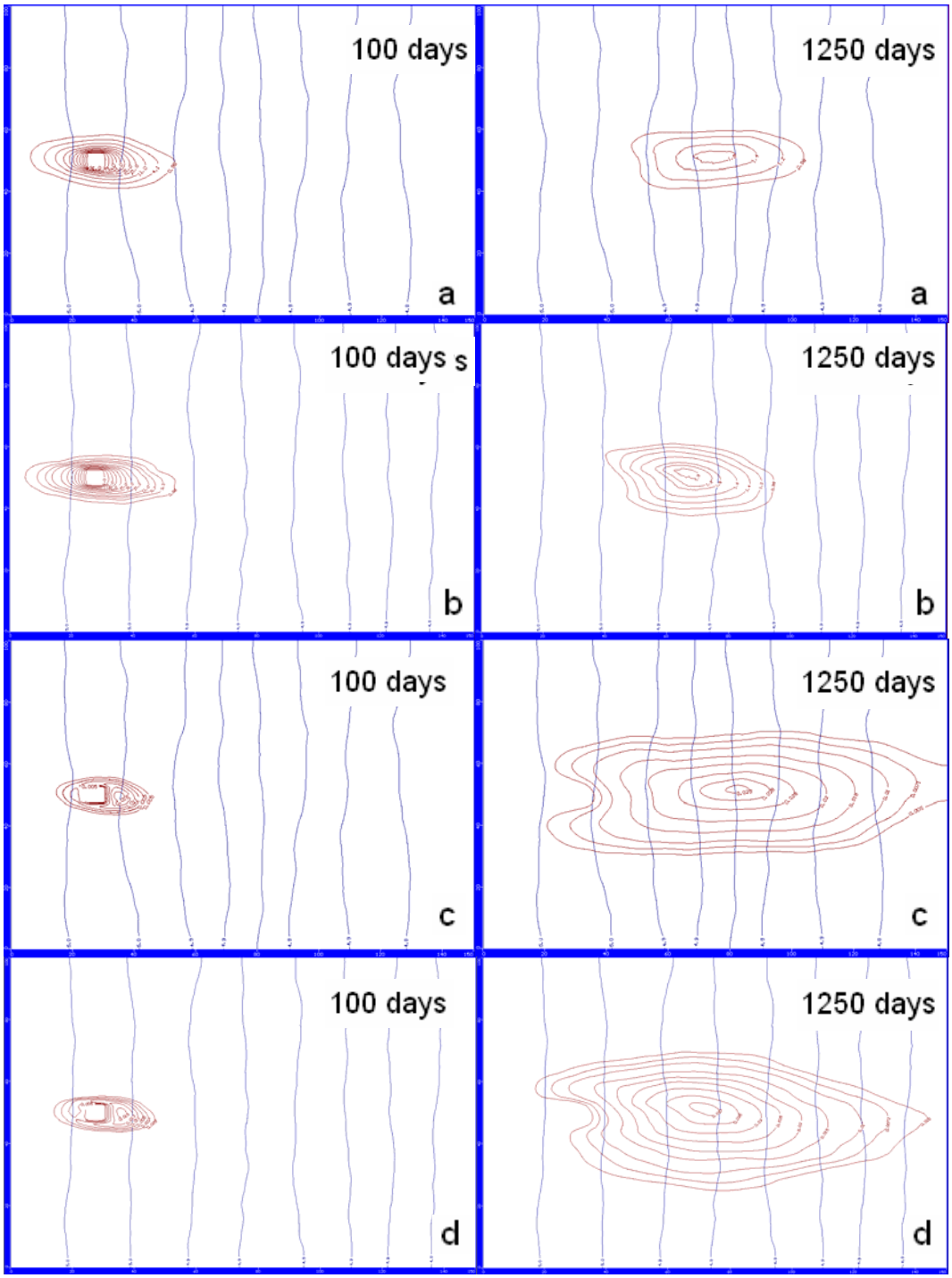

Figure C.19. DCE plumes at 100th and 1250th days for (a) h = 10 m, (b) h_x = 10 m, h_y = 2 m when CV = 50 % and ETH plumes at 100th and 1250th days for (c) h = 10 m, (d) h_x = 10 m, h_y = 2 m when CV = 50 %

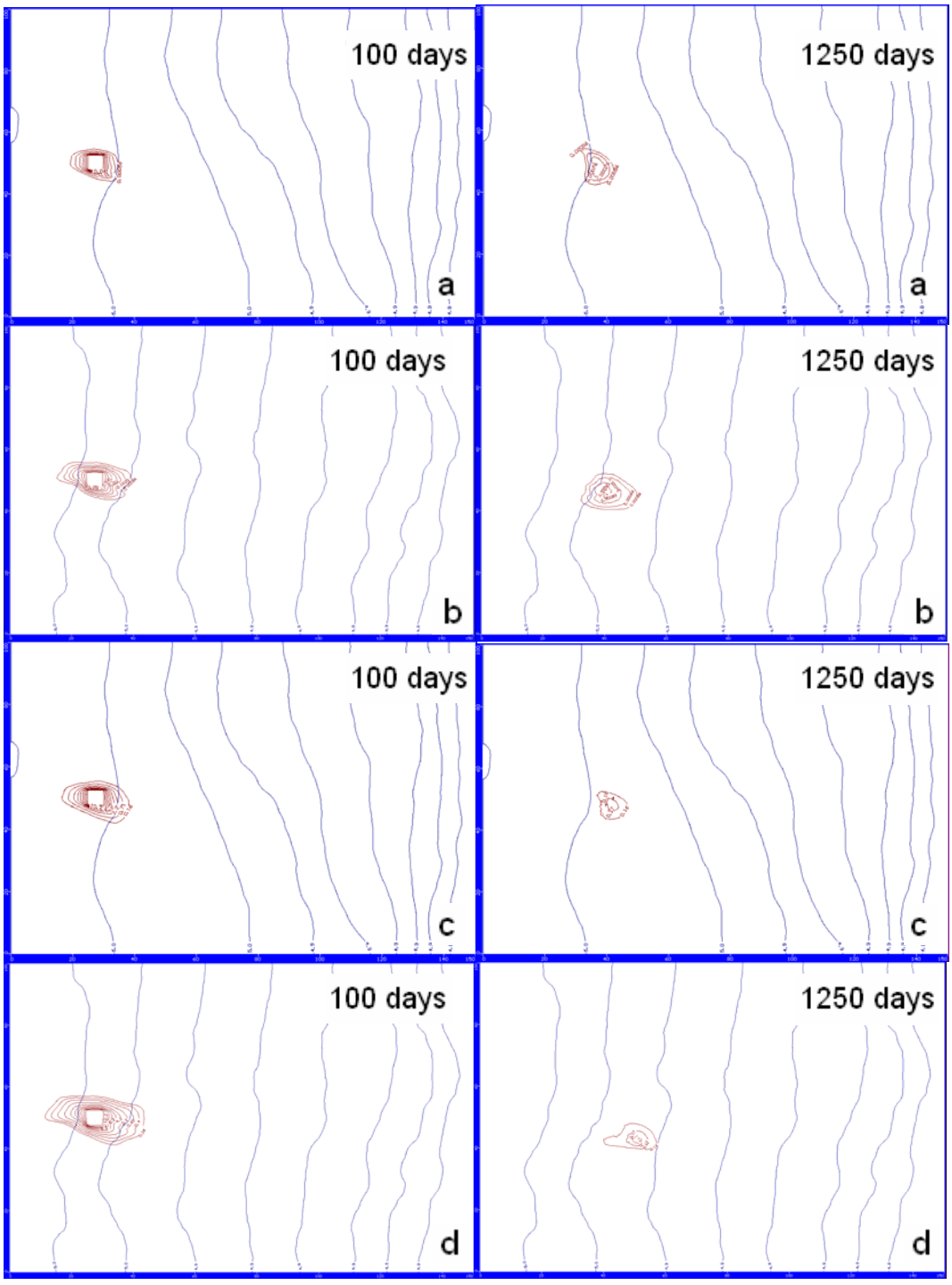

Figure C.20. PCE plumes at 100th and 1250th days for (a) h = 10 m, (b) h_x = 10 m, h_y = 2 m when CV = 50 % and TCE plumes at 100th and 1250th days for (c) h = 10 m, (d) h_x = 20 m, h_y = 4 m when CV = 150 %

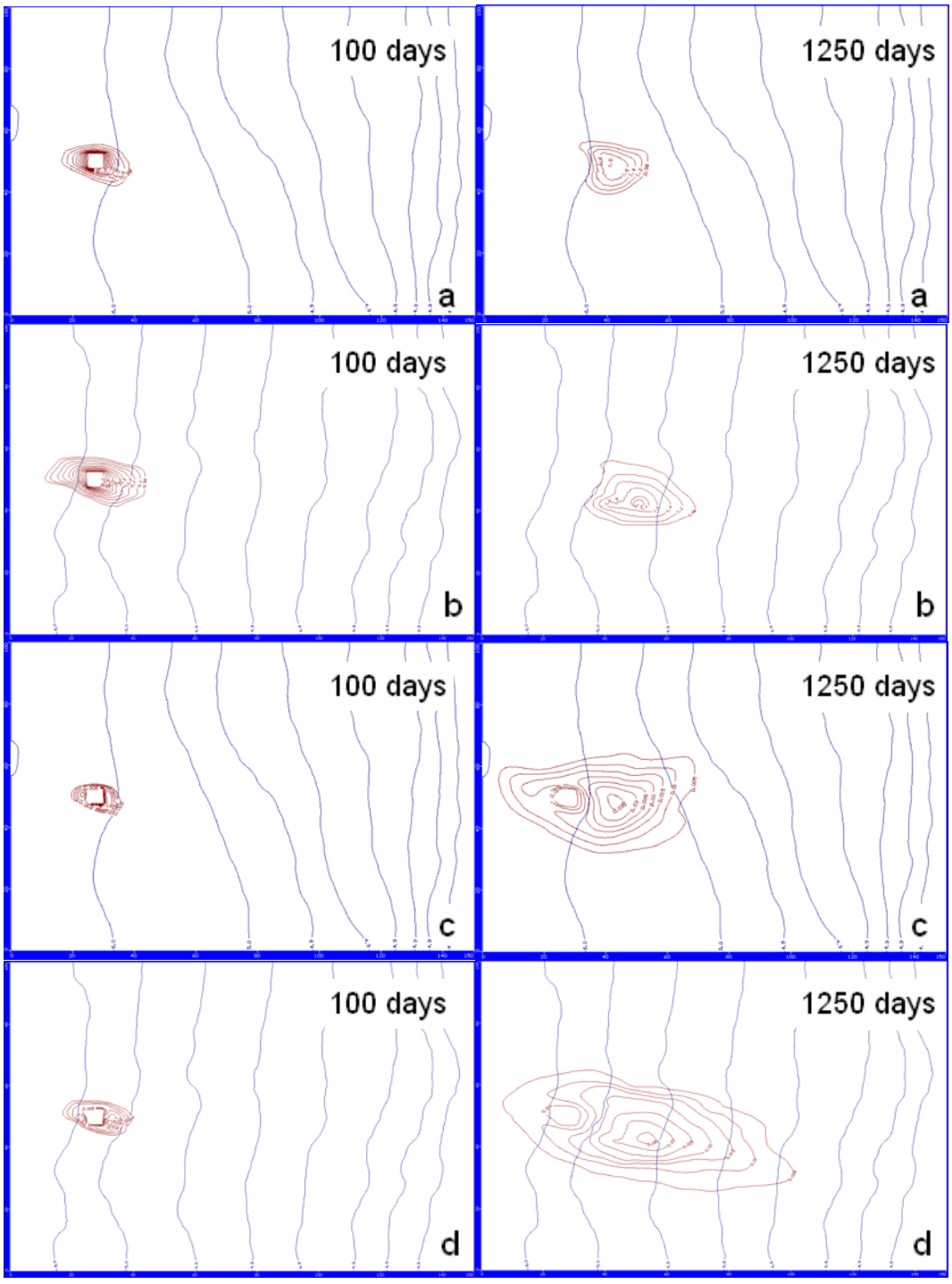

Figure C.21. DCE plumes at 100th and 1250th days for (a) h = 10 m, (b) h_x = 10 m, h_y = 2 m when CV = 50 % and ETH plumes at 100th and 1250th days for (c) h = 10 m, (d) h_x = 20 m, h_y = 4 m when CV = 150 %

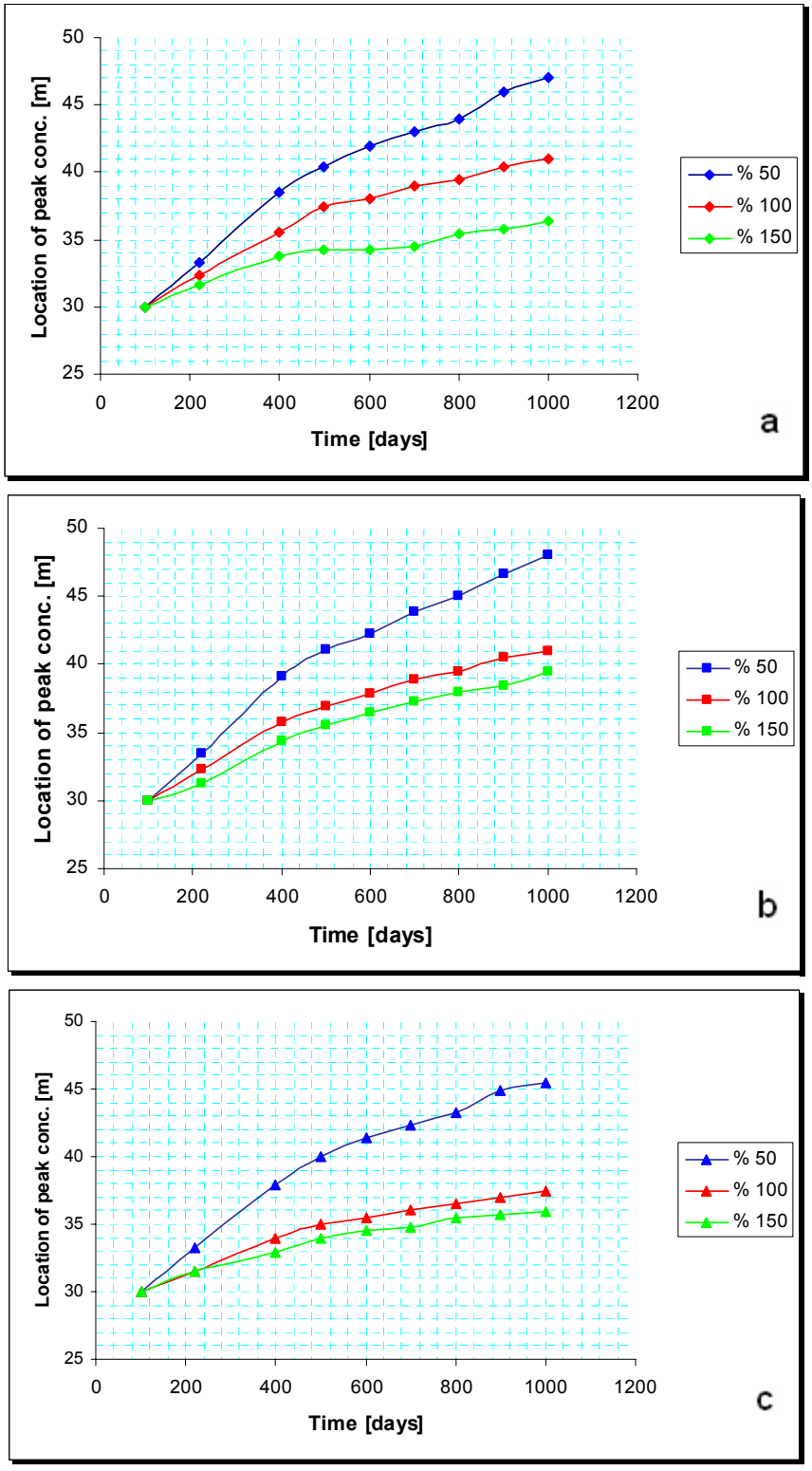

Figure C.22. Location of peak concentration of PCE plume with time for (a) h = 5 m, (b) h = 10 m, (c) h = 20 m.

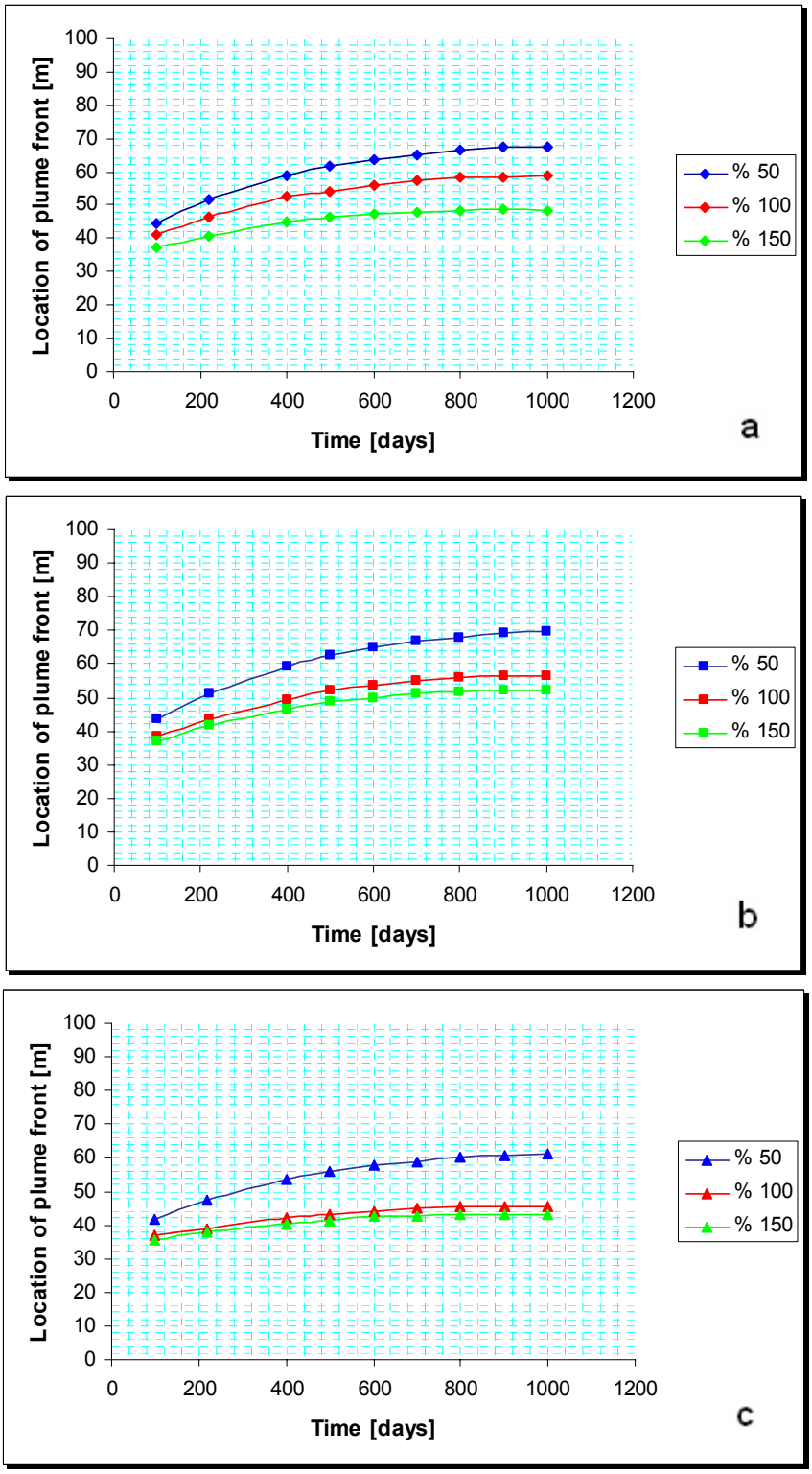

Figure C.23. Location of PCE plume front with time for (a) h = 5 m, (b) h = 10 m, (c) h = 20 m.

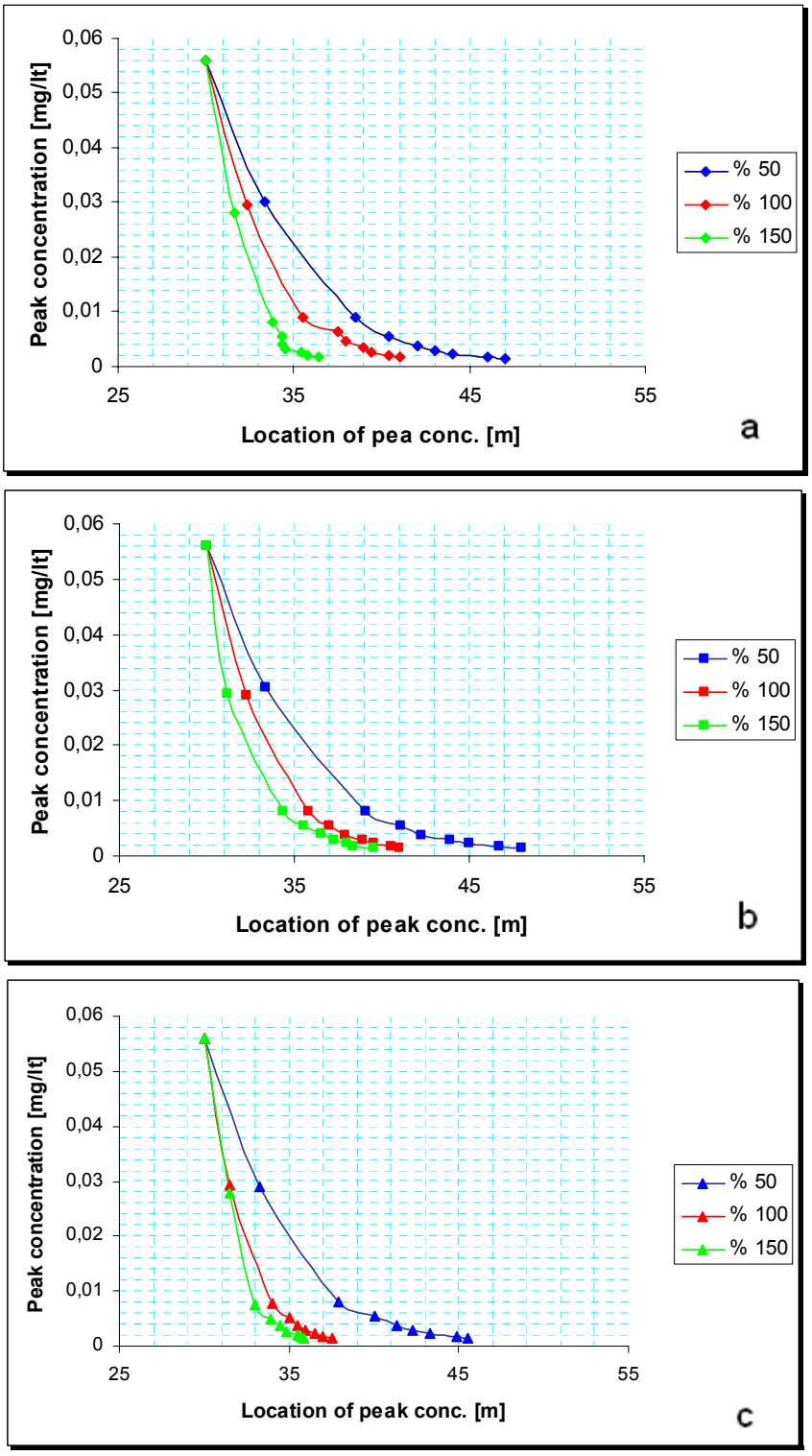

Figure C.24. Peak concentration distribution of PCE plume with distance for (a) h = 5 m, (b) h = 10 m, (c) h = 20 m.

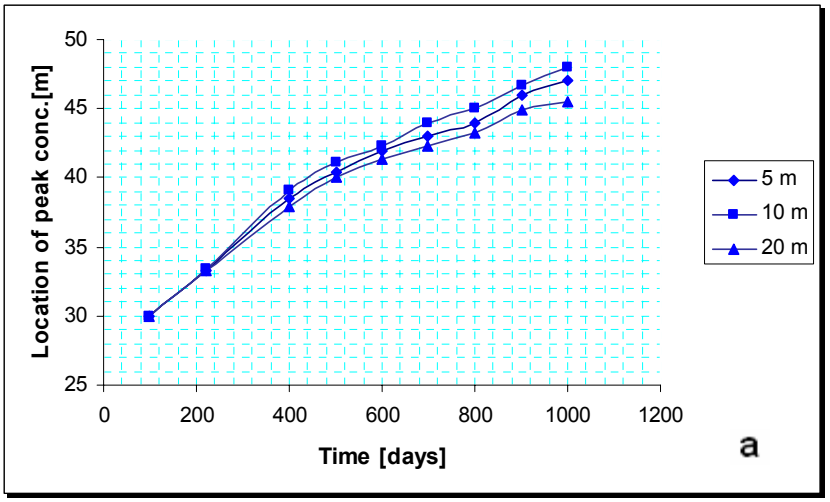

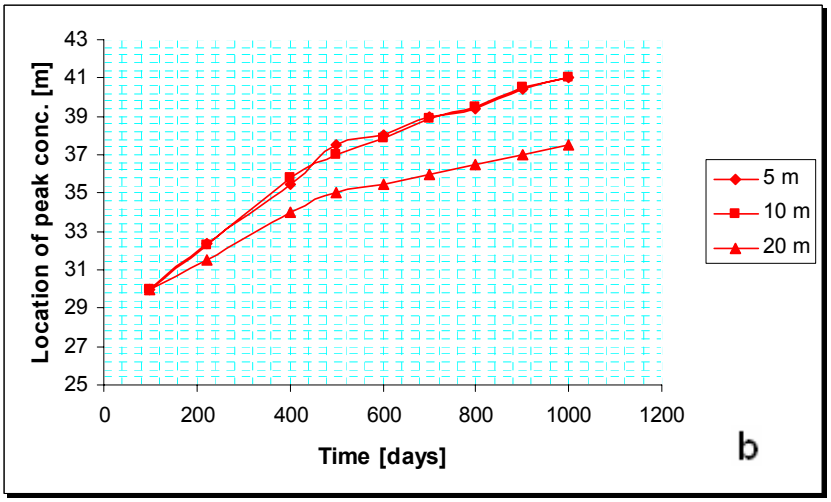

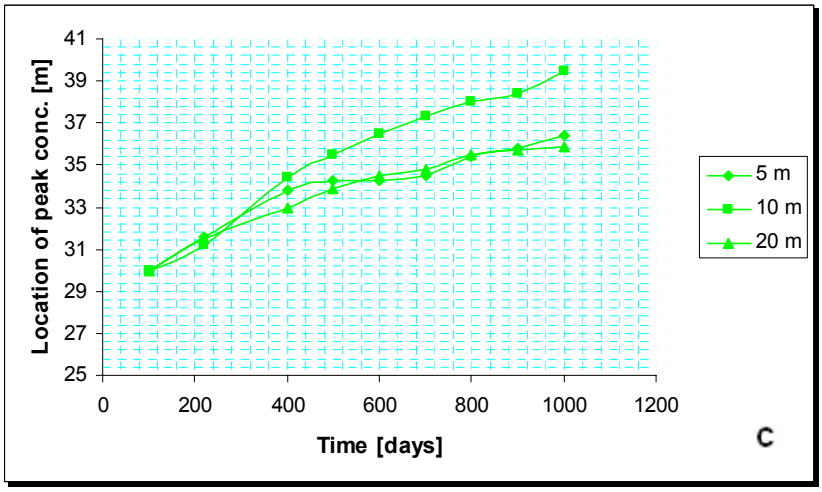

Figure C.25. Location of peak concentration of PCE plume with time for (a) CV = % 50, (b) CV = % 100, (c) CV = % 150

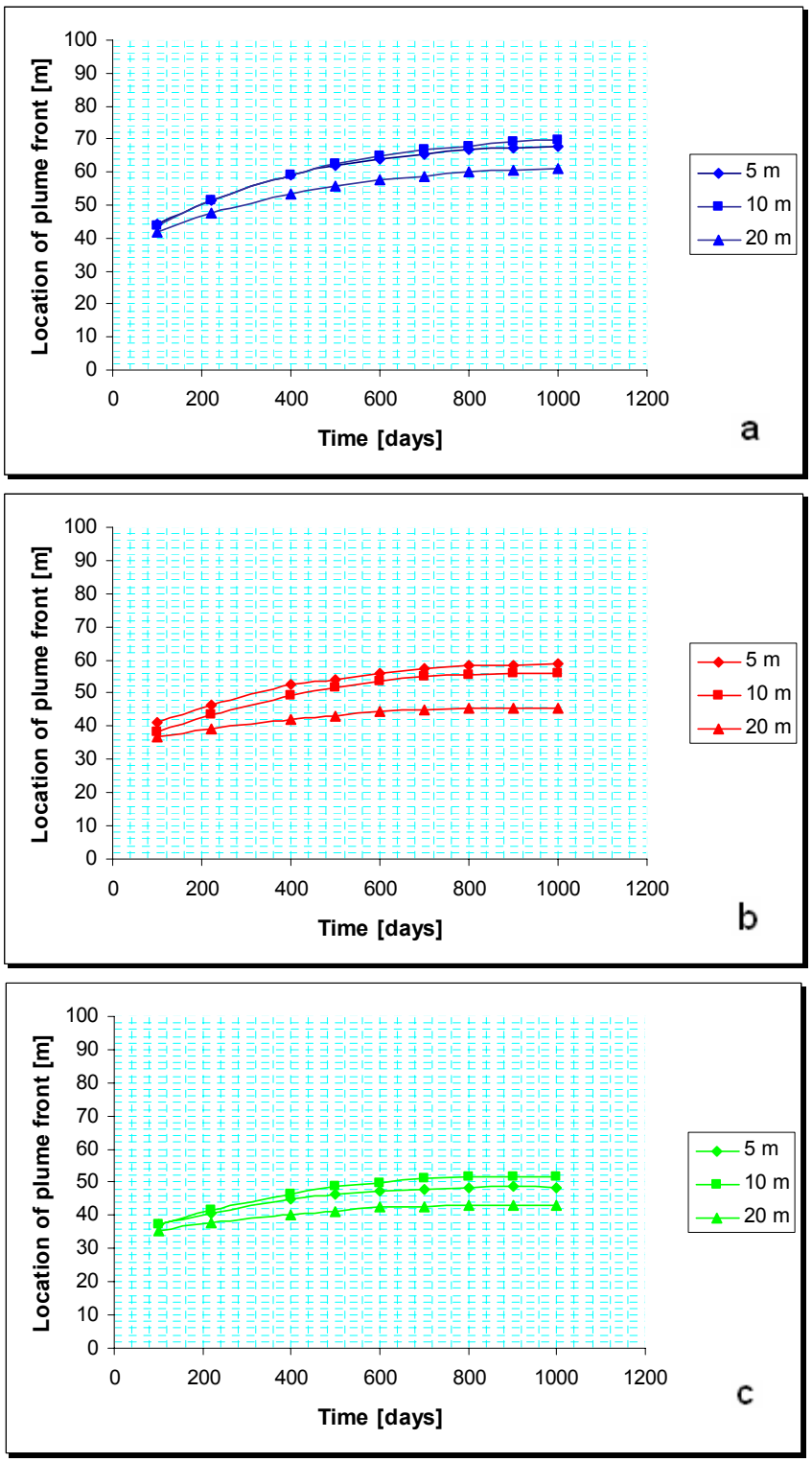

Figure C.26. Location of PCE plume front with time for (a) CV = % 50, (b) CV = % 100, (c) CV = % 150

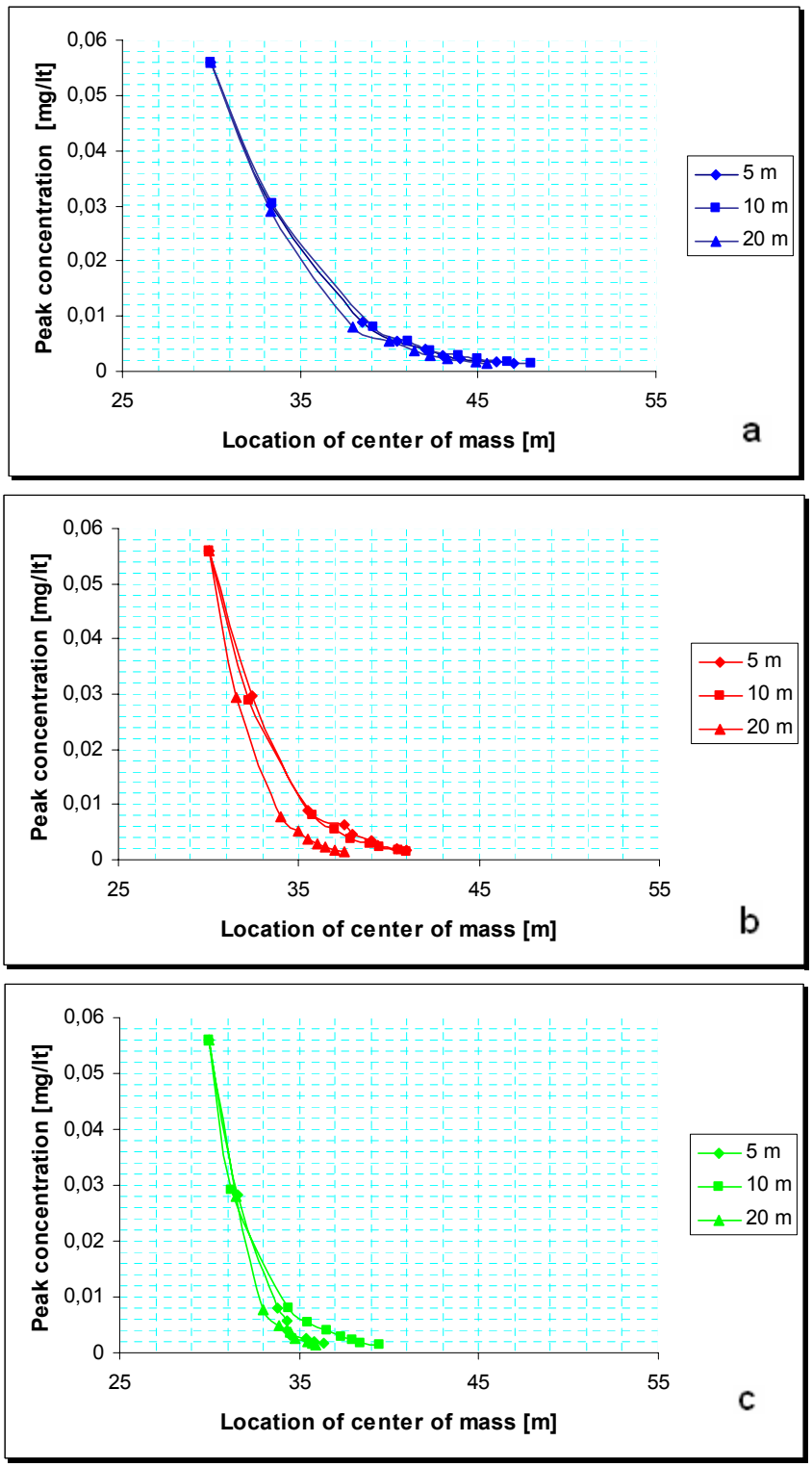

Figure C.27. Peak concentration distribution of PCE plume with distance for (a) CV = % 50, (b) CV = % 100, (c) CV = % 150

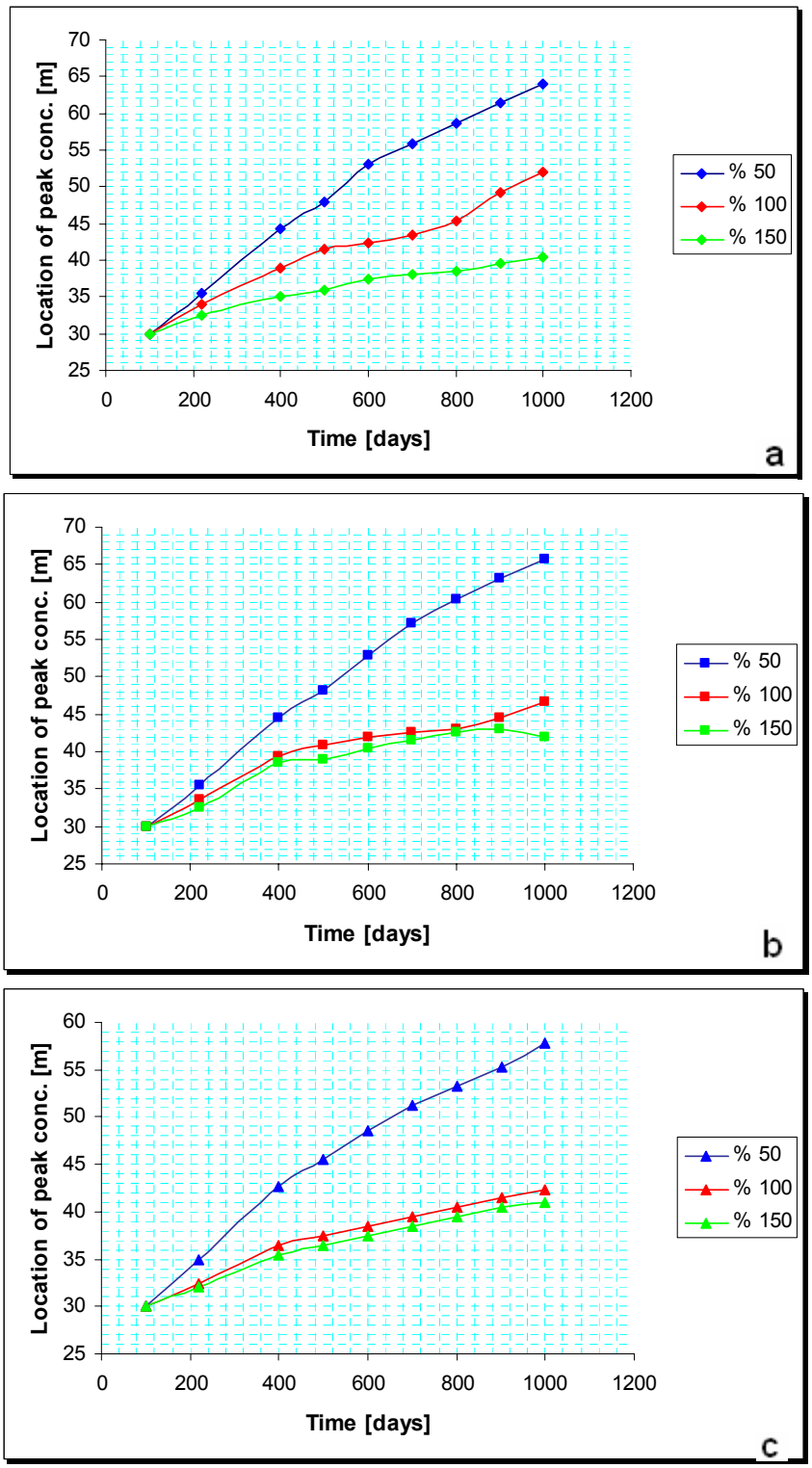

Figure C.28. Location of peak concentration of TCE plume with time for (a) h = 5 m, (b) h = 10 m, (c) h = 20 m.

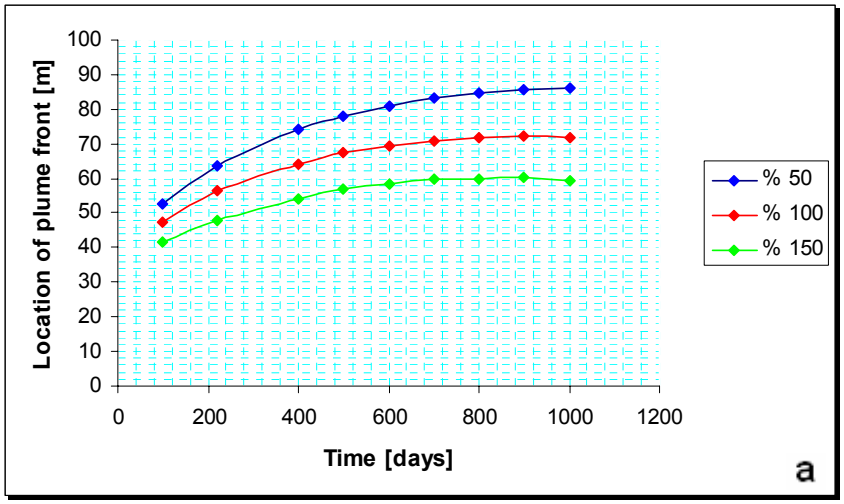

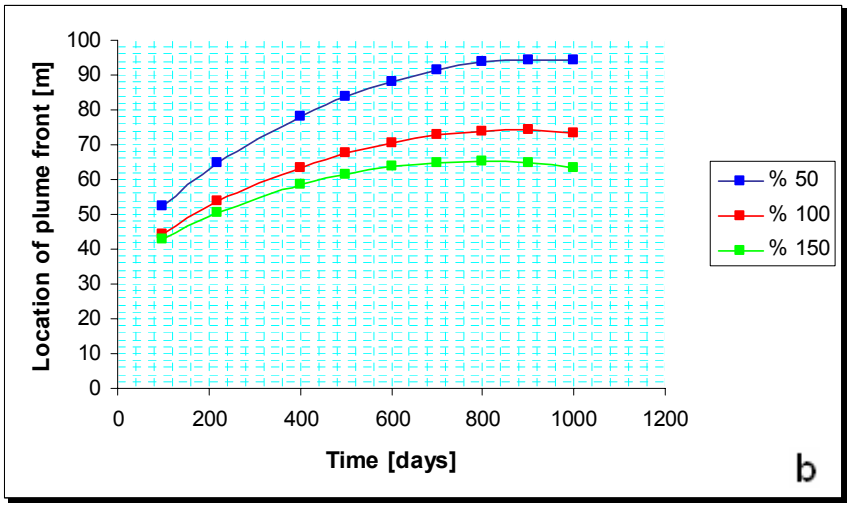

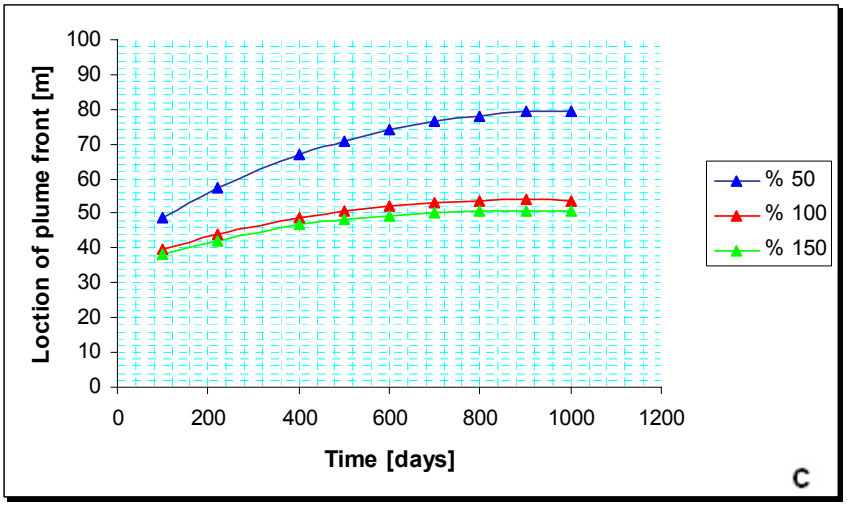

Figure C.29. Location of TCE plume front with time for (a) h = 5 m, (b) h = 10 m, (c) h = 20 m.

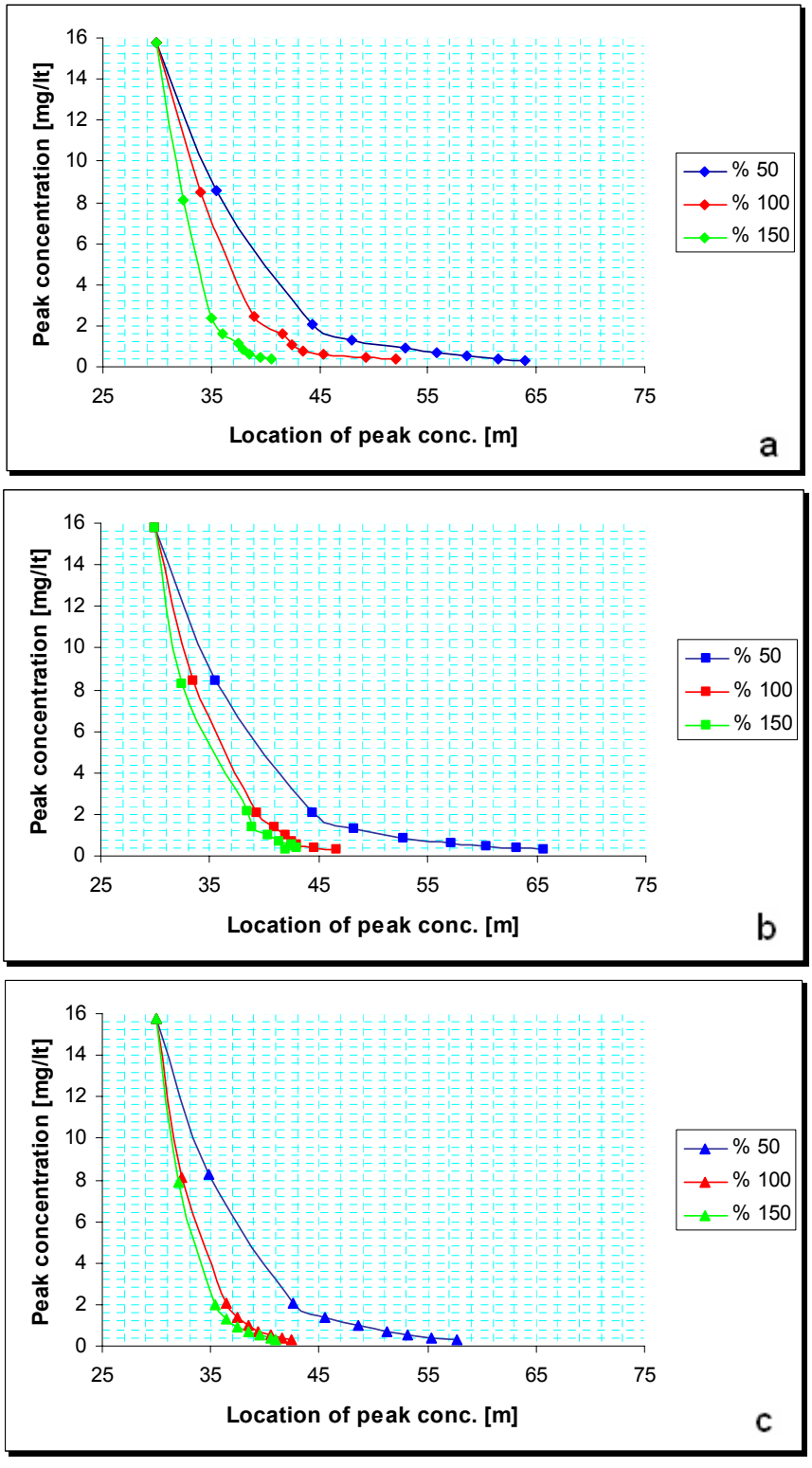

Figure C.30. Peak concentration distribution of TCE plume with distance for (a) h = 5 m, (b) h = 10 m, (c) h = 20 m.

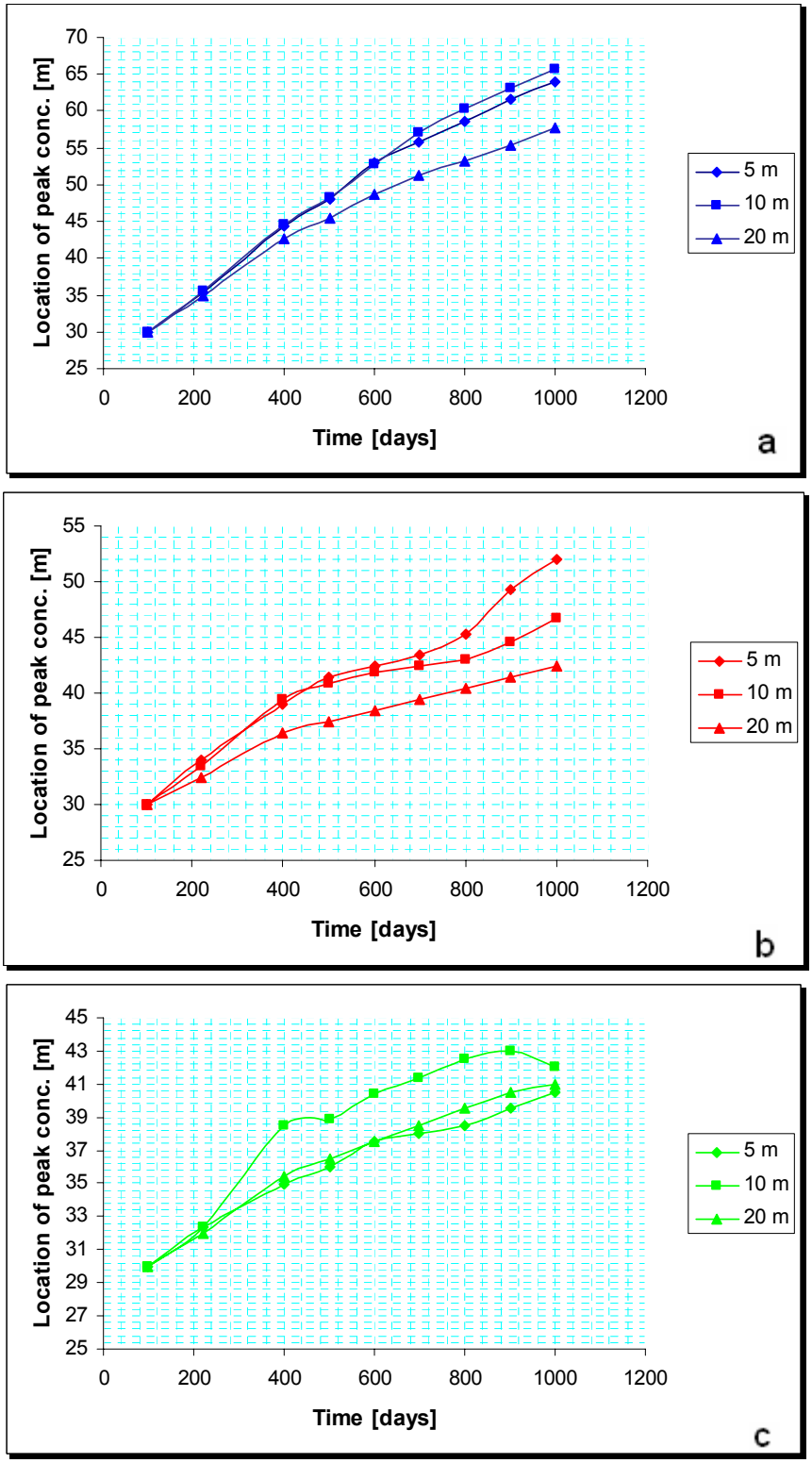

Figure C.31. Location of peak concentration of TCE plume with time for (a) CV = % 50, (b) CV = % 100, (c) CV = % 150

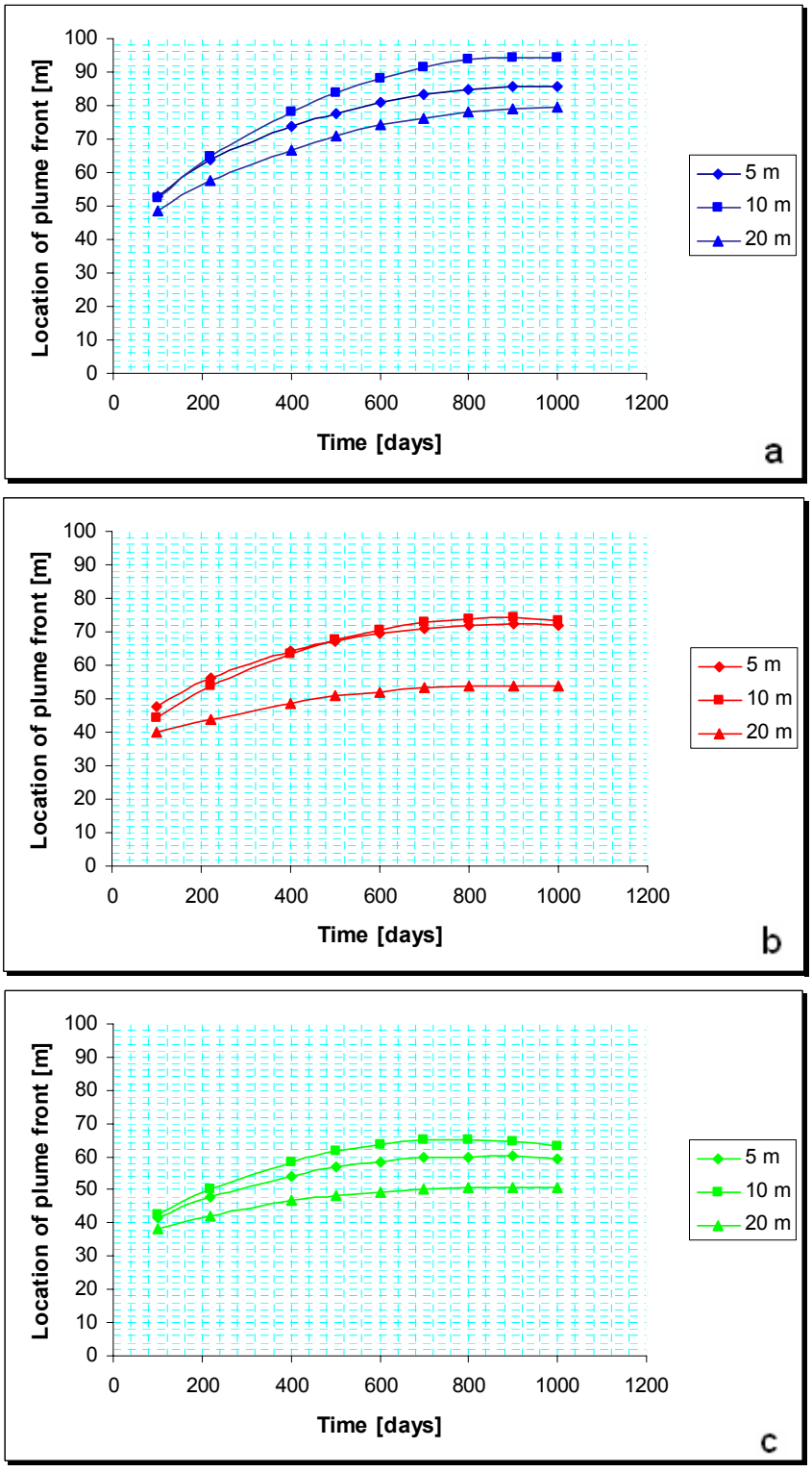

Figure C.32. Location of TCE plume front with time for (a) CV = % 50, (b) CV = % 100, (c) CV = % 150

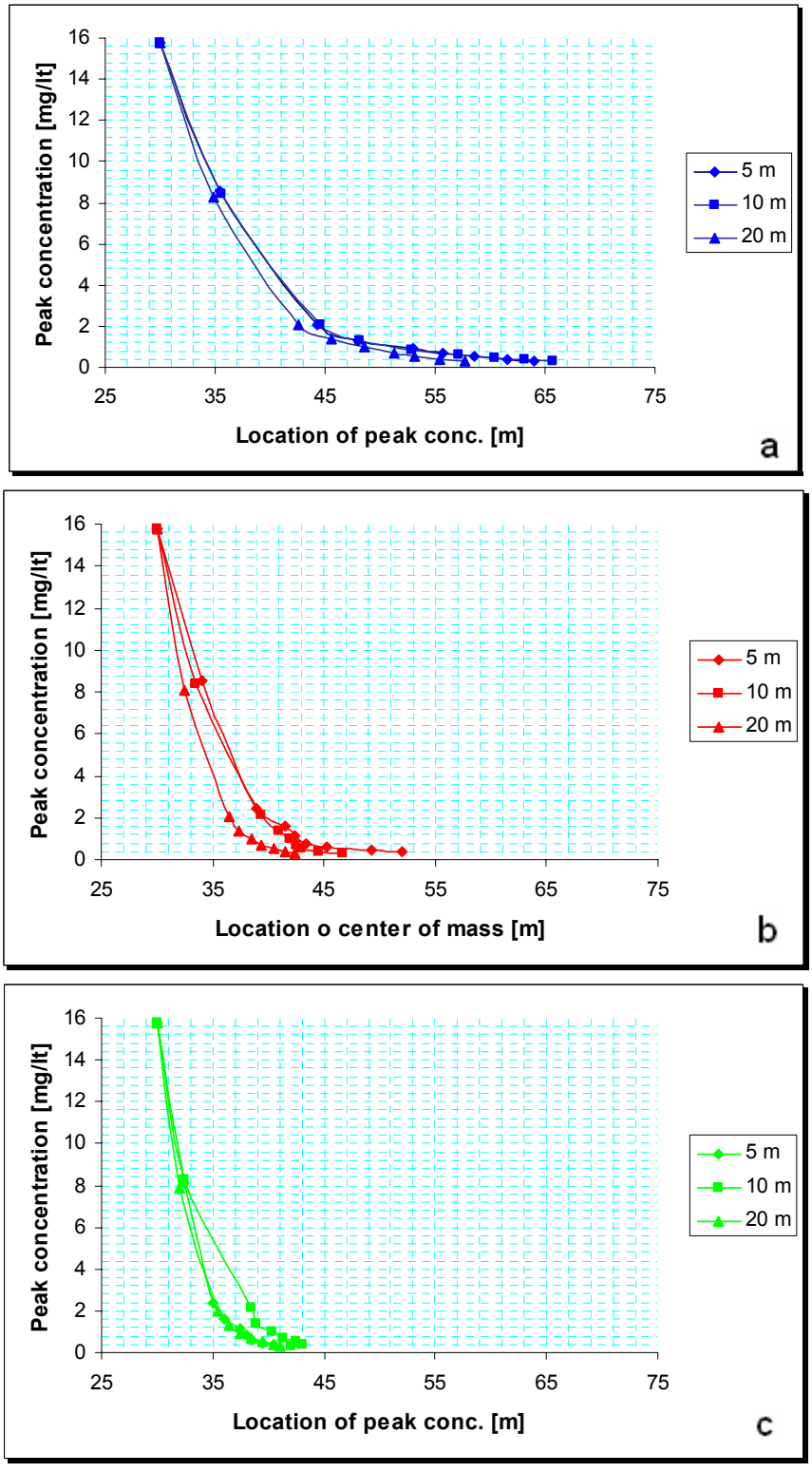

Figure C.33. Peak concentration distribution of TCE plume with distance for (a) CV = % 50, (b) CV = % 100, (c) CV = % 150

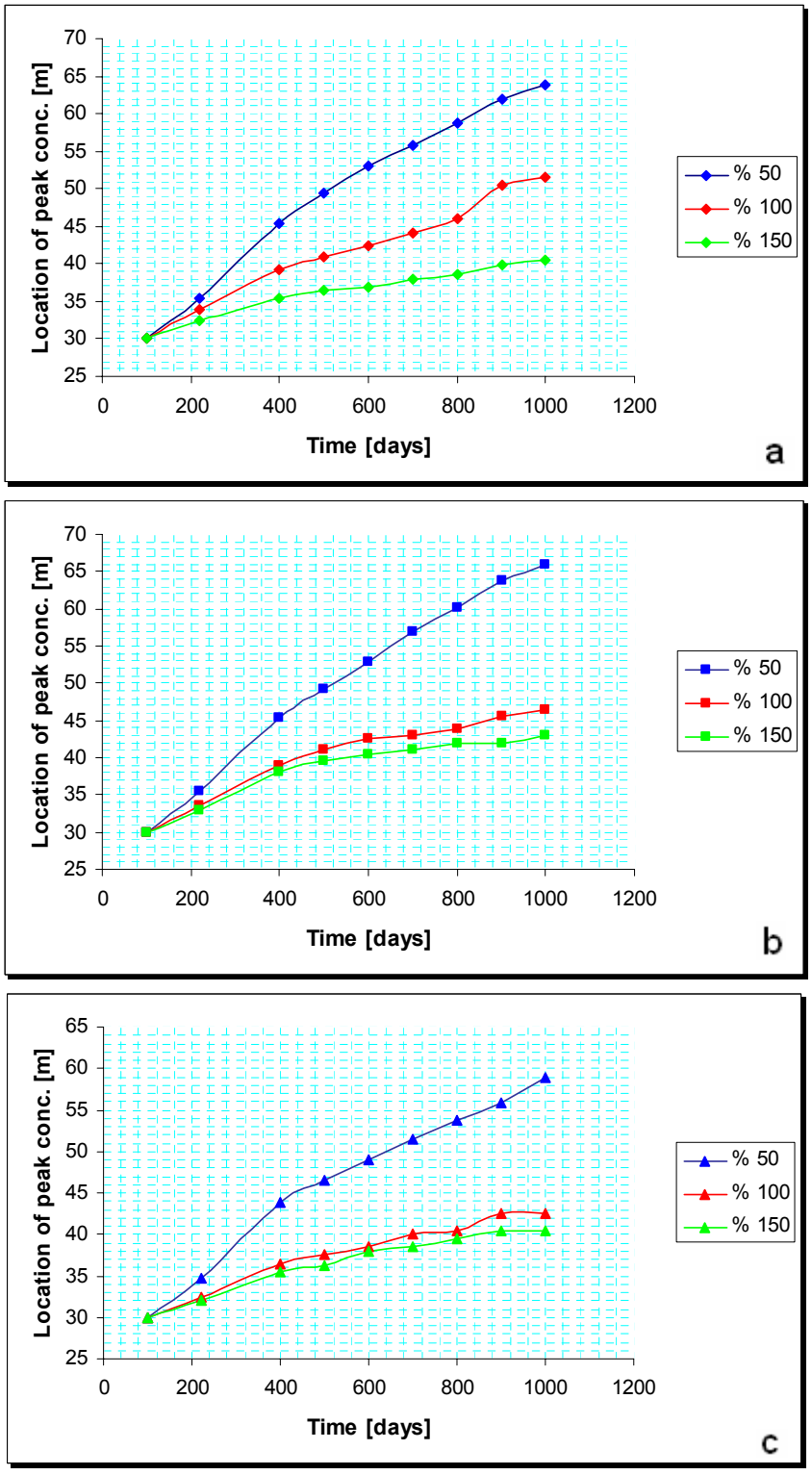

Figure C.34. Location of peak concentration of DCE plume with time for (a) h = 5 m, (b) h = 10 m, (c) h = 20 m.

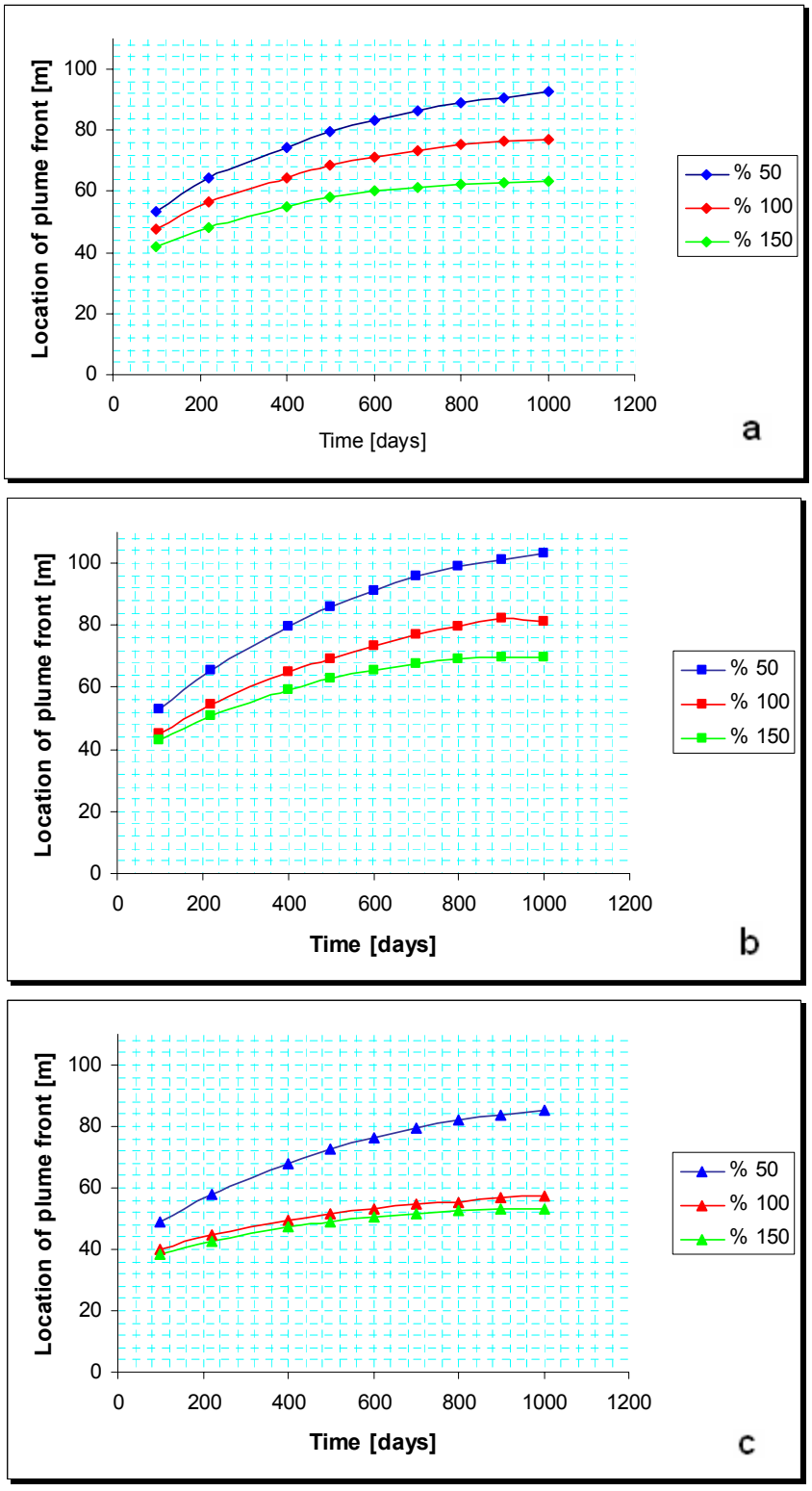

Figure C.35. Location of DCE plume front with time for (a) h = 5 m, (b) h = 10 m, (c) h = 20 m.

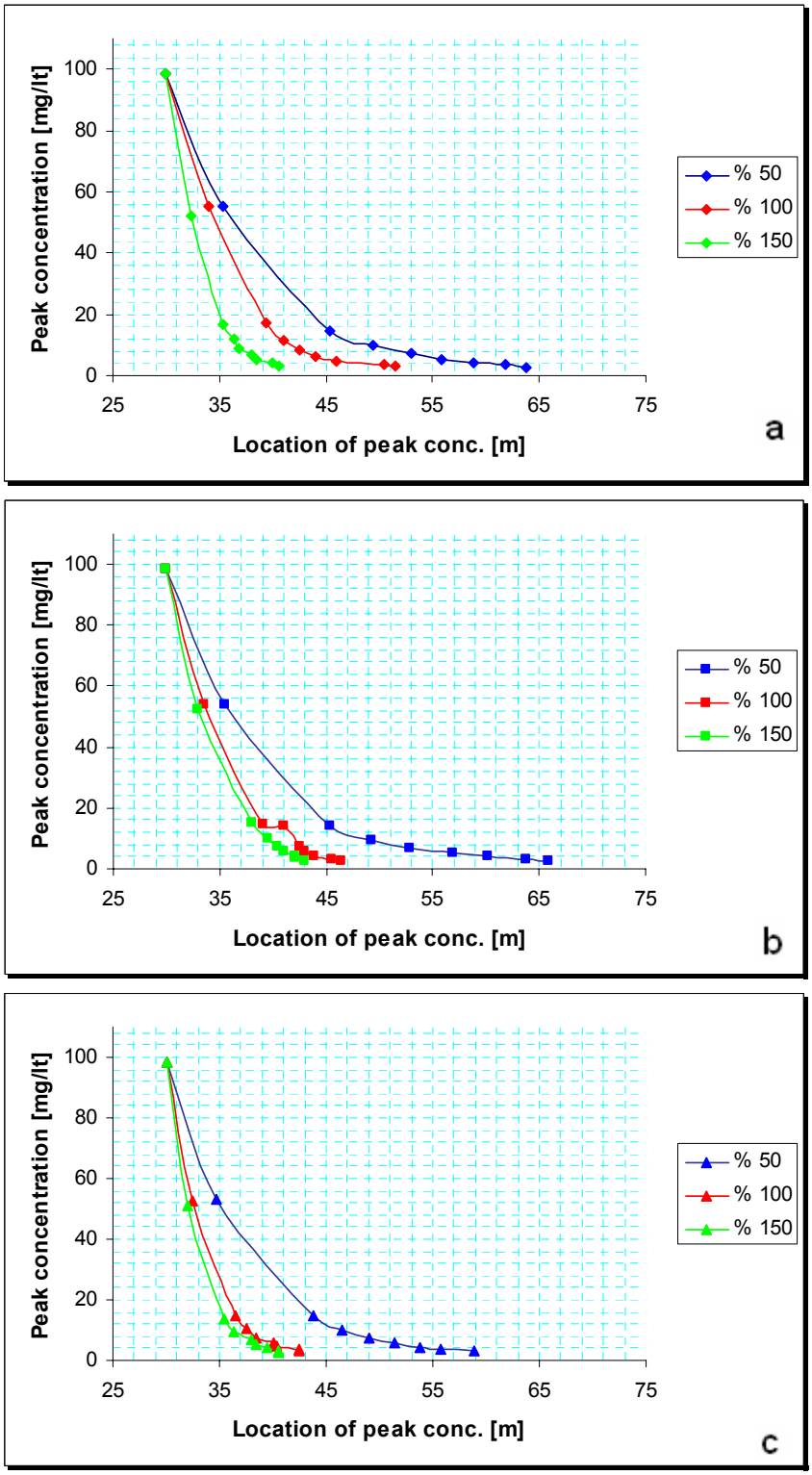

Figure C.36. Peak concentration distribution of DCE plume with distance for (a) h = 5 m, (b) h = 10 m, (c) h = 20 m.

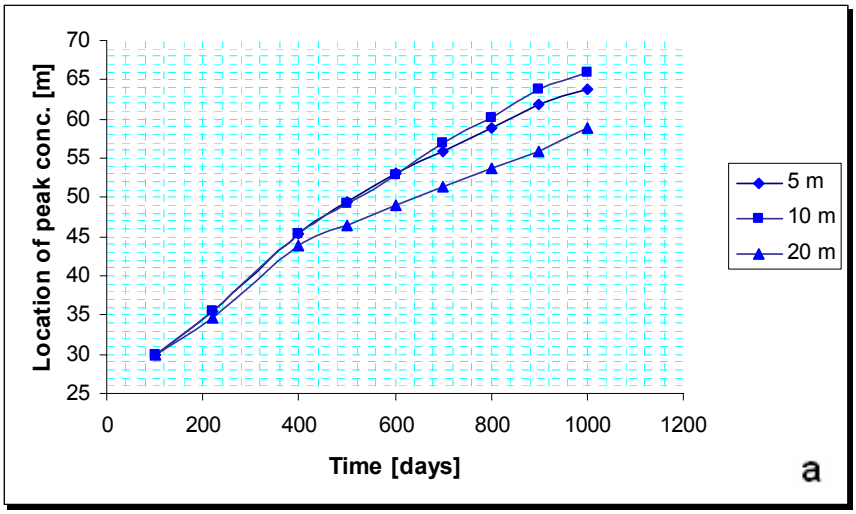

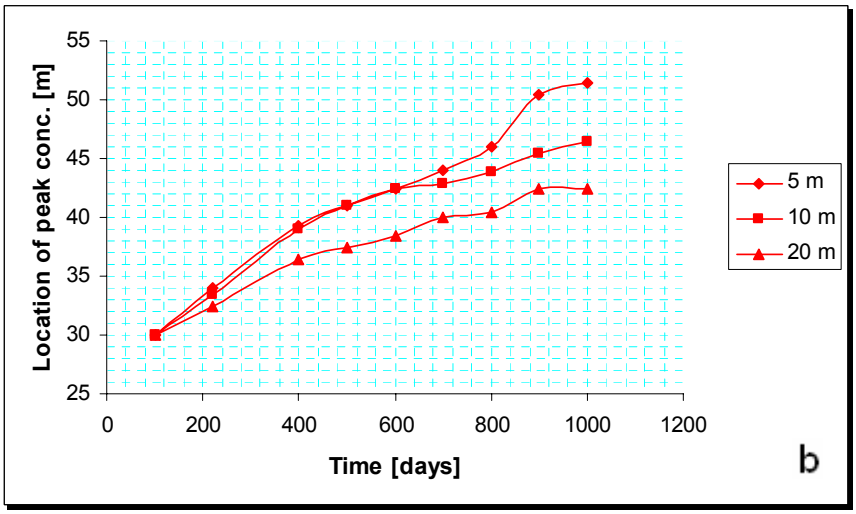

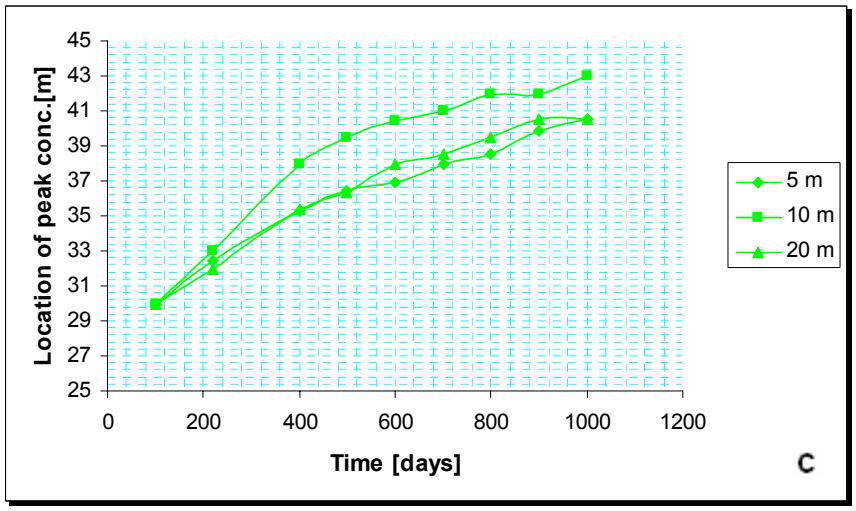

Figure C.37. Location of peak concentration of DCE plume with time for (a) CV = % 50, (b) CV = % 100, (c) CV = % 150

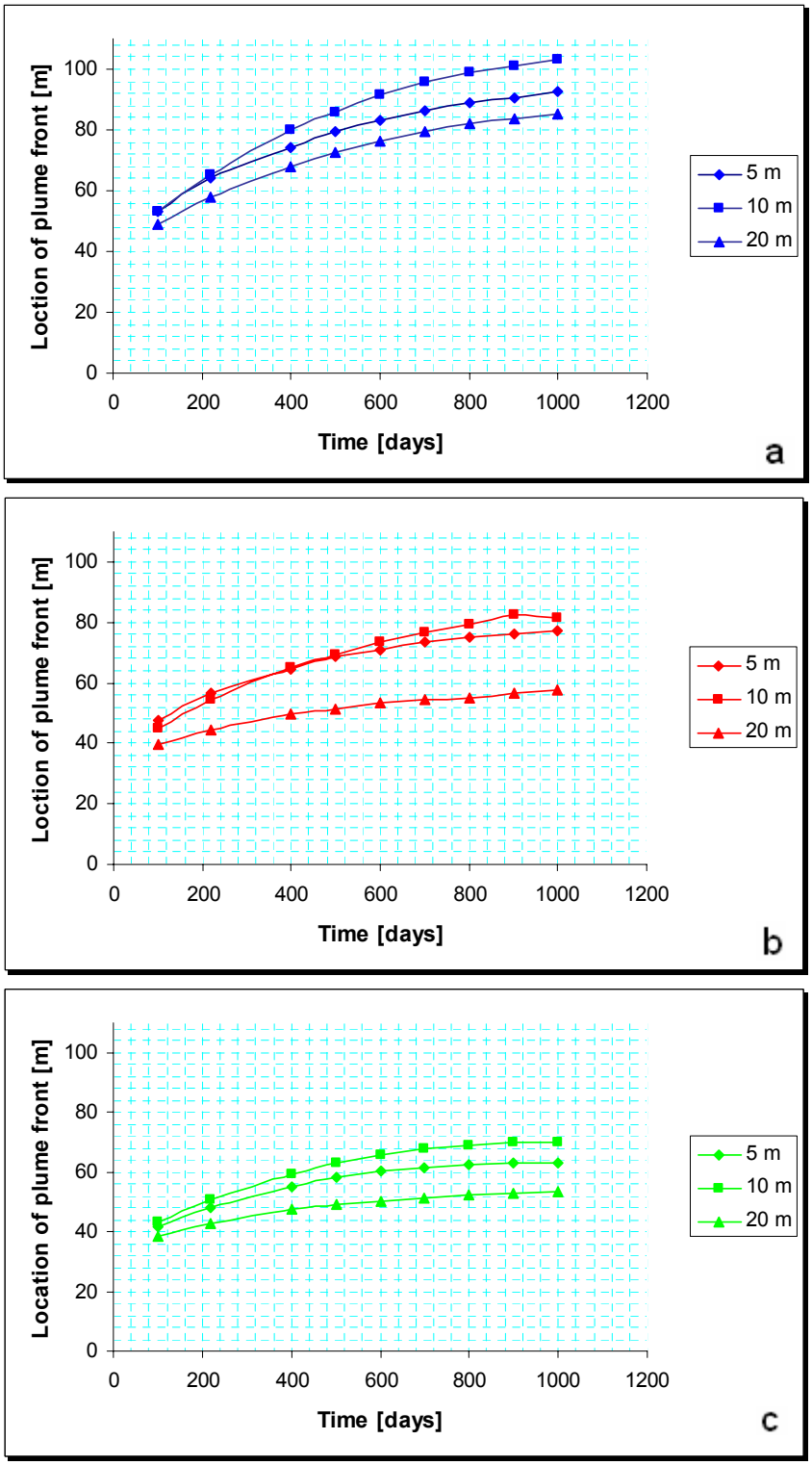

Figure C.38. Location of DCE plume front with time for (a) CV = % 50, (b) CV = % 100, (c) CV = % 150

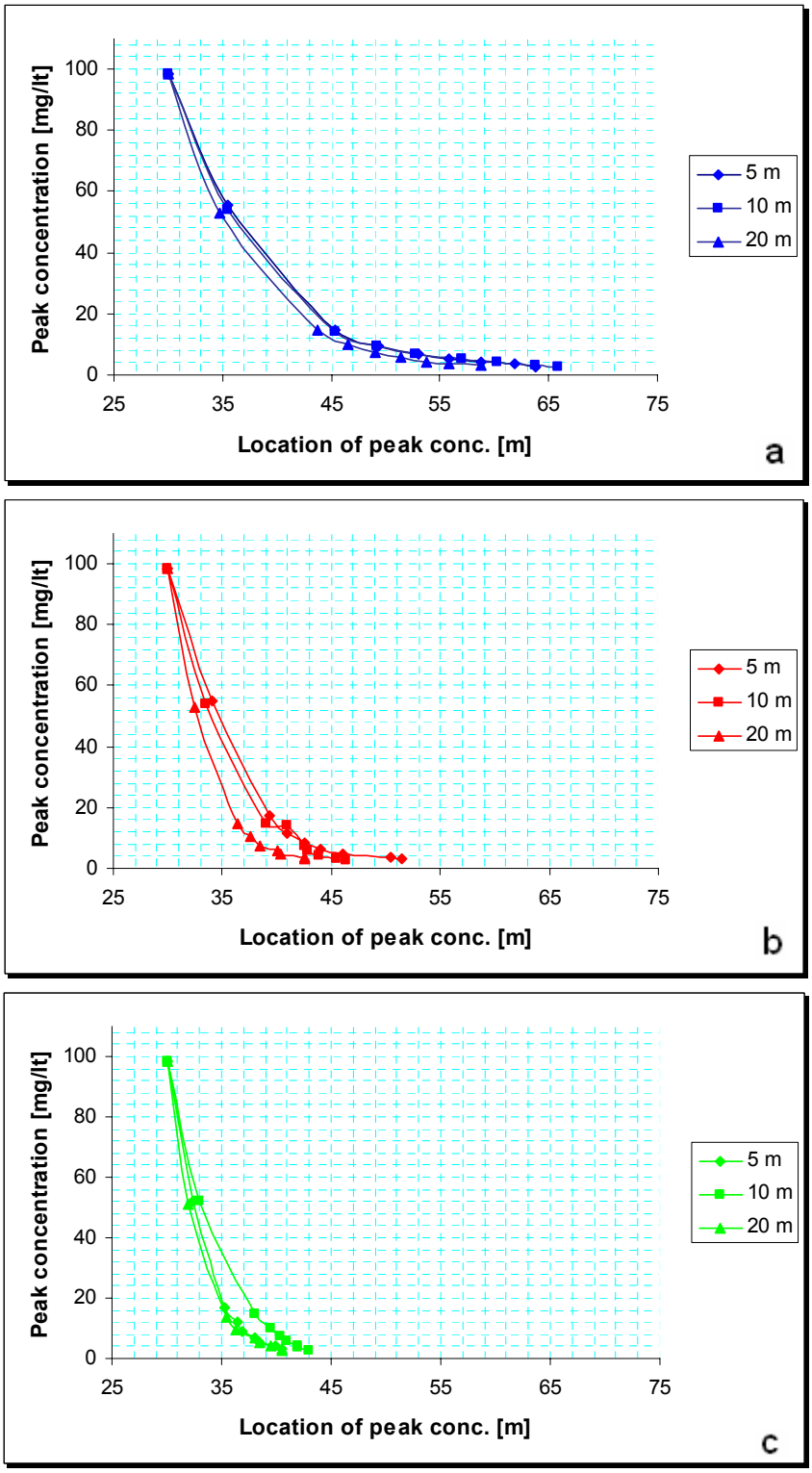

Figure C.39. Peak concentration distribution of DCE plume with distance for (a) CV = % 50, (b) CV = % 100, (c) CV = % 150

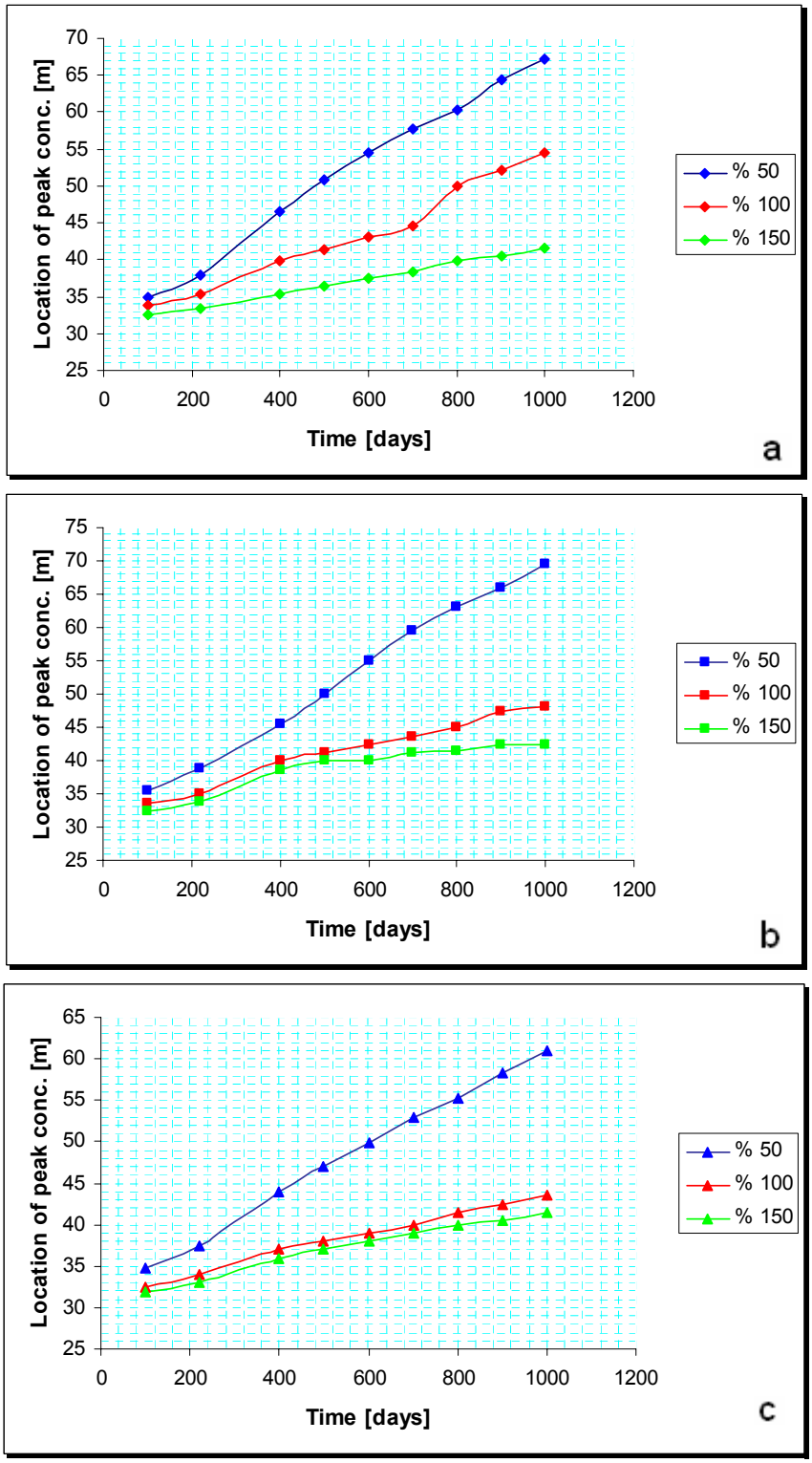

Figure C.40. Location of peak concentration of ETH plume with time for (a) h = 5 m, (b) h = 10 m, (c) h = 20 m.

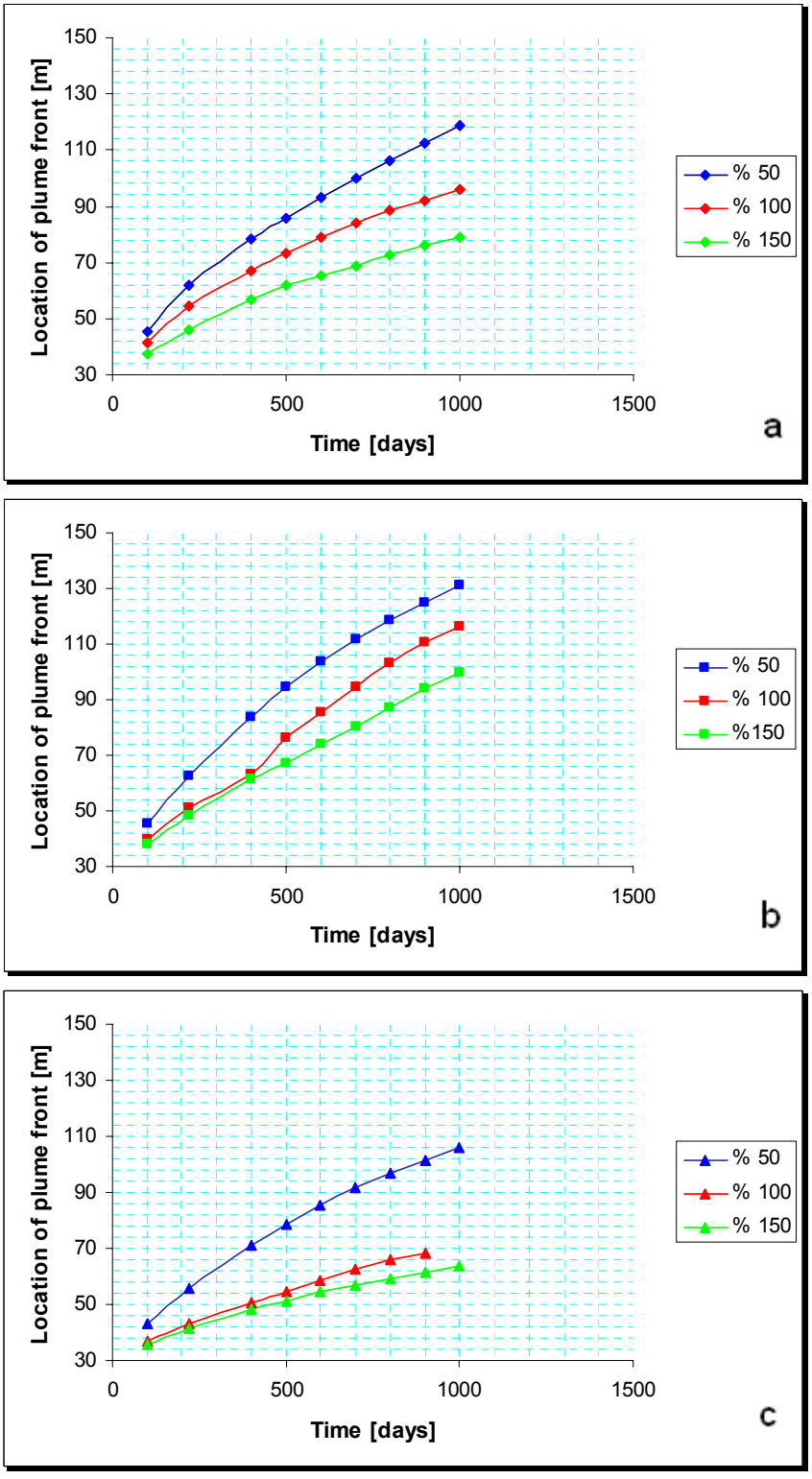

Figure C.41. Location of ETH plume front with time for (a) h = 5 m, (b) h = 10 m, (c) h = 20 m.

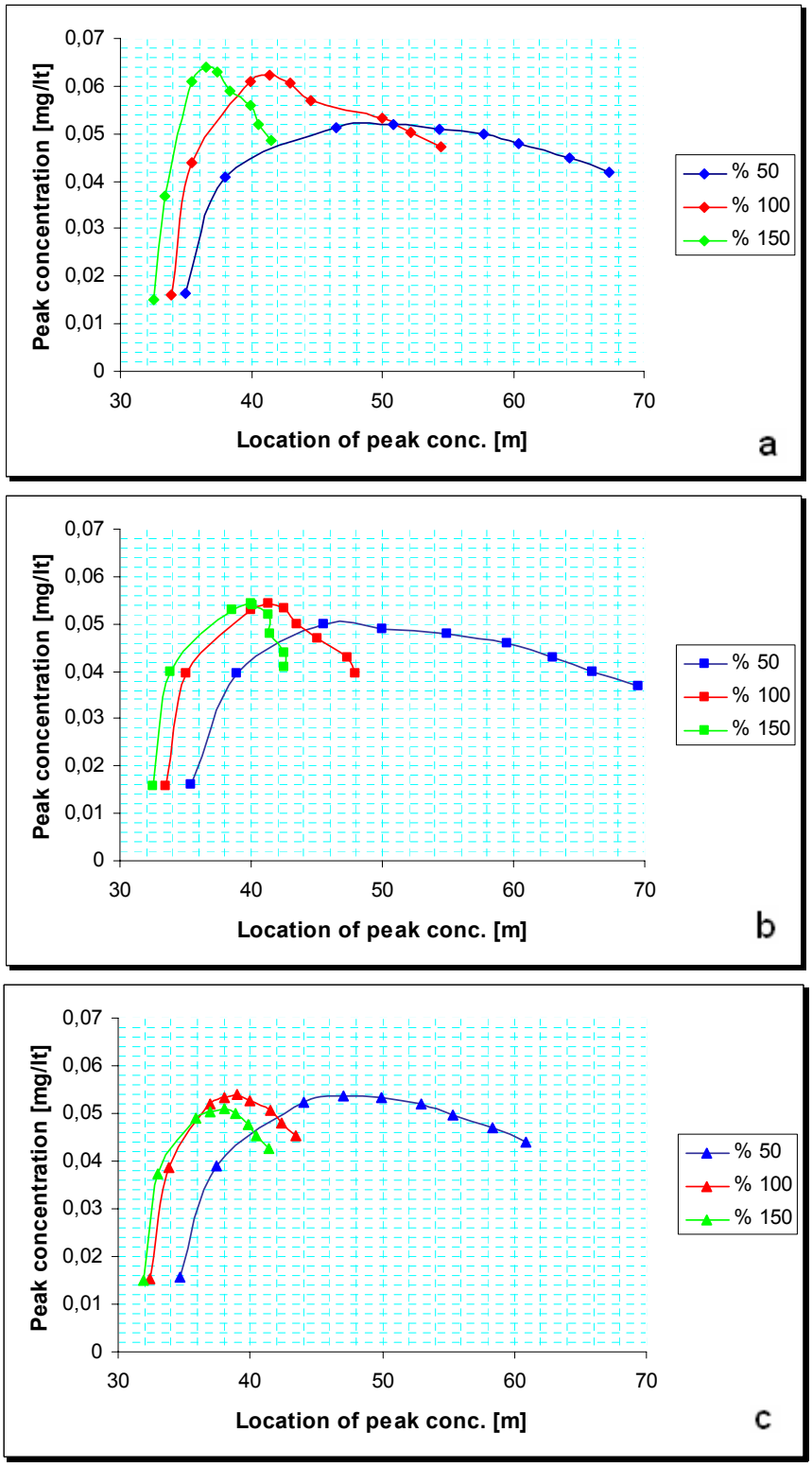

Figure C.42. Peak concentration distribution of ETH plume with distance for (a) h = 5 m, (b) h = 10 m, (c) h = 20 m.

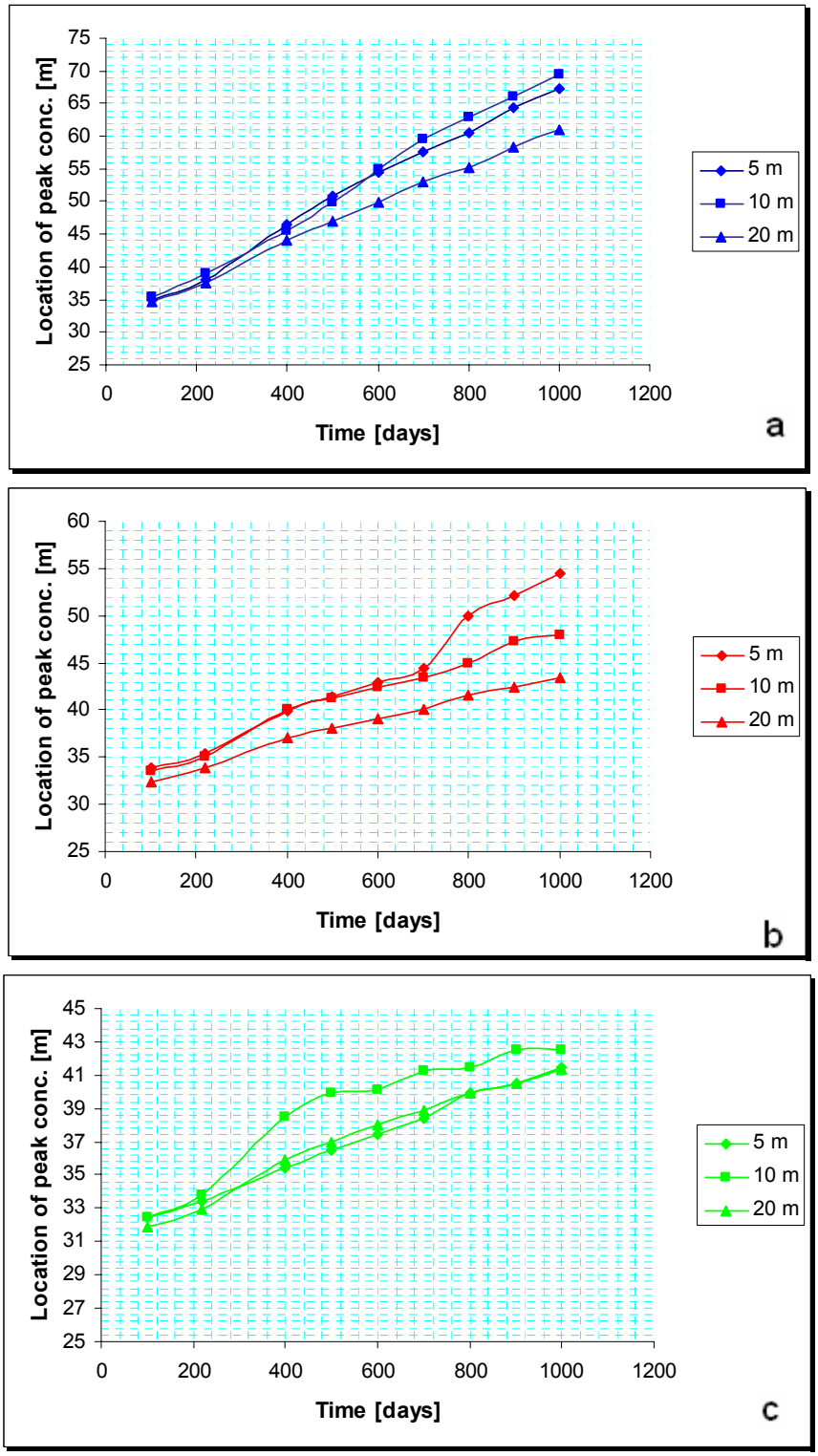

Figure C.43. Location of peak concentration of ETH plume with time for (a) CV = % 50, (b) CV = % 100, (c) CV = % 150

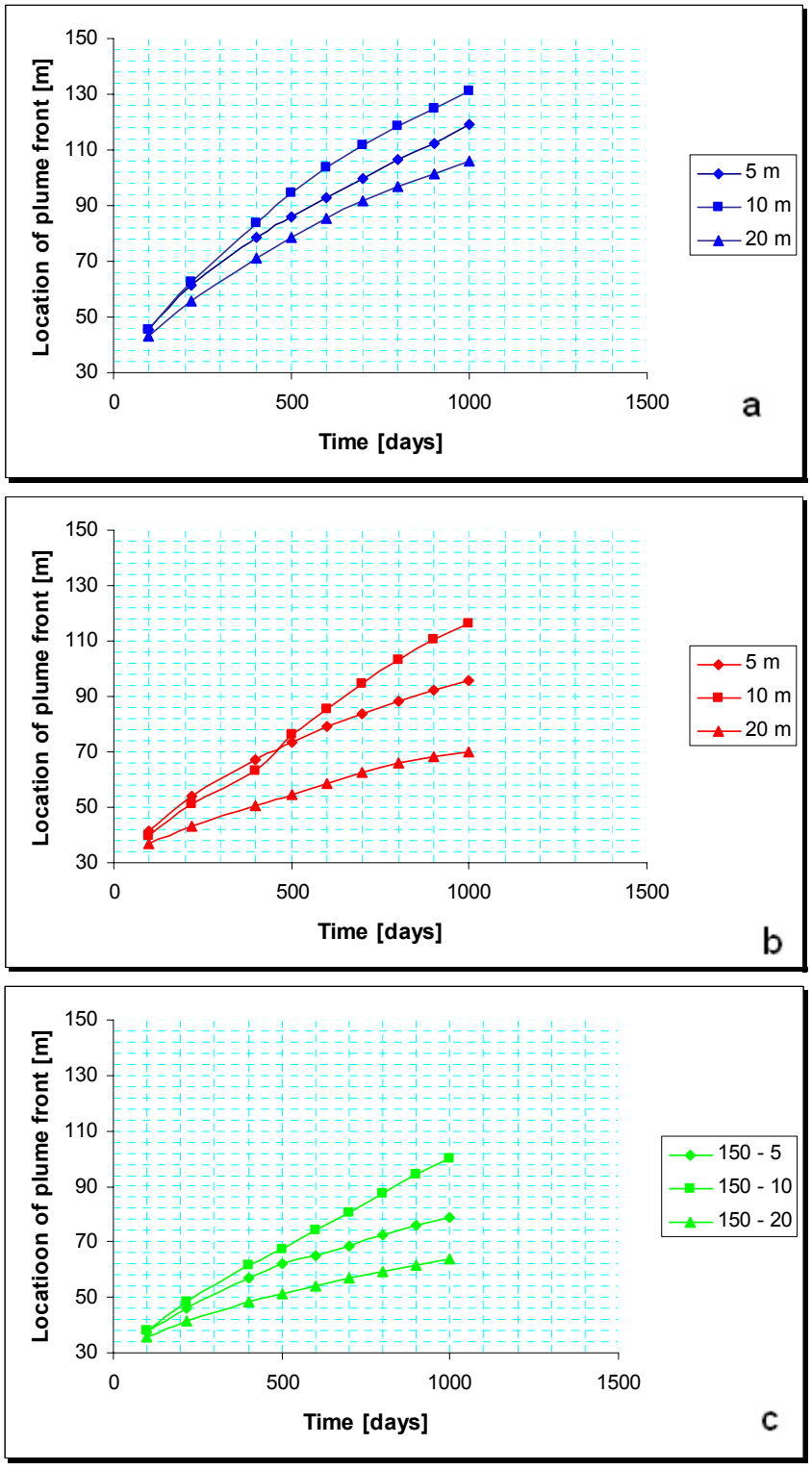

Figure C.44. Location of ETH plume front with time for (a) CV = % 50, (b) CV = % 100, (c) CV = % 150

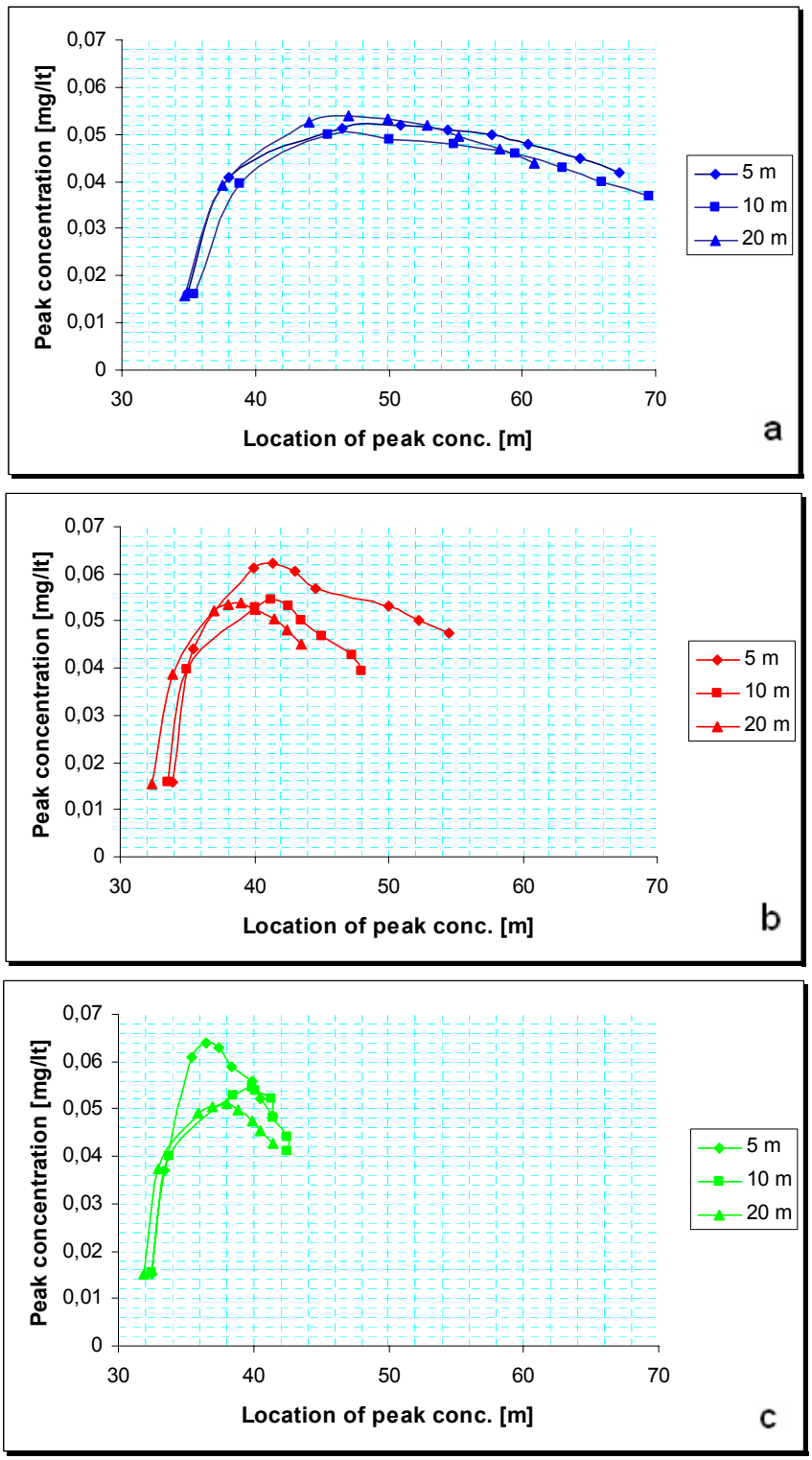

Figure C.45. Peak concentration distribution of ETH plume with distance for (a) CV = % 50, (b) CV = % 100, (c) CV = % 150

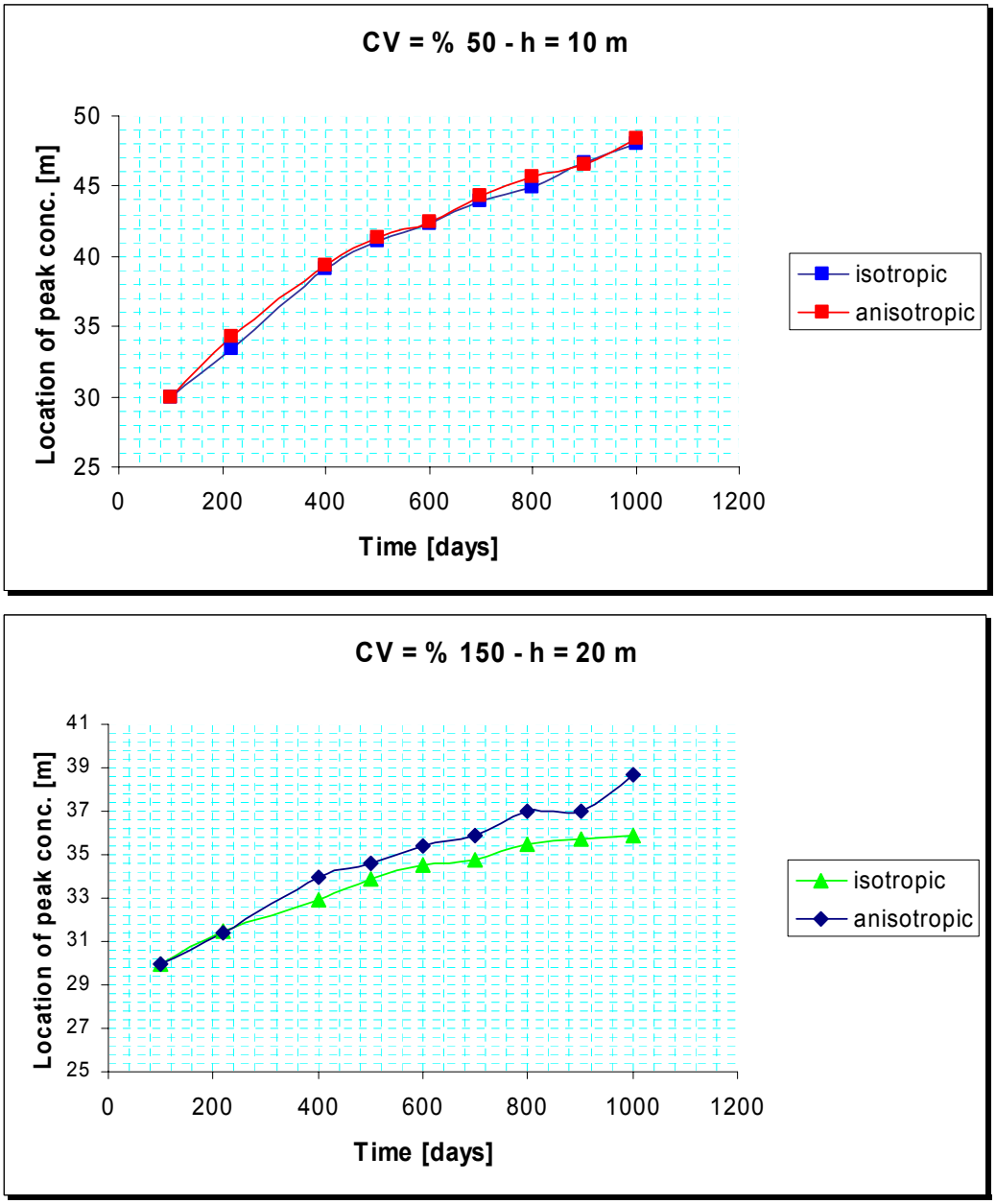

Figure C.46. Location of peak concentration of PCE plume with time for isotropic (h = 10 m when CV = % 50 and h = 20 m when CV = % 150) and anisotropic (h_x = 10 m, h_y = 2 m when CV = % 50 and h_x = 20 m, h_y = 4 m when CV = % 50) fields.

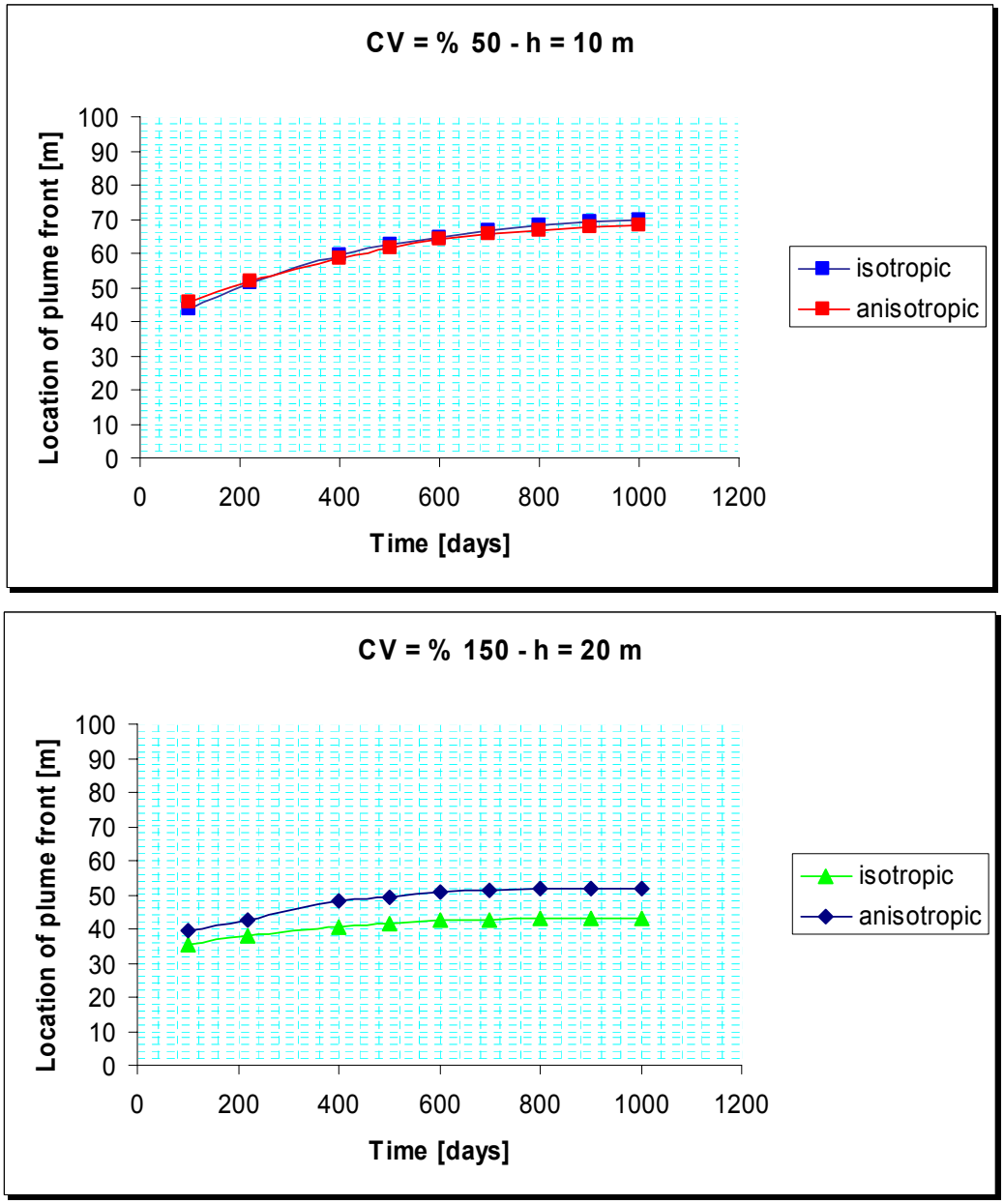

Figure C.47. Location of PCE plume front with time for isotropic (h = 10 m when CV = % 50 and h = 20 m when CV = % 150) and anisotropic (h_x = 10 m, h_y = 2 m when CV = % 50 and h_x = 20 m, h_y = 4 m when CV = % 50) fields.

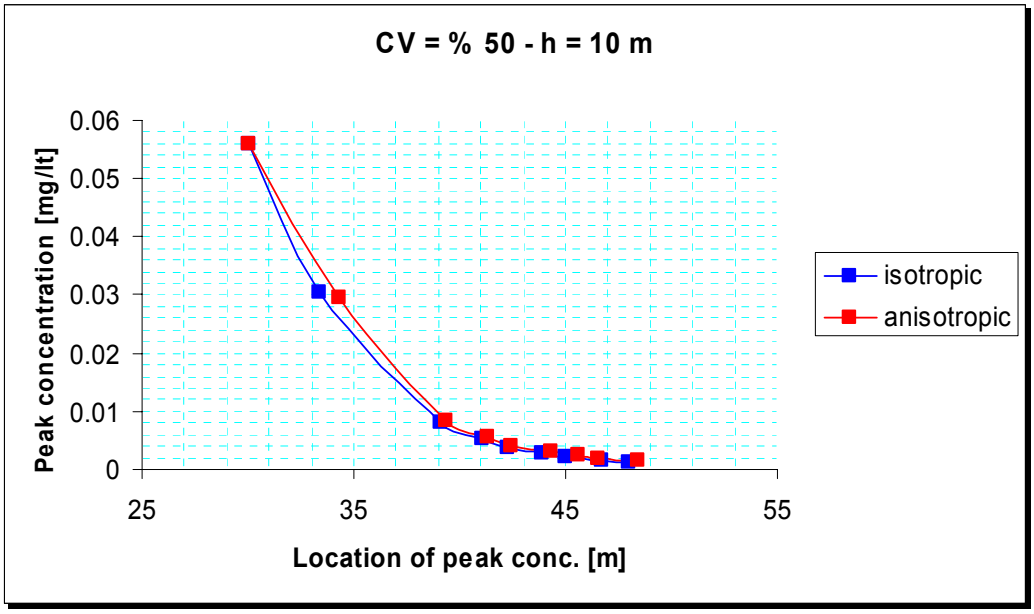

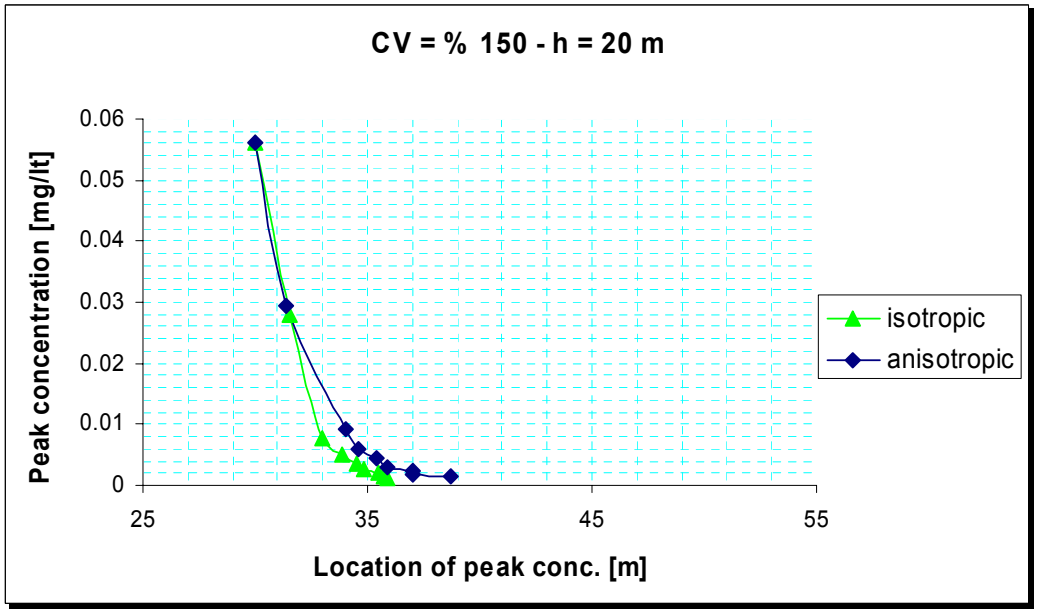

Figure C.48. Peak concentration distribution of PCE plume with distance for isotropic (h = 10 m when CV = % 50 and h = 20 m when CV = % 150) and anisotropic (h_x = 10 m, h_y = 2 m when CV = % 150 and h_x = 20 m, h_y = 4 m when CV = % 150) fields.

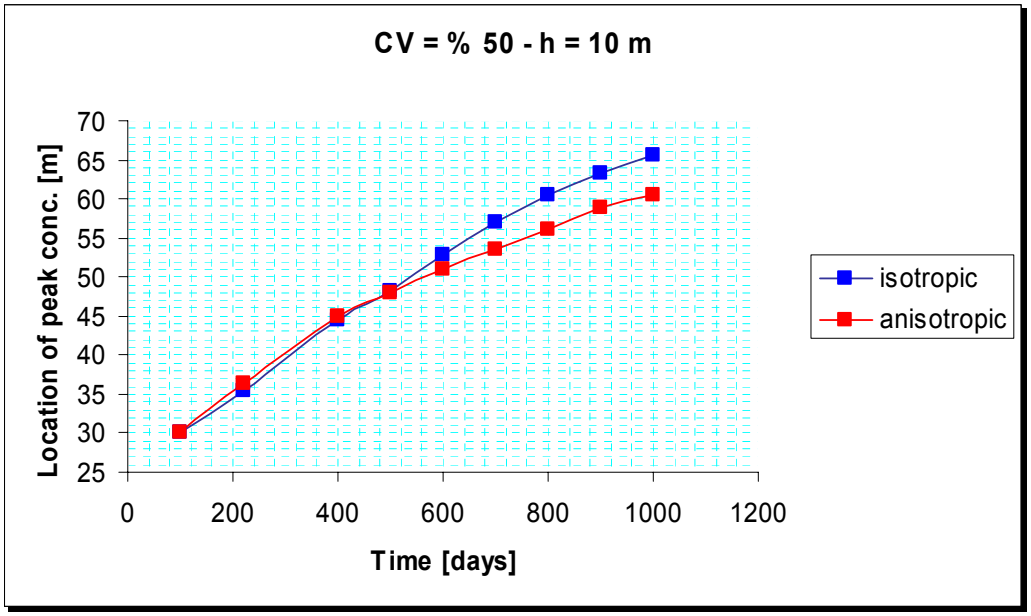

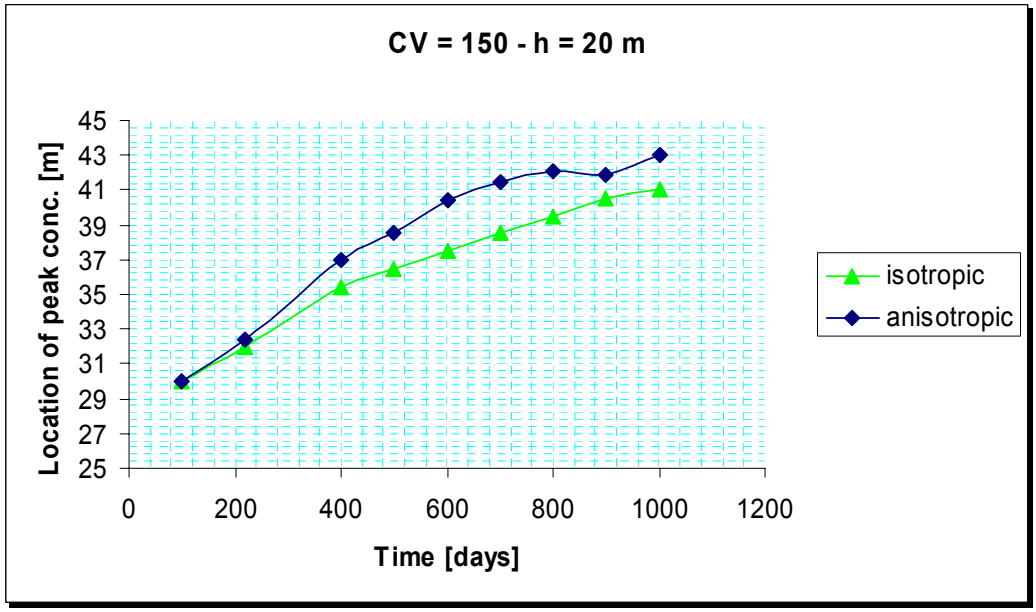

Figure C.49. Location of peak concentration of TCE plume with time for isotropic (h = 10 m when CV = % 50 and h = 20 m when CV = % 150) and anisotropic (h_x = 10 m, h_y = 2 m when CV = % 50 and h_x = 20 m, h_y = 4 m when CV = % 50) fields.

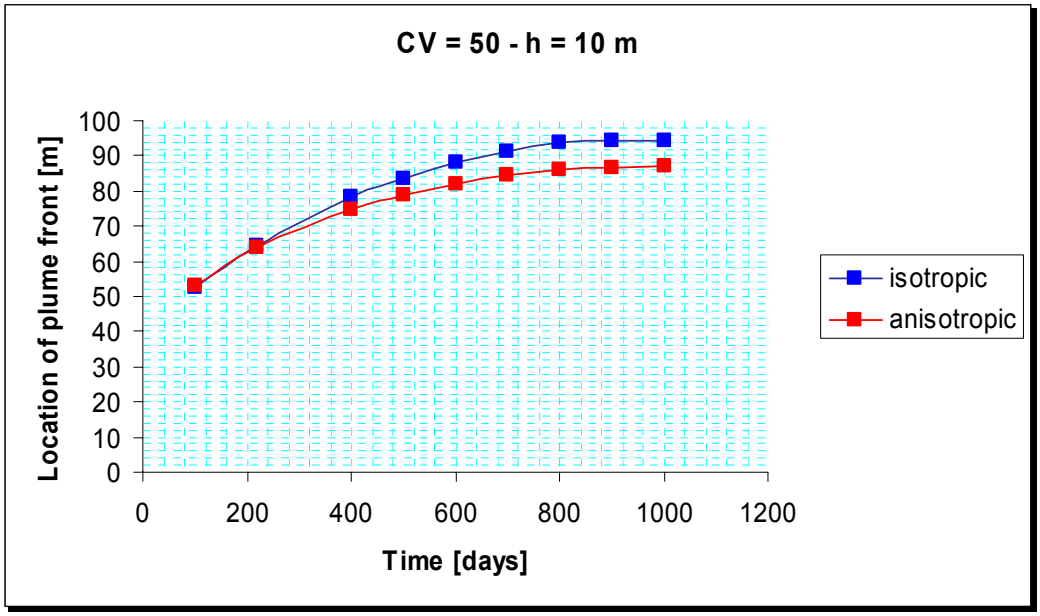

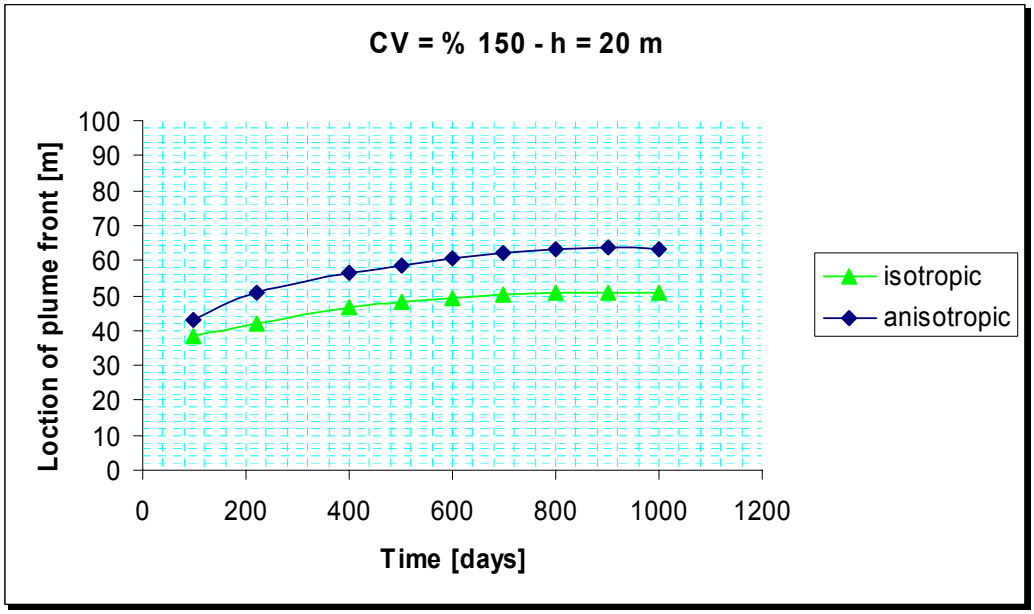

Figure C.50. Location of TCE plume front with time for isotropic (h = 10 m when CV = % 50 and h = 20 m when CV = % 150) and anisotropic (h_x = 10 m, h_y = 2 m when CV = % 50 and h_x = 20 m, h_y = 4 m when CV = % 50) fields.

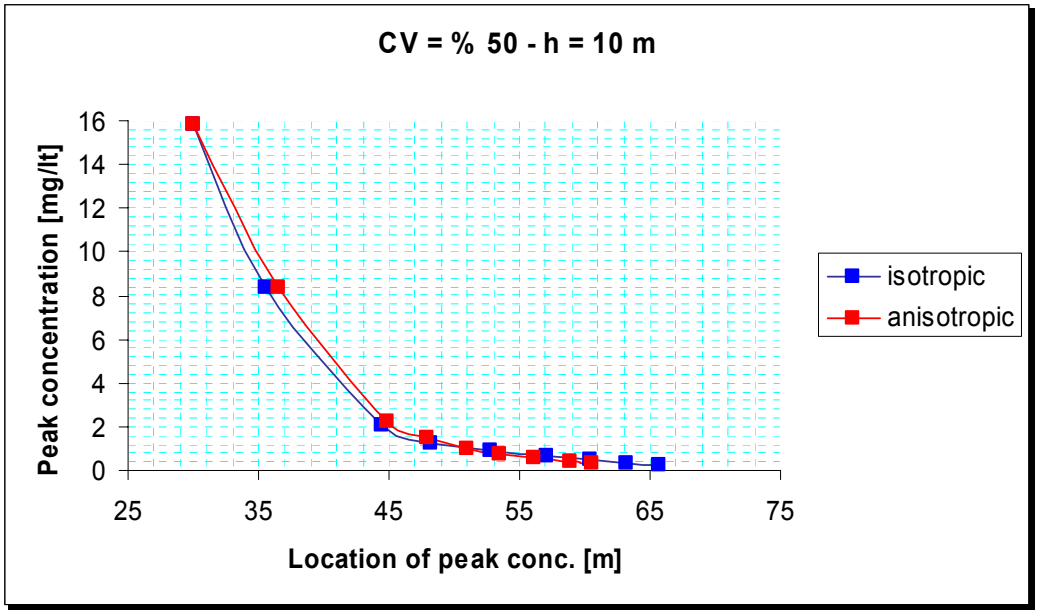

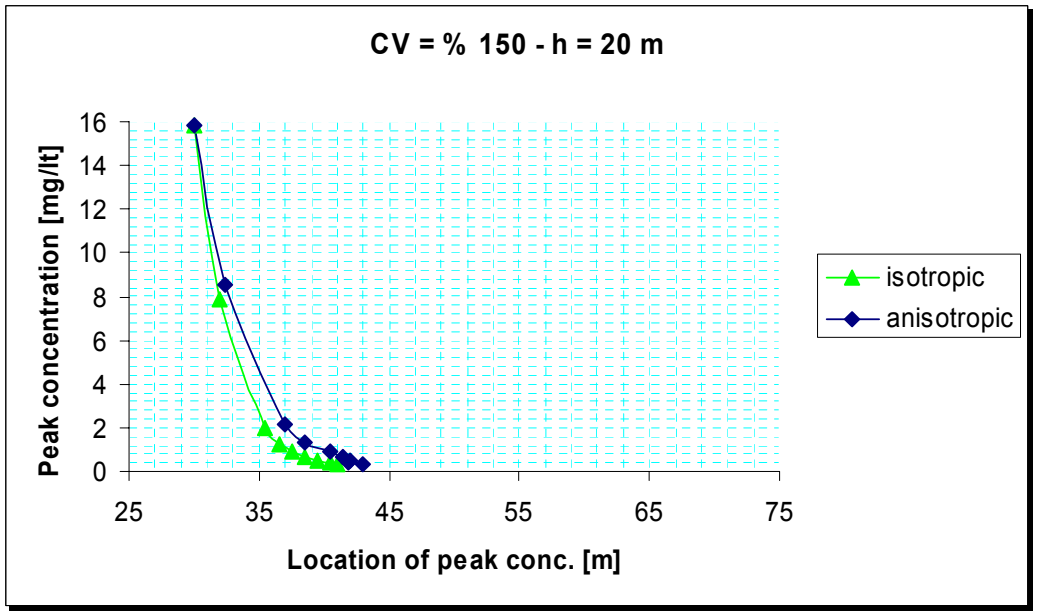

Figure C.51. Peak concentration distribution of TCE plume with distance for isotropic (h = 10 m when CV = % 50 and h = 20 m when CV = % 150) and anisotropic (h_x = 10 m, h_y = 2 m when CV = % 50 and h_x = 20 m, h_y = 4 m when CV = % 50) fields.

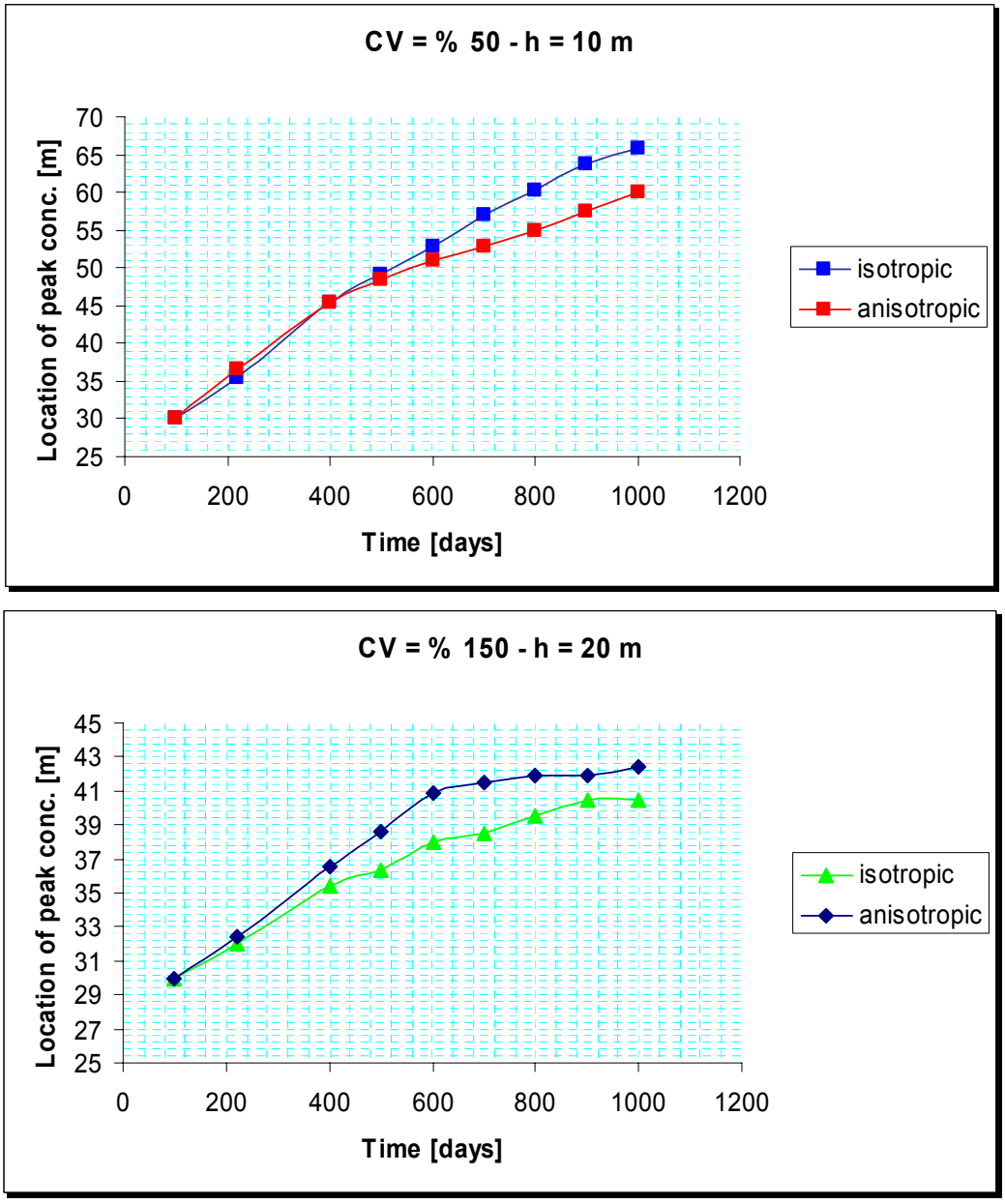

Figure C.52. Location of peak concentration of DCE plume with time for isotropic (h = 10 m when CV = % 50 and h = 20 m when CV = % 150) and anisotropic (h_x = 10 m, h_y = 2 m when CV = % 50 and h_x = 20 m, h_y = 4 m when CV = % 50) fields.

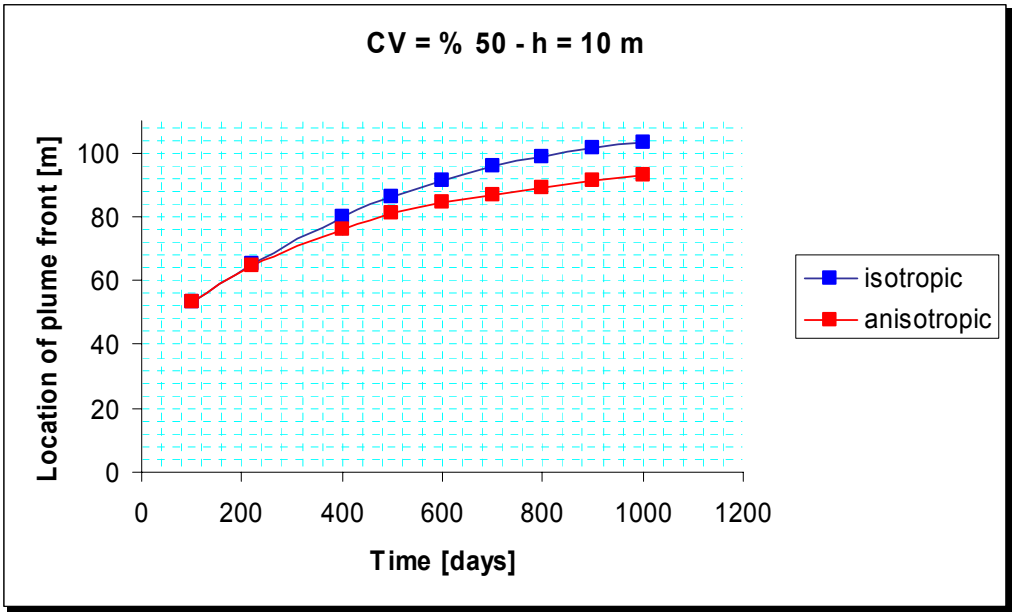

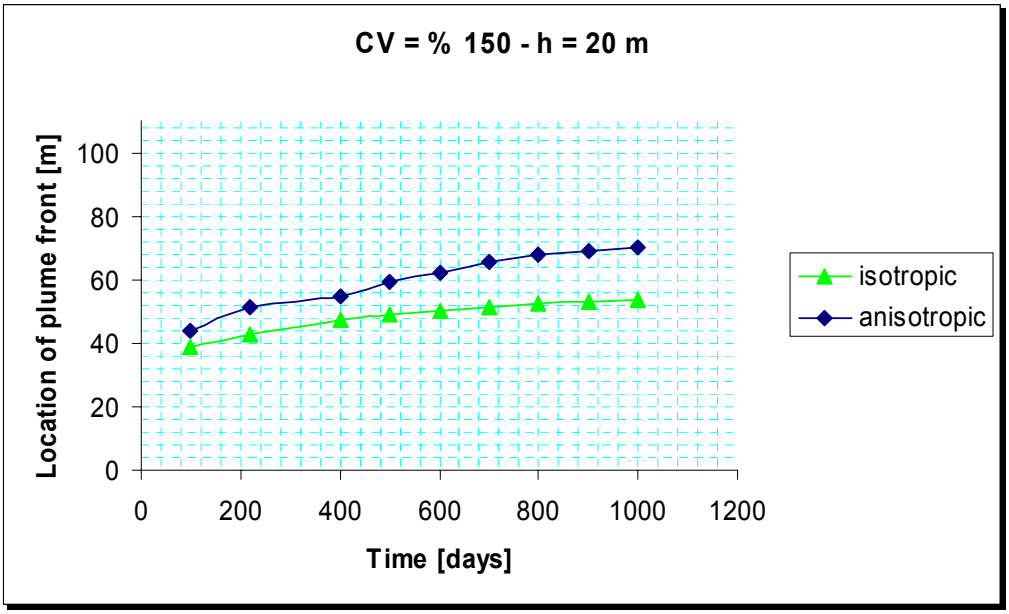

Figure C.53. Location of DCE plume front with time for isotropic (h = 10 m when CV = % 50 and h = 20 m when CV = % 150) and anisotropic (h_x = 10 m, h_y = 2 m when CV = % 50 and h_x = 20 m, h_y = 4 m when CV = % 50) fields.

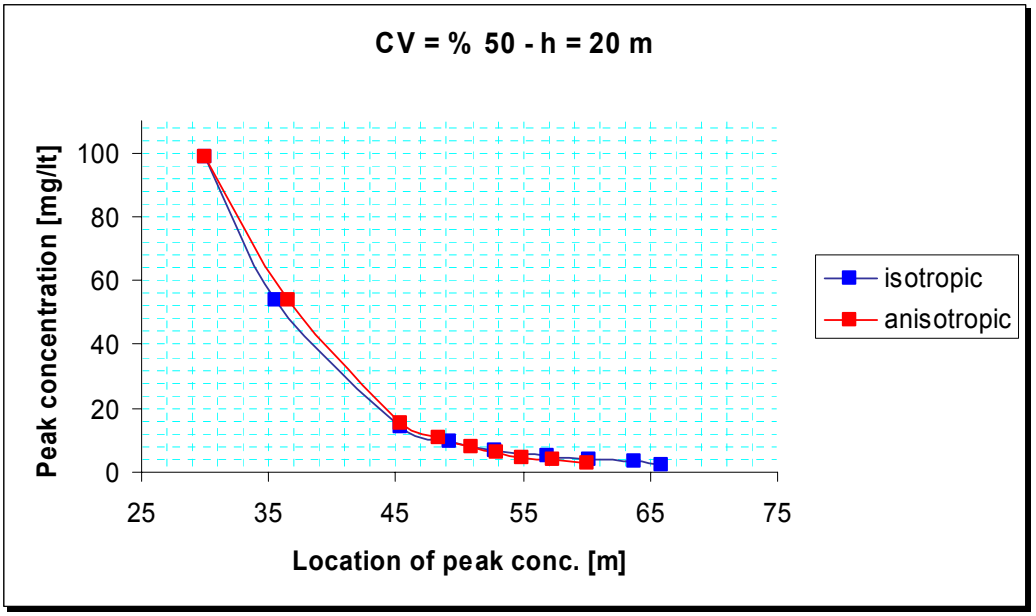

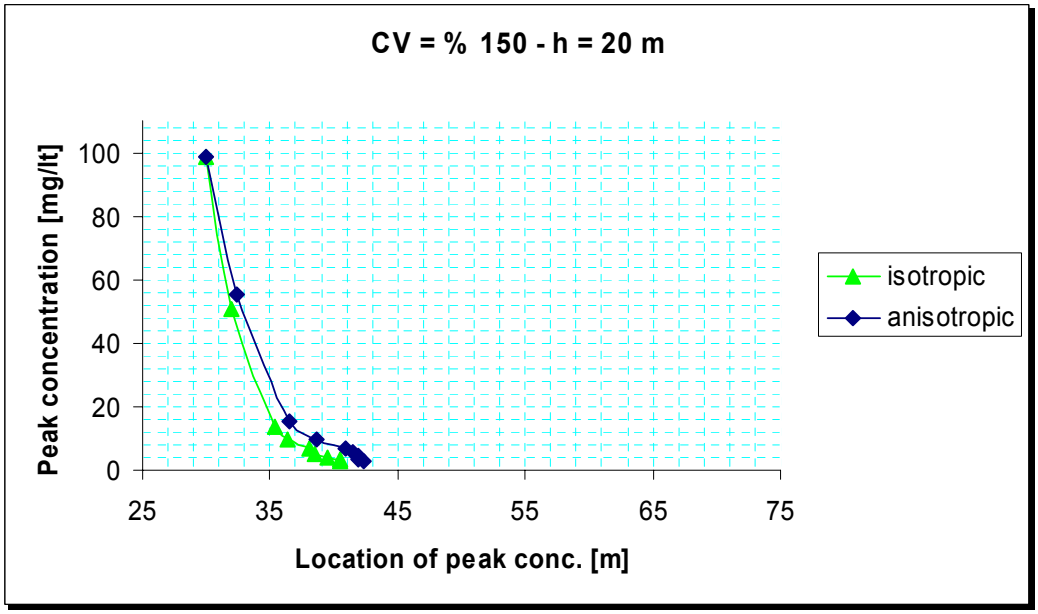

Figure C.54. Peak concentration distribution of DCE plume with distance for isotropic (h = 10 m when CV = % 50 and h = 20 m when CV = % 150) and anisotropic (h_x = 10 m, h_y = 2 m when CV = % 50 and h_x = 20 m, h_y = 4 m when CV = % 50) fields.

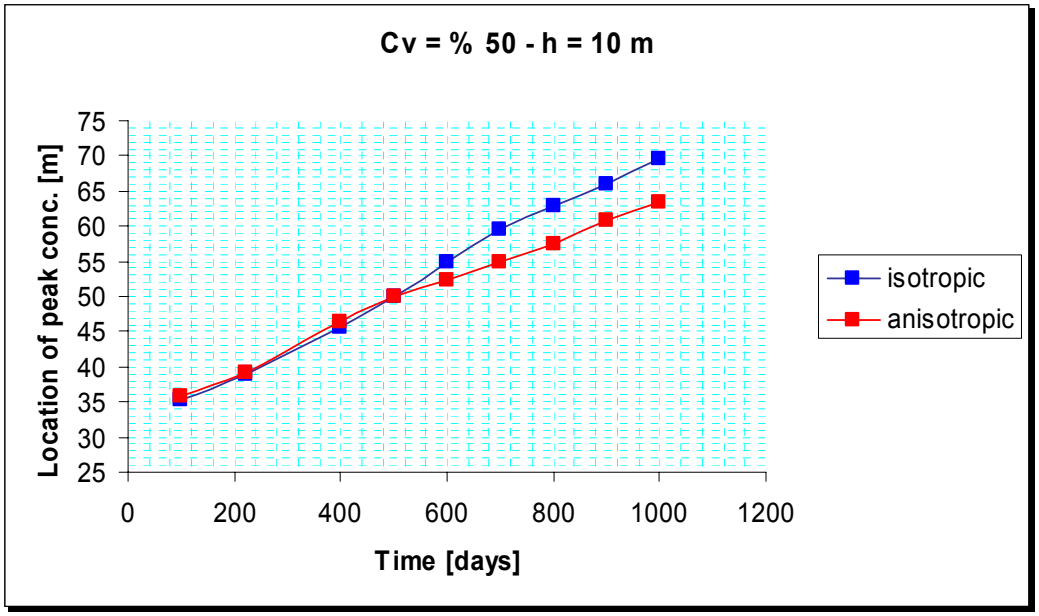

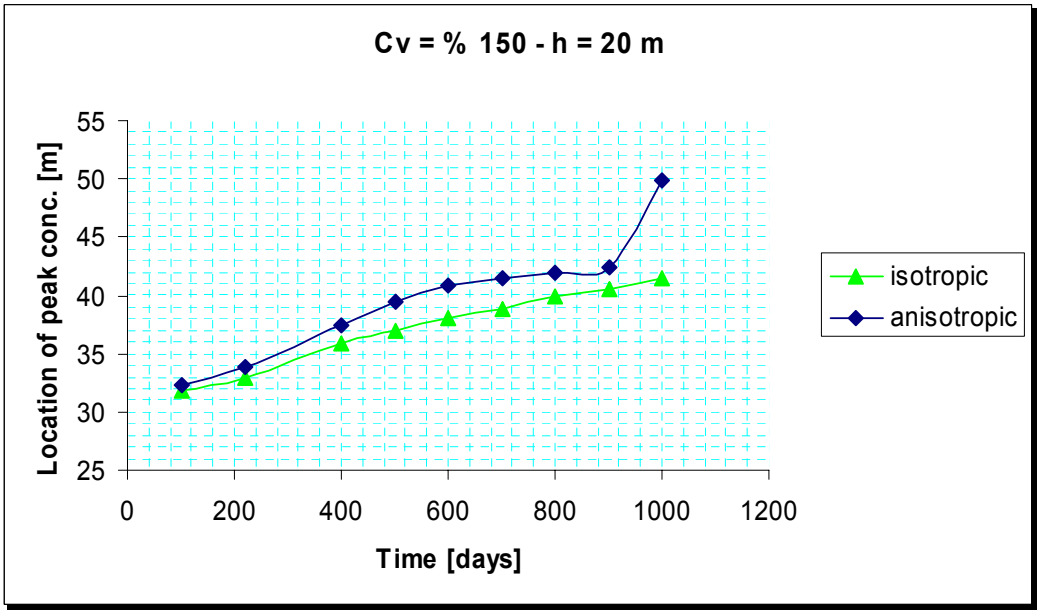

Figure C.55. Location of peak concentration of ETH plume with time for isotropic (h = 10 m when CV = % 50 and h = 20 m when CV = % 150) and anisotropic (h_x = 10 m, h_y = 2 m when CV = % 50 and h_x = 20 m, h_y = 4 m when CV = % 50) fields.

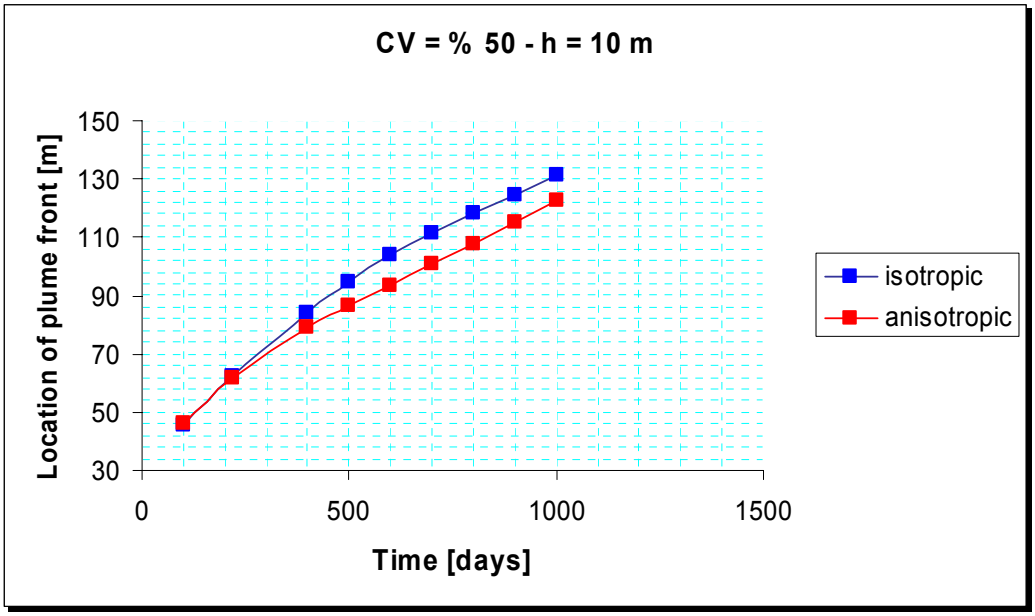

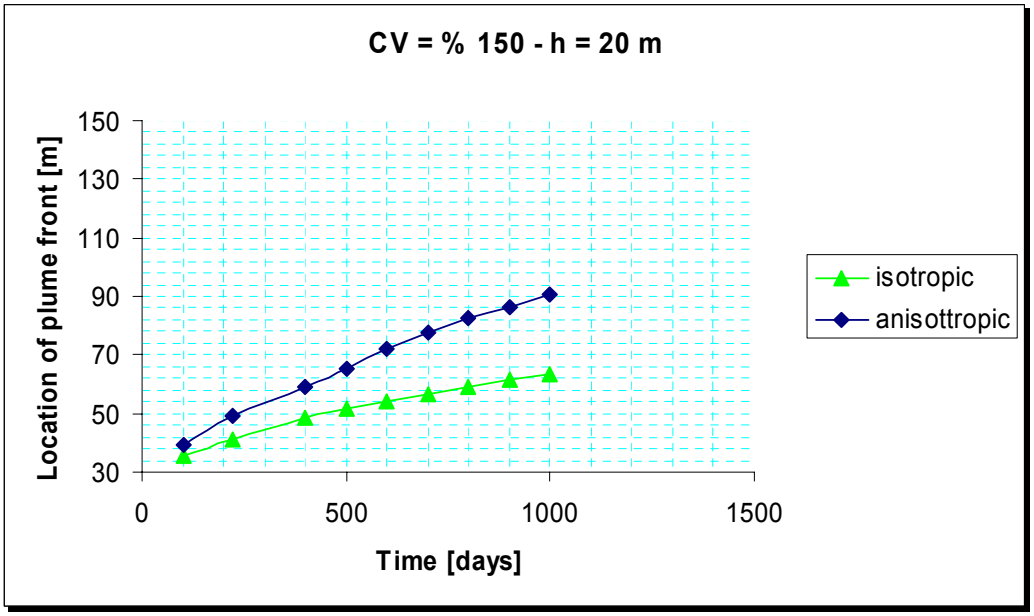

Figure C.56. Location of ETH plume front with time for isotropic (h = 10 m when CV = % 50 and h = 20 m when CV = % 150) and anisotropic (h_x = 10 m, h_y = 2 m when CV = % 50 and h_x = 20 m, h_y = 4 m when CV = % 50) fields.

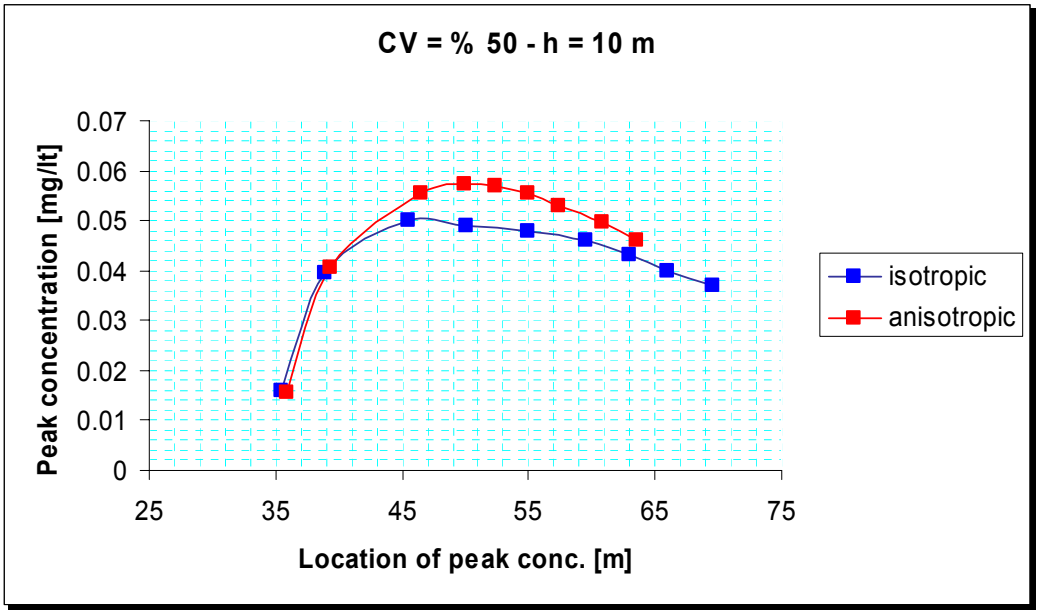

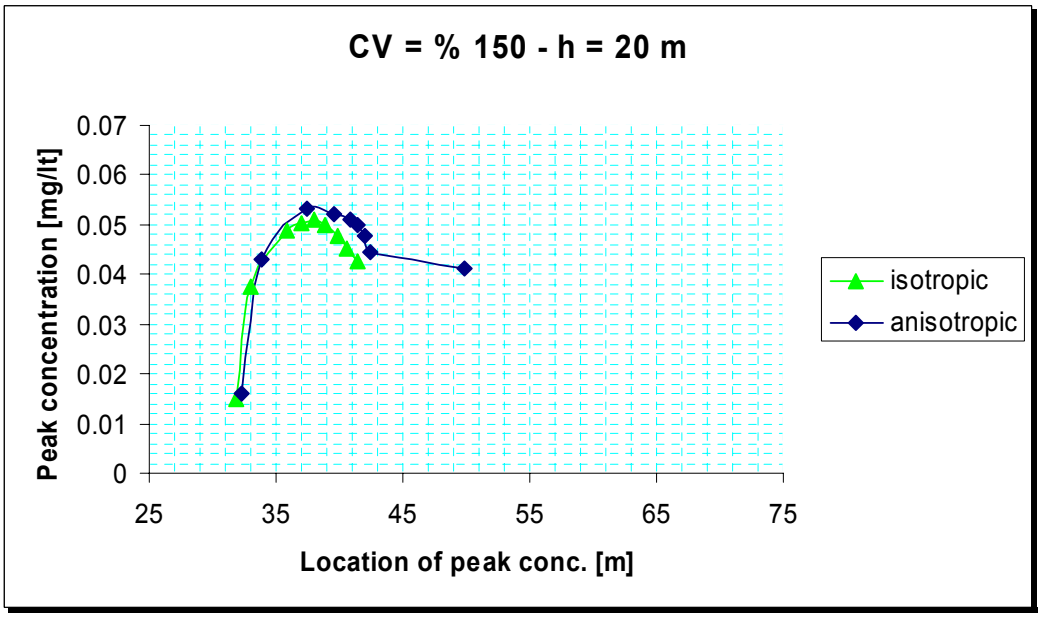

Figure C.57. Peak concentration distribution of ETH plume with distance for isotropic (h = 10 m when CV = % 50 and h = 20 m when CV = % 150) and anisotropic (h_x = 10 m, h_y = 2 m when CV = % 50 and h_x = 20 m, h_y = 4 m when CV = % 50) fields.

APPENDICES D – OBSERVATION WELL TRANSECTS AND PLUME FLOW PATHS

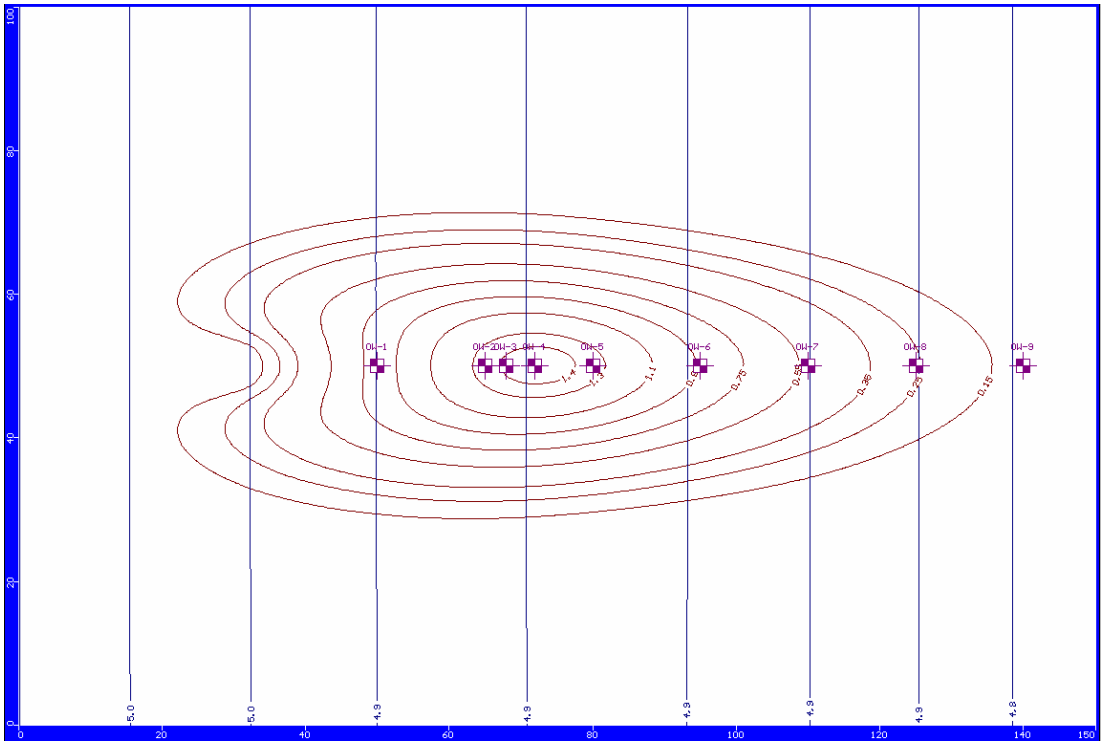

Figure D.1. The VC plume flowpath and observation well configurations for the uniform flow field

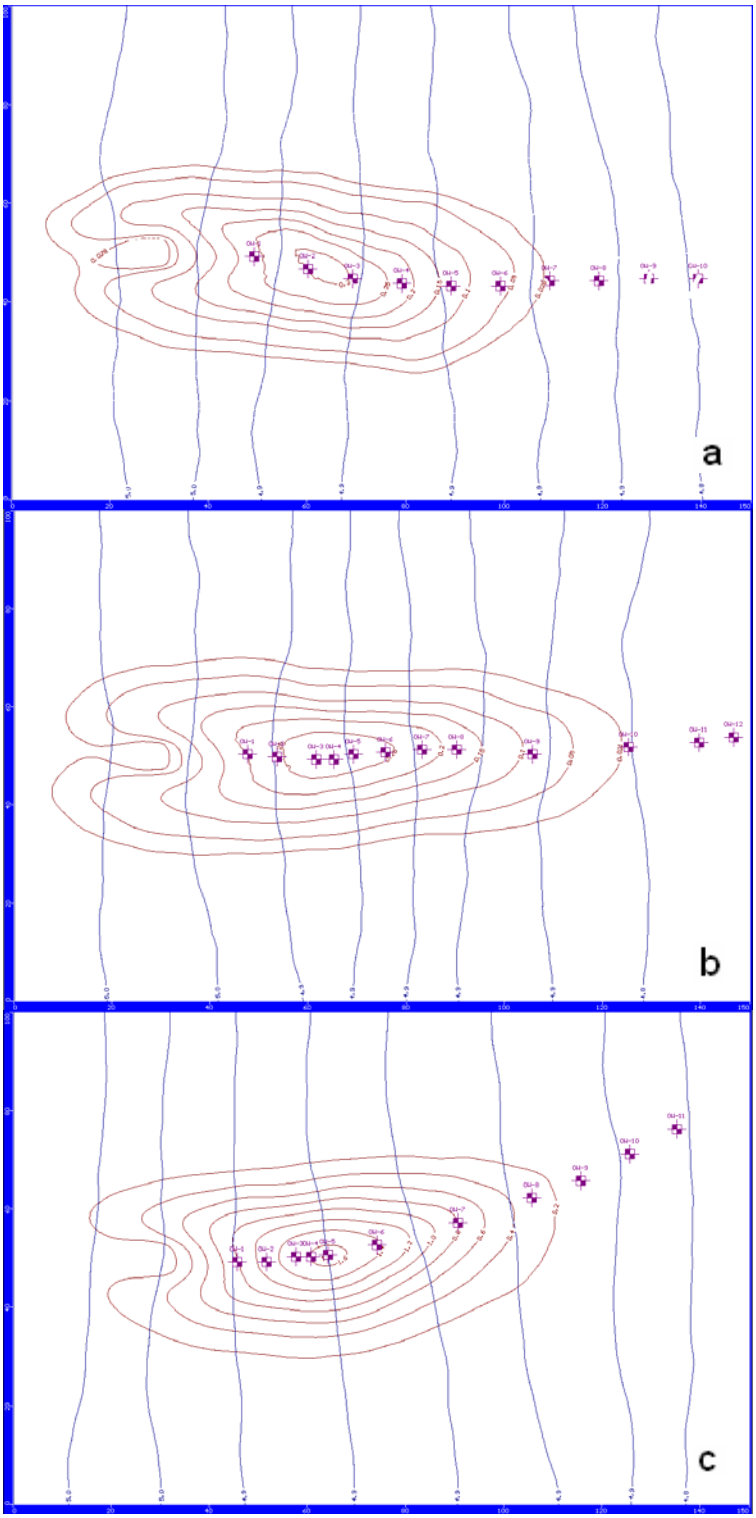

Figure D.2. The VC plume flowpath and observation well configurations for the fields (a) h = 5 m, h = 10 m, h = 20 m when CV = % 50.

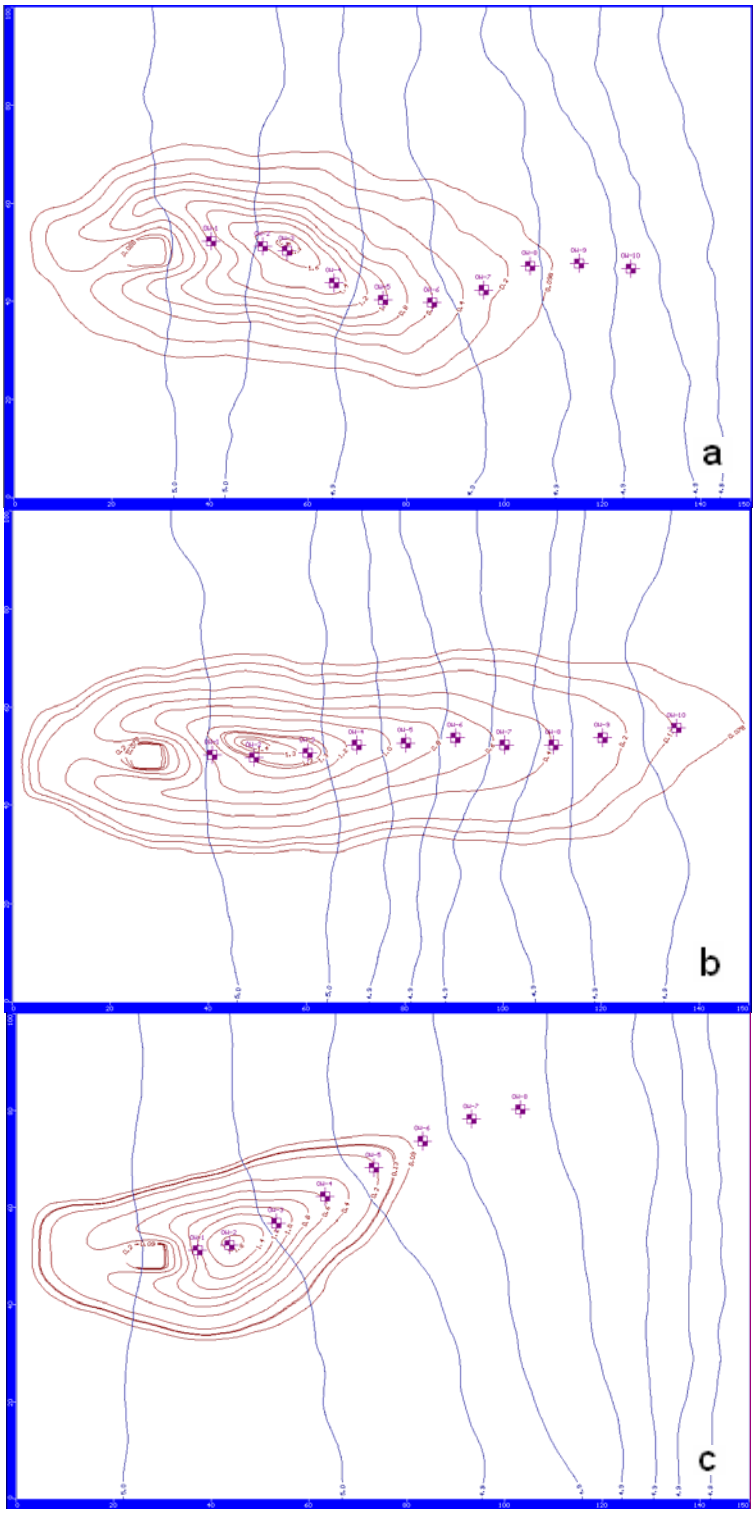

Figure D.3. The VC plume flowpath and observation well configurations for the fields (a) h = 5 m, h = 10 m, h = 20 m when CV = % 100.

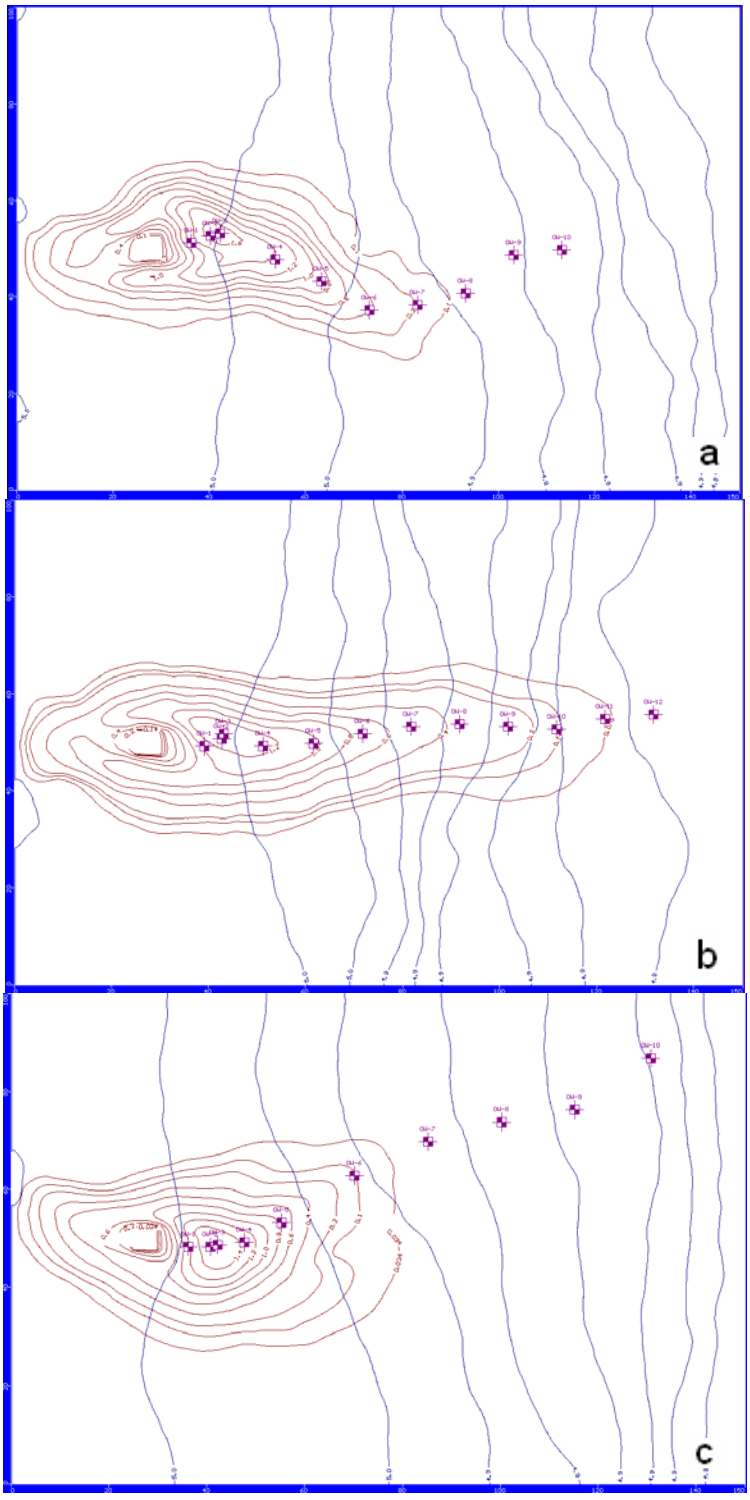

Figure D.4. The VC plume flowpath and observation well configurations for the fields (a) h = 5 m, h = 10 m, h = 20 m when CV = % 150.

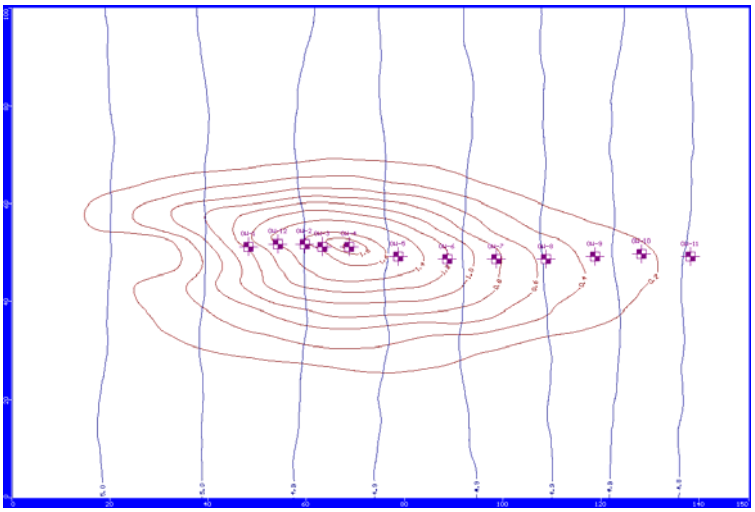

Figure D.5. The VC plume flowpath and observation well configurations for the field h_x = 10 m, h_y = 2 m, when CV = % 50.

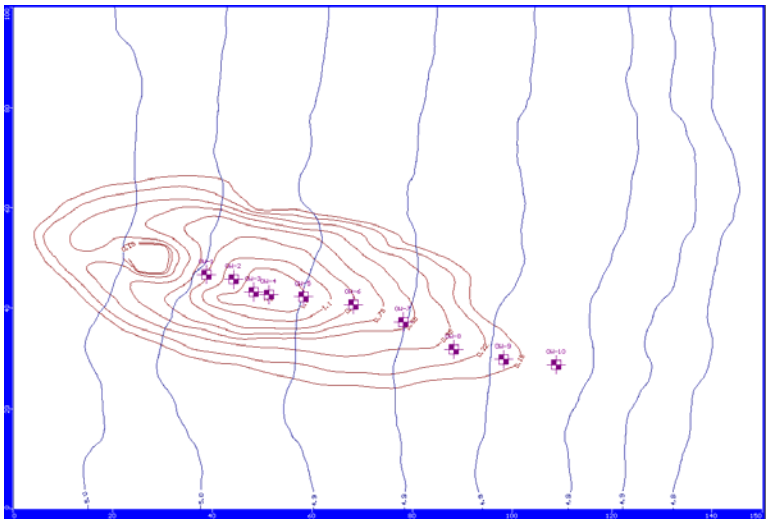

Figure D.6. The VC plume flowpath and observation well configurations for the field h_x = 20 m, h_y = 4 m, when CV = % 150.

APPENDICES E – MEASURED CONTAMINANT CONCENTRATIONS at OBSERVATION WELLS

Table E.1. The observed concentrations of contaminants at locations downgradient of the source of contamination for the field with uniform hydraulic conductivity distribution.

	Distance Downgradient [m]	Concentrations [mg/l] PCE	TCE	DCE	VC	ETH
OW1	0	0.00137 *	0.227	2.005	0.845	
OW2	15	0.0007	0.309	2.77	1.4	
OW3	18	0.0005	0.303 *	2.737 *	1.459	
OW4	22	0.000311	0.282	2.574	1.486	0.0404 *
OW5	30	9.00E-05	0.213	1.98	1.386 *	0.0345
OW6	45	4.00E-06	0.0866	0.862	0.923	0.0196
OW7	60	1.20E-07	0.0271	0.272	0.516	0.00958
OW8	75	1.00E-09	0.00658	0.0726	0.251	0.00423
OW9	90	6.00E-11	0.00145	0.0164	0.122	0.00207

* Located at the center of mass of the plume

Table E.2. The observed concentrations of contaminants at locations downgradient of the source of contamination for the field with Coefficient of Variation (CV) =50 % and Correlation Length (h) = 5 m

	Distance Downgradient [m]	Concentrations PCE [mg/l]	TCE [mg/l]	DCE [mg/l]	VC [mg/l]	ETH [mg/l]
OW1	0	0.00138 *	0.233	2.073	0.909	
OW2	11	0.001	0.303	2.716	1.315	
OW3	21	0.000476	0.297 *	2.677 *	1.509	
OW4	31	0.00011	0.223	2.064	1.435 *	0.0359 *
OW5	40	2E-5	0.128	1.213	1.108	0.0249
OW6	50	2E-6	0.0601	0.584	0.757	0.0153
OW7	60	1E-7	0.0248	0.249	0.492	0.0089
OW8	70	3E-9	0.00857	0.0884	0.282	0.00456
OW9	80	8E-11	0.003	0.0322	0.167	0.00239
OW10	90	2.00E-12	0.001	0.011	0.096	0.00122

* Located at the center of mass of the plume

Table E.3. The observed concentrations of contaminants at locations downgradient of the source of contamination for the field with Coefficient of Variation (CV) =50 % and Correlation Length (h) = 10 m

Distance Downgradient [m]		Concentrations [mg/l] PCE	TCE	DCE	VC	ETH
OW1	0	0.00135 *	0.202	1.78	0.743	
OW2	6	0.00126	0.243	2.13	0.93	
OW3	14	0.00094	0.278	2.455	1.143	
OW4	18	0.00076	0.281	2.5 *	1.21	
OW5	22	0.00057	0.277 *	2.48	1.259	
OW6	28	0.0003	0.258	2.33	1.287 *	0.0358 *
OW7	36	0.00015	0.222	2.04	1.266	0.0332
OW8	43	0.00006	0.182	1.69	1.19	0.0296
OW9	58	0.000005	0.0878	0.841	0.877	0.017
OW10	78	3E-08	0.0178	0.18	0.405	0.0071
OW11	92	2.00E-10	0.00423	0.045	0.204	0.00299
OW12	99	2.00E-11	0.00241	0.0294	0.163	0.00214

* Located at the center of mass of the plume

Table E.4. The observed concentrations of contaminants at locations downgradient of the source of contamination for the field with Coefficient of Variation (CV) =50 % and Correlation Length (h) = 20 m

Distance Downgradient [m]		Concentrations [mg/l] PCE	TCE	DCE	VC	ETH
OW1	0	0.00144 *	0.25	2.191	0.98	
OW2	6	0.00123	0.305	2.71	1.292	
OW3	12	0.0008	0.325	2.915	1.51	
OW4	15	0.00059	0.319 *	2.88 *	1.571	0.044
OW5	19	0.0004	0.301	2.74	1.6 *	0.0432 *
OW6	29	8.00E-05	0.209	1.94	1.425	0.0348
OW7	46	2.00E-07	0.0651	0.632	0.803	0.0162
OW8	61	7.00E-09	0.01	0.101	0.29	0.0047
OW9	72	4.00E-11	0.002	0.0193	0.116	0.00144
OW10	83	2.00E-13	0.00023	0.00307	0.0395	0.00049
OW11	93	7.00E-16	4.00E-05	0.00043	0.0125	0.00012

* Located at the center of mass of the plume

Table E.5. The observed concentrations of contaminants at locations downgradient of the source of contamination for the field with Coefficient of Variation (CV) =100 % and Correlation Length (h) = 5 m

Distance Downgradient [m]		Concentrations [mg/l] PCE	TCE	DCE	VC	ETH
OW1	0	0.00168 *	0.264	2.28	1.018	
OW2	11	0.001	0.347	3.1	1.562	
OW3	16	0.00064	0.337 *	3.034 *	1.7	0.047 *
OW4	26	0.0002	0.245	2.24	1.48	0.0378
OW5	37	0.000025	0.124	1.259	1.038 *	0.0235
OW6	47	0.0000027	0.051	0.446	0.603	0.0123
OW7	56	8.00E-08	0.0132	0.133	0.281	0.0052
OW8	65	1.26E-09	0.00354	0.0366	0.14	0.0019
OW9	75	1.50E-10	0.0008	0.0086	0.0627	0.0007
OW10	86	2.20E-13	0.0002	0.0017	0.0259	0.00026

* Located at the center of mass of the plume

Table E.6. The observed concentrations of contaminants at locations downgradient of the source of contamination for the field with Coefficient of Variation (CV) =100 % and Correlation Length (h) = 10 m

Distance Downgradient [m]		Concentrations [mg/l] PCE	TCE	DCE	VC	ETH
OW1	0	0.00146 *	0.255	2.232	1.046	
OW2	9	0.001	0.284	2.536	1.303	
OW3	20	0.00036	0.247 *	2.238 *	1.335	0.0358 *
OW4	30	1.00E-04	0.177	1.603	1.153 *	0.0287
OW5	40	2.30E-05	0.1158	1.085	0.927	0.0214
OW6	50	5.00E-06	0.0733	0.7	0.735	0.016
OW7	60	1.00E-06	0.043	0.419	0.561	0.0112
OW8	70	1.20E-07	0.0212	0.211	0.391	0.0071
OW9	80	5.00E-08	0.0086	0.088	0.25	0.00401
OW10	95	3.00E-11	0.00237	0.0227	0.119	0.0016

* Located at the center of mass of the plume

Table E.7. The observed concentrations of contaminants at locations downgradient of the source of contamination for the field with Coefficient of Variation (CV) =100 % and Correlation Length (h) = 20 m

	Distance Downgradient [m]	Concentrations [mg/l] PCE	TCE	DCE	VC	ETH
OW1	0	0.00144 *	0.257	2.376	1.165	
OW2	7	0.000722	0.321 *	2.872 *	1.632	0.0451 *
OW3	17	6.00E-05	0.162	1.509	1.21 *	0.0286
OW4	28	2.00E-06	0.0452	0.439	0.583	0.0116
OW5	40	1.50E-08	0.00768	0.0782	0.209	0.00335
OW6	51	5.00E-11	0.00117	0.0123	0.0702	0.00085
OW7	62	3.27E-13	0.000194	0.00212	0.0247	0.00026
OW8	72	3.10E-15	3.25E-05	0.00038	0.0095	9.0E-05

* Located at the center of mass of the plume

Table E.8. The observed concentrations of contaminants at locations downgradient of the source of contamination for the field with Coefficient of Variation (CV) =150 % and Correlation Length (h) = 5 m

	Distance Downgradient [m]	Concentrations [mg/l] PCE	TCE	DCE	VC	ETH
OW1	0	0.00169 *	0.319	2.73	1.259	
OW2	4	0.0012	0.361	3.237	1.634	
OW3	6	0.0007	0.346 *	3.11 *	1.713 *	0.0485 *
OW4	18	0.00025	0.226	2.063	1.37	0.0349
OW5	28	3.20E-05	0.107	1.0093	0.888	0.0202
OW6	40	1.70E-06	0.0321	0.311	0.407	0.0081
OW7	49	9.00E-08	0.00945	0.094	0.1895	0.00325
OW8	58	3.00E-10	0.00128	0.0132	0.0585	0.00075
OW9	67	2.00E-12	0.000207	0.00222	0.02	0.00022
OW10	77	1.30E-14	3.00E-05	0.00032	0.00663	7.E-07

* Located at the center of mass of the plume

Table E.9. The observed concentrations of contaminants at locations downgradient of the source of contamination for the field with Coefficient of Variation (CV) =150 % and Correlation Length (h) = 10 m

	Distance Downgradient [m]	Concentrations [mg/l] PCE	TCE	DCE	VC	ETH
OW1	0	0.00146 *	0.259	2.308	0.0326	
OW2	4	0.00105	0.304	2.772	1.362	
OW3	5	0.0008	0.294 *	2.639 *	1.385	
OW4	12	0.00059	0.251	2.256	1.246 *	0.0348 *
OW5	23	0.000138	0.17	1.56	1.035	0.0264
OW6	33	2.30E-05	0.0944	0.885	0.732	0.017
OW7	43	3.70E-06	0.0507	0.486	0.511	0.011
OW8	53	6.20E-07	0.0277	0.2695	0.365	0.00724
OW9	63	8.70E-08	0.0141	0.141	0.254	0.0046
OW10	73	2.80E-09	0.00534	0.0545	0.152	0.00236
OW11	83	4.60E-11	0.00162	0.017	0.0815	0.00105
OW12	93	1.30E-12	0.000585	0.00557	0.0451	0.00052

* Located at the center of mass of the plume

Table E.10. The observed concentrations of contaminants at locations downgradient of the source of contamination for the field with Coefficient of Variation (CV) =150 % and Correlation Length (h) = 20 m

	Distance Downgradient [m]	Concentrations [mg/l] PCE	TCE	DCE	VC	ETH
OW1	0	0.0134 *	0.259	0.00107	1.137	
OW2	5	0.00088	0.311	2.77	1.53	
OW3	6	0.0007	0.295 *	2.68 *	1.556 *	
OW4	12	0.000157	0.206	1.906	1.348	0.0335 *
OW5	20	8.00E-06	0.0744	0.706	0.762	0.0161
OW6	37	2.50E-09	0.00301	0.031	0.095	0.00151
OW7	54	3.00E-14	4.60E-05	0.00052	0.0109	0.00011
OW8	69	5.00E-18	7.40E-07	9.4E-06	0.00178	1.5E-05
OW9	84	0	1.00E-08	1.3E-07	0.0003	2.0E-06
OW10	102	0	5.00E-11	6.7E-10	1.3E-05	7.7E-08

* Located at the center of mass of the plume

Table E.11. The observed concentrations of contaminants at locations downgradient of the source of contamination for the anisotropic field with Coefficient of Variation, CV =50 % and Correlation Lengths hx = 10 m and hy = 2 m.

Distance Downgradient [m]		Concentrations [mg/l] PCE	TCE	DCE	VC	ETH]
OW1	0	0.00154 *	0.267	2.36	1.049	0.033
OW2	6	0.00125	0.33	2.956	1.4403	0.423
OW3	12	0.00087	0.345 *	3.1 *	1.58	0.0457
OW4	15	0.00072	0.341	3.055	1.625	0.0461 *
OW5	21	0.00043	0.316	2.87	1.666 *	0.0452
OW6	31	0.000146	0.244	2.196	1.55	0.0389
OW7	41	2.13E-05	0.139	1.31	1.218	0.0272
OW8	51	1.98E-06	0.065	0.632	0.833	0.0167
OW9	61	1.67E-07	0.0289	0.278	0.545	0.0099
OW10	71	9.07E-09	0.0116	0.119	0.34	0.0055
OW11	81	6.10E-10	0.0051	0.0544	0.224	0.0032
OW12	91	4.66E-11	0.0023	0.025	0.154	0.0018

* Located at the center of mass of the plume

Table E.12. The observed concentrations of contaminants at locations downgradient of the source of contamination for the anisotropic field with Coefficient of Variation, CV =150 % and Correlation Lengths hx = 20 m and hy = 4 m.

Distance Downgradient [m]		Concentrations [mg/l] PCE	TCE	DCE	VC	ETH
OW1	0	0.00144 *	0.228	2.012	0.945	
OW2	6	0.0012	0.28	2.53	1.252	
OW3	10	0.00079	0.3 *	2.697 *	1.44	
OW4	13	0.000586	0.289	2.616	1.495 *	0.04097 *
OW5	20	0.00016	0.215	1.98	1.37	0.0342
OW6	30	1.91E-05	0.116	1.09	0.956	0.0218
OW7	41	2.83E-06	0.0539	0.52	0.597	0.0124
OW8	52	1.14E-07	0.0166	0.165	0.284	0.00526
OW9	62	1.38E-08	7.76E-03	0.0780	0.171	0.0029
OW10	72	1.47E-09	3.90E-03	0.0394	0.113	0.00173

* Located at the center of mass of the plume

APPENDICES F –DEGRADATION RATE GRAPHS

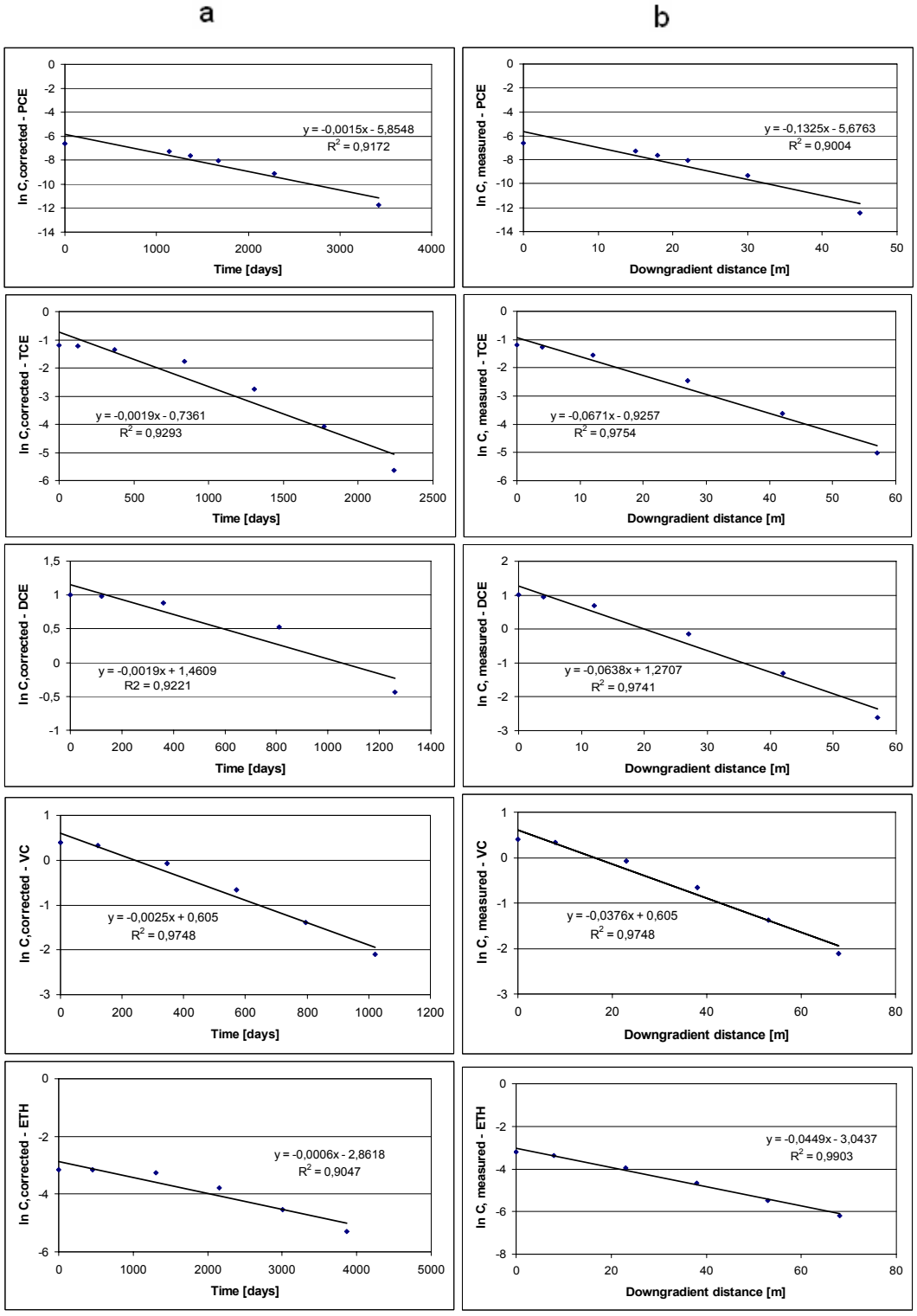

Figure F.1. Linear Regression Plots for (a) Conservative Tracer Method (b) Buscheck-Alcantar Method for uniform field

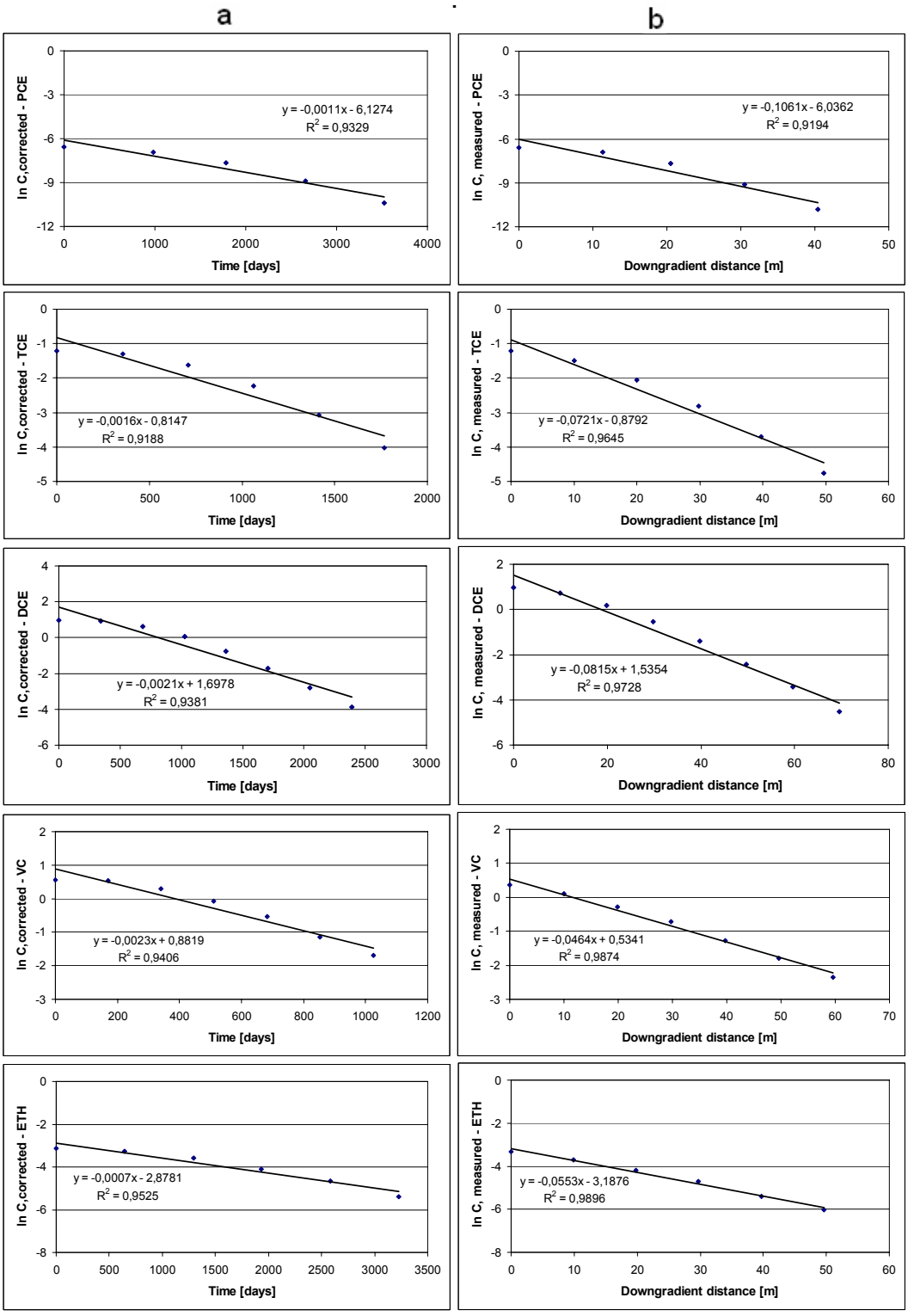

Figure F.2. Linear Regression Plots for (a) Conservative Tracer Method (b) Buscheck-Alcantar Method when CV = % 50 and h = 5 m.

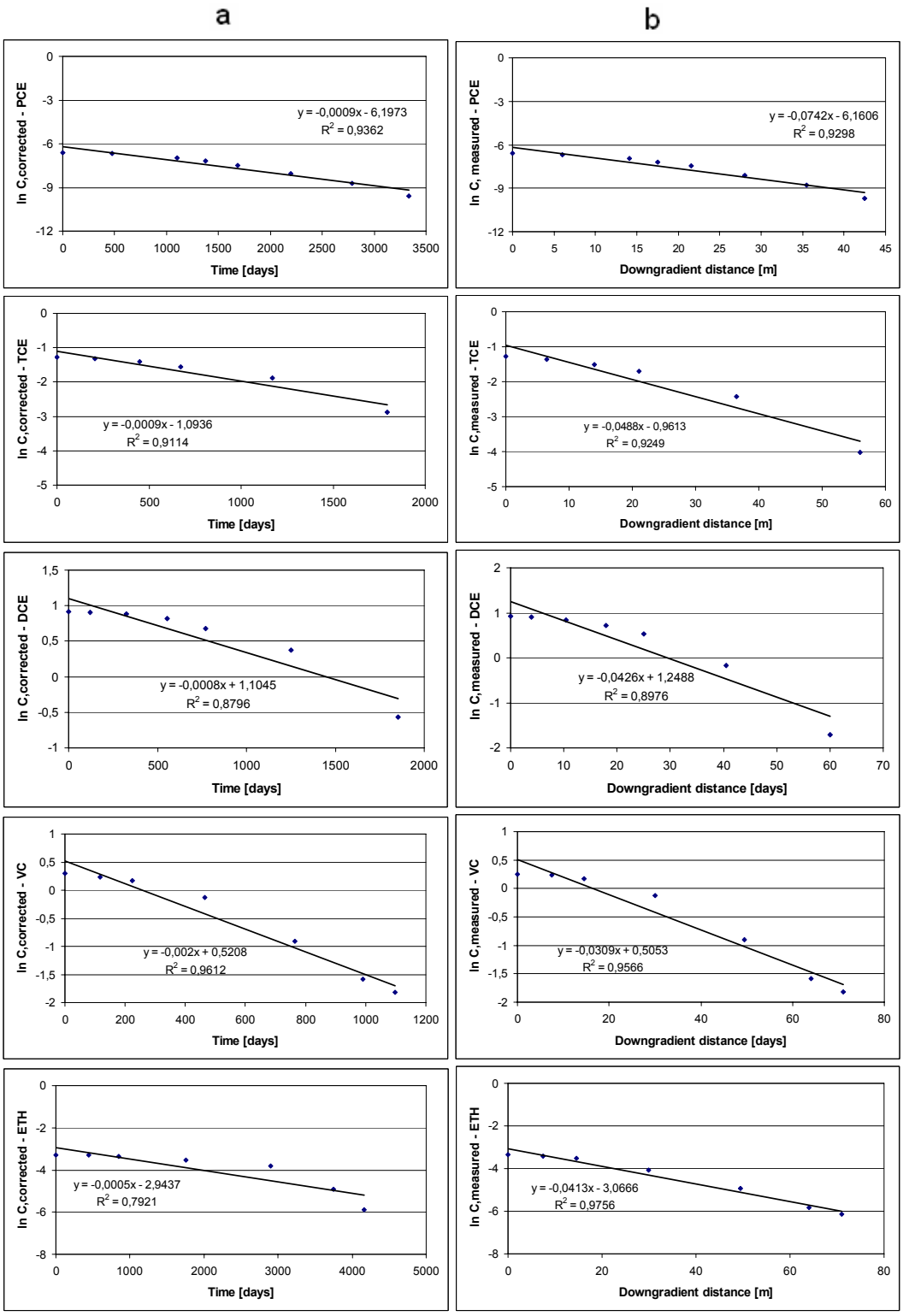

Figure F.3. Linear Regression Plots for (a) Conservative Tracer Method (b) Buscheck-Alcantar Method when CV = % 50 and h = 10 m.

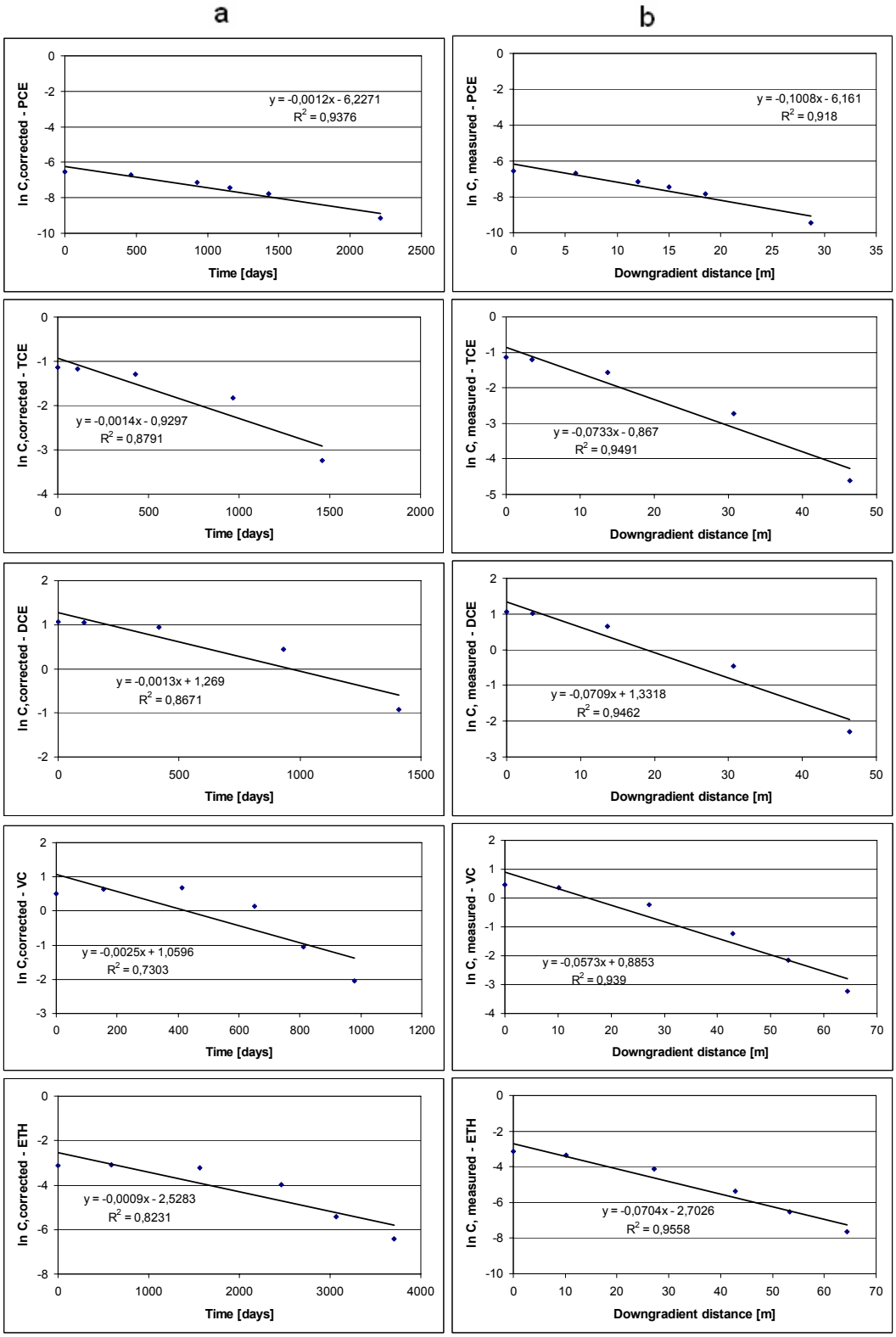

Figure F.4. Linear Regression Plots for (a) Conservative Tracer Method (b) Buscheck-Alcantar Method when CV = % 50 and h = 20 m.

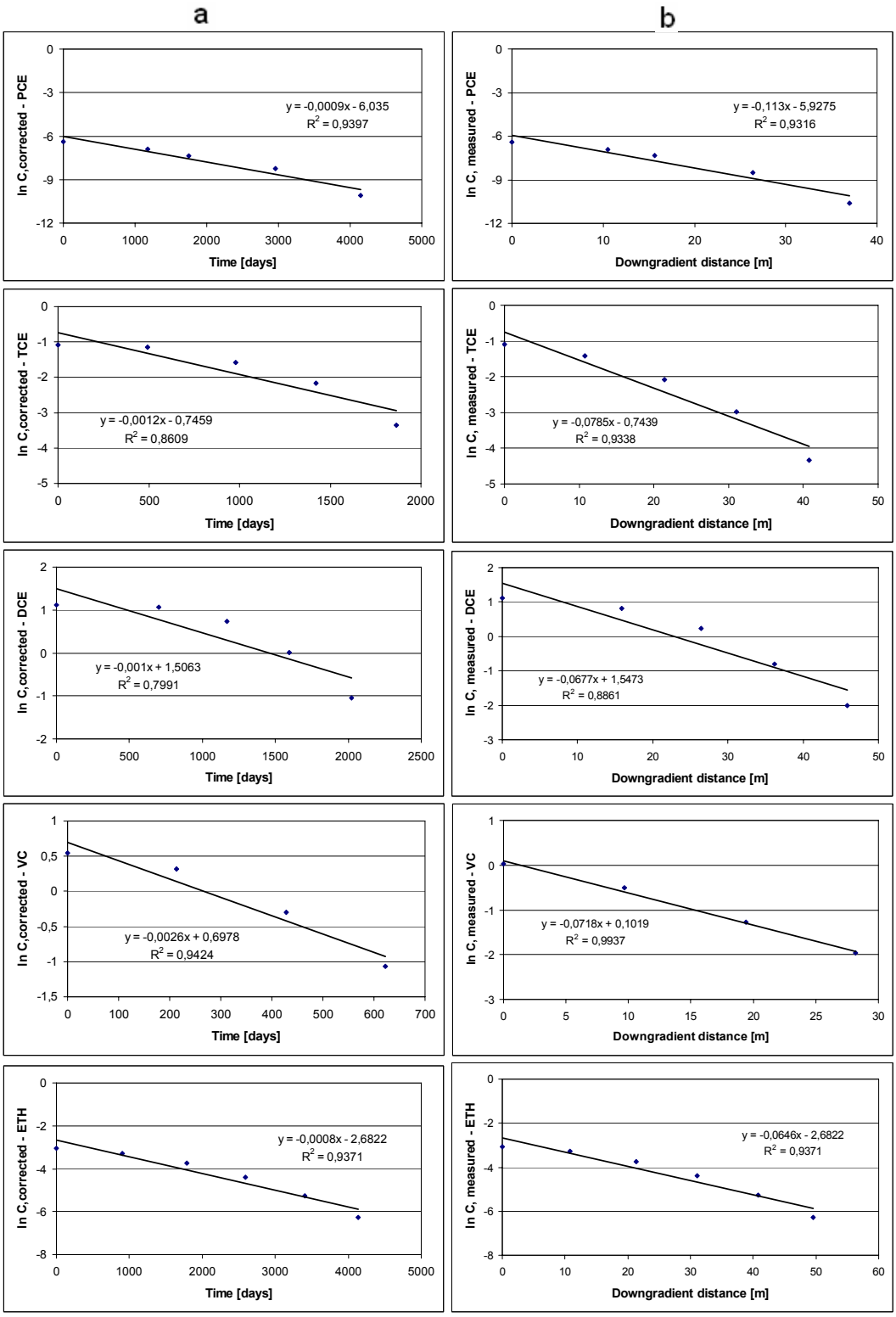

Figure F.5. Linear Regression Plots for (a) Conservative Tracer Method (b) Buscheck-Alcantar Method when CV = % 100 and h = 5 m.

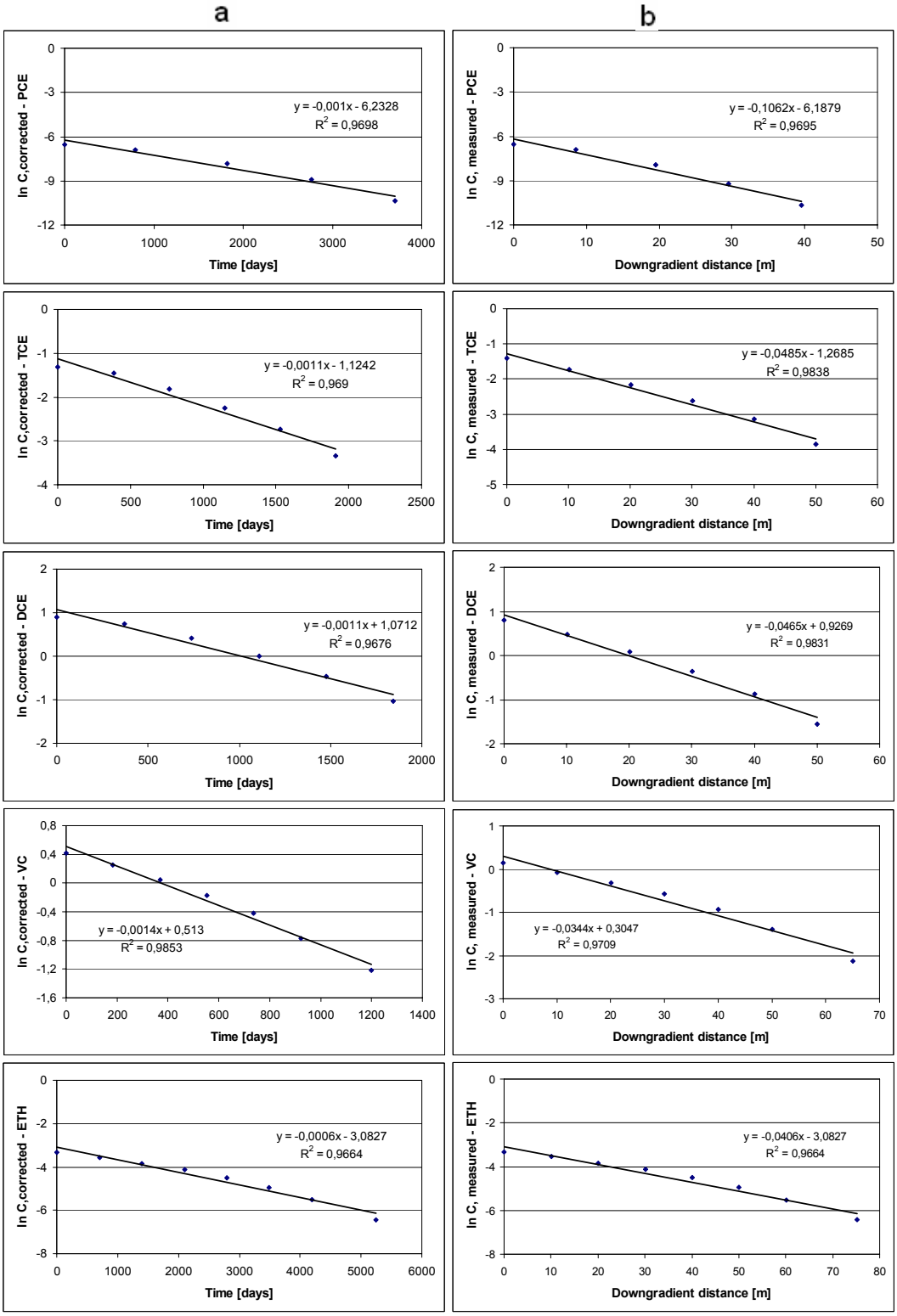

Figure F.6. Linear Regression Plots for (a) Conservative Tracer Method (b) Buscheck-Alcantar Method when CV = % 100 and h = 10 m.

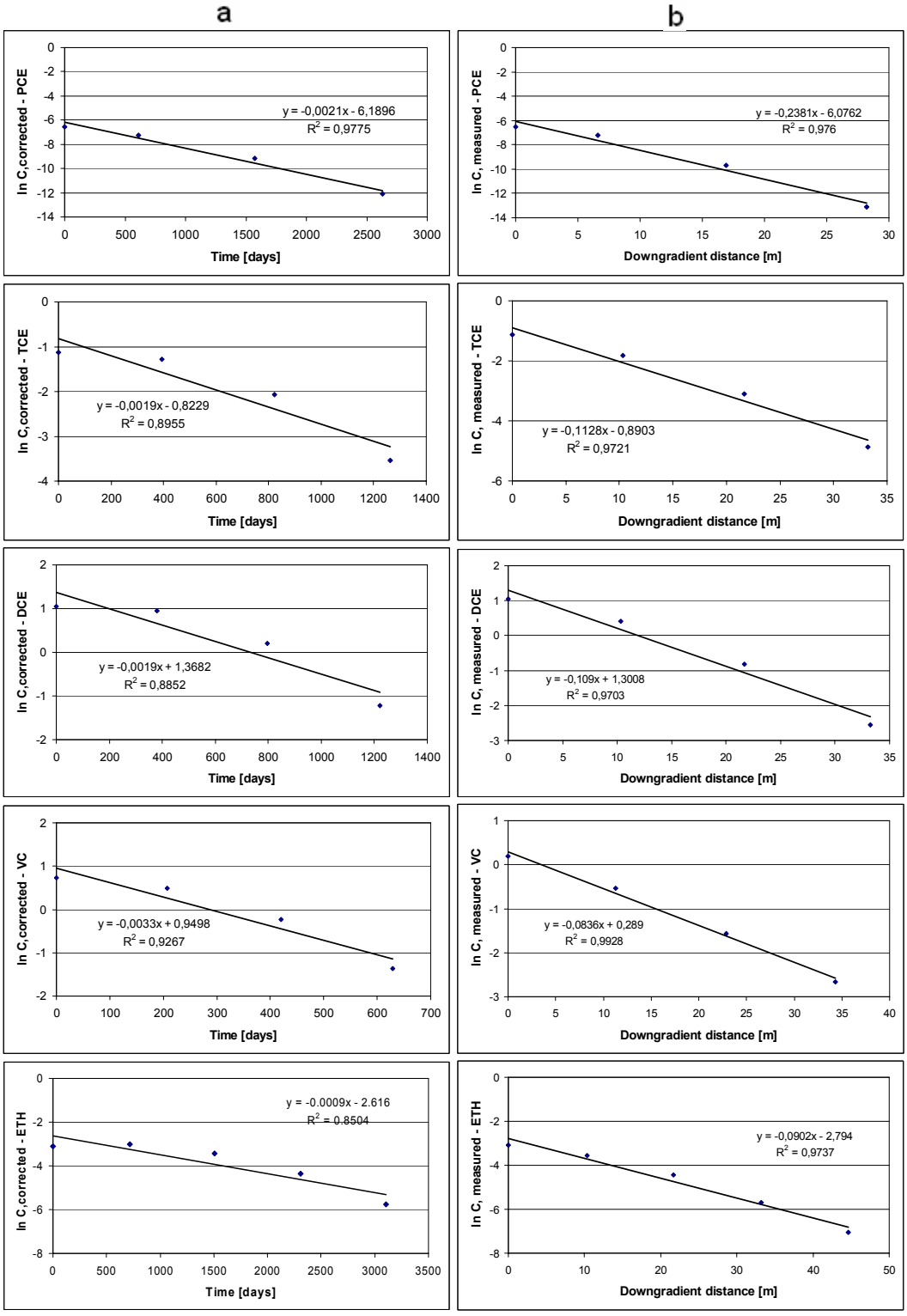

Figure F.7. Linear Regression Plots for (a) Conservative Tracer Method (b) Buscheck-Alcantar Method when CV = % 100 and h = 20 m.

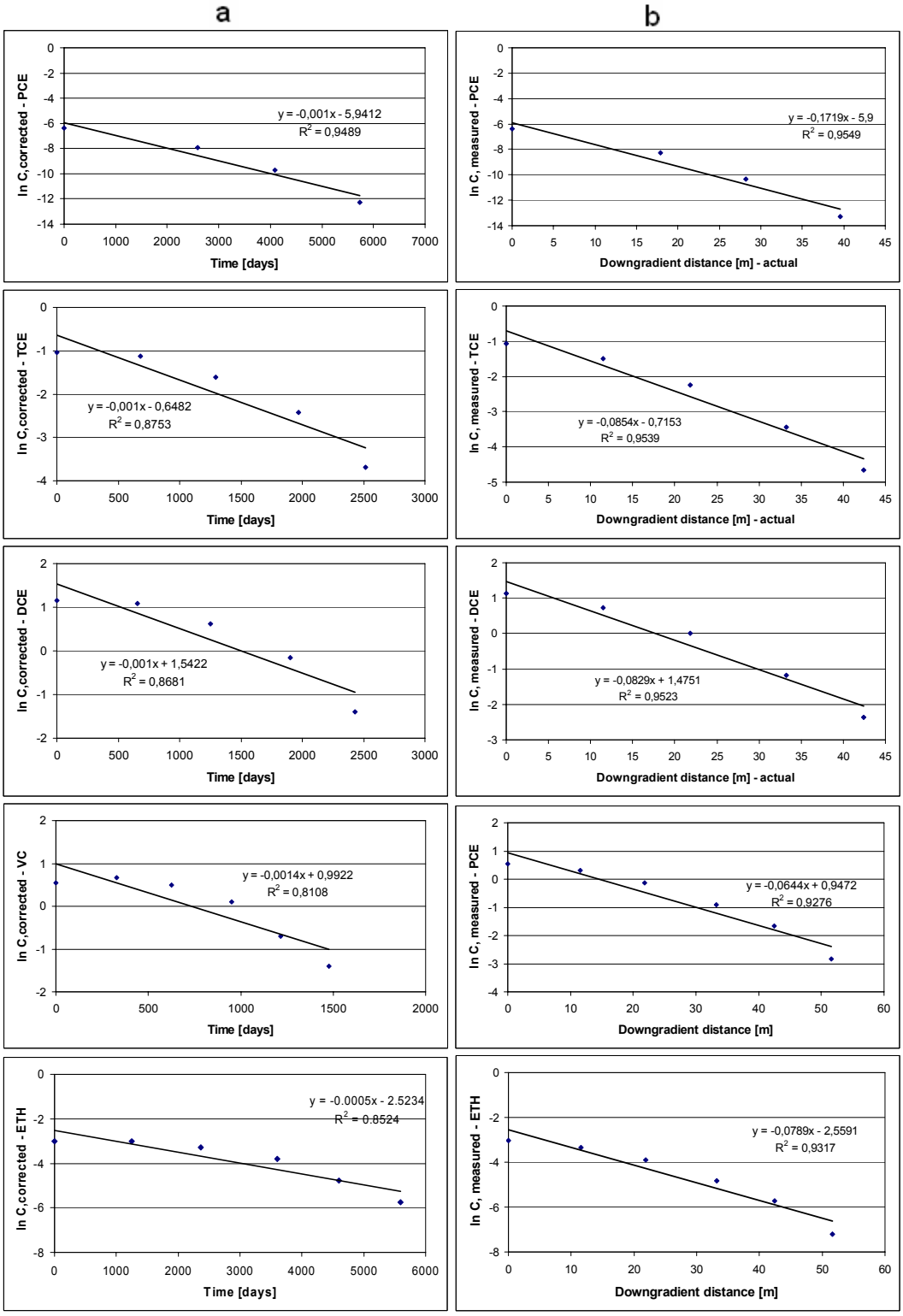

Figure F.8. Linear Regression Plots for (a) Conservative Tracer Method (b) Buscheck-Alcantar Method when CV = % 150 and h = 5 m.

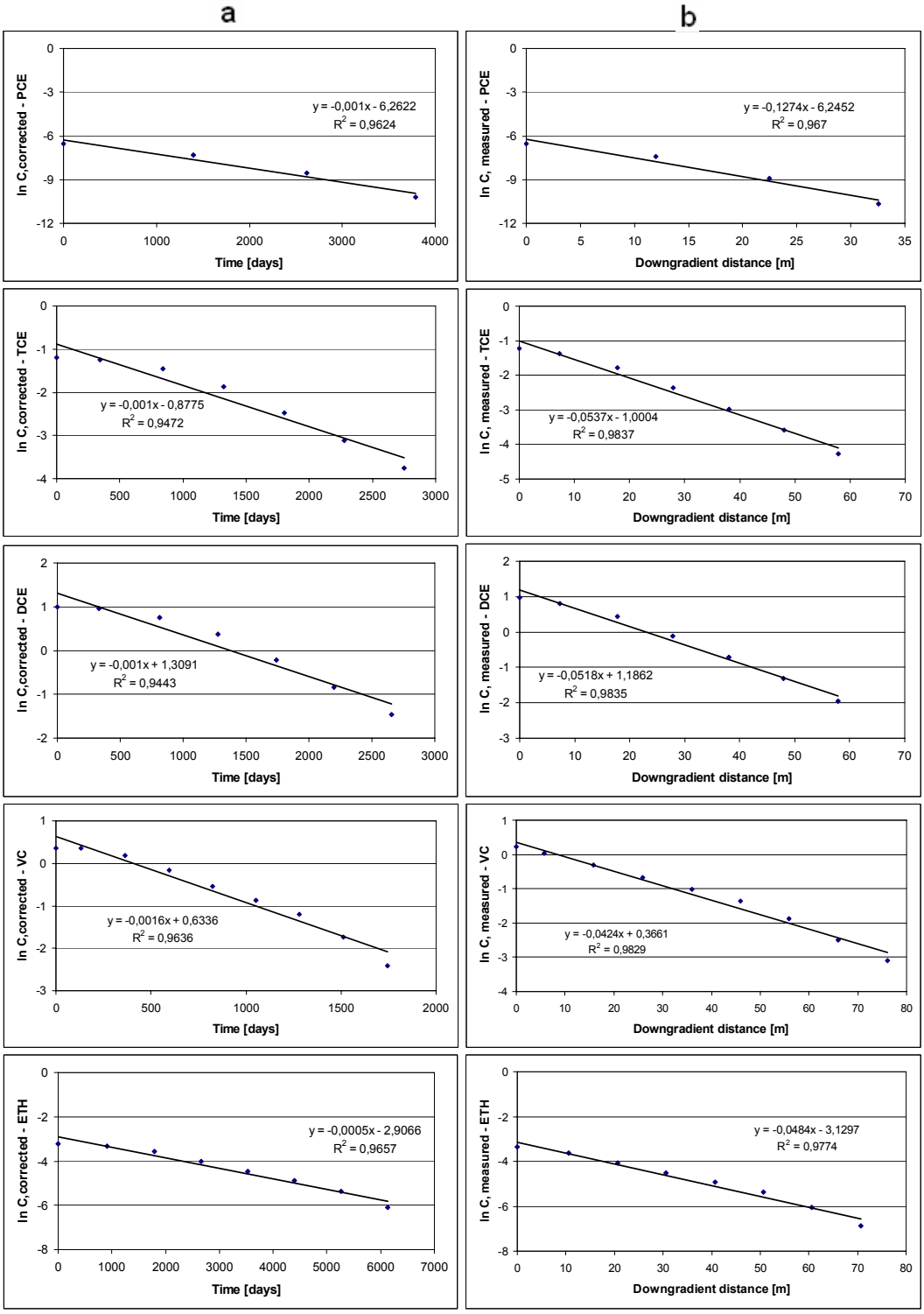

Figure F.9. Linear Regression Plots for (a) Conservative Tracer Method (b) Buscheck-Alcantar Method when CV = % 150 and h = 10 m.

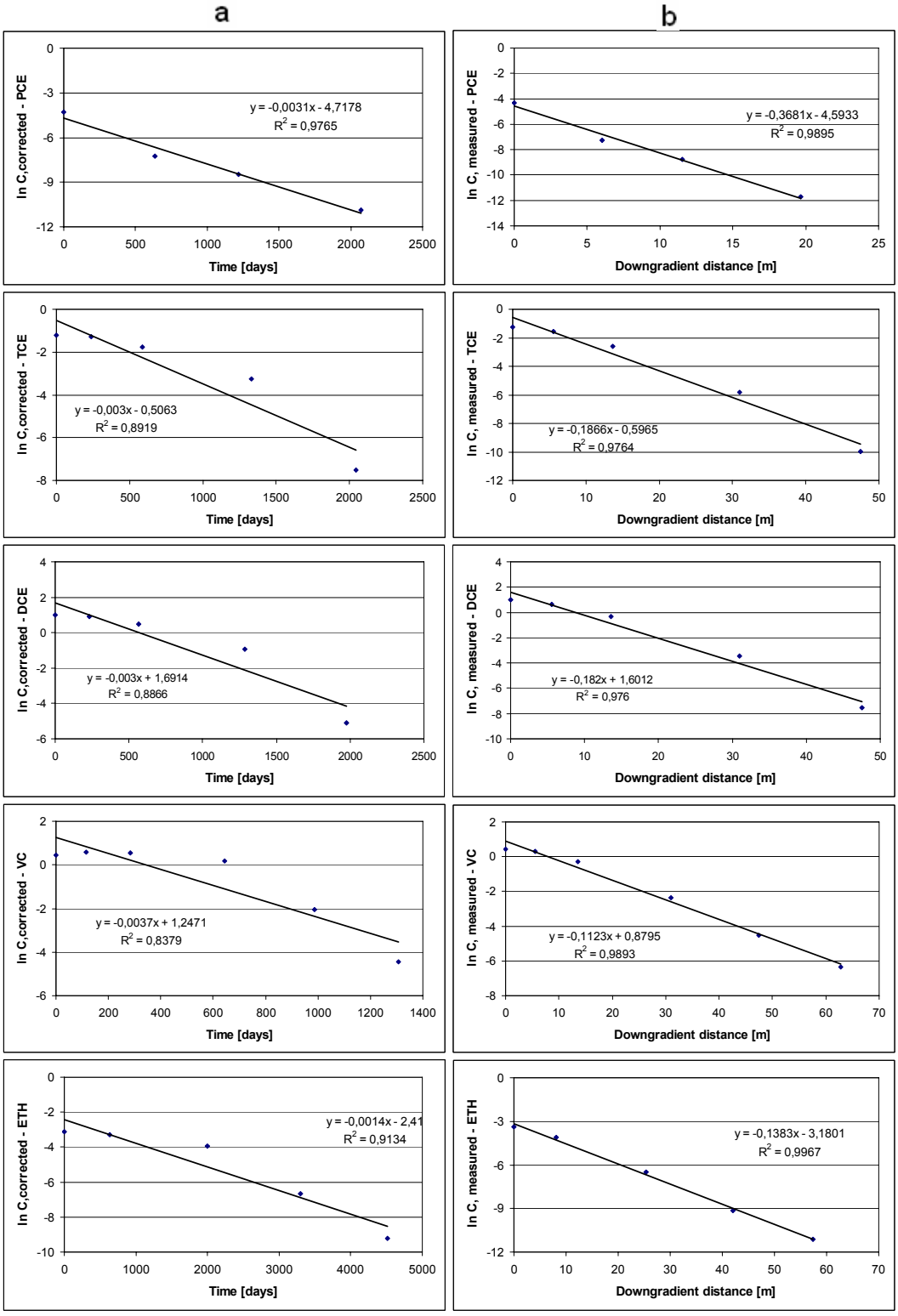

Figure F.10. Linear Regression Plots for (a) Conservative Tracer Method (b) Buscheck-Alcantar Method when CV = % 150 and h = 20 m.

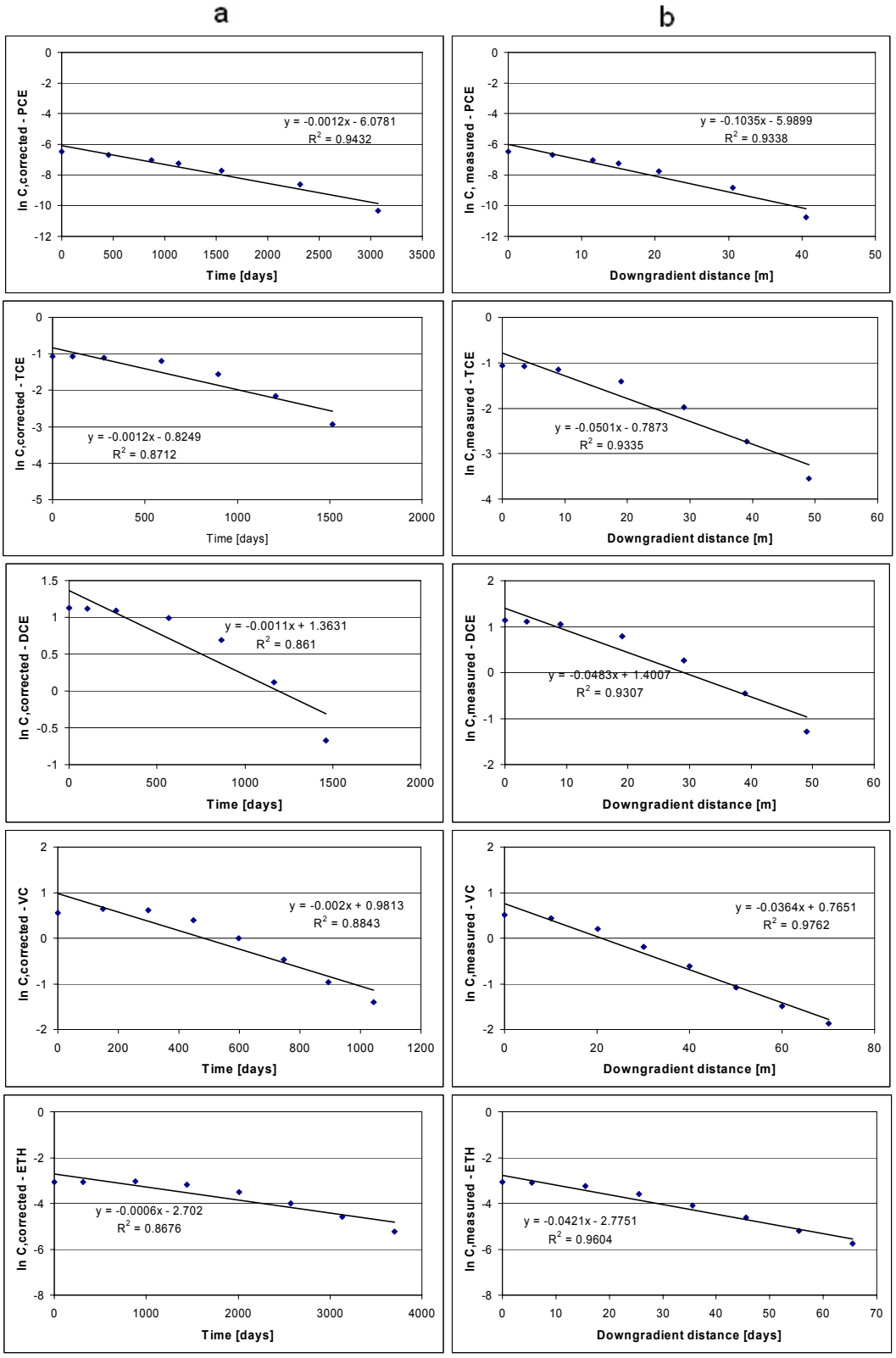

Figure F.11. Linear Regression Plots for (a) Conservative Tracer Method (b) Buscheck-Alcantar Method when CV = % 50, h_x = 10 m and h_y = 2 m.

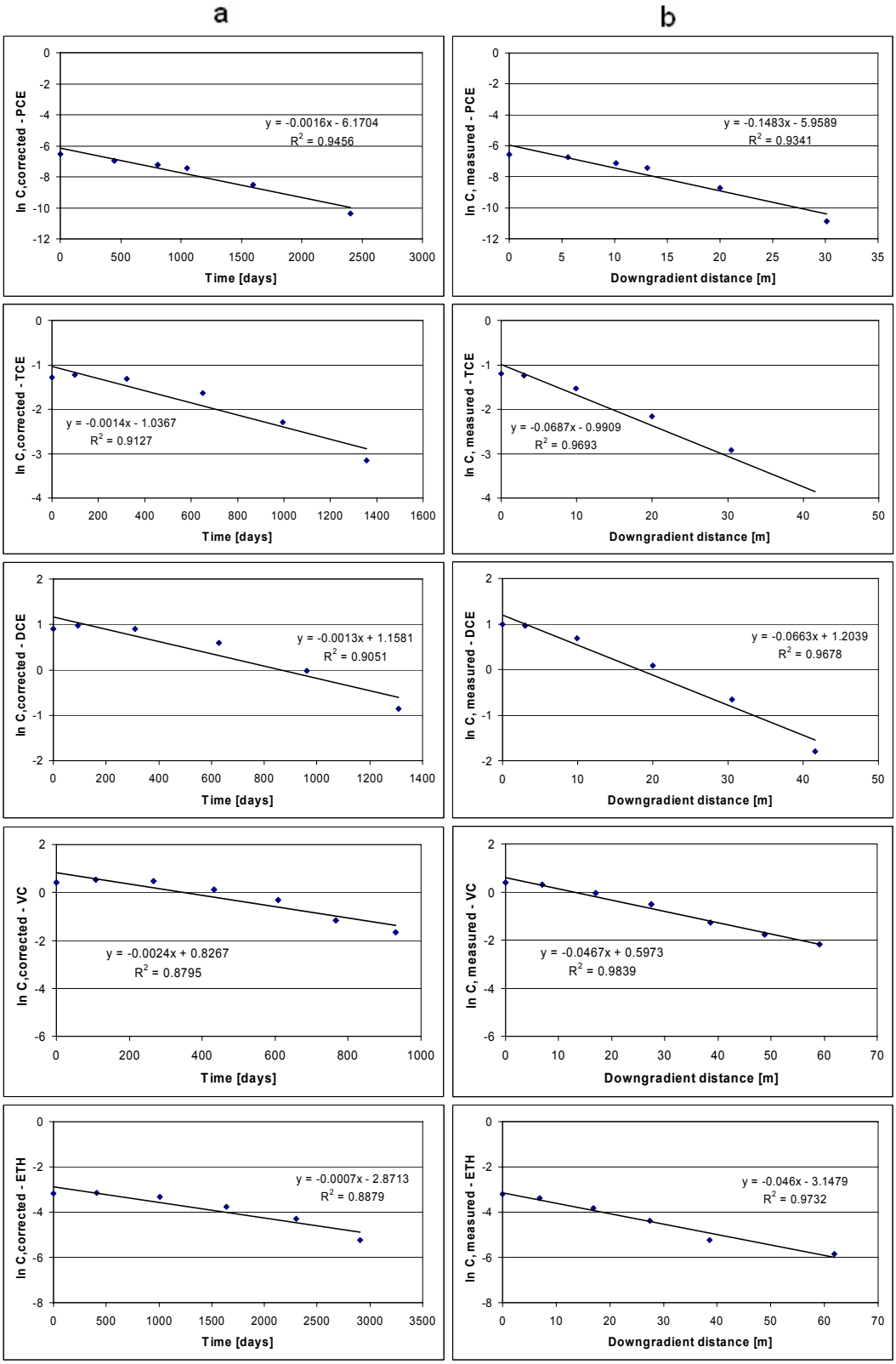

Figure F.12. Linear Regression Plots for (a) Conservative Tracer Method (b) Buscheck-Alcantar Method when CV = % 150, h_x = 20 m and h_y = 4 m.

APPENDICES G – SURFACE PLOTS OF CONTAMINANTS' BIODEGRADATION RATES

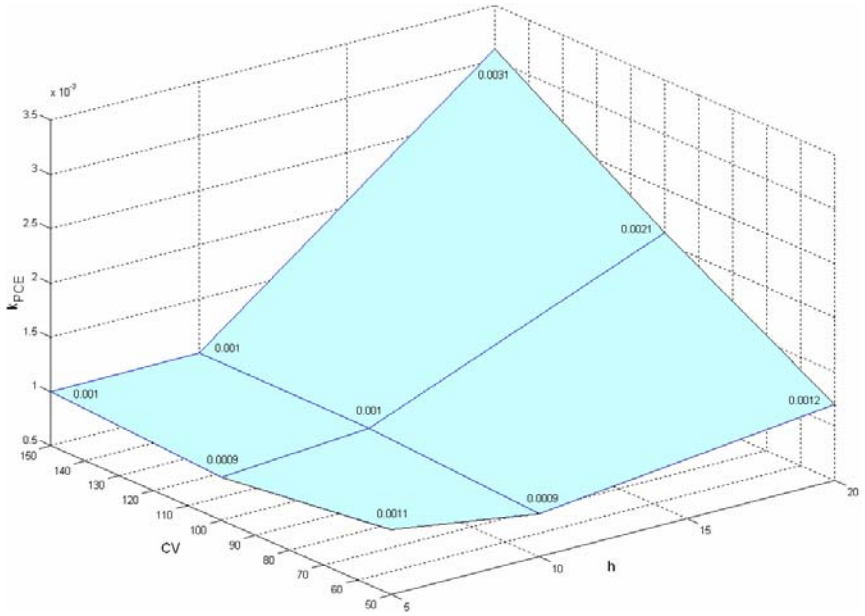

Figure G.1. Surface Plot of PCE biodegradation rates calculated by Conservative Tracer Method.

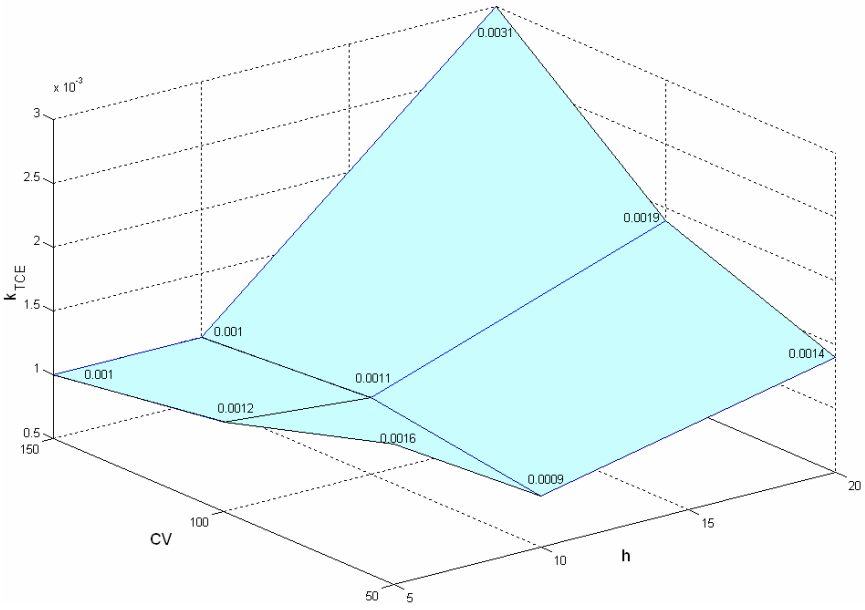

Figure G.2. Surface Plot of TCE biodegradation rates calculated by Conservative Tracer Method

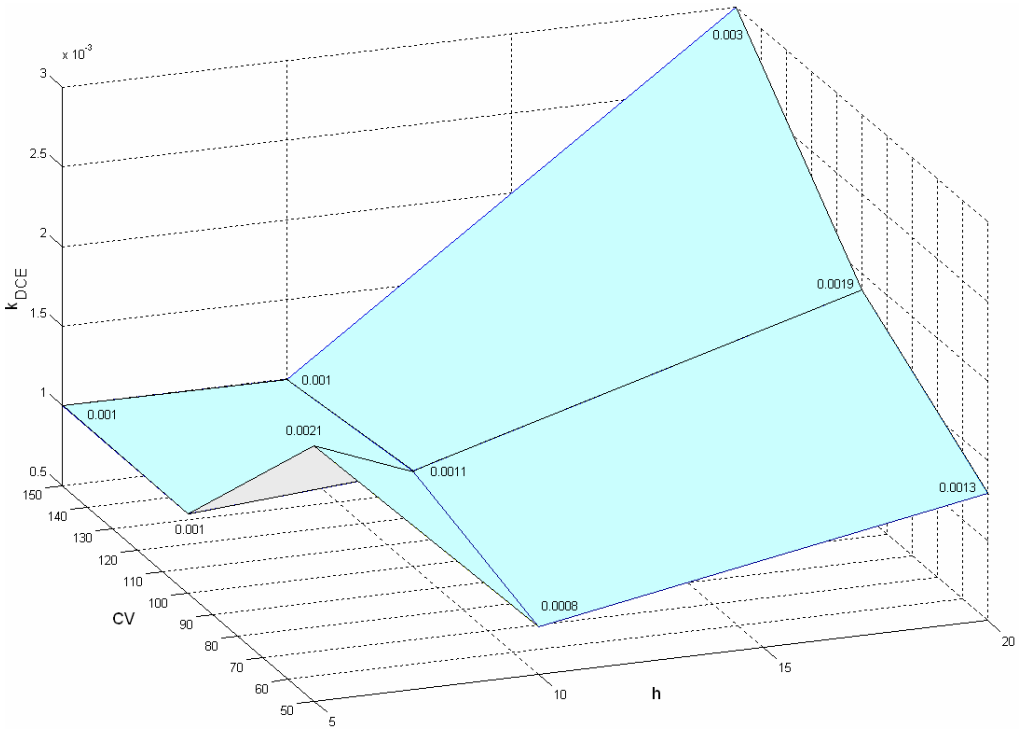

Figure G.3. Surface Plot of DCE biodegradation rates calculated by Conservative Tracer Method

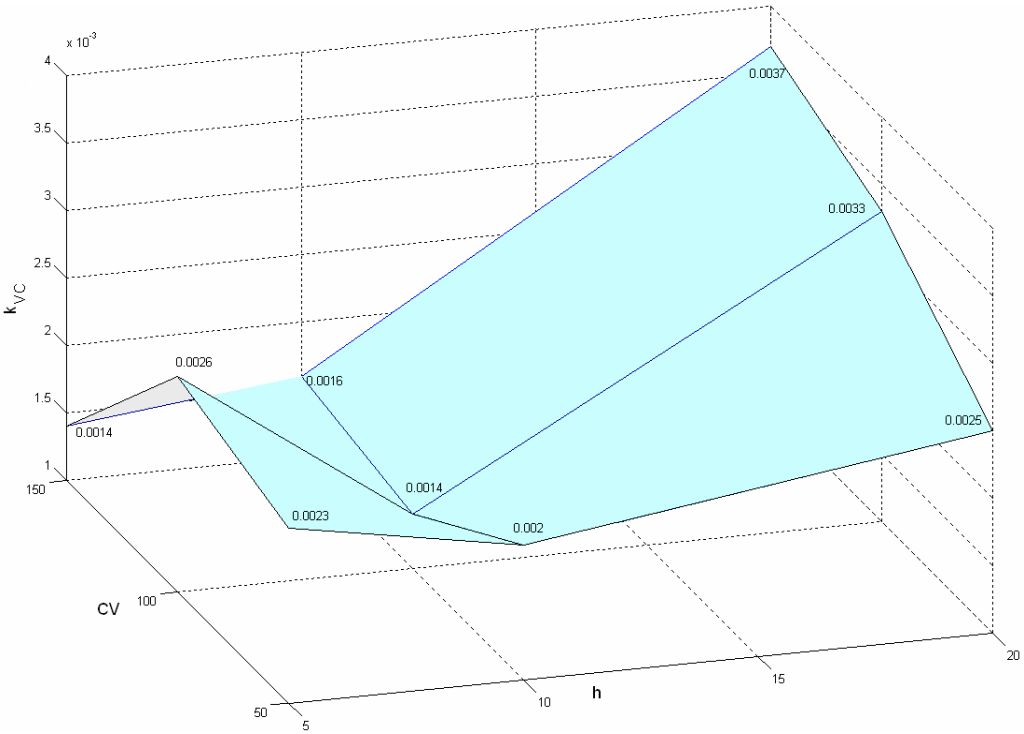

Figure G.4. Surface Plot of VC biodegradation rates calculated by Conservative Tracer Method

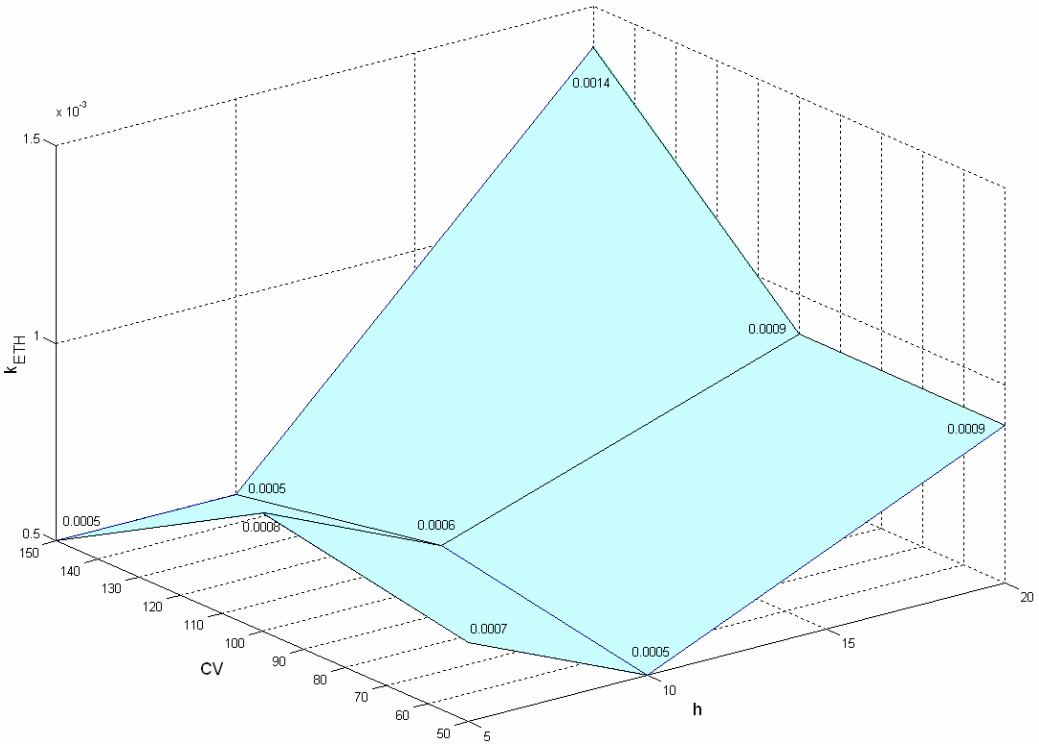

Figure G.5. Surface Plot of ETH biodegradation rates calculated by Conservative Tracer Method

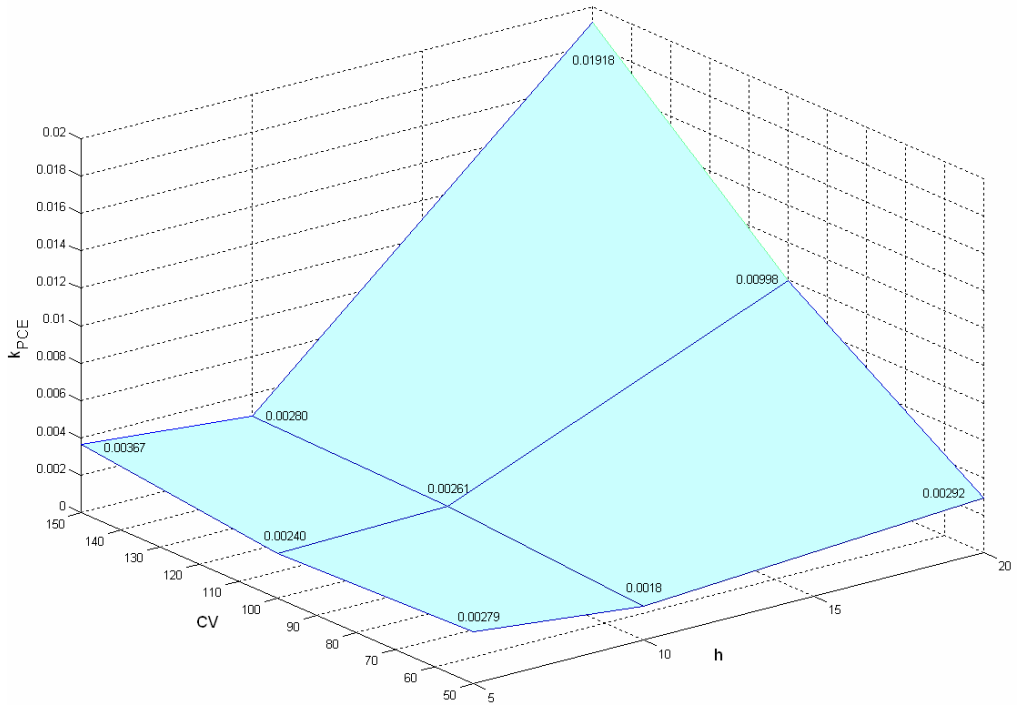

Figure G.6. Surface Plot of PCE biodegradation rates calculated by Buscheck-Alcantar Method

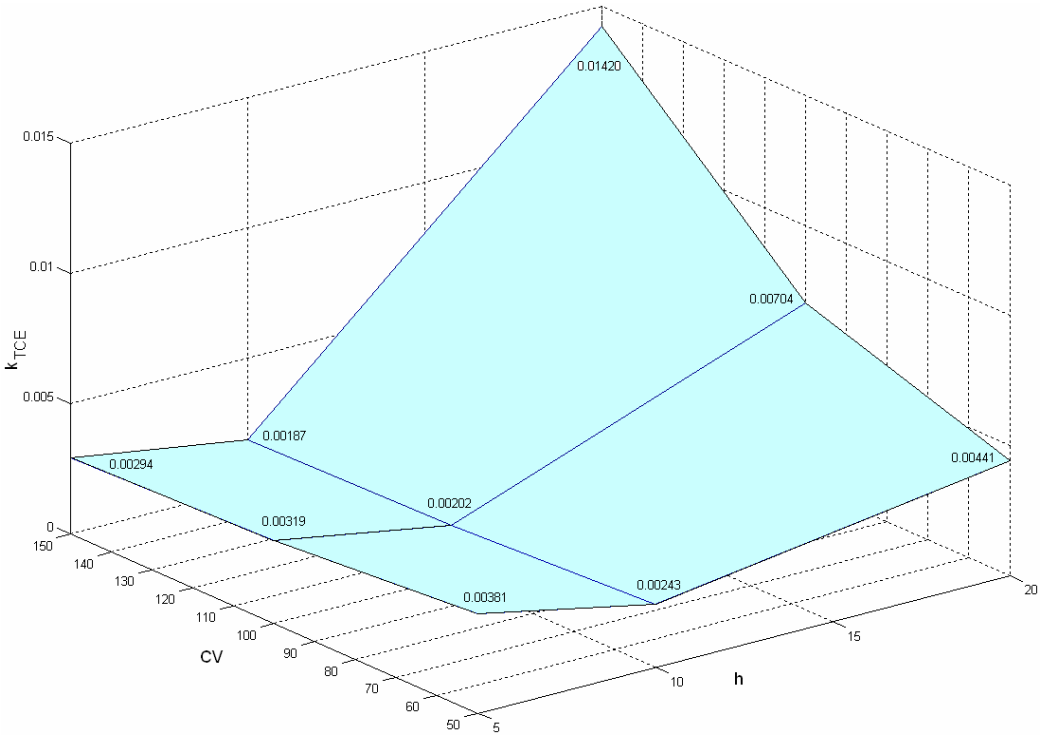

Figure G.7. Surface Plot of TCE biodegradation rates calculated by Buscheck-Alcantar Method

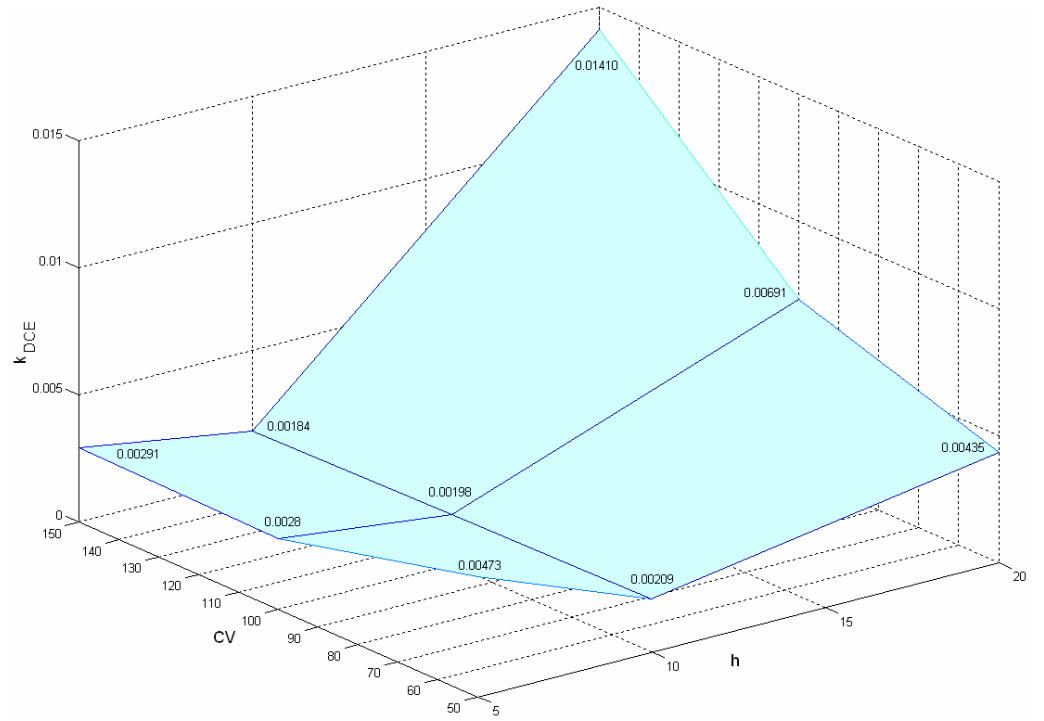

Figure G.8. Surface Plot of DCE biodegradation rates calculated by Buscheck-Alcantar Method

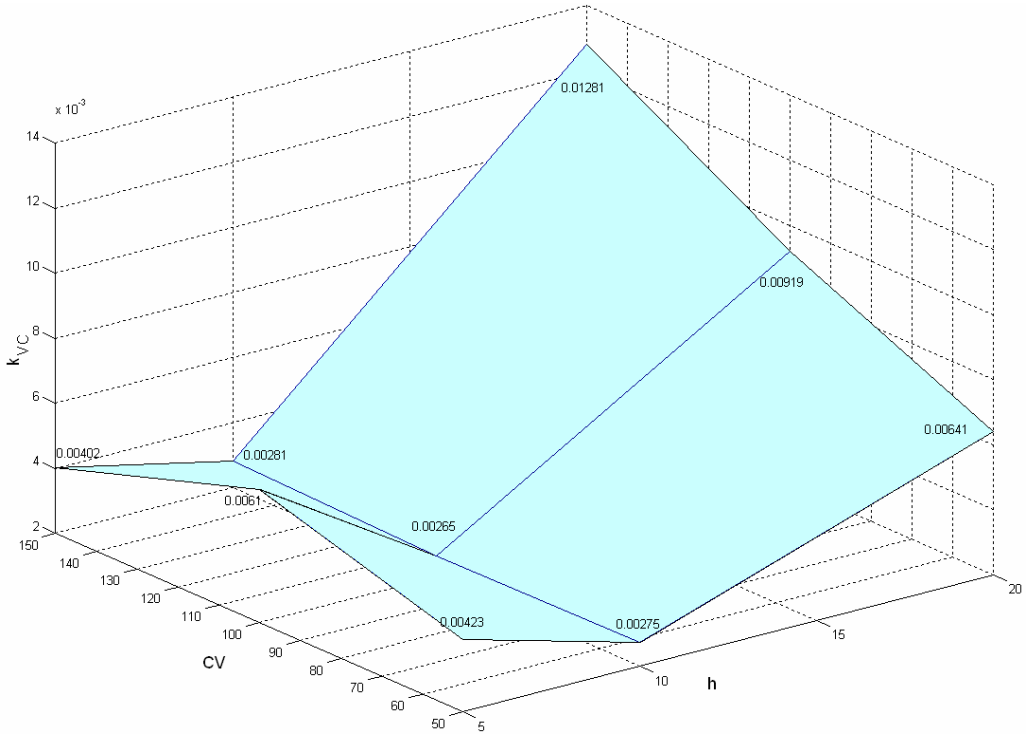

Figure G.9 Surface Plot of VC biodegradation rates calculated by Buscheck-Alcantar Method

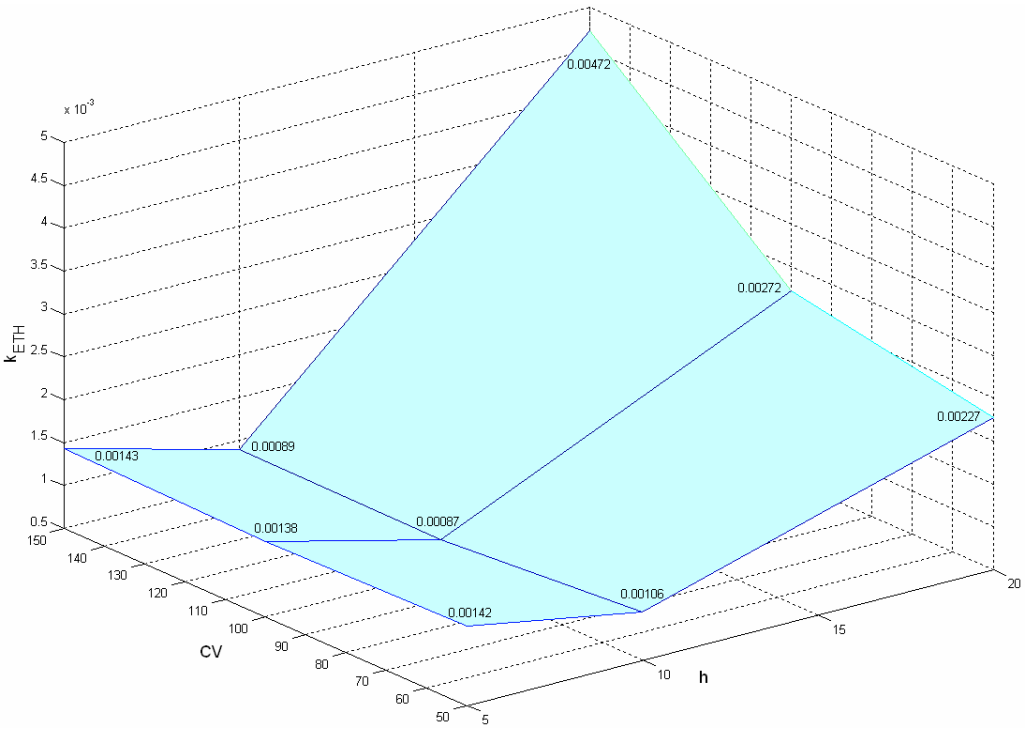

Figure G.10 Surface Plot of ETH biodegradation rates calculated by Buscheck-Alcantar Method